Water Absorption in Two-Layer Masonry Systems - Properties, profiles and predictions

Johansson, Peter

2005

LUND INSTITUTE OF TECHNOLOGY
LUND UNIVERSITY

Division of Building Materials

WATER ABSORPTION IN TWO-LAYER MASONRY SYSTEMS

Properties, profiles and predictions

Report TVBM-1024 Doctoral Thesis

Lund 2005

ISRN LUTVDG/TVBM--05/1024--SE(1-151)
ISSN 0348-7911 TVBM
ISBN 91-628-6680-X

Lund Institute of Technology
Division of Building Materials
P.O. Box 118, SE-221 00 Lund
Sweden

Telephone: 46-46-222 74 15
Telefax: 46-46-222 44 27
www.byggnadsmaterial.lth.se

PREFACE

This research was carried out at the Division of Building Materials, Lund Institute of Technology, under the auspices of the Moisture Research Centre. The project was initiated by Professor Göran Fagerlund, whom I wish to thank for his ideas and support.

I would like to thank Professor Lars-Olof Nilsson for his excellent supervision throughout the final phase of the project. I would also like to acknowledge all the staff at the Division of Building Materials for their help and support. I wish to express special gratitude to Ingemar Larsson, Division of Building Materials, and Agneta Ohlsson, Division of Building Physics, for their generous help in the laboratory. A special thank to Mårten Janz for the collaboration during the early part of the research.

The financial support of the Swedish Council for Building Research, the Development Fund of the Swedish Construction Industry, and Skanska AB is gratefully acknowledged.

SUMMARY

The main impetus for this research was the desire to verify models for determining transient moisture profiles in the capillary range. For the evaluations, transient moisture profiles were both simulated and measured, after which the results of the two methods were compared. The study was performed for on specimens exposed to continuous water absorption, using specimens of both single and combined materials. The materials used for the study were two mortars and a lime silica brick. For testing, we chose materials with moisture properties corresponding to those of common inorganic façade materials.

As input for the simulations, data such as sorption isotherms and moisture diffusivities were determined for the studied materials. Sorption isotherms were experimentally determined over the complete moisture range, two separate methods having to be used for the hygroscopic and the capillary parts of the moisture range. In the hygroscopic moisture range, both absorption and desorption isotherms could be determined, but in the capillary moisture range only desorption isotherms could be determined. To allow measurement of absorption isotherms in the capillary moisture range, the measuring equipment had to be modified; however, despite the modifications, reliable absorption measurements were still not possible. The desorption isotherms determined by the two different methods generally agreed well for all tested materials.

Moisture diffusivities were determined by evaluating a series of water absorption tests using a Boltzmann transformation principle. To determine moisture diffusivities over the complete moisture range, the water absorption tests were performed on specimens conditioned to different initial moisture contents, ranging from completely dry to the vacuum saturation point. The variation in the results was significantly reduced when the water content was expressed as the degree of vacuum saturation; thus, moisture diffusivity was determined as a function of moisture content, expressed as a degree of vacuum saturation.

Different methods for measuring the transient moisture profiles were considered. The moisture profile measurements were supposed to be performed on specimens of both single and combined materials. Two of the most interesting methods were the nuclear magnetic resonance (NMR) technique and the slice and dry method. The NMR technique displayed excellent precision in terms of both moisture content measurement and the spatial resolution. However, the method was severely limited, in that even an insignificant amount of iron in the specimen disturbed the measurements. Another limitation was restricted access to the measuring equipment.

For the larger-scale measurements of the moisture profiles, the slice and dry technique was chosen. This method offered high and conclusive precision in terms of moisture content measurement, and only relatively simple laboratory equipment was needed. One drawback of the method was that the specimens had to be sliced for testing, meaning that a particular specimen could not be tested repeatedly. Other drawbacks were limited spatial resolution and the destruction of the specimen.

Moisture profiles were measured after a continuous wetting phase, for both the specimens of three single materials and the two material combinations. The combinations were intended to simulate a façade consisting of a layer of mortar on masonry: the outer layer of mortar was exposed to continuous wetting, and the moisture profiles were then measured for the material combination.

Both the thickness of the outer mortar layer and the properties of the mortar were varied. The measurements showed that the moisture properties of the outer layer of mortar depended more significantly on both the moisture penetration depth and moisture levels in the underlying material than on mortar thickness.

Moisture profile simulations were performed using off-the-shelf software, using as inputs the absorption isotherms and moisture diffusivities determined in this work. The simulations were intended to reflect the larger-scale experimental portions of this research. To this end, the boundary conditions and wetting durations used as inputs corresponded to the conditions of the larger-scale moisture profile measurements.

The simulated and measured results for the combined materials largely agreed with each other, in terms of both moisture levels and depth of moisture front. However, the simulated moisture profiles of the two mortars as single materials significantly diverged from the measured values. The simulated profiles lacked a clear front in the moisture levels and moreover were overestimated after the front. Alternative simulations were carried out in which the deviation between the simulations and the measurements was clarified, and was shown to depend on errors in the technique for evaluating diffusivities at low moisture levels.

Comparison between the simulated and measured moisture profiles indicated that moisture profiles can be predicted with considerable precision in the high moisture range. However, by determining additional material data pertaining to moisture diffusivity in the low moisture range, the precision of the predictions can be improved. A primary conclusion of the research is that moisture profiles can be predicted for combined materials using off-the-shelf software.

CONTENTS

1 INTRODUCTION

1.1 BACKGROUND

1.1.1 General

The choice of façade material as the outer layer on a different underlying material is frequently based on insufficient knowledge, with the result that the combined materials experience early degradation. In some cases it is the outer layer that loosens from the underlying material, while in other cases a new finish on the façade causes the original underlying material to experience early degradation. The difficulties in choosing suitable materials for different combinations often arise because the moisture mechanics between the two materials is unknown. Thus, while two materials may show good resistance to frost when used separately, when combined they may well be extremely sensitive to frost attacks. The difference in resistance to frost attacks between the single and combined materials arises from unfavourable moisture conditions appearing in the interface between the combined materials. This interface can also increase the sensitivity to frost attacks, since moisture transport across the interface will be partly hindered during freezing.

The following are examples of material combinations and degradation processes:

- Finishing materials based on cement or polymers over underlying concrete, brick, or other mineral-based materials: The finishing often causes a greater range of degradation from frost attacks in the underlying material than is the case for the underlying material without the finishing layer. The moisture balance in the material combination is what determines the performance.
- Different types of paint applied to underlying materials of wood, concrete, mortar, or brick: The problem described in the first paragraph is often seen here as well.
- A layer of mortar on masonry: When the same type of mortar is used in different thicknesses, thinner layers are often observed to cause a greater range of degradation in the underlying masonry than is the case under thicker mortar layers. The reason for the lower frequency of damage occurring under thicker layers of mortar is likely the delayed temperature decrease during frost attacks. As well, a thinner layer of mortar often has a different pore structure from that of a thicker layer, resulting in a change in moisture balance; this change in moisture balance is known to cause frequent damage via shrinkage or frost attacks.
- Damage can also be caused by the differential shrinkage of two combined materials, which often results from the differing properties of the two materials.
- Damage from frost attacks more frequently occurs after an additional isolation on the inside of a façade. This happens when moisture levels are generally increasing at the same time as cycles of frost attack are occurring more often to a certain depth in the façade.

1.1.2 Moisture mechanics

To understand moisture-related durability problems relating to combined materials, it is crucial to be able to predict moisture conditions over the complete moisture range under a certain external moisture load. Knowledge of diffusion processes in porous building materials is fairly good, and methods for determining moisture transport data as sorption isotherms and moisture diffusivities are relatively well established over the hygroscopic range. Thus, moisture conditions can be determined within this moisture range with a fairly high degree of precision.

A problem with determining moisture conditions at interfaces between materials in facades is that the moisture levels are usually well above the hygroscopic range. In the capillary range, methods for measuring material properties and moisture profiles and for prediction have been studied to some extent for some years. Early significant studies include those performed by Lykow (1958), Vos and Tammes (1968), van der Kooi (1971), Bomberg (1974), and Nielsen (1974). In recent years, further studies of moisture properties in the capillary range have been published by Plagge et al (2004), Janz (1997), Hjorslev (1998) and Hall and Hof (2002). However, all these studies were of single materials.

The present research, however, focuses especially on the moisture balance between combined materials. The literature includes very few studies of moisture transport in the capillary range in material combinations, studies such as Sandin (1980) and Brocken (1998). These studies mainly examine the material properties of single materials and present experiments on material combinations; verified prediction methods valid in the capillary range are extremely rare.

1.2 ORIGINAL OBJECTIVES

A major objective of this work was to develop a tool for determining moisture levels in combined materials under a certain external moisture load. Inputs for the calculations include the moisture transport and fixation properties of the materials.

Durability problems with combined materials caused by an external moisture load should also be studied, mainly using experimental methods. A method should also be developed by which the durability of combined materials under a high external moisture load can be determined.

During the course of the research the original objectives were revised, and the development of a method for determining the durability under a high external moisture load was excluded.

1.3 STRUCTURE OF THE THESIS

Chapter 2 describes the measurement of moisture fixation data for the studied materials. Two different methods are used, one for the hygroscopic moisture range and the other for the capillary moisture range, and results obtained using the two methods are compared. Fundamental material data for the studied materials are also presented in this chapter.

Moisture diffusivities for the studied materials are presented in Chapter 3. The moisture diffusivities are determined from a series of water absorption tests conducted using a Boltzmann transformation principle.

Four different methods for measuring transient moisture profiles were chosen, and these are examined in Chapter 4. Moisture contents or moisture profiles are measured for different materials and the results are discussed.

In Chapter 5, moisture profiles are measured for specimens of both single and combined materials. The absorption tests are performed after a continuous wetting phase, and the particular measurement method used was determined according to the evaluation presented in Chapter 4.

The simulation of transient moisture profiles is outlined in Chapter 6; in calculating the moisture profiles, the input data regarding material properties were based on the moisture fixation data presented in Chapter 2 as well as the moisture diffusivities in Chapter 3. For the moisture profile simulations, both the boundary conditions and the duration of the wetting time were adapted to the conditions of the moisture profile measurements presented in Chapter 5. As a summation, the measured and simulated moisture profiles are compared.

Conclusions of the work are presented together with a proposal for future studies in Chapter 7.

2 MOISTURE FIXATION MEASURED OVER THE COMPLETE MOISTURE RANGE

2.1 INTRODUCTION

Sorption isotherms covering the hygroscopic range are usually determined using the well-tried climate box method. During the tests, specimens are put into equilibrium with different levels of relative humidity created using saturated salt solutions. To verify the exact time when the equilibrium state is achieved, the specimens are weighed at certain intervals; moreover, the specimens must be of a certain minimum size depending on the accuracy of the balance used. With a normal laboratory balance having an accuracy of thousandths of a gram, the specimens normally have to be of such a size that a relatively long time is needed to achieve equilibrium. The measuring time can of course be shortened if different specimens are used for the different relative humidity steps. However, when this is done, variation in pore size distribution and in other material-related properties that vary spatially in the material will of course affect the results. By using the same specimen throughout the measurement process these sources of error can be avoided.

The sorption balance method can be used as an alternative to the climate box method. This method is based on the continuous weighing of a single sample: the surrounding climate is changed in terms of relative humidity and temperature while the mass of the sample is registered continuously. Since one objective is to determine a complete sorption isotherm in a relatively short time, the specimen should be quite small. Even if the specimens of the different materials tested are of the same weight, the time needed to reach the equilibrium state will still be utterly dependent on the pore size distribution in a given specimen. In this research, sorption isotherms representing both desorption and absorption were determined for three different materials (see Section 2.3) using the sorption balance technique (see Section 2.3). For testing purposes, materials were chosen with properties representative of those of normally used inorganic façade materials.

Since a major share of the moisture storage capacity of common inorganic building materials lies above the hygroscopic range, another measurement method, other than the sorption balance or climate box method, was needed to enable measurement of the entire sorption isotherm from complete dryness to vacuum saturation. Instead of refining the previously mentioned methods, the pressure plate technique was used to complement the sorption balance technique above the hygroscopic range. This method was first developed in the field of soil mechanics for studying the negative water pressure in different soil layers. One of the first reports in the literature concerning the pressure plate method was that of Richards (1948). The pressure plate technique was originally designed for making desorption measurements. Its principle of operation is based on the equilibrium existing between the excess pressure in the pressure plate extractor and the suction under the meniscus in the water-filled pores. Since the excess pressure can be regulated with considerable accuracy, high precision in terms of relative humidity can be attained. Sorption isotherms above the hygroscopic range were determined using the pressure plate method, which is further described in Section 2.4.

2.2 MATERIALS

For the moisture diffusivity tests three types of materials were chosen, representing commonly used inorganic façade materials, i.e. lime–silica brick, lime–cement mortar, and cement mortar that contains air. The lime–silica brick used in the tests was obtained on the regular building material market. However, the mortars were produced within the project, partly to facilitate control of the proportions of the different constituents and partly to allow the use of white cement instead of ordinary Portland cement. White cement has a considerably lower iron content than Portland cement does, a quality required when measuring moisture content using nuclear magnetic resonance (NMR; see Chapter 4).

One aim of the project was to use the same materials for the determination of material data with respect to moisture fixation (see this chapter), moisture transport (see Chapter 3), moisture profile measurements under a certain moisture load (see Chapter 5), and corresponding moisture profile simulations (see Chapter 6).

Lime–silica brick consists mainly of finely ground burned lime, plus quartz sand or crushed sandstone in fractions of 0–4 mm. During manufacturing, the raw materials are mixed together and water is added; the water admixture produces heat as the lime is slaked. The raw mass can then be shaped as desired under pressure; subsequently it is cured in an autoclave containing steam at a temperature of 200–220ºC, according to Burström (2001).

Two types of mortar were produced in the laboratory, a cement mortar and a lime–cement mortar. The cement mortar had a water–cement ratio of 0.8 and was mixed from white cement and Baskarp aggregate in the 0–3-mm fraction; the cement–aggregate ratio was 2:7 by weight. The cement mortar was produced in two versions, with and without air entrainment agent (AEA). With AEA the fresh mortar had a total air content of approximately 4% by volume, and without AEA it had a total air content of approximately 1.2%. The lime–cement mortar was produced in four quality grades from A to D, according to Hus AMA 98 (1998). The binder was white cement and slaked lime in different proportions for the different quality grades (see Table 2.1). When mixing the fresh mortars, water was added until the consistency of the mixture corresponded to that required for bricklaying. The aggregate used was Baskarp in the 0–3-mm fraction.

Table 2.1 Mixture properties for lime–cement mortar of quality classes A to D.

	Proportion by weight		
Lime–cement mortar	Slaked lime	White cement	Aggregate
A	10	90	350
B	35	65	550
C	50	50	650
D	50	50	950

All types of tested mortar were cast in bar-shaped forms measuring 50 × 50 × 500 mm. The forms were made of surface-coated plywood and the upper surfaces of the specimen were covered with a wet cloth and plastic foil for approximately 24 h after casting. Shrinkage cracks caused by too-rapid drying could be prevented by keeping the surface wet. After the first 24 h, the cement mortar was stored for five days in a water basin. To reach optimal carbonation the lime–cement mortar was stored in a climate chamber for approximately two months. The climate chamber had a relative humidity of 65–75%, which is optimum for carbonation according to Hinderson (1958).

After the cement mortar was cured in the water basin and the lime–cement mortar was cured in the climate chamber, the cast-mortar prisms were sawn into specimens measuring 50 × 50 × 100 mm. During sawing it was discovered that the lime–cement mortar of quality classes C and D were of low strength and tended to fall apart during handling; even though some specimens of these mortars could be cut, the surface aggregate tended to loosen during handling. If such specimens were used during the pressure plate experiments described in Section 2.4, the dry weight would change during the course of the experiment since the specimens had to be handled for weighing after each pressure level. The measuring procedure thus required relatively strong specimens. Also, the cement mortar without AEA was excluded, since preliminary studies showed a significantly low capillary absorption rate, not corresponding to that of any common façade material.

After the prisms were sawn into smaller specimens of 50 × 50 × 100 mm, the degree of carbonation was checked by splitting the specimens and spraying the fresh surfaces with an indicator fluid. The fluid was a mixture of 3% phenolphthalein and 95% ethyl alcohol by weight, according to the Svensk standard (1988). In contact with a basic environment (pH ≥ 9.2), the fluid turns red, and so is a suitable indicator of carbonation. Since the specimens were not carbonated throughout, they were placed in sealed boxes; to increase the rate of carbonation, a cylinder of carbon dioxide gas was connected to the box. Since the cylinder provided the box with completely dry carbon dioxide and the optimum humidity for carbonation is approximately 65–75% relative humidity, a small basin of water was placed in the box; evaporation from the basin kept the relative humidity at approximately 70%. The relative humidity was regularly measured during the curing phase. The carbonation of the specimen was checked approximately once a month using the indicator fluid. This forced carbonation process had to be performed for approximately one year until all of the specimens were carbonated throughout.

The pressure plate experiments performed on lime–cement mortar A failed, as further discussed in Section 2.4, so this mortar was excluded from further study. Material data regarding the materials used in the moisture fixation tests are presented in Table 2.2. The material properties were determined from 15 prisms of each material, each of the dimensions 50 × 50 × 100 mm. Vacuum-saturated specimens were weighed in air and in water, thus allowing the volume and porosity to be determined using the Archimedes principle. Vacuum saturation was performed according to the schedule described in Section 2.4.2. Two separate batches of lime–silica bricks were used: batch 1 was initially used for the capillary water absorption tests described in Chapter 3, but was excluded due to damage during drying, so batch 2 was also used for these tests; batch 2 lime–silica bricks were exclusively used in the testing described in the remaining chapters.

Table 2.2 The density, compact density, and porosity of test materials, given as mean values and standard deviation.

Material	Density, ρ [kg/m^3]		Compact density, ρ_c [kg/m^3]		Porosity, P [%]	
	$\bar{x}$	s	$\bar{x}$	s	$\bar{x}$	s
Lime–silica brick, batch 1	1911	15.6	2644	2.2	27.7	0.6
Lime–silica brick, batch 2	1898	31.4	2624	5.3	27.7	1.2
Lime–cement mortar	1673	9.6	2631	3.5	36.4	0.4
Cement mortar	1897	16.3	2556	26.1	25.8	0.3

2.3 SORPTION BALANCE

2.3.1 General

The basic principle of the sorption balance technique is essentially the same as that of the climate box technique, except that the specimen is weighed continuously while the complete sorption isotherm is being determined. During the measurement process a small sample was weighed continuously while the surrounding relative humidity was changed in a stepwise manner.

2.3.2 Method

The current study used the dynamic vapour sorption (DVS) method. DVS is a relatively new technique for water vapour sorption analysis, based on the principle of an air flow passing two sample holders connected to a microbalance (see Figure 2.1). When the sample holders are symmetrically hung and balanced, distortions arising from differing buoyancy effects caused by the gas flow can be avoided (such differences can occur if the relative humidity or temperature of the gas flow passing one of the two sample holders differs from that passing the other). For this type of DVS apparatus, the type of gas, relative humidity, and temperature surrounding the two sample holders are equivalent, since the gas is mixed before entering the microbalance.

Because great temperature stability is required when sorption measurements are being performed, the DVS apparatus was placed in an incubator, permitting the temperature to be kept constant with a precision of ± 0.1ºC. The required relative humidity was created by mixing two gas flows of known relative humidity: one was a completely dry gas supplied directly from a gas cylinder; the other was the same type of gas, but moisture saturated by having passed through a water jar. Each flow was controlled by thermal conductivity mass flow controllers. The relative humidity of the mixed gas flow could be varied between 0 and 98%. Combined relative humidity and temperature probes were mounted in the gas flows beneath the sample holders to allow monitoring of the conditions of the sample and sample holder.

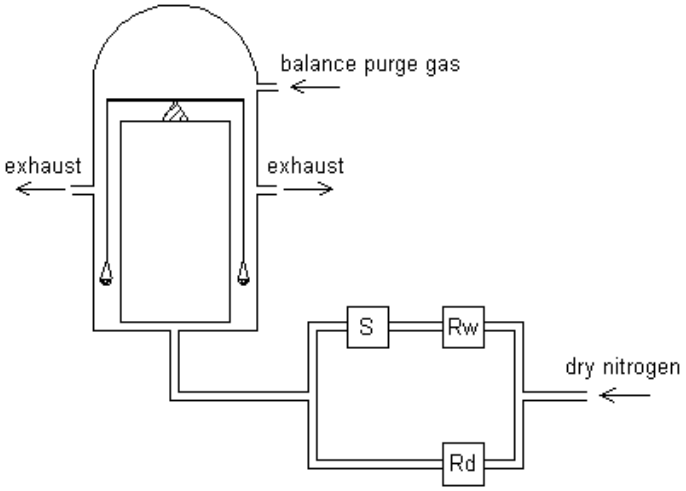

Figure 2.1 Schematic sketch of the DVS instrument. The dry nitrogen gas is partly saturated by the vapour humidifier, S, and mixed in the requested proportions by the flow regulators, R_w and R_d.

The main component of the DVS system is a Cahn D-200 microbalance, Cahn Instruments, U.S.A, which continuously registers the weight as a function of time. For a sample weight of 1.5 mg, the precision of the balance is 0.1 µg, according to Levoguer and Williams (1997). Using as small a sample as possible allows the time to achieve the equilibrium state to be minimized. The microbalance was protected against high relative humidity by a continuous flow of purge gas (see Figure 2.1). The purge gas used during the measurement process was dry nitrogen.

Sorption measurements for lime–silica brick, lime–cement mortar, and cement mortar were performed. Before the measurement process started, specimens of 50 × 50 × 4 mm were completely saturated with deionized water. The vacuum principle was used to saturate the specimen and is further described in Section 2.4.2. After saturation, the specimens were ground in a mortar to produce an approximately 1-mm fraction. From the ground sample, 50–60 µg was randomly chosen and put in the sample holder, which had been thoroughly cleaned with deionized water and alcohol before the tests were performed.

A full cycle of measurements was performed, starting with desorption at 93% relative humidity and continuing stepwise in seven steps to a completely dry gas flow of 0% relative humidity. After equilibrium with the completely dry gas flow, an inverted cycle was performed, consisting of seven steps reaching a final relative humidity of 93% (see Figure 2.2). A maximum relative humidity of approximately 97% could have been used; however, 93% relative humidity was chosen, since the time needed to reach equilibrium at a higher relative humidity was estimated to be too long. Nitrogen gas of high purity was used in all the experiments, but since the specimens were well cured and carbonized before testing (see Section 2.2), dry air could also have been used. Nitrogen gas is normally used to prevent carbonization during testing, when tests are performed on non-carbonized cement-based materials. All measurements were performed at 20 ± 0.1ºC.

The equilibrium state could be defined in two ways, either by setting a fixed duration for each relative humidity step or by using the time differential coefficient of the mass. The time differential coefficient of the mass was defined as the rate of the change in mass over a certain period. Preliminary testing revealed that the balance was insufficiently stable to allow use of the time differential coefficient of mass as an equilibrium criterion. The swaying of the specimens being weighed hindered the measured specimens from reaching the equilibrium state, so a fixed duration was used for each relative humidity step, as shown in Figure 2.2.

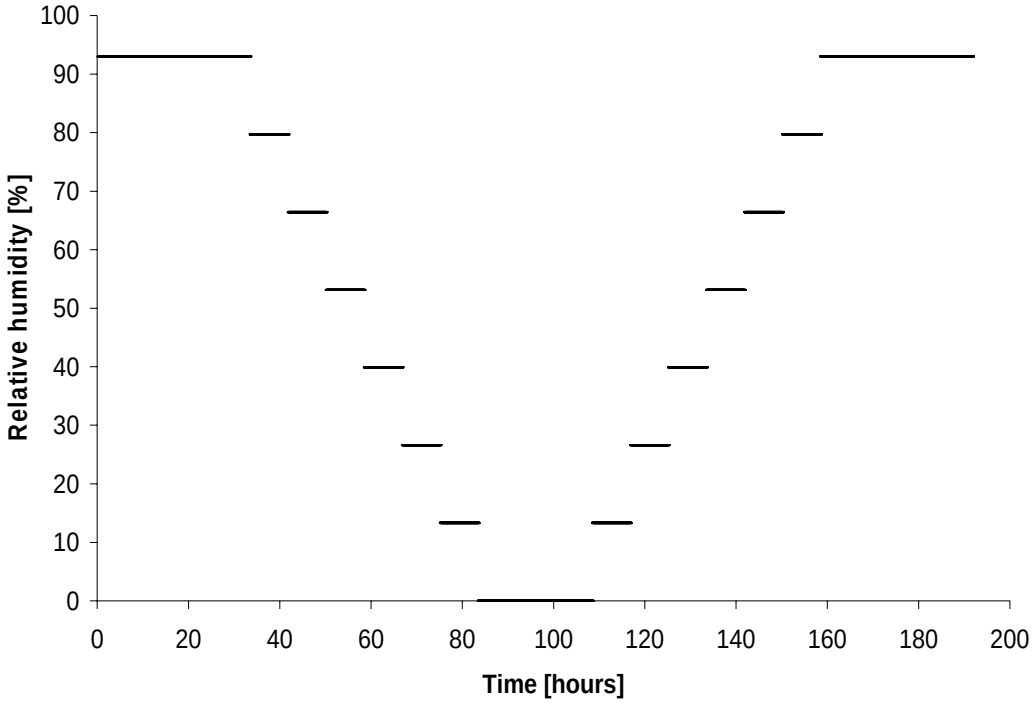

Figure 2.2 Relative humidity steps as a function of time for a full measurement cycle with vacuum-saturated specimens.

Several different combinations of relative humidity steps of various durations were tested for lime–silica brick until satisfactory equilibrium could be reached for all relative humidity steps in the cycle (see Figure 2.3). The highest and the lowest relative humidity steps needed the longest durations to achieve a sufficiently low rate of weight change. Even if the duration of a specific step was increased considerably, weight change was still detectible. To estimate the final weight at equilibrium, extrapolation was performed for the weight change at each relative humidity step. A general expression according to Equation 2.1 was used to extrapolate the equilibrium state without needing an infinite measuring duration (see Anderberg and Wadsö, 2004). The first 10% of the measurement data was excluded when the extrapolation was performed, since the rate of weight change in this first part of the phase was not representative (see Figure 2.3).

$$m = e^{k \cdot t} \tag{2.1}$$

where

m is the mass of the specimen,

k is a general constant, and

t is the time needed for the measurement.

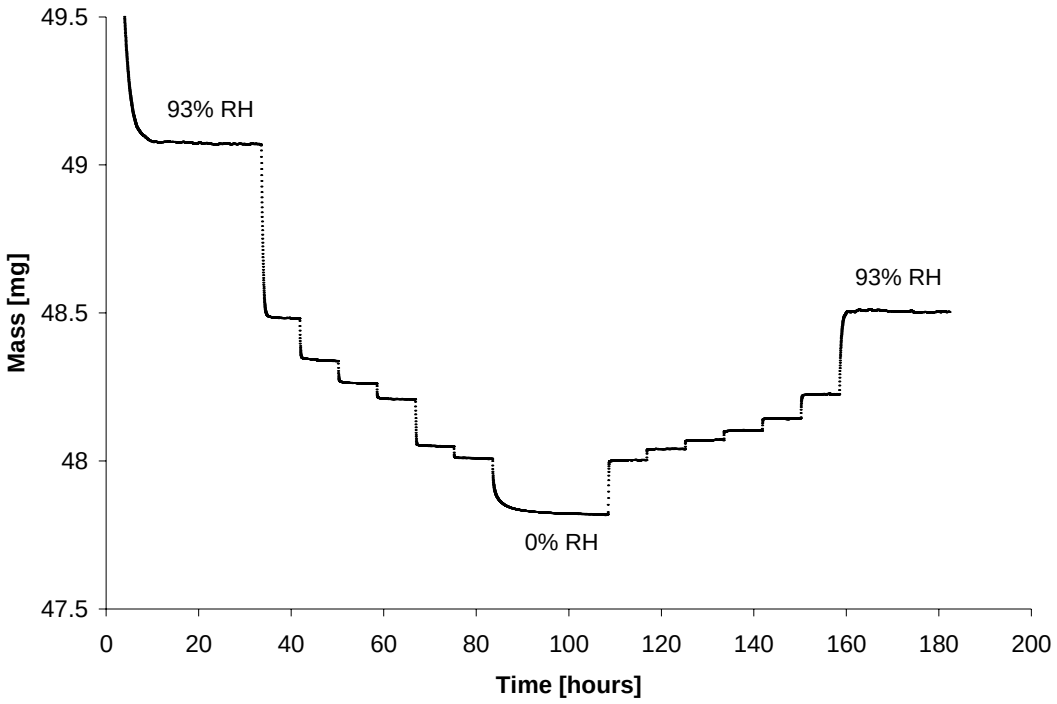

Figure 2.3 Mass as a function of time to complete a full sorption cycle for lime–silica brick.

The equilibrium state for a given relative humidity step could be found by extrapolation when the slope of the line for the step was approaching (see Figure 2.3). Since the equilibrium state was almost reached during the measurement process (see lime–silica brick example presented in Figure 2.3), the use of Equation 3.1 had a negligible effect on the results. As can be seen in Table 2.3, the difference between the original and the extrapolated results is very small.

Table 2.3 Moisture content by mass as a function of relative humidity for a full sorption cycle for lime–silica brick. The measured moisture content by mass is represented by u, and the corresponding value extrapolated according to Equation 2.1 is represented by u_e.

Relative humidity [%]	u [%]	u_e [%]
93	2.6187	2.6199
80	1.3905	1.3830
66	1.0904	1.0608
53	0.9306	0.9221
40	0.8193	0.8114
27	0.4874	0.4750
13	0.3975	0.3945
0	0	0
13	0.3902	0.3831
27	0.4678	0.4605
40	0.5337	0.5211
53	0.5987	0.5909
66	0.6855	0.6757
80	0.8538	0.8470
93	1.4367	1.4328

2.3.3 Results

Tests were performed on each material until two complete desorption and absorption isotherms had been determined for each of the three tested materials. The variation between the results of the two tests for each material was negligible, so a mean value was used without stating the standard deviation.

The sorption isotherms for the different materials are shown in Figure 2.4 for lime–silica brick, in Figure 2.5 for lime–cement mortar, and in Figure 2.6 for cement mortar. In the sorption isotherms, moisture content by mass is shown as a function of different relative humidities. When the moisture content by mass was determined, the dry weight of the specimen at 0% relative humidity was used to calculate the mass-time relationship (see Figure 2.3 for lime–silica brick).

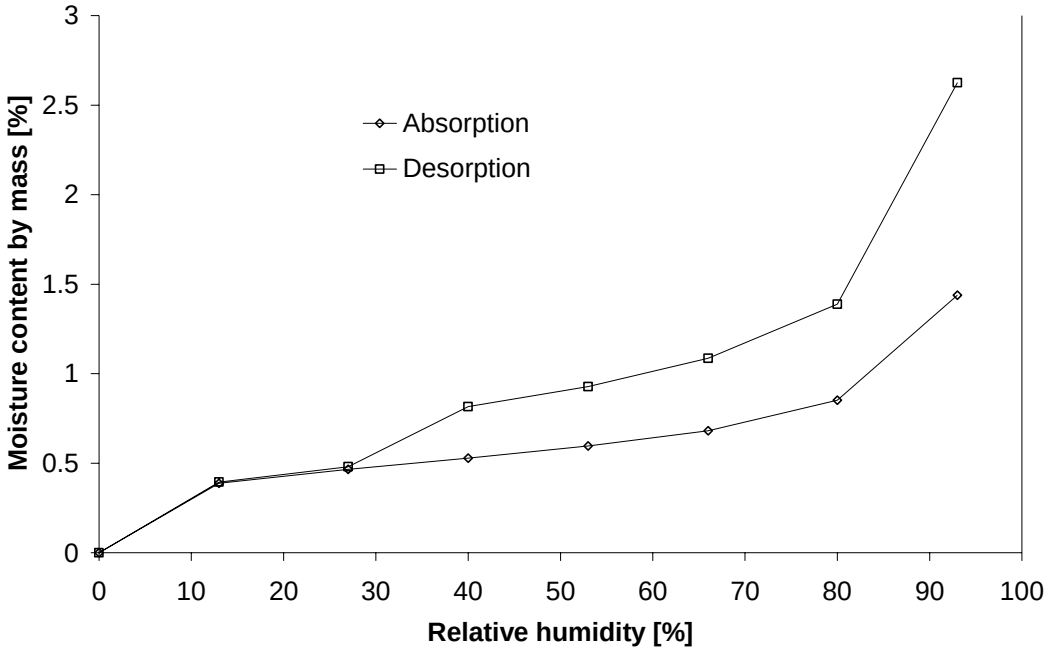

Figure 2.4 Sorption isotherms for lime–silica brick.

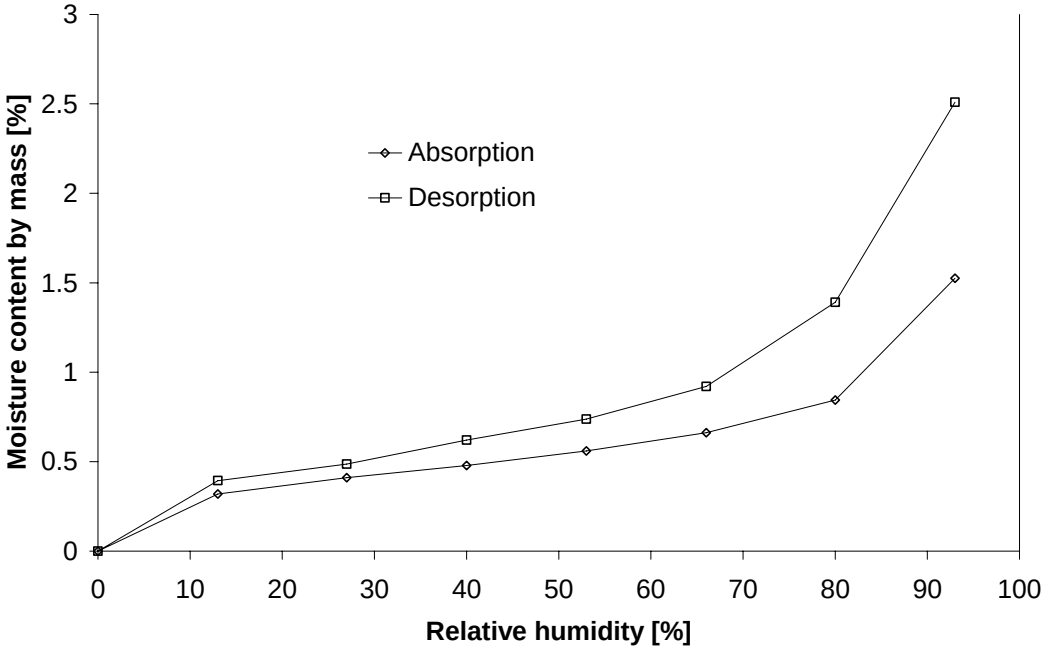

Figure 2.5 Sorption isotherms for lime–cement mortar.

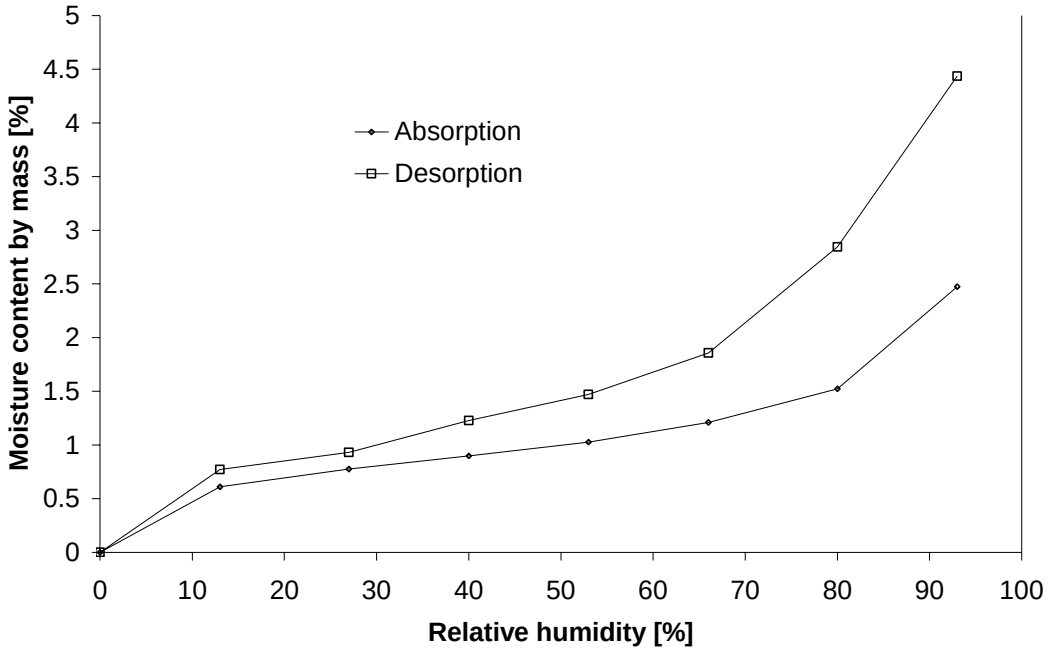

Figure 2.6 Sorption isotherms for cement mortar.

2.4 PRESSURE PLATE

2.4.1 General

The sorption isotherm above the hygroscopic range is called the "suction curve" or "water retention curve", and it shows the relationship between moisture content and pore water pressure. The pore water pressure, ΔP, or "suction", can be transformed into a corresponding relative humidity, ϕ, using the Kelvin equation.

$$\ln \Phi = -\frac{v_s}{R \cdot T} \cdot \Delta P \tag{2.2}$$

where

Φ is the relative humidity above a curved meniscus,

v_s is the molar volume of water [0.018 m^3/kmol],

R is the gas constant [8314 J/kmol·K],

T is the temperature [K], and

ΔP is the capillary suction [Pa].

The simplest way to determine a suction curve is to expose a specimen to a negative water pressure (cf. Fagerlund, 1973) on a suction plate. However, such a technique can only be used for a pressure range of $-0.098 \cdot \text{MPa} < \Delta P < 0$ MPa, which corresponds to a relative humidity of between 99.92% and 100%. To measure moisture fixation properties at lower humidity levels, corresponding to pore water pressures lower than –0.098 MPa, a pressure plate may be used. In such an apparatus, a positive gas pressure is applied to a wet specimen placed on a fine porous plate. When the water menisci in a material are exposed to a certain pressure difference, an equilibrium state is eventually reached. According to Equation 2.3, a specific pore radius corresponds to a certain suction level.

$$\Delta P = \frac{2 \cdot \sigma}{r} \tag{2.3}$$

where

ΔP is the capillary suction [Pa],

σ is the surface tension of water at 293ºK [0.074 N/m], and

r is the radius of a meniscus [m].

For pores of larger radius, the suction forces will be unable to resist the pressure difference and the pores will be drained, while pores of smaller radius retain greater suction and will remain water filled (the capillary principle is further described in Section 3.2). The pressure plate technique can also be used for determining pore size distribution, according to Fagerlund (1973) and Krus and Kieβl (1998).

2.4.2 Method

Retention curves have been measured for three different inorganic materials, namely lime–silica brick, lime–cement mortar B, and cement mortar. These materials were described in detail in Section 2.2, where the bulk density, compact density, and porosity were presented in Table 2.2. Since the results of the pressure plate and sorption balance tests were to be combined (see Section 2.4.3), it was of greatest importance that all materials be thoroughly cured and carbonized before testing. The curing and carbonizing of the different materials was described in Section 2.2.

The specimens as prepared for pressure plate testing were 50 × 50 × 4 mm, and each of the three materials was represented by eleven specimens. The length of the side of the specimen was chosen so that the area of the pressure plate membrane would be optimally used. Of course, a greater part of the membrane area could still have been covered even if smaller specimens had been pieced together. The risk of weight loss or gain caused by incidental desorption or absorption during specimen handling (while weighing and storing) would be greater with smaller specimens, since they have a larger area in relation to volume. There was also the risk that imperceptibly small pieces of aggregate could loosen and separate from the specimen during handling. The problems of both incidental desorption or absorption and the loosening of ballast

are almost unavoidable, but have only a marginal effect when larger specimens are used in testing.

The thickness of the specimen was chosen so that the smallest representative unit in the tested materials would be properly represented. For the mortars using the Baskarp aggregate in the 0–3-mm fraction, the smallest representative unit was 3 mm, while for the lime–silica brick using a limestone aggregate in the 0–4-mm fraction the smallest representative unit was 4 mm (see Section 2.2). Therefore, the smallest possible thickness was determined to be 4 mm. Of course, a greater thickness could have been used, but that would have prolonged the testing. Initial testing showed that the test duration for the cement-based materials was approximately four weeks at each pressure step.

Before the tests took place, all specimens were vacuum saturated using a procedure described by Fagerlund (1977). The moisture content at vacuum saturation was used as the starting moisture level, since the vacuum saturation point is a more rigid criterion than the capillary saturation point is. At the capillary saturation point the pore system of a given material still retains enclosed air voids. When a capillary-saturated specimen is put into contact with the wet membrane in the pressure plate cell, the material starts to absorb water until a sufficiently high pressure is reached. The phenomenon of a capillary-saturated specimen absorbing water from the membrane in a pressure plate extractor under low pressures was further discussed in Janz (2000). Guidance regarding the use of the pressure plate extractor was given by Christensen and Strømdahl (1996).

The vacuum saturation process, described in chronological order (Fagerlund, 1977), is as follows:

1. The dried specimens are evacuated in a vacuum chamber for 3 h under a residual pressure of 100 to 250 Pa.
2. Water of room temperature is let into the vacuum chamber while the pump is still running, so that the specimens are covered with water within 1 min. Tap water is used.
3. The pump is allowed to run for 1 h after the water has been let into the vacuum chamber.
4. Ordinary atmospheric pressure is let into the vacuum chamber.
5. The specimens can be rapidly moved from the vacuum chamber into another water-filled vessel, until the pore volume and/or volume is determined.

For the test, three different pressure plate extractors were used with maximum pressures of 0.5, 1.5, and 10 MPa, respectively. Before the test was performed, all specimens were vacuum saturated according to the schedule described above. When the test started, certain pressures (see Table 2.4) were chosen for the study; the corresponding relative humidity levels are also shown in the table. The pressure steps were set so that a relatively even distribution was reached in terms of change of moisture content, i.e. a relatively even resolution over the complete moisture range in terms of moisture content by mass. Since the estimated sorption isotherm displayed an increasing slope from the hygroscopic range up to complete saturation for the studied materials (see Figures 2.4 to 2.6), the pressure steps were chosen so as to be smaller as saturation was being approached.

Table 2.4 Target pressure levels for retention measurements performed, the corresponding relative humidity levels given by Equation 2.2, and the radii of menisci according to Equation 2.3.

Pressure [MPa]	Relative humidity [%]	Radii of menisci [μm]
0.004	99.997	37
0.008	99.994	18.5
0.02	99.985	7.4
0.1	99.926	1.48
0.3	99.779	0.493
1	99.264	0.148
3	97.807	0.049
6.5	95.310	0.023
10	92.876	0.015

The schematic design of the two pressure plate extractors for pressures up to 0.5 and 1.5 MPa, respectively, is depicted in Figure 2.7. A room equipped with a climate control unit was used for the tests, and the room temperature was logged for the complete duration of the testing. Measurements showed that the temperature in the testing room was 20ºC ± 1ºC. An electric heater was used to keep the room temperature stable in the winter, since the climate control unit was not equipped with a heating element. The climate control unit broke down for three weeks in the summer while measurements were being made, and room temperature in the laboratory reached approximately 27ºC for two days. The results were checked according to deviation from estimated moisture contents (moisture contents could be estimated by comparison with the moisture contents for the nearby pressure steps determined at 20ºC ± 1ºC). No deviation could be found between the moisture contents determined at 27ºC and the expected moisture contents.

To ensure hydraulic contact between the ceramic plate and the specimen, a thin layer of kaolin clay was applied to the ceramic plate, as specified in the Nordtest standard (1997). Before the kaolin clay was applied, it was diluted with water to give a low enough viscosity that the kaolin could easily be applied to the ceramic plate. After an approximately 2-mm-thick layer of kaolin was applied, a nylon cloth was applied above the kaolin to prevent the specimen from being contaminated by direct contact with the clay. Keeping the specimens clean was of the greatest importance, since the specimens were to be weighed when equilibrium was achieved at each pressure step.

The need for a layer of kaolin clay to serve as an intermediary between the specimen and the ceramic plate was investigated by Janz (1997). In tests of brick, the bed of kaolin was replaced with a micro-fibre cloth comprising 85% polyester and 15% polyamide, or the specimen was placed directly on the ceramic plate with no intermediate layer. Results of the three different setups showed that, regardless as to whether no bed, a kaolin clay bed, or a micro-fibre cloth was

used, the water retention curve was not changed. However, the time required to reach equilibrium with the different bedding materials was not considered by Janz (1997), as the test started with the vacuum-saturated specimen being placed on the porous ceramic plate. To ensure that the equilibrium state was reached within a reasonable amount of time, kaolin clay was used as an intermediate layer in the present research.

Before the next higher pressure was applied, the specimens were removed from the extractor for weighing. The kaolin was cleaned off the ceramic plate and the plate was vacuum saturated (see above description) before being coated anew with kaolin and then covered with the textile cloth. After this, the eleven specimens were placed on the textile cloth, the lid of the extractor was fastened into place, and the outflow tube connected to a pipette – an arrangement that allowed the extracted water to be measured. To prevent evaporation through the opening of the pipette, the opening was blocked with a stopper that contained a hole for the outlet tube. When water entered the pipette, excess air was allowed to escape through a narrow notch in the stopper. Since the notch was only approximately 0.10 mm wide, no significant evaporation could occur.

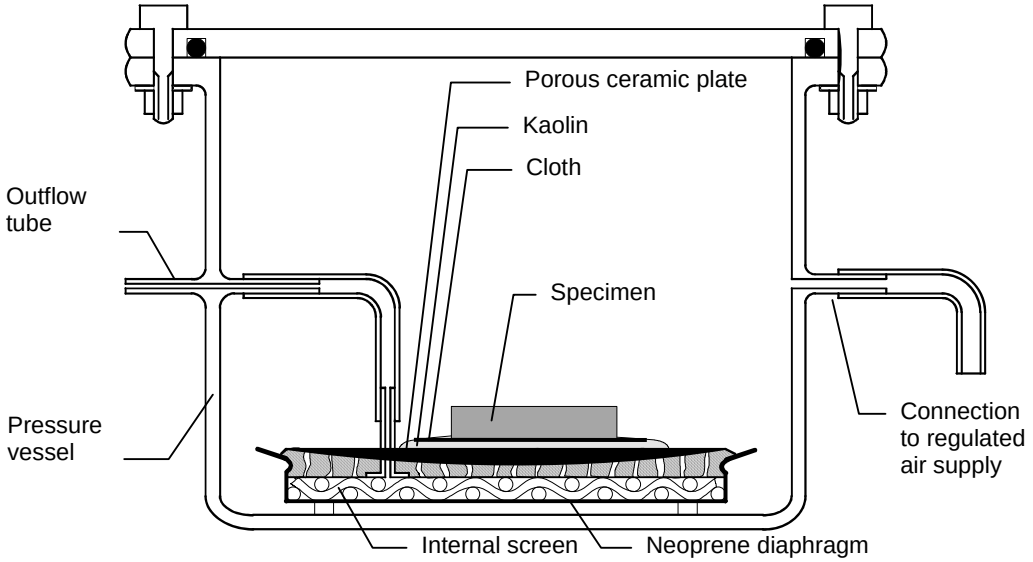

Figure 2.7 Schematic sketch of the pressure plate extractors for pressures up to 0.5 and 1.5 MPa (Janz, 1997).

The inlet tube depicted on the right in Figure 2.7 was then connected to a cylinder of nitrogen gas. To enable fine adjustment of the pressure in the extractor, a pressure regulator was connected between the gas cylinder and the extractor, providing a control precision of $1 \cdot 10^{-4}$ MPa for the 0.5- and 1.5-MPa extractors. Nitrogen was used instead of air to prevent further carbonization during the test. This was probably an unnecessary precaution, since each material had been completely carbonized before testing began (see Section 2.2).

When a certain pressure was applied to the pressure plate extractor, the water from both the specimen and the kaolin clay was extracted through the outflow tube and into the pipette. As the pores of the ceramic plate were considerably smaller than those of the tested materials, the

pressures used were not sufficient to empty the pores in the ceramic plate. By means of the small pores in the ceramic plate, it was possible to have atmospheric pressure on the underside of the plate and excess pressure on the upper side. Since the ceramic plate was still water saturated despite the excess pressure, excess pressure was applied as a pressure difference over all the water menisci in the water-filled pores of the specimen. The amount of extracted water was continuously measured and the equilibrium state was defined when there was no increase in the water level in the pipette for 48 h; at that point all specimens were assumed to be in equilibrium with the excess pressure. When equilibrium was reached, the excess pressure in the pressure plate extractor was equal to the suction in the still water-filled pores of the specimen. Since there is a relationship between the suction and the relative humidity in the specimen (see Equation 2.2), a point on both the retention curve and the sorption isotherm could be determined. To determine the moisture content after equilibrium at a specific pressure level, the pressure plate extractor was opened and the specimen was brought out for weighing. A high-precision balance having a precision of thousandths of a gram was used; the balance was calibrated before and after the weighing of each series.

To minimize evaporation from the specimens when opening the extractor, the specimens were immediately removed from the extractor after the lid was lifted off and put in plastic containers. Two containers were used for the eleven specimens. Since the different steps were relatively close together in pressure, there was a significant risk that evaporation during careless handling could result in considerable loss of moisture. A great enough loss in moisture could result in the occurrence of absorption instead of desorption in the next pressure step. Therefore, a piece of wet cloth was placed inside both of the plastic containers used for storing the specimens, to keep the humidity close to the saturation point. The specimens were removed one at a time from the containers for weighing, and then replaced in the containers. Since the room was equipped with a climate control unit, resulting in considerable air movement and dehumidification, increased evaporation could easily have resulted from careless specimen handling. The balance was placed in a Plexiglas box, partly to prevent evaporation from the specimens during weighing and partly to prevent air currents from disturbing the balance. As an extra precaution, the climate control unit was switched off during specimen handling. After weighing the specimens, the vacuum-saturated ceramic plate was again prepared with kaolin clay and cloth coverings. Then the specimens were removed from the plastic containers and replaced in the extractor. The next higher pressure step was then applied until equilibrium was reached. After equilibrium was reached at the new pressure step, the weighing procedure was repeated. During the measurements, the 0.5-MPa extractor was used for pressure steps from 0.004 MPa to 0.3 MPa, while the 1.5 MPa extractor was used for the 1-MPa pressure step. The various pressure steps are shown in Table 2.4.

For pressure steps from 3 MPa to 10 MPa, a pressure plate extractor allowing pressures up to 10 MPa was used. The 10-MPa pressure plate extractor operated on the same principle as did the extractors with maximum pressures of 0.5 and 1.5 MPa. Instead of a ceramic plate, however, the extractor used a cellulose membrane with considerably smaller pores than those of the ceramic plate. The extractor consisted of metal top and bottom discs linked by a mantle. Around the outside of the mantle, along the edges of the top and bottom discs, sturdy bolts were mounted linking the top and bottom discs. A 6-mm-thick plate of Plexiglas was placed on the bottom

metal disc to provide a smoother bed for the samples. To provide a layer allowing water transport to the cellulose membrane, a thin disc-shaped metal grid was placed on the top of the Plexiglas plate. The metal grid had a smaller diameter than the mantle did, and was sealed around its circumference to the Plexiglas plate. A disc-shaped cellulose membrane was then placed on top of the metal grid. Since the cellulose membrane had a greater diameter than the mantle did, the membrane was squeezed between the mantle and the Plexiglas plate. To ensure a good seal between the membrane and the mantle, a rubber gasket was placed in a slit in the mantle.

After the mantle was mounted, the specimen could be placed on the cellulose membrane. Since a soft cellulose membrane was used instead of the ceramic plate, the kaolin clay was not needed to ensure hydraulic contact between the specimen and the membrane. After the specimen was put in place, the upper metal top was put on and sealed with a rubber gasket placed in a small slit in the mantle. Finally, the bolts were tightened systematically and by a certain torque given by the manufacturer of the pressure plate cell.

For the tests, the pressure plate extractor was connected to a cylinder containing nitrogen gas, as was the case with the two lower-pressure extractors. A pressure regulator was installed between the gas cylinder and the extractor (see Figure 2.8), providing a control precision of 0.01 MPa. By means of the excess pressure, moisture was extracted from the specimens. The moisture was removed from the extractor through a tube, connected to a collar in the Plexiglas plate, which exited the extractor through a narrow hole in the bottom metal disc. As with the setup for the 0.5- and 1.5-MPa pressure extractors, the outlet tube led into a pipette, which was provided with a stopper to prevent evaporation during the measurement process. To let the remaining air out, the cork was provided with a narrow notch.

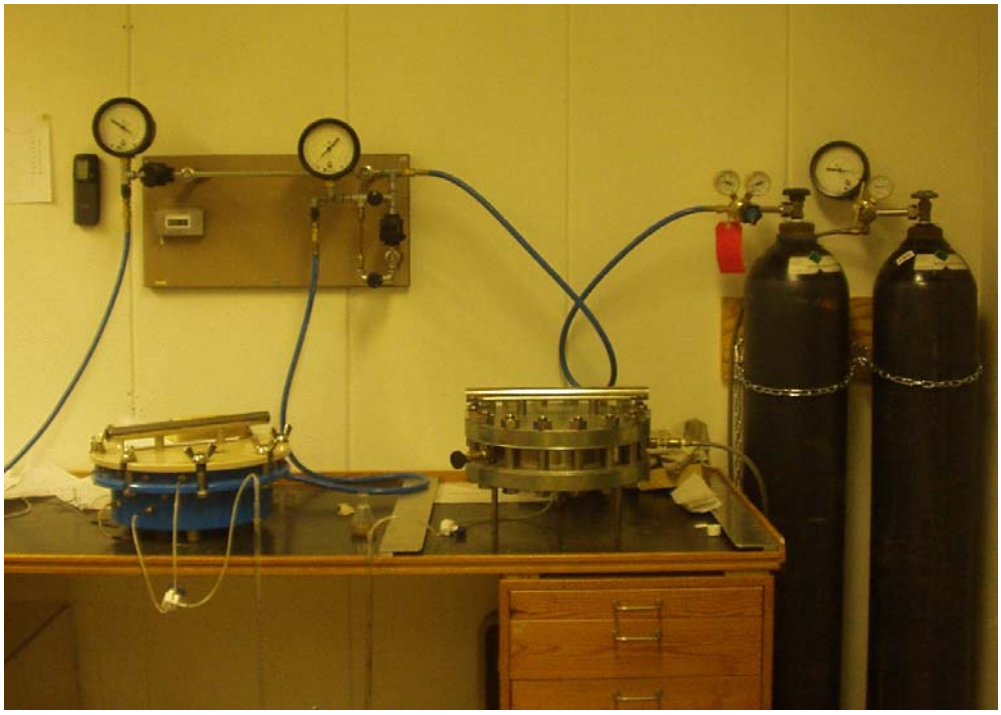

Figure 2.8 Two different pressure plate extractors operating at maximum pressures of 1.5 MPa and 10 MPa, connected to gas cylinders.

With the 10-MPa extractor, the equilibrium state was defined as it was for the two lower-pressure extractors. At each pressure step, the level in the pipette was observed until it showed a constant value for at least 48 h. After equilibrium was reached, the excess pressure was let out of the extractor via a valve. Different rates of pressure decrease were tested, and the highest possible rate was found to be approximately 3 min per 1 MPa. If a higher rate was used, there was a significant risk that air currents inside the extractor might move the specimens; however, a considerably lower rate of pressure decrease might result in moisture absorption from the cellulose membrane. This posited risk of absorption during the pressure decrease phase was not, however, verified experimentally.

During the pressure plate tests we also attempted to determine absorption isotherms, despite the fact that the equipment was designed for desorption tests. The material used for the initial absorption test was the lime–silica brick. Before the test took place, the lime–silica brick was dried until equilibrium was reached at 40°C. Since a high suction corresponds to a low relative humidity (see Equation 2.2), the tests had to be started using the 10-MPa extractor; for higher relative humidity levels, the 1.5- and 0.5-MPa pressure plate extractors could be used.

The 10-MPa pressure plate extractor had to be modified, as the outflow tube passing through the lower metal disc was not completely sealed to the plastic collar in the Plexiglas bed. In the desorption tests, the seal between the collar and the plastic tube was able to contain the water, as the tube simply led downwards to the collecting pipette. In the absorption tests, the outflow pipe was instead used as an inflow pipe, and was connected to a pipette at the surface of the water just

above the membrane in the extractor; thus, the underside of the membrane was supplied with water at atmospheric pressure.

Before the specimens were placed on the membrane, a continuous water phase was created from the pipette to the underside of the cellulose membrane. The specimens were then placed on the membrane; the upper metal disc of the pressure plate extractor was put in place and the bolts were tightened as quickly as possible. The initial absorption test was started at the highest pressure of 10 MPa. Shortly after the pressure was applied, air bubbles began to be transported from the pressure plate extractor through the pipe and into the pipette. The rate of such bubbling remained relatively continuous over time, showing no decrease for several weeks. The disturbance caused by the bubbling made the water level in the pipette hard to read and equilibrium hard to determine with any certainty; even so, a certain degree of water consumption was registered and equilibrium could be suspected. After an equilibrium state was estimated to have been reached, the specimens were removed from the extractor and weighed. The specimens displayed moisture contents reasonable for an absorption isotherm, in comparison with the moisture contents of the already determined desorption isotherm. The measuring procedure was repeated using a new cellulose membrane, but the air bubbles still appeared; even at lower pressures the air bubble problem persisted. All absorption tests were performed using the 10-MPa pressure plate extractor.

2.4.3 Results

The results of the pressure plate tests are presented as water retention curves for the three tested materials: for lime–silica brick in Figure 2.10, lime–cement mortar in Figure 2.13, and cement mortar in Figure 2.16. These figures also present the results of the sorption balance tests described in Section 2.3, which show moisture content by mass at specific relative humidity steps above 50%. Relative humidity levels below 50% were excluded, since the tested materials showed insignificant moisture capacity in this range. Before the results of the sorption balance tests were included in the figures, the relative humidity levels were transformed into suction using Equation 2.2.

As well as the three materials presented in Table 2.2, retention curves were also determined for lime–cement mortar A (see Table 2.1). However, its retention curves could not be completed since the specimens exploded when the excess pressure from the 10 MPa level was being released. The damage to the specimens is visible in Figure 2.9 as pop-out craters. Since the specimens occupied the exact same position on the cellulose membrane both before and after the 10-MPa pressure step was performed, other causes of the damage could be excluded. The selection of the specific pressure steps used in determining the retention curves was discussed in Section 2.4.2 and presented in Table 2.4.

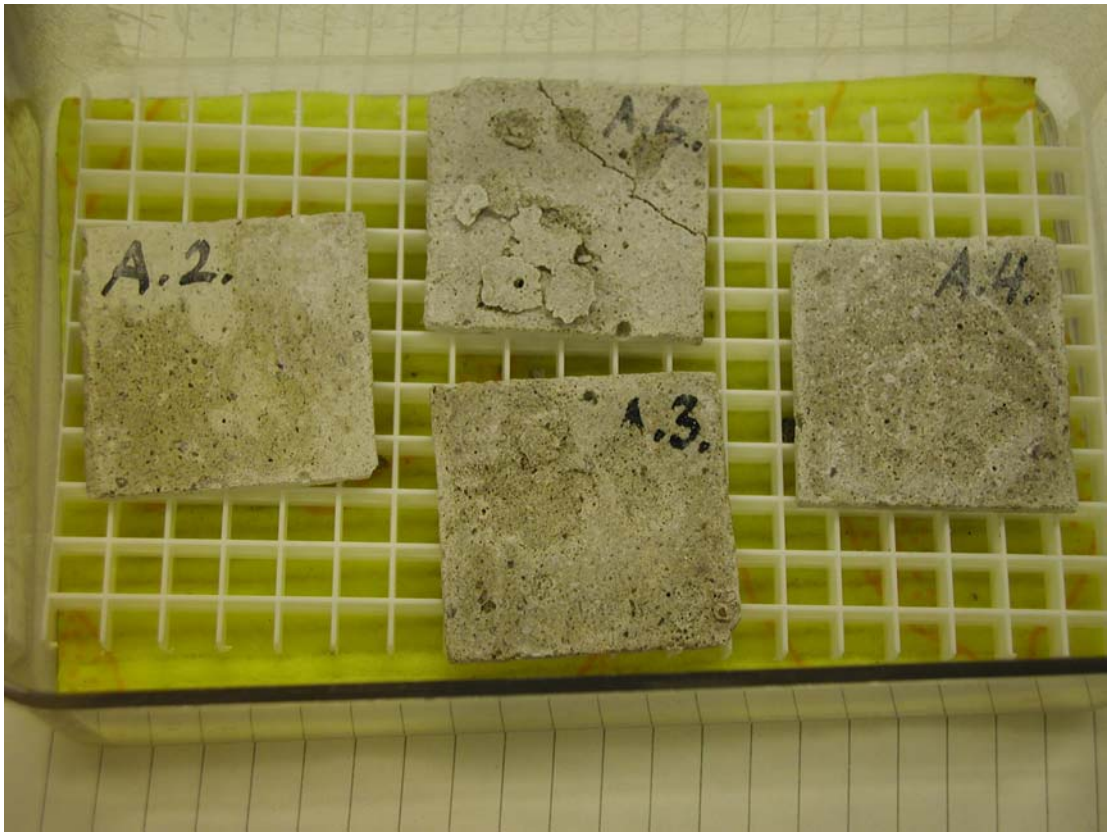

Figure 2.9 Damaged specimens of lime–cement mortar A after measurement in the pressure plate extractor.

The results of the pressure plate tests for the three tested materials are also presented as the degree of vacuum saturation by different suction levels, in Figures 2.11, 2.14, and 2.17. These figures also present the results of the sorption balance tests described in Section 2.3. To illustrate the high resolution provided by the pressure plate technique above the hygroscopic range, the retention curves were also transformed into conventional sorption isotherms. The transformed retention curves are shown in Figures 2.12, 2.15, and 2.18 for the three materials.

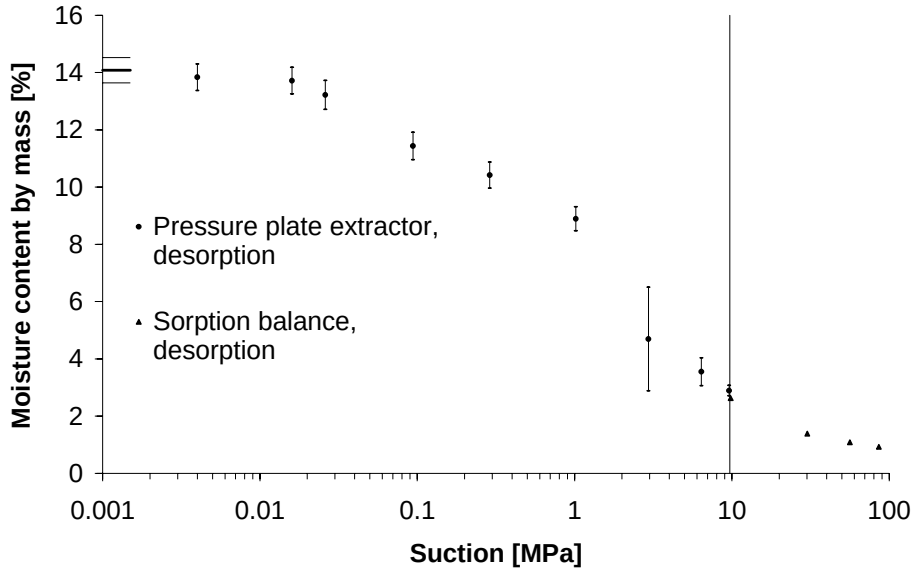

Figure 2.10 Retention measurements performed using the pressure plate extractor on individual specimens of lime–silica brick. The moisture content by mass is presented as mean values, with the scatter expressed as one standard deviation. The horizontal lines represent vacuum saturation. Results of desorption measurements made using the sorption balance method, originally discussed in Section 2.3.3, are shown as mean values without scatter, to the right of the vertical line.

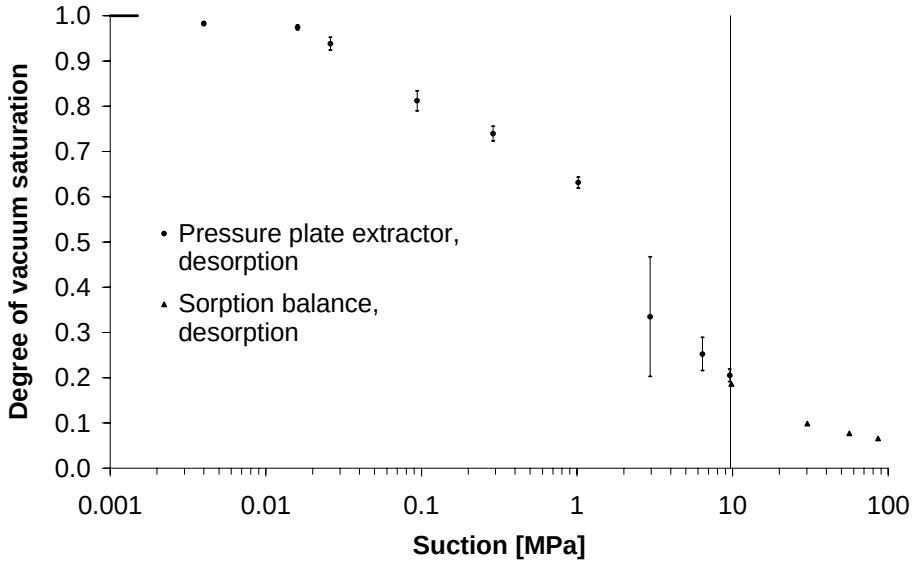

Figure 2.11 Retention measurements performed using the pressure plate extractor on individual specimens of lime–silica brick. The degree of vacuum saturation is presented as mean values, with the scatter expressed as one standard deviation. The horizontal lines represent vacuum saturation. Results of desorption measurements made using the sorption balance method, originally discussed in Section 2.3.3, are shown as mean values without scatter, to the right of the vertical line.

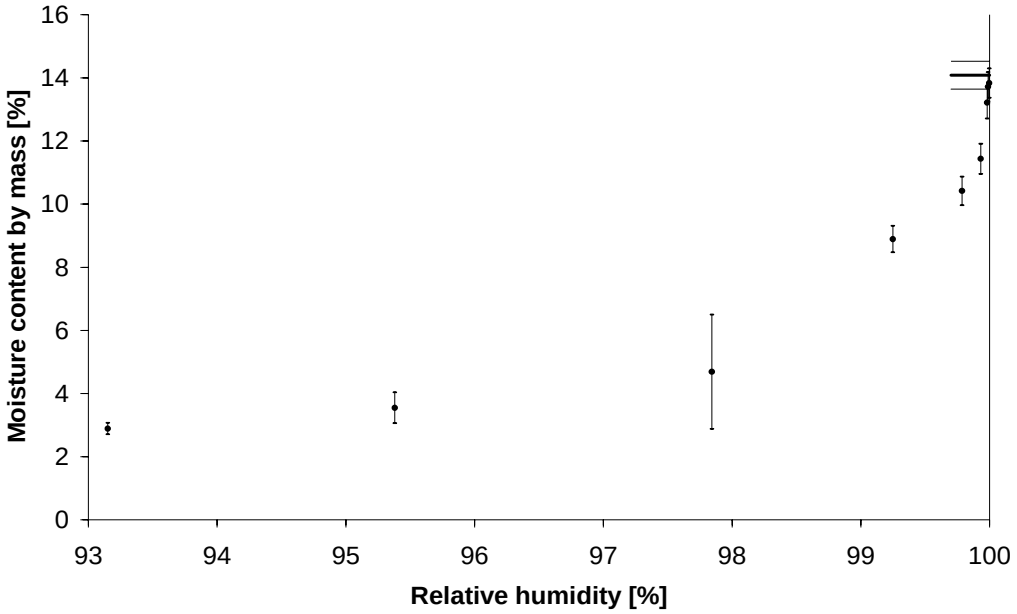

Figure 2.12 Retention measurements shown as the upper part of the sorption isotherm, performed on individual specimens of lime–silica brick. The moisture content by mass is presented as mean values, with the scatter expressed as one standard deviation. The horizontal lines represent vacuum saturation.

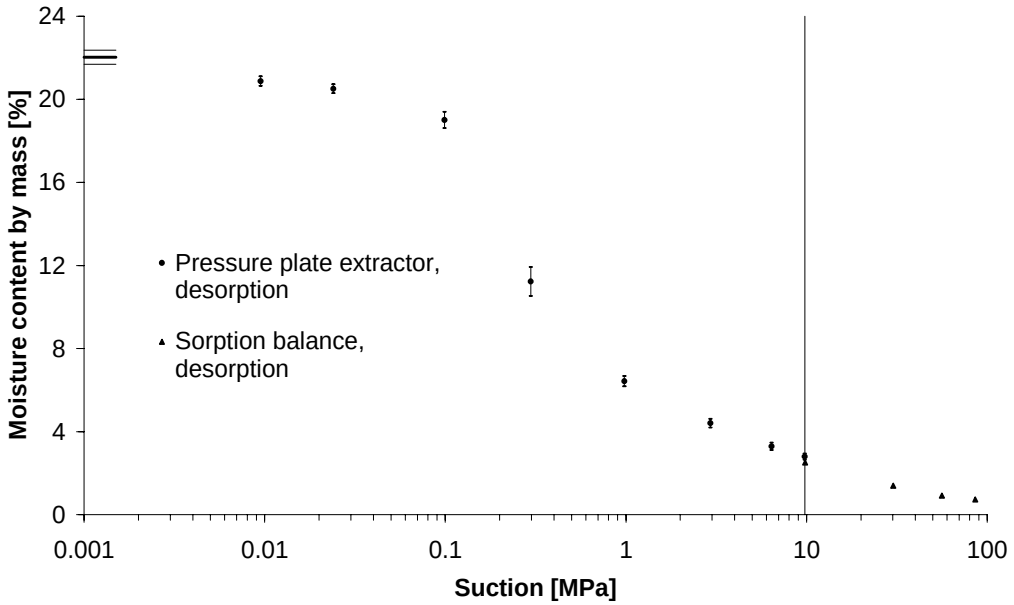

Figure 2.13 Retention measurements performed using the pressure plate extractor on individual specimens of lime–cement mortar. The moisture content by mass is presented as mean values, with the scatter expressed as one standard deviation. The horizontal lines represent vacuum saturation. Results of desorption measurements made using the sorption balance method, originally discussed in Section 2.3.3, are shown as mean values without scatter, to the right of the vertical line.

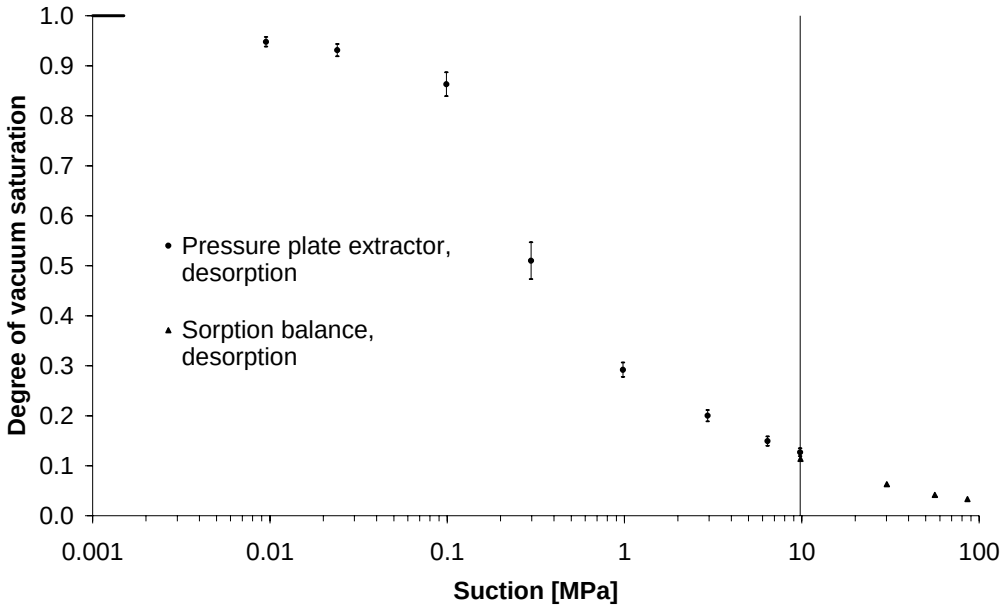

Figure 2.14 Retention measurements performed using the pressure plate extractor on individual specimens of lime–cement mortar. The degree of vacuum saturation is presented as mean values, with the scatter expressed as one standard deviation. The horizontal lines represent vacuum saturation. Results of desorption measurements made using the sorption balance method, originally discussed in Section 2.3.3, are shown as mean values without scatter, to the right of the vertical line.

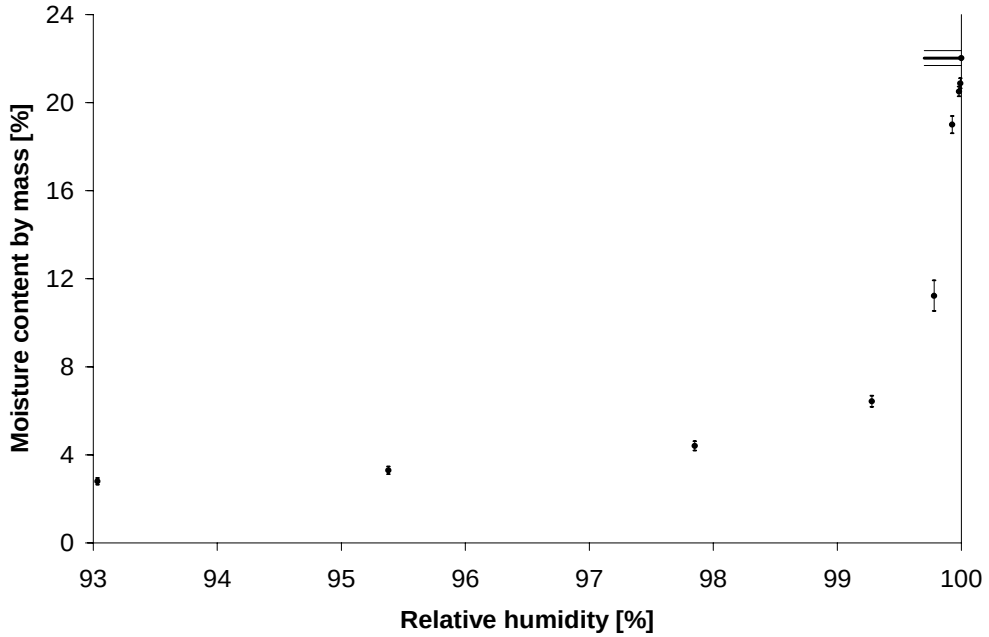

Figure 2.15 Retention measurements, shown as the upper part of the sorption isotherm, performed on individual specimens of lime–cement mortar. The moisture content by mass is presented as mean values, with the scatter expressed as one standard deviation. The horizontal lines represent vacuum saturation.

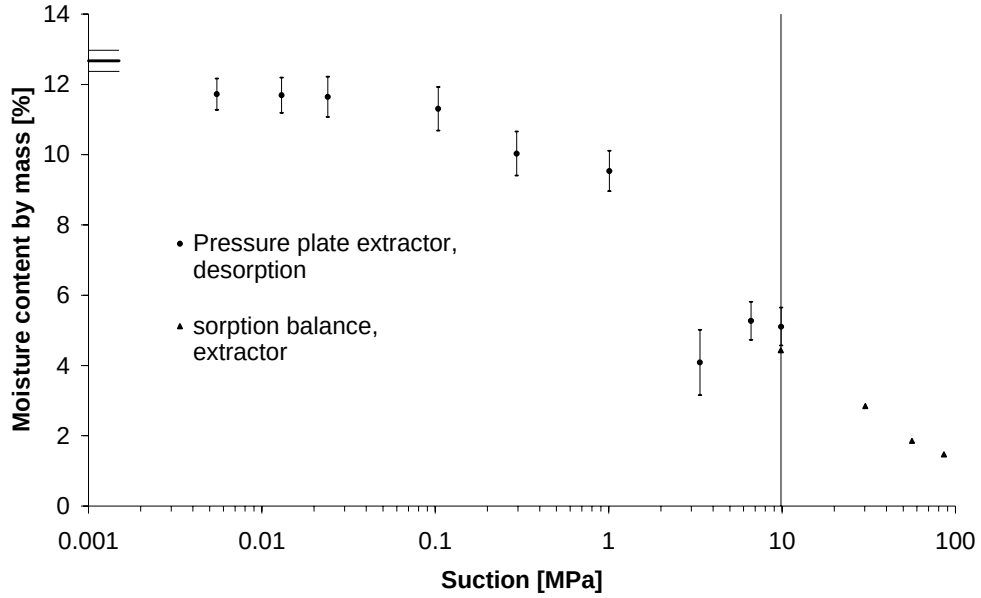

Figure 2.16 Retention measurements performed using the pressure plate extractor on individual specimens of cement mortar. The moisture content by mass is presented as mean values, with the scatter expressed as one standard deviation. The horizontal lines represent vacuum saturation. Results of desorption measurements made using the sorption balance method, originally discussed in Section 2.3.3, are shown as mean values without scatter, to the right of the vertical line.

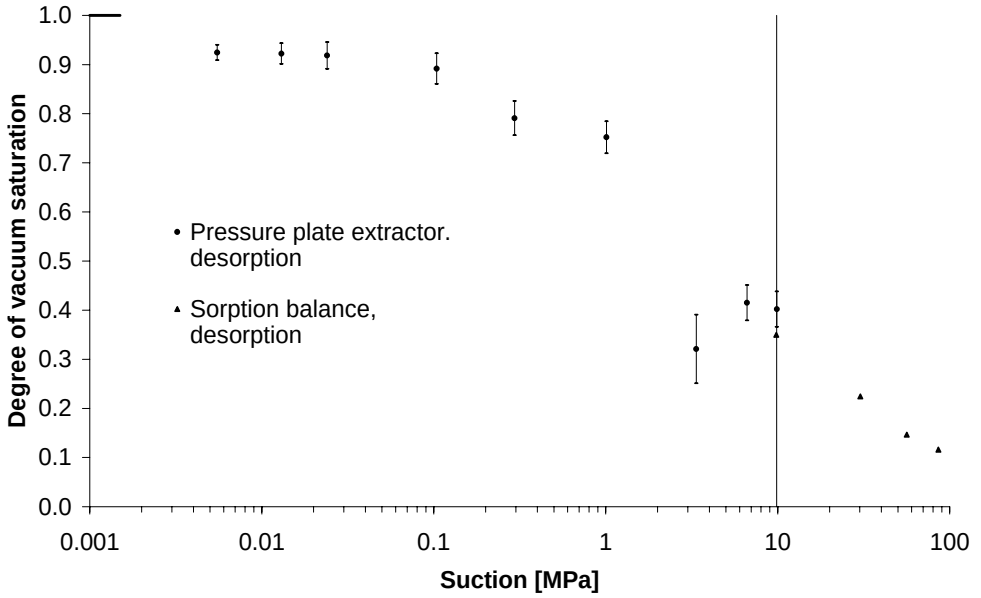

Figure 2.17 Retention measurements performed using the pressure plate extractor on individual specimens of cement mortar. The degree of vacuum saturation is presented as mean values, with the scatter expressed as one standard deviation. The horizontal lines represent vacuum saturation. Results of desorption measurements made using the sorption balance method, originally discussed in Section 2.3.3, are shown as mean values without scatter, to the right of the vertical line.

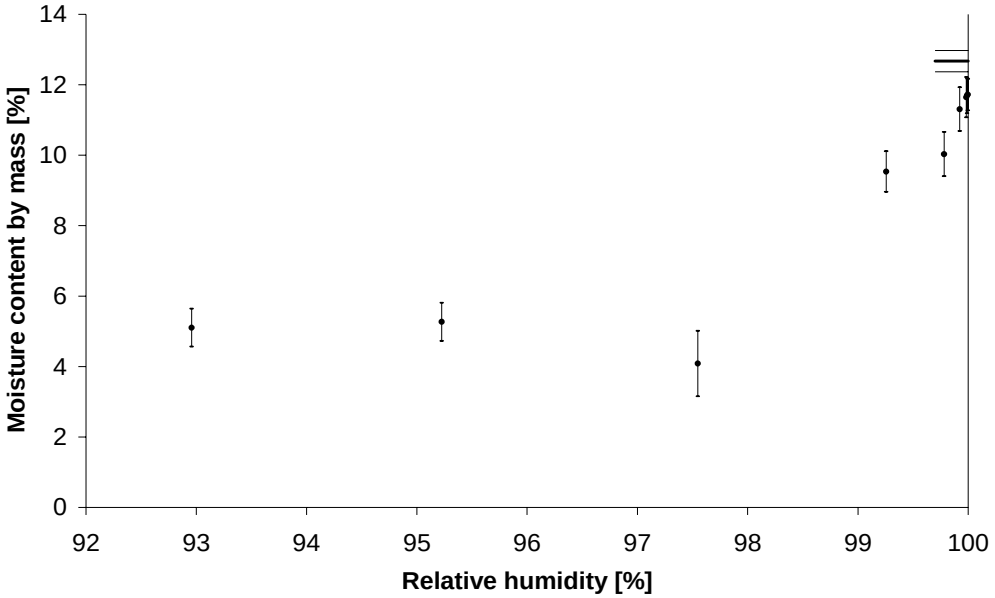

Figure 2.18 Retention measurements, shown as the upper part of the sorption isotherm, performed on individual specimens of cement mortar. The moisture content by mass is presented as mean values, with the scatter expressed as one standard deviation. The horizontal lines represent vacuum saturation.

2.4.4 Discussion

For the testing, nine different pressure steps were chosen according to Table 2.4, so as to cover various representative points on the suction curve. Before the pressure plate experiments were performed, we examined the literature to find desorption isotherms for materials with a pore size distribution relatively close to that of the three studied materials. Since both the moisture content by mass for the highest relative humidity step in the hygroscopic range, and the moisture content at vacuum saturation were known experimentally from the present research, an approximate desorption isotherm could be estimated. The estimated desorption isotherm showed an increasing slope in the moisture range close to vacuum saturation, compared to the slope in the lower moisture range near the hygroscopic range. Since a relatively fine resolution in terms of moisture content by mass was required for the desorption isotherm, the pressure and relative humidity steps had to be chosen so as to be relatively close together in the high moisture range (see Table 2.4). The results presented in Section 2.4.3 for the three tested materials indicate that the selected pressure steps generally provided sufficient resolution. To achieve better resolution, the pressure steps would have had to be even closer together in the mid relative humidity range, corresponding to relative humidity levels from 96% to 99%.

The considerable difference in the durations of the pressure plate versus the sorption balance tests required materials that did not change in terms of structure or pore size distribution during the course of testing. Since cement- and lime-based materials were studied, both hydration and carbonation had to be considered. The curing of the mortars was carefully considered, and was described in Section 2.2. After the curing process, the cement-based materials were put into a carbonation chamber for approximately two years. Before the cement-based mortars were used

for the tests, they were checked for complete carbonation. According to the comparison of the results of the pressure plate versus the sorption balance testing presented in Section 2.4.3, there was excellent agreement. Carefully ensuring the thoroughness of carbonation was most likely a major reason why the results of the two measuring methods were in good agreement, despite their different measurement durations.

The results of the pressure plate tests generally showed moderate deviation in terms of moisture content by mass (see Figures 2.10, 2.13, and 2.16 for the respective materials). To determine whether the deviation was caused by the measuring method or by a possible variation in the porosity of the different specimens, the degree of vacuum saturation, rather than moisture content, is shown in Figures 2.11, 2.14, and 2.17 for the different materials. Since the relative deviation was smaller for the degree of vacuum saturation than for the moisture content of mass at several pressure levels, the difference in deviation was most likely due to variation in porosity between individual specimens.

Considerable scatter was noted for lime–silica brick at a pressure of 3 MPa, in terms of both the moisture content by mass and degree of saturation. The considerable spread in the degree of saturation was not a result of variation between specimens, but of the measuring method. When studying the notes from the laboratory work, we noted that the gas cylinder had to be replaced during the testing process at the 3-MPa level, because the gas had run out. When replacing the gas cylinder, the excess pressure had to be let out of the pressure plate extractor, since the pressure regulator did not have a reverse valve. Because the pressure plate extractor was not subject to excess pressure when the gas cylinder was being changed, absorption from the wet cellulose membrane most likely took place.

The results for cement mortar revealed an unexpectedly low moisture content by mass and degree of vacuum saturation at the pressure of 3 MPa. Also, the deviation was considerably higher at this pressure step than at other pressure steps for the same material. In the lab notes we noted that the pressure level in the gas cylinder was significantly low at the end of this pressure step, but since the equilibrium state had been reached, the gas cylinder was not changed. However, it was noticed during the experimental work that the outflow pressure provided by the pressure regulator could increase of its own accord when the pressure level in the gas cylinder approached the outflow pressure from the pressure regulator. A temporary increase in the outflow pressure caused by the gas regulator was most likely the cause of the deviation in results at the 3-MPa pressure step; the increased pressure could have caused the moisture content by mass and degree of saturation at the 6.5-MPa pressure step to be determined by absorption instead of desorption.

Initial absorption tests were also carried out using the pressure plate technique. For these tests, the 10-MPa pressure plate extractor was used, since the highest pressure corresponded to the lowest relative humidity. The test results just barely allowed the equilibrium state to be estimated, because of the interference caused by a continuous flow of air bubbles through the water supply pipe and the appurtenant pipette. Several factors could have caused the air bubbles. Possibly, the air pressure gradient over the cellulose membrane was sufficient to cause the diffusion of air through the water-filled pores in the membrane. As well, the pressure decrease of the water transported across the membrane might have caused an increase in the volume of the

dissolved air, even a very small defect in the cellulose membrane could have caused an air stream, due to the extremely high pressures used.

2.5 CONCLUSIONS

Results determined for the three tested materials using the sorption balance and pressure plate methods are compared in Figures 2.19, 2.20, and 2.21, in terms of the material properties set forth in Table 2.2. The results obtained using the different methods are in significant agreement, despite the fact that different specimens were used for the two methods. There was also a considerable difference in the time required for the two measurement methods: the sorption balance method required approximately one week per material, while the pressure plate method required approximately six months per material. The agreement between the results of the different measuring methods most likely stemmed from the fact that the specimens were well cured and thoroughly carbonated before testing took place. In cases in which cement-based materials are allowed to carbonize during testing and when different measurement methods with different time requirements are used, it can be hard to obtain agreement in the results. Good agreement between the results of the two measuring methods used here was also found by Janz (2000) and Johannesson and Janz (2002), while good agreement between the results of the pressure plate technique and pore size measurements using mercury was found by Krus and Kieβl (1991).

At a relative humidity of 93% the moisture content by mass for lime–silica brick and lime–cement mortar was approximately 2.5%, but the cement mortar showed a moisture content by mass of approximately 5%. The higher moisture content at this specific relative humidity confirms that cement-based mortar has a larger share of small pores than either the lime–silica brick or the lime–cement mortar does.

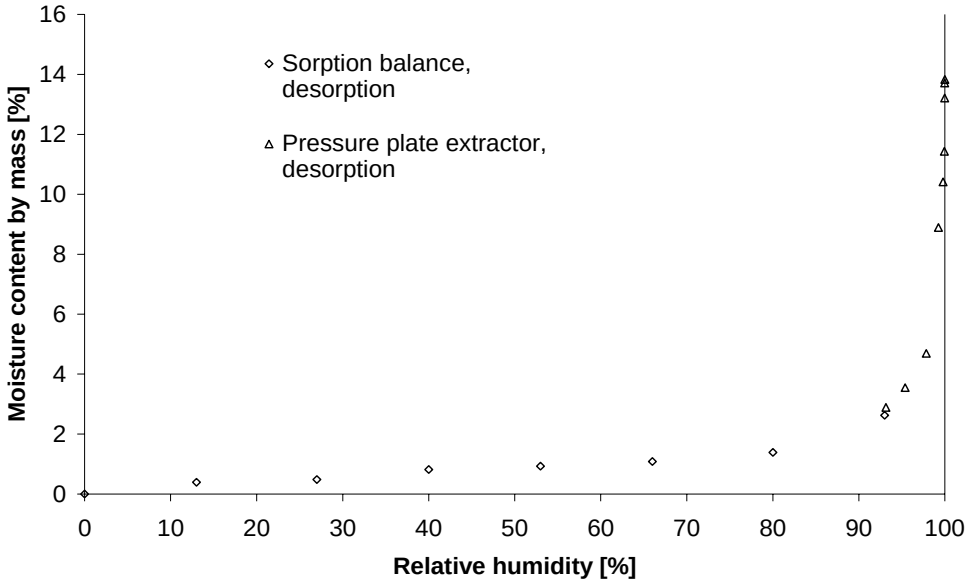

Figure 2.19 Sorption isotherms for lime–silica brick measured using the sorption balance and pressure plate extractor methods. Moisture content by mass is presented as mean values.

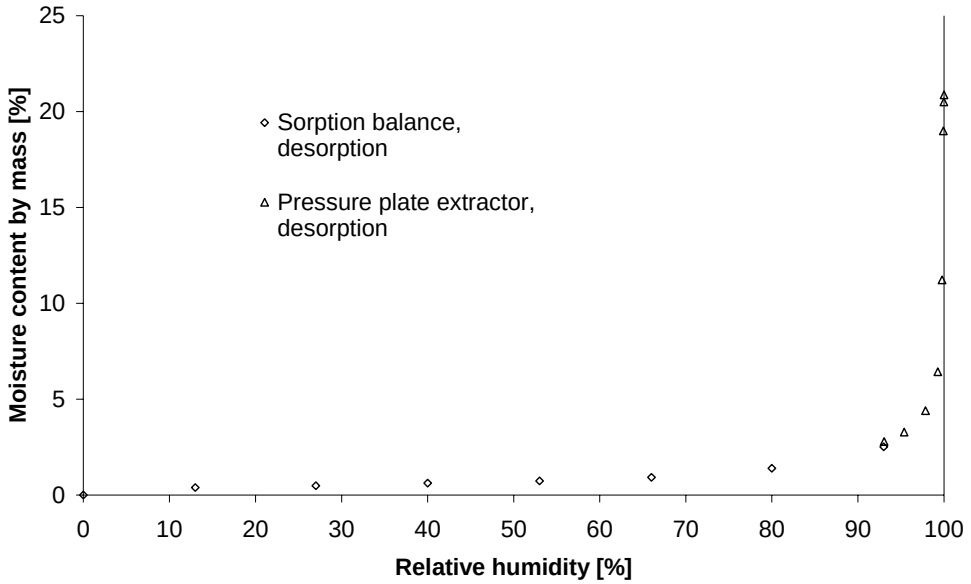

Figure 2.20 Sorption isotherms for lime–cement mortar measured using the sorption balance and pressure plate extractor methods. Moisture content by mass is presented as mean values.

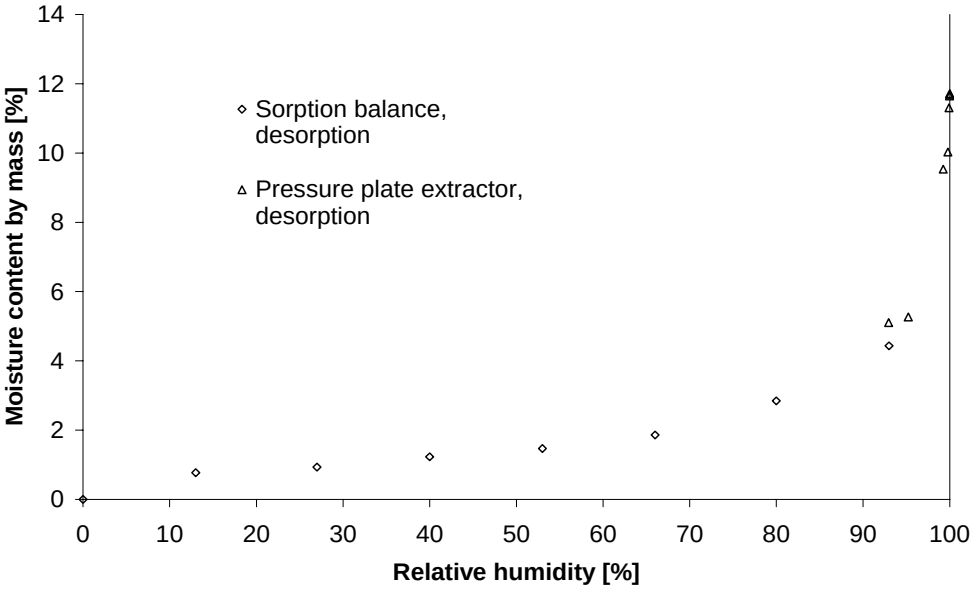

Figure 2.21 Sorption isotherms for cement mortar measured using the sorption balance and pressure plate extractor methods. Moisture content by mass is presented as mean values.

3 MOISTURE TRANSPORT PROPERTIES MEASURED OVER THE COMPLETE MOISTURE RANGE

3.1 INTRODUCTION

Moisture transport properties can be determined using several common methods. For example, moisture diffusivity can be evaluated directly from transient moisture profiles (see e.g. Kieβel and Krus, 1991), or capillary water uptake tests can be performed on individual specimens conditioned to different moisture levels (see Janz, 1997, 2000). Before capillary tests are performed the moisture content in the specimen must be evenly distributed throughout the volume of the specimen. Then capillary water uptake tests can be performed on specimens with various initial moisture contents, and the relationship between the sorption coefficient and the initial moisture content can be determined. Using this relationship, moisture diffusivity values can be determined as a function of the initial moisture content of the specimen. Since the moisture transport properties can be evaluated without reference to transient moisture profiles, the method is eminently suitable for evaluating different models for calculating moisture profiles. This stands in marked contrast to reports in the literature, which often describe how moisture transport properties are evaluated from transient moisture profiles, and how the specific moisture transport data is then used in determining the corresponding moisture profiles.

3.2 METHOD FOR EVALUATING TRANSPORT DATA

When water absorption tests are performed in the capillary range, i.e. when a free surface of water is put into contact with the specimen, the water uptake process occurs in two phases (see Figure 3.1). The capillary phase can be approximately described by a straight line representing the amount of absorbed water as a function of the square root of time. The water sorption coefficient, A [kg/(m^2·s^{½})], is represented by the slope of the line, a steep slope giving a higher sorption coefficient value (see Equation 3.1 for a definition of the sorption coefficient). A high sorption coefficient value does not necessarily imply a rapid water intrusion front. In comparing different materials, a material with a relatively slow water intrusion front can have a large water absorption coefficient value if the material has relatively high capillary porosity. On the other hand, a material that shows a rapid water intrusion front does not necessarily have a high absorption coefficient if the capillary porosity is small.

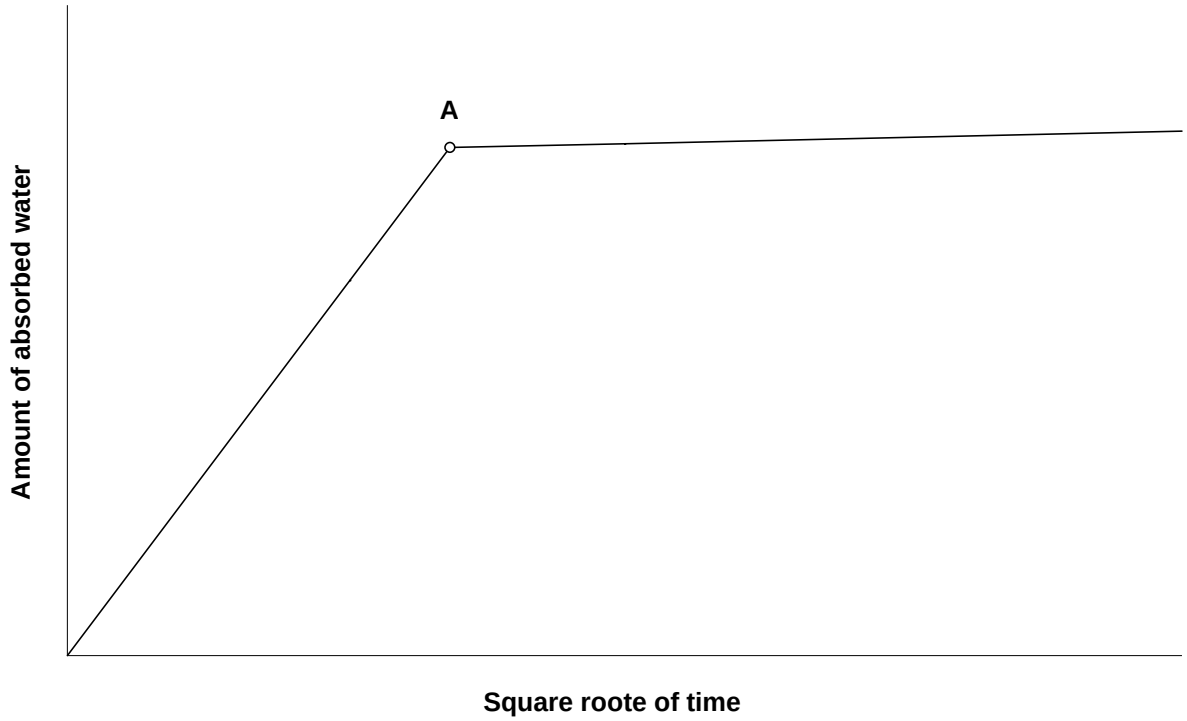

Figure 3.1 Representation of an ideal capillary water uptake process, showing the amount of absorbed water as a function of the square root of time.

The over capillary water uptake phase occurs in the moisture range above the capillary break point, indicated by A in Figure 3.1. The sorption rate in the over capillary phase, above the capillary break point, is considerably lower than that occurring in the capillary phase. When the capillary break point is reached, there is always a certain amount of enclosed air in the pore system. When a material has reached point A in Figure 3.1 and still has free access to a water surface, the enclosed air bubbles will slowly be dissolved in the already water-filled capillary pore system. The dissolved air escapes by diffusing slowly through this system (Ahlgren et al., 1976); thus, the slope of the line above the capillary break point is considerably smaller than it is in the capillary phase below the break point.

To calculate moisture transport at high moisture levels, the moisture diffusivity at these levels must be known. There are several methods for determining these diffusivities. The experimental data that are normally used can either be evaluated with reference to transient moisture profiles or the results of water uptake tests. However, the evaluation using moisture profiles is experimentally complicated, since such profiles are difficult to measure with a high degree of precision (see Chapter 4). A capillary water uptake test is simpler to perform, since only a high-precision balance is needed.

The sorption coefficient, A [kg/(m^2·s^{½})], is shown in Equation 3.1 as a function of the amount of absorbed water per square meter, ΔW [kg/m^2], by a specimen exposed to a free surface of water after a certain time, t [s].

$$A = \frac{\Delta W}{\sqrt{t}} \tag{3.1}$$

Normally, when absorption tests are evaluated, the amount of absorbed water per square meter, ΔW [kg/m^2], is considered as a function of the square root of time. Since the water absorption is like a moving boundary, with a higher moisture content per volume unit after the boundary, it is more relevant to study the amount of water per square meter, W [kg/m^2], than the change in moisture content per cubic meter, w [kg/m^3].

The effect of the initial amount of water per square meter, W_{start} [kg/m^2], on the sorption coefficient, A [kg/(m^2·s^{½})], can be determined using absorption tests with different start levels. After rewriting Equation 3.1, the sorption coefficient, A [kg/(m^2·s^{½})], applicable to a particular starting moisture level can be described as A_{Wstart} [kg/ (m^2·s^{½})] using Equation 3.2.

$$A_{Wstart} = \frac{W - W_{start}}{\sqrt{t}} \tag{3.2}$$

Transport data can be obtained using Boltzmann transformation with a series of capillary water uptake tests in which the specimens are conditioned to certain moisture levels before the capillary water uptake test is performed (Claesson, 1994). Specimens with different initial moisture contents will display different capillary absorption rates. When the initial moisture content, moisture content at capillary saturation, and sorption coefficient are known, the moisture diffusivity can be determined as an average value in the moisture content interval from the initial moisture content up to the capillary saturation point, using Equation 3.4.

When the distribution of the moisture content, $w(x)$ [kg/m^3], is known for a material, the one-dimensional moisture flux, g [kg/(m^2·s)], can be determined using Equation 3.3.

$$g = -D(w)\frac{\partial w}{\partial x} \tag{3.3}$$

Since moisture diffusivity, $D(w)$ [m^2/s], is dependent on moisture content in a porous material, the variable must be described as a function of the moisture content of the material. According to Equation 3.4, moisture diffusivity, $\overline{D}(w_{start}, w_{cap})$ [m^2/s], can be described as a function of the initial moisture content, w_{start} [kg/m^3], the moisture content at capillary saturation, w_{cap} [kg/m^3], and the sorption coefficient, A [kg/(m^2·s^{½})] (see Claesson, 1994, and Arfvidsson and Janz, 1994). Moisture diffusivity is an average value representing the moisture transport for the complete interval from w_{start} [kg/m^3] to w_{cap} [kg/m^3] at capillary saturation.

$$\overline{D}(w_{start}, w_{cap}) = \frac{\pi A_{Wstart}^{\,2}}{4(w_{cap} - w_{start})^2} \tag{3.4}$$

When the moisture content per cubic meter, w [kg/m^3], is used for determining the moisture content in absorption tests, the moisture content is considered to be a fictive mean value, $\overline{w}$

[kg/m^3], for the entire specimen. The moisture content described as $\overline{w}$ [kg/m^3] can only be used as a measure of the amount of absorbed water in specimens with a uniform cross-sectional area. The relationship between moisture content per volume, $\overline{w}$ [kg/m^3], and the amount of absorbed water, W [kg/m^2], is described in Equation 3.5, where h [m] represents the height of the specimen provided that the cross-sectional area is constant.

$$W = \overline{w}h \tag{3.5}$$

The moisture diffusivity, $\overline{D}(w_{start}, w_{cap})$ [m^2/s], according to Equation 3.4 can now be written using Equation 3.5 as a function of the initial amount of water per square meter, W_{start} [kg/m^2], where the sorption coefficient, A_{Wstart} [kg/(m^2·s^{½})], is expressed as Equation 3.2.

$$\overline{D}(w_{start}, w_{cap}) = \frac{h^2 \pi A_{Wstart}^{\ 2}}{4(W_{cap} - W_{start})^2} \tag{3.6}$$

The units of diffusivity according to Equation 3.6, $\overline{D}(w_{start}, w_{cap})$ [m^2/s], will remain unchanged, allowing the diffusivity to be applied directly to Equation 3.3 in undertaking moisture flow calculations. Instead of just determining the average moisture diffusivity for an interval from a certain initial moisture level up to capillary saturation, moisture diffusivity, $D(w)$ [m^2/s], can be calculated using a computer program, JAM-KAP (Arfvidsson and Janz, 1994), stepwise for the intervals between different initial moisture levels. Moisture diffusivities calculated using JAM-KAP are shown in Figures 3.19, 3.21, and 3.23; the calculation routine used by the computer program is described in greater detail in Janz (1997).

3.3 CAPILLARY TEST

3.3.1 General

Capillary absorption tests can be performed using several methods, the common principle of which is to let a specimen of porous material absorb water. The amount of absorbed water is normally registered by weighing of the specimen during the water uptake phase. This weighing can either be performed continuously throughout the water uptake phase (see Plagge et al., 2004), or manually, the water absorption process being temporarily left off when the weighing is performed (see Section 3.3.2). After finished a weighing step, the water absorption is resumed. In comparing the results of the continuous and manual weighing methods, the time required for the weighing in the manual method must be excluded from the total amount of time.

Another method for determining the amount of water absorbed during a water uptake test is to register the amount of water consumed directly at the water supply. The water supply, for example a plastic cup, can be placed upon a balance. Then the specimen can be suspended just above the surface of water. To start the water uptake phase, one adds enough water to the supply that its surface comes into contact with the underside of the specimen. The forces caused by the surface tension can be disregarded if the balance is set to zero just after the surface of water is allowed to contact the specimen. The water level in the supply will of course sink as long as the water absorption test is in progress, resulting in increased forces caused by the surface tension

between specimen and the water surface. However, the change in surface tension can be ignored if the surface area of the water in the supply is considerably larger than the cross-sectional area of the specimen. Another way to keep the force of the surface tension constant is to keep the water level constant, by adding water to the supply corresponding to the amount of water absorbed by the specimen.

Instead of putting a water supply in contact with the specimen, a nozzle can be attached directly to the wetted surface of the specimen. The nozzle can be connected to a tube that supplies the nozzle with water from a water supply. For continuously determining the amount of absorbed water, the water supply is then placed on a balance. The principle of using a nozzle instead of a free water surface is further described in Section 4.2.2 and also in Janz (1997).

3.3.2 Method

Capillary water uptake tests have been performed on three different façade materials, namely lime–silica brick, lime–cement mortar, and cement mortar (see Chapter 3). Two different batches of lime–silica brick were tested. Before the test was performed, thirteen individual specimens of each material were produced. The production and preparation of the specimens before capillary water uptake testing is described in detail in Section 2.2. The specimens used were shaped like rectangular parallelepipeds measuring 50 × 50 × 100 mm. The variation in the length of the longest side of the specimen was ± 2 mm and of the two other sides was ± 0.5 mm.

Before testing started, the specimens were dried in heating cabinets at a temperature of 40ºC, except for specimens of lime–silica brick, batch 1, that were dried at 105ºC. After the specimens reached equilibrium with their respective drying conditions, all specimens were vacuum saturated with deionized water (for a detailed description, see Section 2.4.2). After the vacuum saturation process was finished, all specimens were assumed to be completely water saturated. When these specimens were weighed and their weights were compared to the dry weights of the specimens, the total amount of absorbed water per square meter could be determined as W_{sat} [kg/m^2]. The volume of the specimens was determined during the vacuum saturation process by weighing the saturated specimen both under water and in air. The sides of the specimen were not completely perpendicular to each other, since the specimens had been produced by hand, therefore the cross-sectional area was determined by dividing the volume by the height of the specimen. By only measuring the height of a specimen in determining its cross-sectional area, the uncertainty could be minimized.

After vacuum saturation, the maximum amount of absorbed water per square meter, W_{sat} [kg/m^2], was established for each specimen. Then each specimen was dried to a specific starting amount of moisture per square meter, W_{start} [kg/m^2], i.e. the specimens were conditioned so that the W_{start}/W_{sat} ratios for each specimen together represented twelve even intervals from one completely dry specimen up to one vacuum-saturated specimen. The specimens were dried to their respective degrees of saturation, W_{start}/W_{sat}, in a heating cabinet at a temperature of 40ºC.

When a specimen had dried to its predetermined degree of saturation, its long sides were wrapped with several layers of plastic kitchen film and both ends were sealed with small plastic bags. The plastic bags overlapped the film and were affixed to the ends of the specimen with elastic rubber bands. Each specimen was then put into a separate sealed plastic bag. To minimize

moisture loss, all the sealed specimens were stored in a box with a relative humidity close to saturation. The box was equipped with a sealed lid and contained a water-filled bowl to maintain the high relative humidity. The specimens were stored in the sealed container more than a month. The high relative humidity in the box was chosen in view of the fact that most specimens were conditioned to moisture levels corresponding to relative humidity levels close to saturation, according to the sorption isotherms for the actual materials determined as described in Chapter 2.

After the moisture redistribution phase was completed, each specimen was taken out of the plastic bag and simultaneously one of its ends was uncovered. Then the specimen, still wrapped in the plastic film along its sides and with the small plastic bag still covering its upper end, was put into contact with deionized water. The upper plastic bag was attached relatively loosely to allow air to escape through the top of the specimen.

During the water intake phase, one end of the specimen was put into contact with a water surface: the specimen was positioned vertically in a plastic basin, with a permeable interlayer between it and the water to ensure a continuous water supply to the specimen. The level of water in the basin was adjusted so that only the end of the specimen was allowed to be in contact with the water. If the basin contained too much water during this phase, there was the risk that the water would not only be in contact with the end of the specimen, but also with part of the mantle surface. In that case, the area of the wetted surface would be difficult to estimate. To prevent the water from being transported between the specimen and the plastic film along its sides, the plastic film ended approximately 5 mm from the wetted end. Since there was a small gap between the wetted surface and the plastic film along the sides, evaporation could take place during the wetting phase; to hinder such evaporation, however, the basin was covered with a lid, resulting in a relative humidity close to the saturation point.

The continuously increasing amount of absorbed water was detected by regular weighing of the specimen during the water uptake phase. At the beginning of the phase the specimen was weighed fairly frequently; however, as the specimen approached the saturation point, the intervals between weighing were extended. The time was registered using a stop watch, which was stopped during the weighing procedure. Before the specimens were put on the balance, free water was removed using a wet cloth. The balance used for the test had a precision of thousandths of a gram; each specimen was weighed for approximately 10 s.

3.3.3 Results

The results of the water absorption tests of the different materials are presented as the total amount of absorbed water per square meter, ΔW [kg/m^2], as a function of square root of time in Figures 3.2, 3.4, 3.6, and 3.8. The initial amount of absorbed water can be seen as the starting point for each specimen in the figures.

During the conditioning process it was observed that the amount of absorbed water at vacuum saturation, W_{sat} [kg/m^2], varied considerably between different specimens of the same material. Therefore, the specimens were conditioned according to the degree of saturation, W_{start}/W_{sat}, in regular intervals from one dry to one vacuum-saturated specimen. The results of the absorption tests of the different materials can thus just as well be presented as the degree of saturation, W/W_{sat}, as as a function of the square root of time in Figures 3.3, 3.5, 3.7, and 3.9.

The absorption tests were performed on two batches of lime–silica brick, partly batch 1 and partly batch 2. The test on batch 2 was performed afterwards, since the results obtained from testing batch 1 were unrealistic. The different handling methods used for these two batches were described in Section 3.3.2.

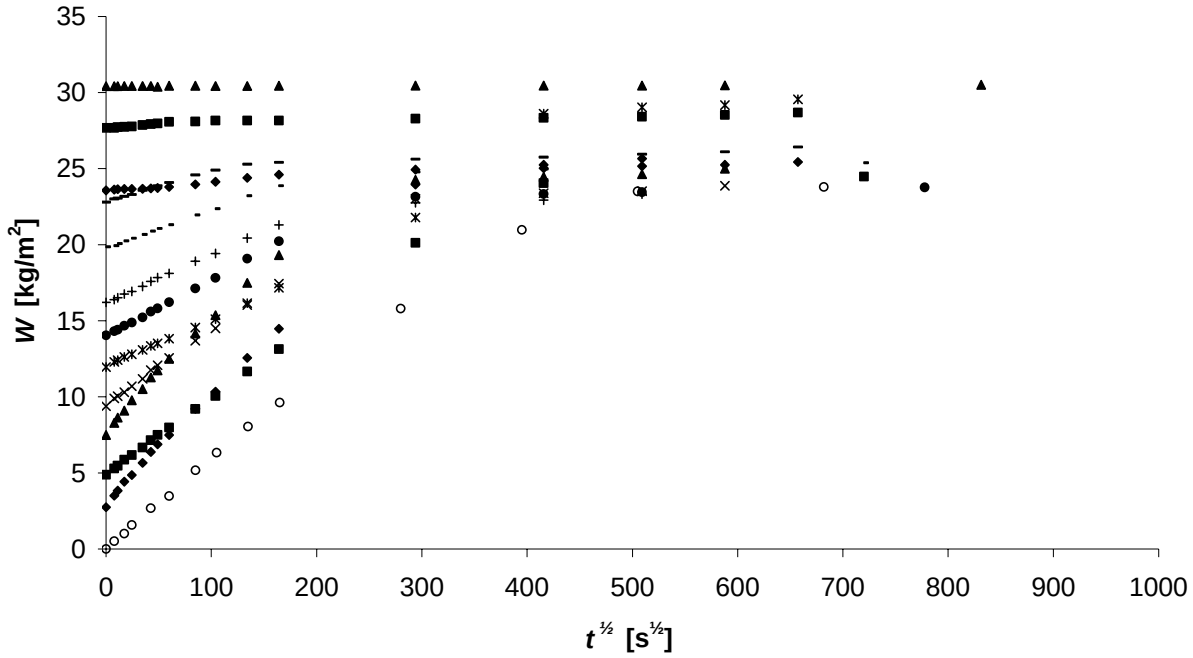

Figure 3.2 The amount of absorbed water per square meter, W, as a function of the square root of time, $t^{1/2}$, for individual specimens of lime–silica brick, batch 1.

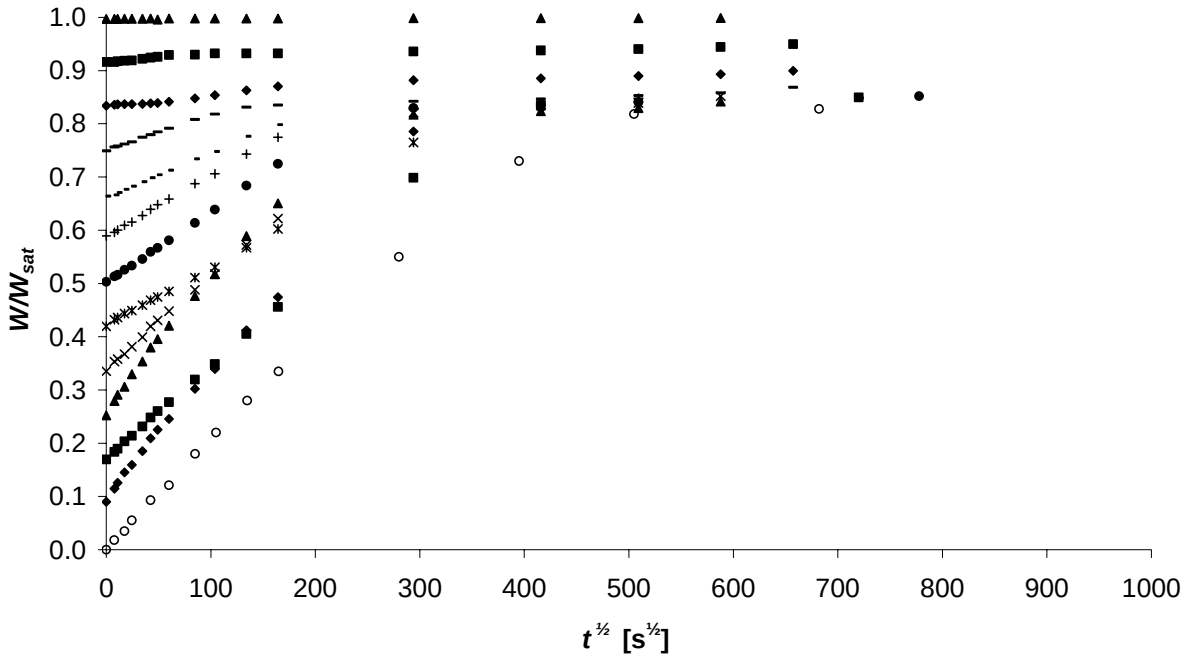

Figure 3.3 The amount of absorbed water per square meter divided by the amount of absorbed water per square meter at vacuum saturation, W/W_{sat}, as a function of the square root of time, $t^{1/2}$, for individual specimens of lime–silica brick, batch 1.

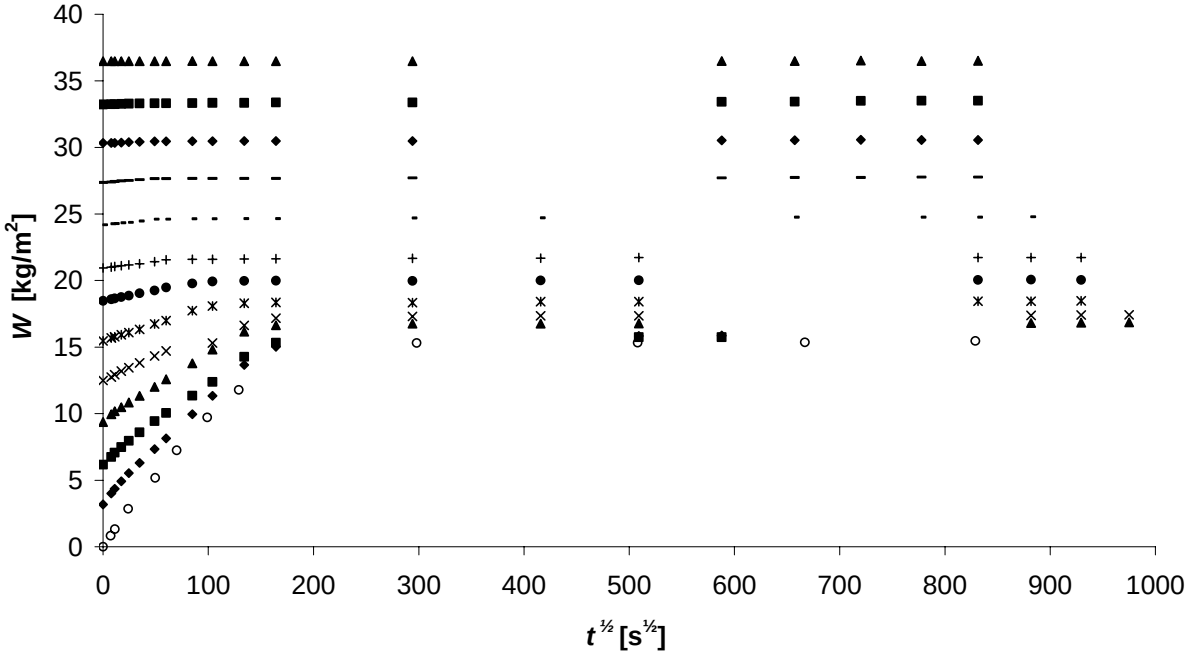

Figure 3.4 The amount of absorbed water per square meter, W, as a function of the square root of time, $t^{1/2}$, for individual specimens of lime–cement mortar.

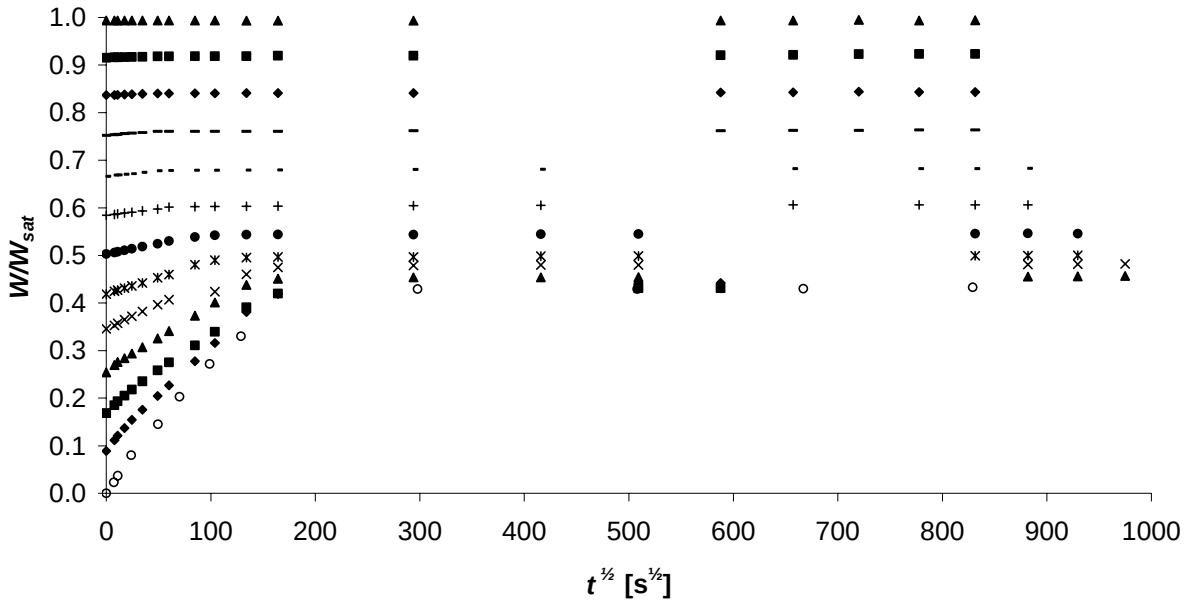

Figure 3.5 The amount of absorbed water per square meter divided by the amount of absorbed water per square meter at vacuum saturation, W/W_{sat}, as a function of the square root of time, $t^{1/2}$, for individual specimens of lime–cement mortar.

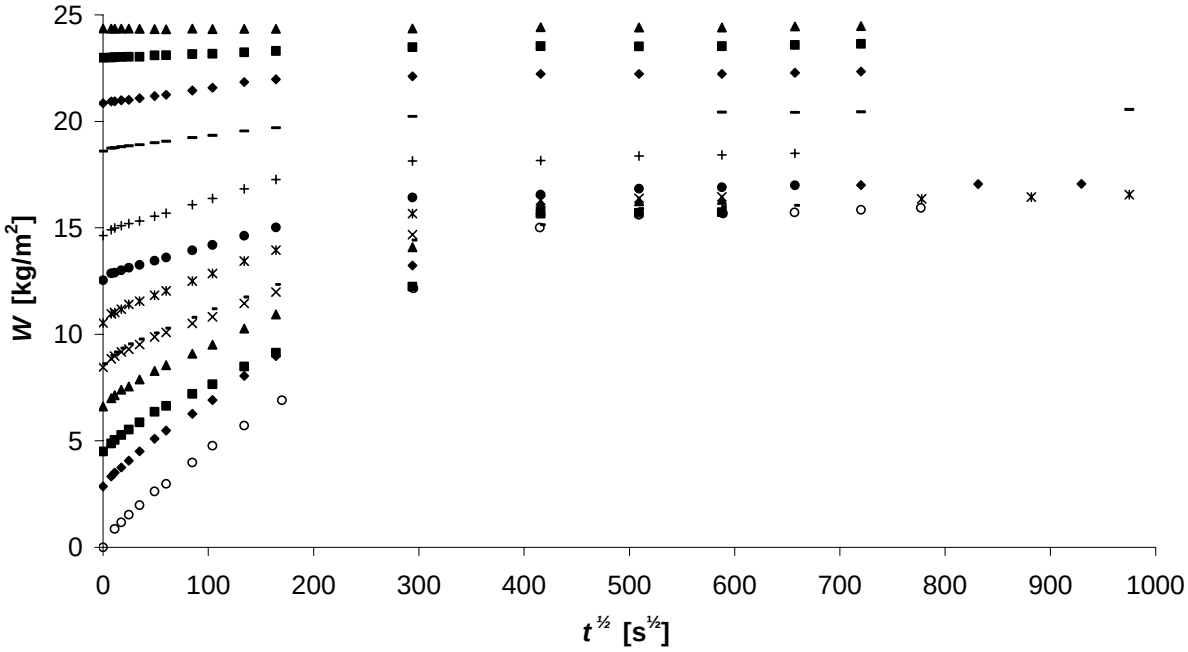

Figure 3.6 The amount of absorbed water per square meter, W, as a function of the square root of time, $t^{1/2}$, for thirteen specimens of cement mortar.

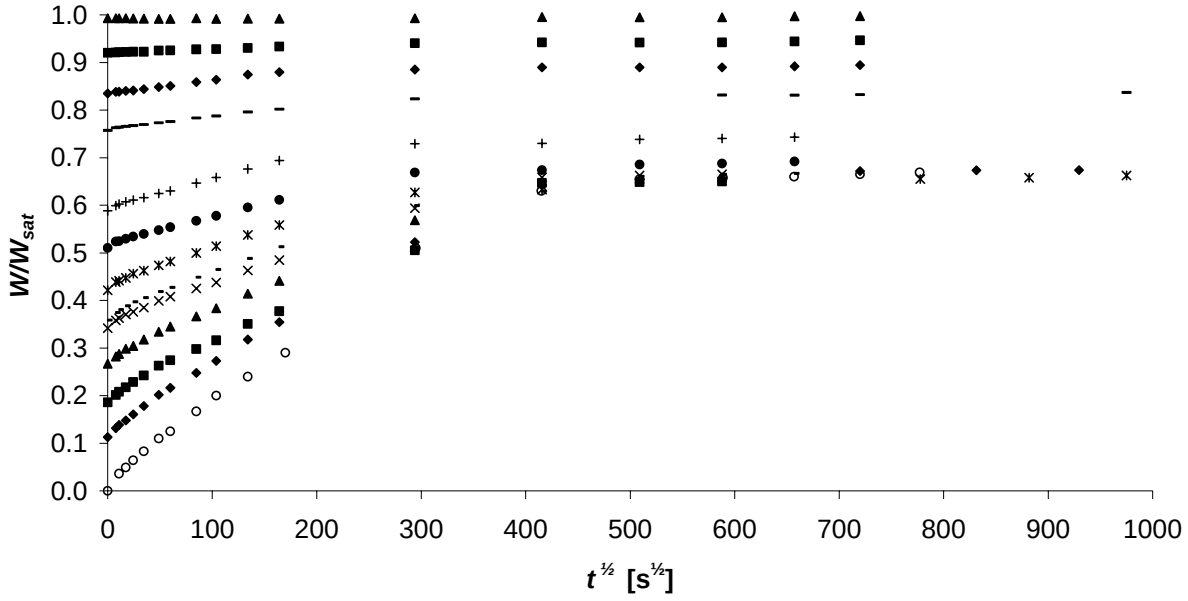

Figure 3.7 The amount of absorbed water per square meter divided by the amount of absorbed water per square meter at vacuum saturation, W/W_{sat}, as a function of the square root of time, $t^{½}$, for individual specimens of cement mortar.

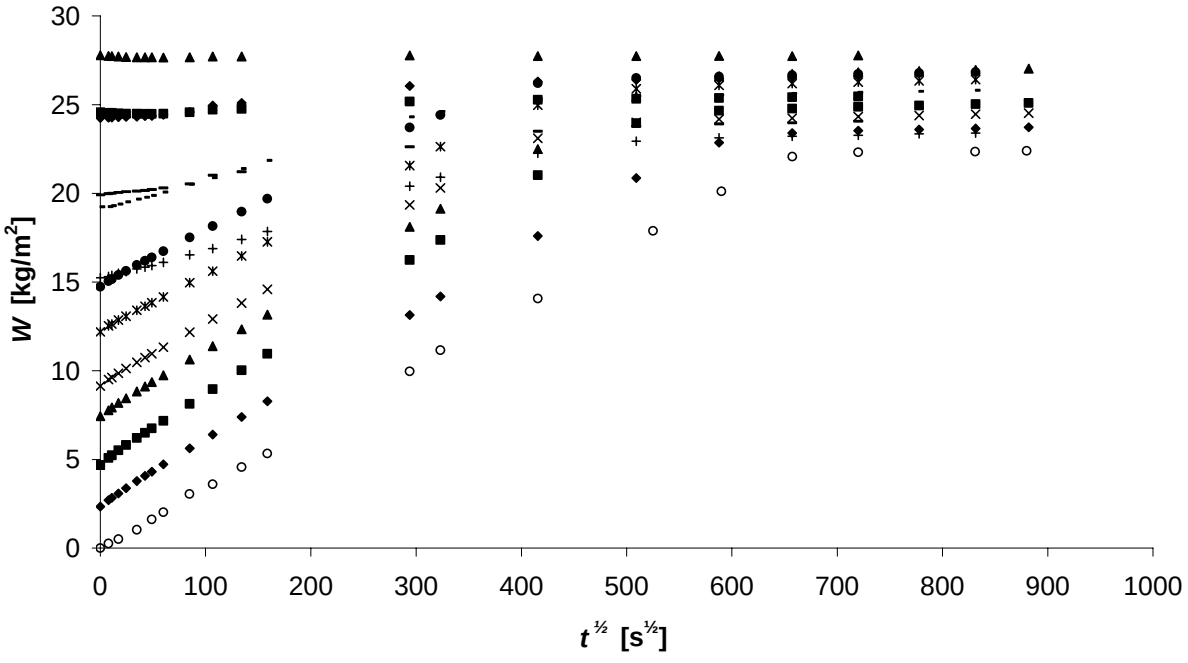

Figure 3.8 The amount of absorbed water per square meter, W, as a function of the square root of time, $t^{½}$, for individual specimens of lime–silica brick, batch 2.

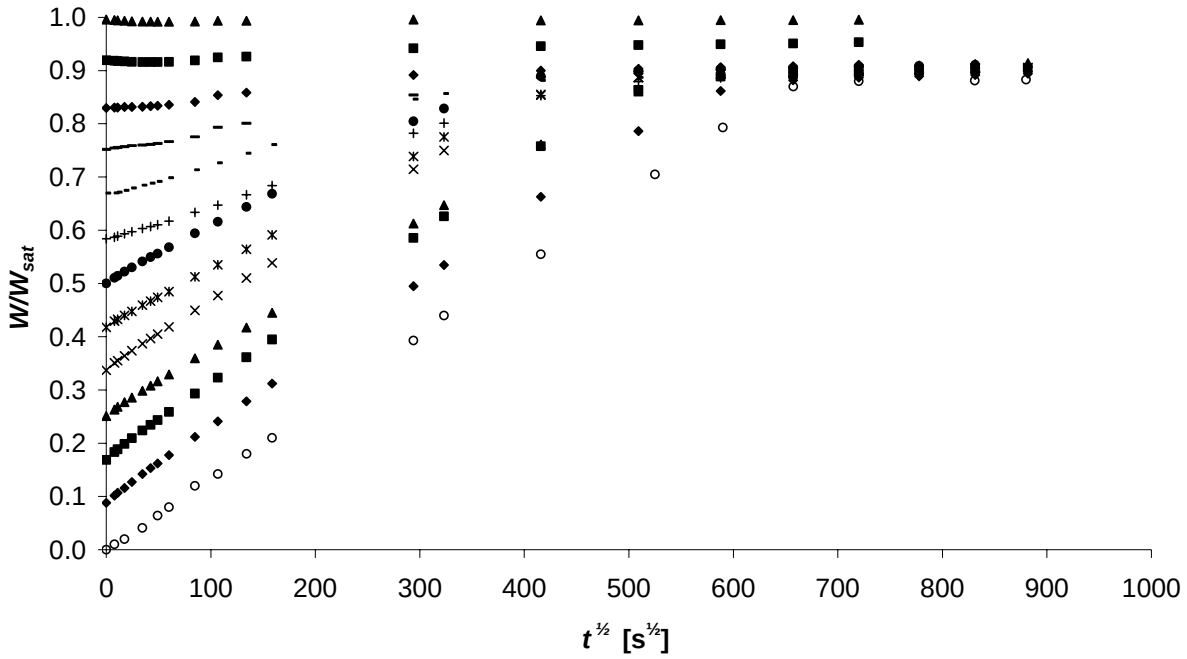

Figure 3.9 The amount of absorbed water per square meter divided by the amount of absorbed water per square meter at vacuum saturation, W/W_{sat}, as a function of the square root of time, $t^{½}$, for individual specimens of lime–silica brick, batch 2.

3.4 ANALYSIS OF RESULTS

3.4.1 Effect of drying

Before testing took place, it was decided that the cement-based materials (i.e. lime–cement mortar and cement mortar) would be dried in heating cabinets at a temperature of 40ºC. A maximum temperature of 40ºC was used, instead of the normal dry specimen definition of 105ºC, to avoid the occurrence of structural changes inside the materials. The lime–silica brick, batch 1, was estimated to be able to be dried at 105ºC without displaying any structural changes. However, the results presented in Figures 3.2 and 3.3 for lime–silica brick, batch 1, were unrealistic, since several specimens with a relatively high initial moisture content were found to have a higher sorption coefficient than did specimens with a considerably lower initial moisture content. The structure of the lime–silica brick, batch 1, had most likely been affected during drying at 105ºC; a reasonable reason for the inexplicable results could be that the specimen acquired micro cracks during drying at that temperature.

Since the absorption tests of lime–silica brick, batch 1, produced inexplicable results, a new test was arranged using exactly the same conditions, except that the drying was performed at 40ºC instead of the previous 105ºC. The results of the repeated sorption test of lime–silica brick, batch 2, are shown in Figures 3.8–3.9, in which specimens with a relatively high moisture content showed lower absorption rates than specimens with a relatively low initial moisture content. The results presented in Figures 3.8–3.9 correspond to those of other comparable tests presented in

this chapter. The variation in the results obtained from testing lime–silica brick, batches 1 and 2, indicates that precautions must not only be taken when drying cement-based materials, but when drying other materials as well.

3.4.2 Effect of hysteresis

During the conditioning process, described in detail in Section 3.3.2, all specimens were dried to their predetermined average moisture levels from vacuum saturation. The specimens were allowed to dry through all of their surfaces. Since this drying was a relatively quick process, it is most likely that most of the evaporated water came from the outer parts of the specimens, while the interior of the specimens retained moisture at closer to vacuum saturation levels.

During the following redistribution phase, the specimens were sealed, as previously described, for approximately a month. During this phase, the outer parts of the specimens absorbed water from the inner parts until an equilibrium state was reached. Since the outer parts of the specimens were under absorption and the inner parts were under desorption, the moisture contents differed within the specimens even when the equilibrium state was reached. Therefore, the moisture contents were most likely somewhat lower in the outer parts of the specimens than in the inner parts.

The effects of the lower moisture contents in the outer parts of the specimens can be seen in Figures 3.10A–C, in which the increased slope of the plots at the beginning of the water uptake phase represents a higher absorption capacity. The increased slope at the beginning of the moisture uptake phase is more noticeable for the specimens with lower initial moisture contents, most likely since they were exposed to a longer drying period. However, the hysteresis effects caused by the redistribution phase are quite small and can thus be ignored. A study of different conditioning methods and their effects was performed by Janz (1997).

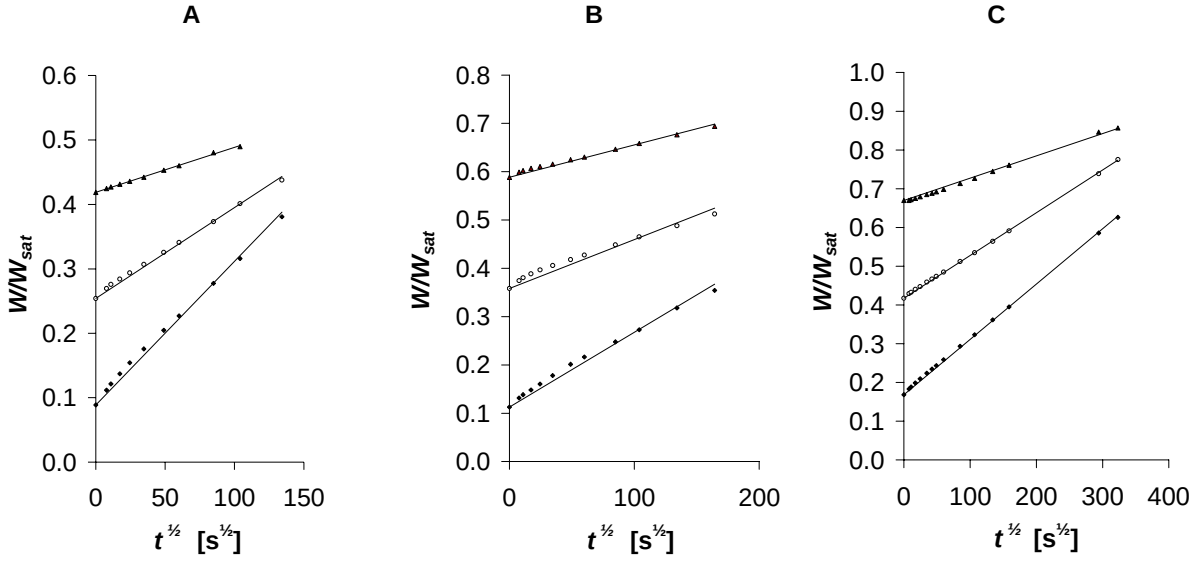

Figure 3.10 Comparison between the slopes of the data and a straight line. Figures A, B, and C represent lime–cement mortar, cement mortar, and lime–silica brick, batch 2, respectively.

3.4.3 Capillary break point

When a dry material is exposed to a water surface, an ideal absorption curve, as depicted by plot A–B–C of Figure 3.11, was expected. However, the most common porous building materials contain pores of various sizes, and the moisture front of a relatively large pore will extend higher than that of a relatively small pore at a particular time (Ahlgren et al., 1976). The difference in capillary absorption rates for different pore sizes results in indistinct capillary break points, shown as the principal curve from A to C in Figure 3.11. The capillary break point can still be defined, since the rectilinear plot from the origin to point A and the rectilinear plot from C onwards can be extrapolated until their point of intersection is reached; this point of intersection is defined as the capillary break point. The capillary break points for the water absorption tests presented in Figures 3.2 to 3.9 correspond well with the general appearance of the capillary break point, A to C, depicted in Figure 3.11.

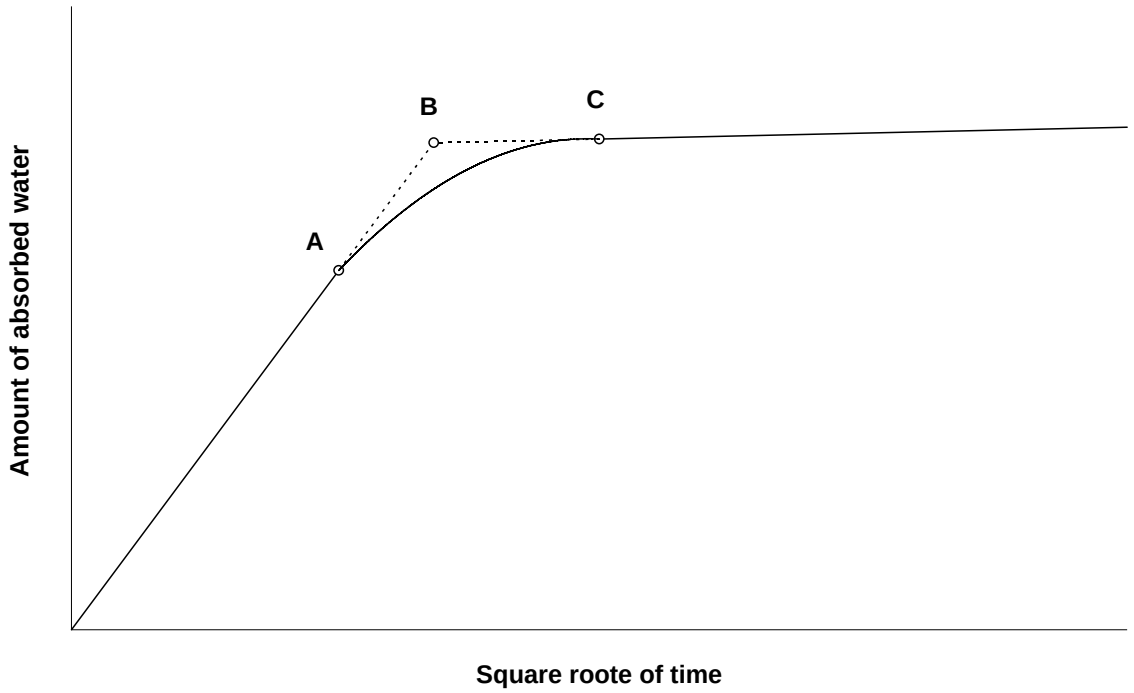

Figure 3.11 Principal representation of an ideal capillary water uptake process represented by the plot A–B–C. The curved plot from A to C represents the capillary water uptake process as often observed when testing common building materials.

According to Ahlgren et al. (1976), the time required to reach capillary break point is independent of the initial moisture content. However, the time required to reach the capillary break point for specimens with different initial moisture contents in the present experiments was found to vary considerably according to the initial moisture level. The variation in time to the capillary break point can most clearly be seen in Figures 3.8 and 3.9 for absorption tests of lime–silica brick, batch 2, and in Figures 3.4 to 3.5 for lime–cement mortar, in which the capillary break point was reached considerably earlier for specimens with higher initial moisture contents. Almost the same type of variation in time to capillary break point for specimens with different initial moisture levels was observed for cement-based mortar, as presented in Figures 3.6 to 3.7.

The variation in time required to reach the capillary break point, depending on the initial moisture level, can be explained in terms of the earlier discussion of the fact that the moisture front of a relatively large pore will extend higher than the moisture front of a relatively small pore at a particular time. For specimens with a given initial moisture content, a certain proportion of the pore volume will be water filled, the smallest pores becoming water filled first while the larger pores are still empty. Since the smallest pores are already water filled for a specimen with a given moisture content, they will not contribute to the water uptake process. Then, when a specimen with a given initial amount of water is exposed to a water surface, the larger pores will preferentially participate in the capillary transport process. Since the water front moves quicker in the larger pores with less resistance, a specimen with sufficient initial moisture content will reach the capillary break point earlier than a dry specimen will, provided that the height of the specimen is less than the capillary limit.

Results of the absorption tests indicate that the degree of saturation at the capillary break point varies with the initial moisture content, according to Figure 3.12, which presents the results for lime–cement mortar, cement mortar, and lime–silica brick, batch 2. The unfilled dots represent moisture levels above the capillary moisture range, so these data points must be excluded from the analysis. The degree of saturation at the capillary break point is observed to increase with increased initial moisture content for lime–cement mortar and cement mortar, according to Figure 3.12. However, any significant relationship between variation in the degree of saturation by the capillary break point and the initial moisture level for lime–silica brick, batch 2, could not be observed. It is also known from other experimental studies (e.g. Schwarz, 1972) that the moisture content at the capillary break point may depend on the initial moisture content.

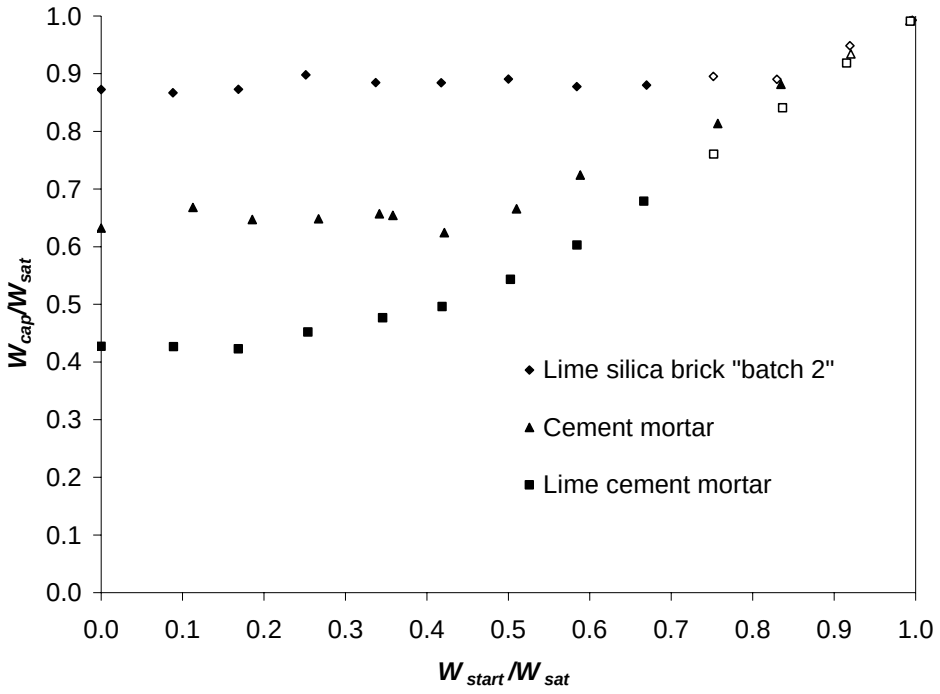

Figure 3.12 The degree of vacuum saturation at the capillary saturation point, W_{cap}/W_{sat} , as a function of the degree of vacuum saturation at the starting point, W_{start}/W_{sat}. Observations above the capillary moisture range are indicated by unfilled dots.

The higher degree of saturation at the capillary break point for specimens with higher initial moisture contents could occur because part of the pore system that is normally empty, instead becomes water filled. During the conditioning process, the vacuum-saturated specimens were dried to various moisture levels, ranging from completely dry up to a moisture level nearly corresponding to vacuum saturation. During the drying process, the bubbles of vapour most likely arose in the water-filled pore system, because of the suction created by the meniscus. At the beginning of the drying process, larger-diameter pores still retained water; as the drying process continued, the larger pores became progressively more emptied, resulting in only the smaller pores finally retaining water. Since the meniscus in the smaller pores is of a smaller radius, the suction in the pore system increased further, resulting in more vapour bubbles in the pore system. As a result, the pore system was gradually emptied, some parts of the pore system coming into contact with atmospheric pressure via connected unfilled pores.

As soon as the specimens were again put into contact with water after the drying phase, the suction in the pore system began disappearing, most likely because the vapour bubbles imploded. Depending on the initial moisture level, some of the larger pores containing vapour bubbles may come into contact with atmospheric pressure via connected pores that emptied during the drying phase. When the specimen was then exposed to water during the capillary tests, the air in these larger pores became enclosed. A lower initial moisture level therefore resulted in a lower degree of saturation at the capillary break point, and conversely, a higher initial moisture level resulted in a higher degree of saturation.

The relationship between different initial moisture contents and capillary properties was also studied by Schwarz (1972). Results of a study of brick showed that the capillary break point was reached earlier for specimens of brick with higher initial moisture contents; as well, the capillary break point was found to be reached at a higher moisture content when the initial moisture contents of the specimens were increased. The initial moisture contents were reached by absorption performed on dry specimens, after which the specimens were sealed for approximately a month to allow for moisture redistribution. Despite the fact that the specimens in the present study were conditioned using different techniques from those used by Schwarz (1972), similar results were obtained. A study of concrete in which the water–cement ratios ranged from 0.31 to 0.62 was performed by Nokken and Hooton (2002). In that study, the time to reach capillary break point was studied for specimens with different initial moisture contents; however, the results indicated that the time to capillary break point was relatively independent of the initial moisture content. Since the literature reports different results for different materials, it is crucial to consider the initial moisture content when determining the degree of saturation or the time to capillary saturation either by experiment or by calculation.

3.4.4 Sorption coefficient

Since it was observed in Section 3.3.3 that the amount of absorbed water at vacuum saturation, W_{sat} [kg/m^2], varied considerably for different specimens of the same material, the degree of vacuum saturation, W/W_{sat}, was used instead of the moisture content, W [kg/m^2]. Therefore, the sorption coefficient according to Equation 3.2, A_{Wstart} [kg/(m^2·s^{½})], was instead described as an alternative sorption coefficient, $A_{Wstart}/_{Wsat}$ [s$^{-½}$], as a function of the initial degree of saturation, W_{start}/W_{sat}, according to Equation 3.7.

$$A_{Wstart/\ Wsat} = \frac{\left(\frac{W}{W_{sat}} - \frac{W_{start}}{W_{sat}}\right)^2}{\sqrt{t}} \tag{3.7}$$

The alternative sorption coefficient has been determined for lime–cement mortar, cement mortar, and lime–silica brick, batch 2, as a function of a certain initial degree of saturation, W_{start}/W_{sat}. The alternative sorption coefficient represents the slope of the line from the beginning of the capillary water uptake phase to the capillary break point, described as point B in Figure 3.11. Therefore, the alternative sorption coefficient was not necessarily an expression for the migration rate of the capillary water front, since the porosity varied considerable between different materials. A material with high porosity can display a low migration rate during capillary uptake, even though the alternative sorption coefficient was very high.

Since the results of the capillary water uptake test described in Section 3.3.3 showed anomalous results for lime–silica brick, batch 1, the sorption coefficient was not determined for this batch.

The alternative sorption coefficients presented in Figures 3.13 to 3.15 are valid for specimens exposed to unhindered one-dimensional capillary absorption with particular initial degrees of saturation, W_{start}/W_{sat}. The relationship between the alternative sorption coefficients and the initial moisture contents for all three materials could almost be described as a perfect fit to an equation of the second degree. However, the alternative absorption coefficients for lime–cement mortar were almost twice as high for dry or almost dry specimens, as were those of the other materials. The higher absorption rate could be because the lime–cement mortar had a considerably higher porosity and thus a higher moisture storage capacity (see Table 2.2).

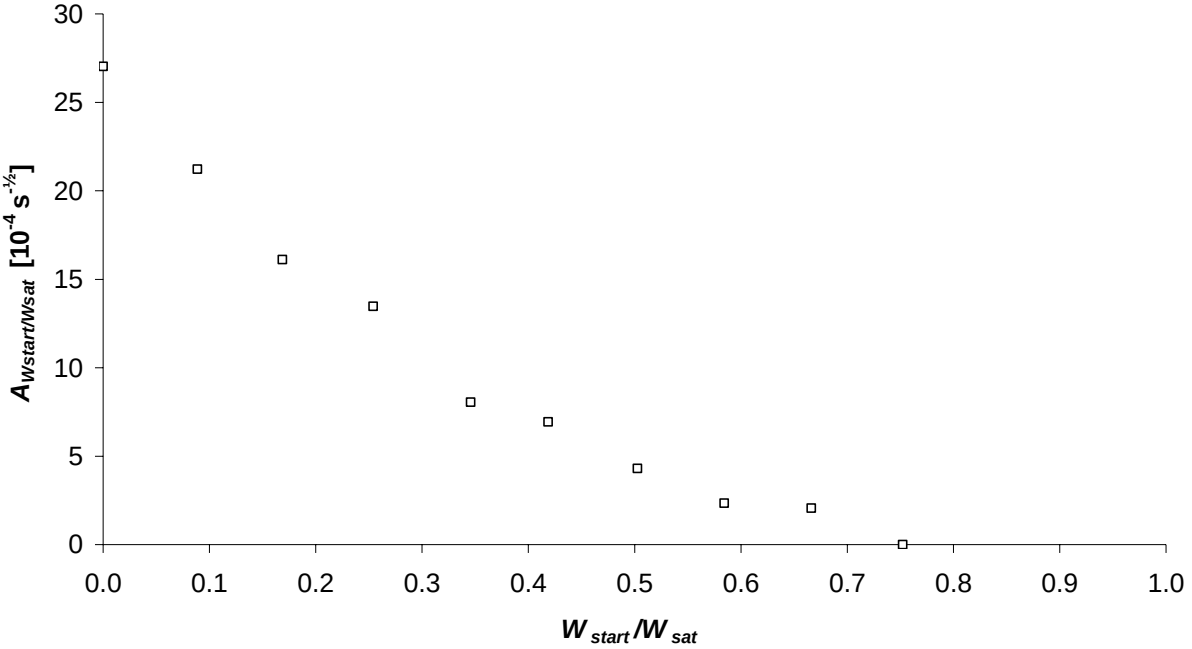

Figure 3.13 The alternative sorption coefficient, $A_{Wstart/Wsat}$, according to Equation 3.7, as a function of the degree of vacuum saturation at the starting point, W_{start}/W_{sat}, for individual specimens of lime–cement mortar exposed to a free surface of water.

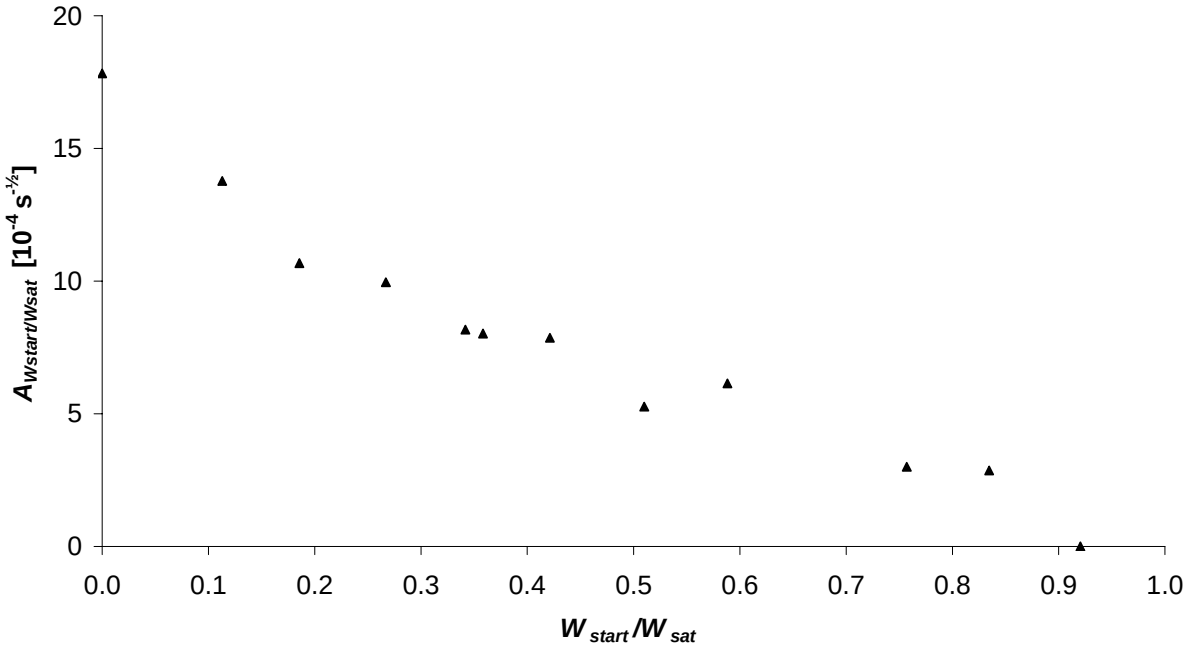

Figure 3.14 The alternative sorption coefficient, $A_{Wstart/Wsat}$, according to Equation 3.7, as a function of the degree of vacuum saturation at the starting point, W_{start}/W_{sat}, for individual specimens of cement mortar exposed to a free surface of water.

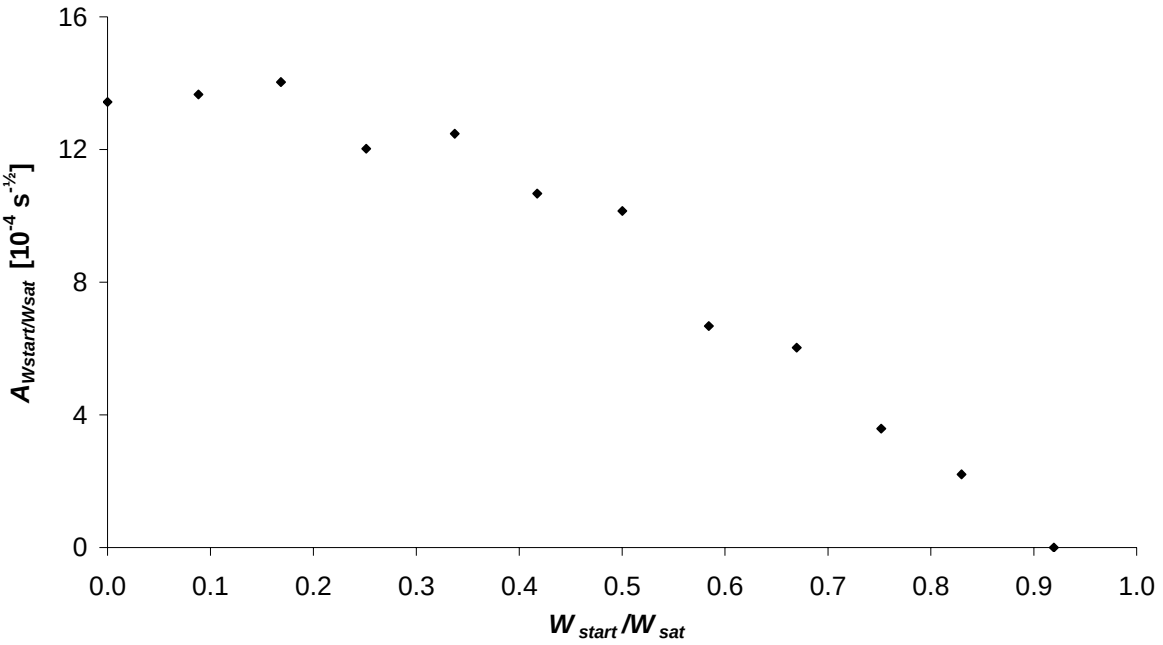

Figure 3.15 The alternative sorption coefficient, $A_{Wstart/Wsat}$, according to Equation 3.7, as a function of the degree of vacuum saturation at the starting point, W_{start}/W_{sat}, for individual specimens of lime–silica brick, batch 2, exposed to a free surface of water.

3.4.5 Average moisture diffusivity

If the expression for the sorption coefficient, A_{Wstart} [kg/(m^2·s^{½})], according to Equation 3.2 is combined with Equation 3.6, the moisture diffusivity, $\overline{D}(w_{start}, w_{cap})$ [m^2/s], can be expressed as Equation 3.8.

$$\overline{D}(w_{start}, w_{cap}) = \frac{h^2 \pi (W - W_{start})^2}{4t (W_{cap} - W_{start})^2} \tag{3.8}$$

Since the variation in porosity is considerable for some of the most common façade materials (see Table 2.2), the possible amount of absorbed water per square meter, W [kg/m^2], will also vary correspondingly for individual specimens. If the amount of absorbed water is considered in relation to the amount of absorbed water at vacuum saturation, W_{sat} [kg/m^2], i.e. the amount of absorbed water for a completely saturated specimen, the W/W_{sat} ratio will vary less than the water content per square meter, W [kg/m^2]. Thus, moisture diffusivity according to Equation 3.8 can be expressed as a function of the W/W_{sat} relationship, rather than as the amount of absorbed water according to Equation 3.9, in which both the numerator and denominator are divided by the square of the amount of absorbed water per square meter at vacuum saturation, W_{sat} [kg/m^2].

$$\overline{D}\left(w_{start}, w_{cap}\right) = \frac{h^2 \pi \left(\frac{W}{W_{sat}} - \frac{W_{start}}{W_{sat}} \right)^2}{4t \left(\frac{W_{cap}}{W_{sat}} - \frac{W_{start}}{W_{sat}} \right)^2} \tag{3.9}$$

The moisture diffusivity, $\overline{D}\left(w_{start}, w_{cap}\right)$ [m^2/s], can then be expressed by Equation 3.10, in which the alternative sorption coefficient according to Equation 3.7, $A_{Wstart/Wsat}$ [s$^{-½}$], is combined with Equation 3.9.

$$\overline{D}\left(w_{start}, w_{cap}\right) = \frac{h^2 \, \pi \, A_{Wstart/\,Wsat}{}^2}{4 \left(\frac{W_{cap}}{W_{sat}} - \frac{W_{start}}{W_{sat}} \right)^2} \tag{3.10}$$

With Equation 3.10 available, the moisture diffusivity, $\overline{D}\left(w_{start}, w_{cap}\right)$ [m^2/s], can be determined as the "average moisture diffusivity" for capillary absorption in the moisture interval from W_{start}/W_{sat} to W_{cap}/W_{sat}. The alternative sorption coefficients, $A_{Wstart/Wsat}$ [s$^{-½}$], were taken from Figures 3.13 to 3.15 as discreet values, described as a function of the initial moisture level, W_{start}/W_{sat}. Note that the units of moisture diffusivity expressed in Equation 3.10 will be unchanged from the original $\overline{D}\left(w_{start}, w_{cap}\right)$ [m^2/s] in Equation 3.6, even though the degree of vacuum saturation was used in determining them. The unchanged units imply that the driving potential of the moisture content, w [kg/m^3], should still be used for calculating the moisture flux, g [kg/(m^2·s)], using Equation 3.3, instead of the degree of saturation, W/W_{sat}.

The average moisture diffusivity values for lime–cement mortar, cement mortar, and lime–silica brick, batch 2, are shown in Figures 3.16 to 3.18, respectively. The results for lime–silica brick, batch 2 (Figure 3.18), are considerably higher than the average moisture diffusivities for the other materials. The parameter in Equation 3.10 that varied the most between the different materials was the alternative sorption coefficient, $A_{Wstart/Wsat}$ [s$^{-½}$]; the other parameters remained approximately the same. In this test, the high sorption coefficient of lime–silica brick, batch 2, resulted in a high average moisture diffusivity.

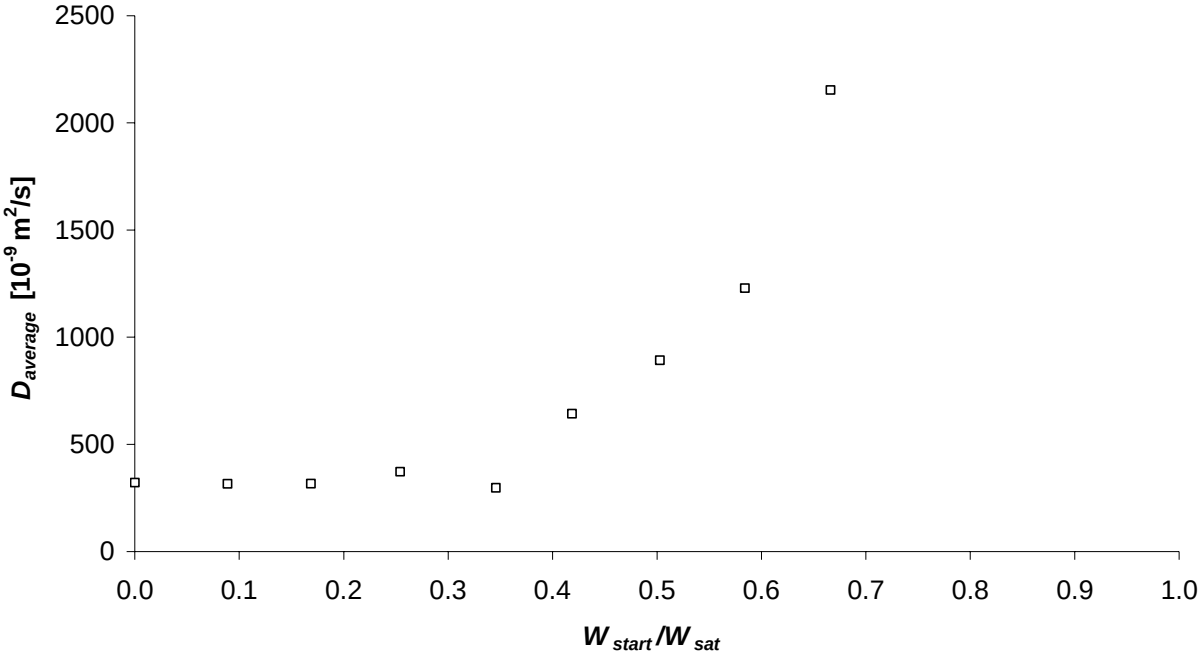

Figure 3.16 Average moisture diffusivity, $\overline{D}(w_{start}, w_{cap})$, as a function of the lower moisture content interval limit, expressed as a function of the degree of vacuum saturation at the starting point, W_{start}/W_{sat}, for individual specimens of lime–cement mortar.

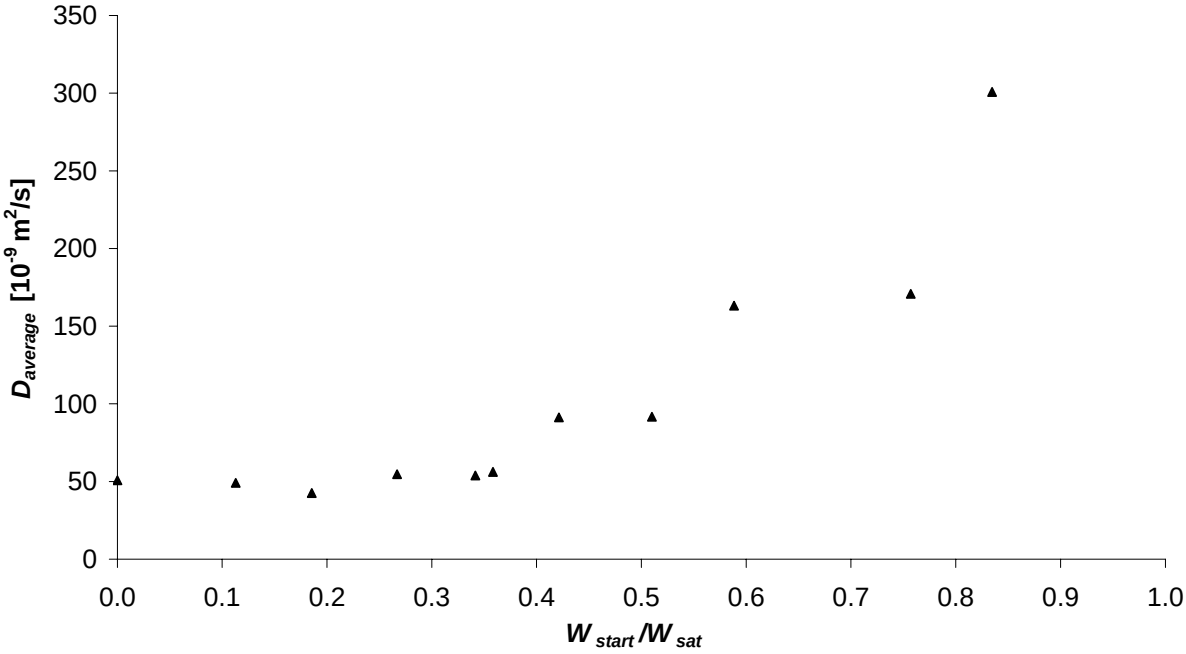

Figure 3.17 Average moisture diffusivity, $\overline{D}(w_{start}, w_{cap})$, as a function of the lower moisture content interval limit, expressed as a function of the degree of vacuum saturation at the starting point, W_{start}/W_{sat}, for individual specimens of cement mortar.

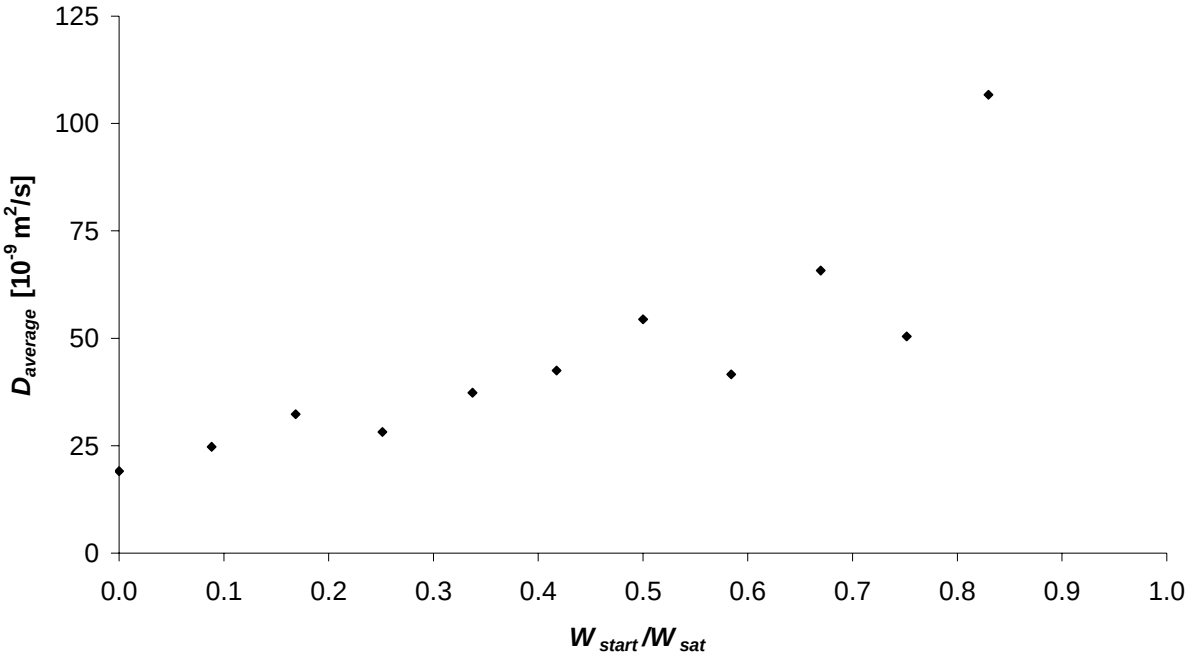

Figure 3.18 Average moisture diffusivity, $\overline{D}(w_{start}, w_{cap})$, as a function of the lower moisture content interval limit, expressed as a function of the degree of vacuum saturation at the starting point, W_{start}/W_{sat}, for individual specimens of lime–silica brick, batch 2.

3.4.6 Moisture diffusivity

As a complement to the average moisture diffusivity, moisture diffusivity has also been determined in stepwise fashion using a computer program, JAM-KAP, briefly introduced in Section 3.2. The calculation routine used by this program was further described in Arfvidsson and Janz (1994). Before the computer calculation was carried out, curve fitting was performed for the relationship between the alternative sorption coefficients, $A_{Wstart/Wsat}$ [$s^{-1/2}$], and the initial moisture contents, W_{start}/W_{sat}, shown in Figures 3.13 to 3.15 for the different materials. The curve fitting could successfully be performed using equations of the second degree, in which the capillary saturation point was used as a boundary condition. Then the moisture diffusivities were calculated as mean values between chosen values of the W_{start}/W_{sat} ratio and corresponding sorption coefficients, $A_{Wstart/Wsat}$ [$s^{-1/2}$], on the adapted second-degree curves. Closer intervals were chosen where the adapted curves displayed greater bending; when large intervals were chosen in these areas, the computer program was unable to find a solution. The computer calculation was performed stepwise, from the point of capillary saturation to the level corresponding to a completely dry specimen. The first step of the calculation started at capillary saturation, or from an arbitrary point close enough to it given the degree of bending. In cases when the program was unable to find a solution, a new point could be chosen closer to the capillary saturation point; alternatively, the value on the *y*-axis could be adjusted until a solution was found. In cases when the value on the *y*-axis had been adjusted, the solution was often found for a new value of *y* that was too far from the original equation to be used. Instead, a more successful approach was to adjust the span of the interval until the solution was reached. To find a solution in areas marked

by considerable bending, the span was decreased; in areas where the bending of the second-degree equation was slight or even non-existent, the span could successfully be increased. Then, when a solution to the first moisture interval starting from capillary saturation was found by the program, a second step was tested. The procedure previously described for the first step was then repeated for the second step until a solution could be found for it as well. After a new solution was found, the process was repeated over and over until a moisture condition corresponding to the dry specimen definition was reached.

The reason for performing the computer simulation stepwise, instead of attacking all of the moisture steps simultaneously, was that the input data had to be adjusted for almost every step. Since the program had no input data folder where the data could be stored for the various simulations, all input data had to be input manually before each new simulation. The process was very time consuming: the input data had to be adjusted for every moisture step until a solution could be found, and all input data for the simulations had to be handled manually and could not be stored by the program.

The adjusted input data regarding the three materials (lime–cement mortar, cement mortar, and lime–silica brick, batch 2) used in computer simulations to determine the moisture diffusivity are shown in Table 3.1. In the table, input data are described by the sorption coefficient, A, multiplied by the individual height of each specimen, h, as a function of the degree of vacuum saturation, W/W_{sat}. As a constant, the moisture content by capillary saturation was also used as input data for each specimen in the form of the ratio, W_{cap}/W_{sat}.

Table 3.1 Input data for determining the moisture diffusivity, $D(w, w_{cap})$ [m^2/s], using the JAM-KAP computer program.

Lime–cement mortar		Cement mortar		Lime–silica brick, batch 2	
W_{start}/W_{sat}	$h \times A(W_{start}/W_{sat})$ [10^{-8} $ms^{-½}$]	W_{start}/W_{sat}	$h \times A(W_{start}/W_{sat})$ [10^{-8} $ms^{-½}$]	W_{start}/W_{sat}	$h \times A(W_{start}/W_{sat})$ [10^{-8} $ms^{-½}$]
0.75	0	0.92	0	0.92	0
0.74	250	0.91	300	0.87	1200
0.72	750	0.89	850	0.80	3000
0.69	1350	0.84	1950	0.74	4300
0.65	2000	0.80	2700	0.69	5200
0.58	2900	0.74	3500	0.63	6400
0.50	4100	0.60	4950	0.55	8000
0.44	5900	0.48	6400	0.48	9200
0.39	7500	0.38	7900	0.32	11600
0.30	10800	0.26	9850	0.24	12800
0.21	15000	0.14	12100	0.18	13600
0.14	18800	0.06	14100	0.12	14400
0.06	23300	0.00	16100	0.06	15100
0.00	27100			0.00	15800

Moisture diffusivities, $D(w, w_{cap})$ [m^2/s], as determined by computer simulation are presented for lime–cement mortar, cement mortar, and lime–silica brick, batch 2, in Figures 3.19, 3.21, and 3.23, respectively. The diffusivities are shown stepwise, as a function of different initial moisture levels stated as the W/W_{sat} ratio. How the steps were chosen was described thoroughly at the beginning of this section.

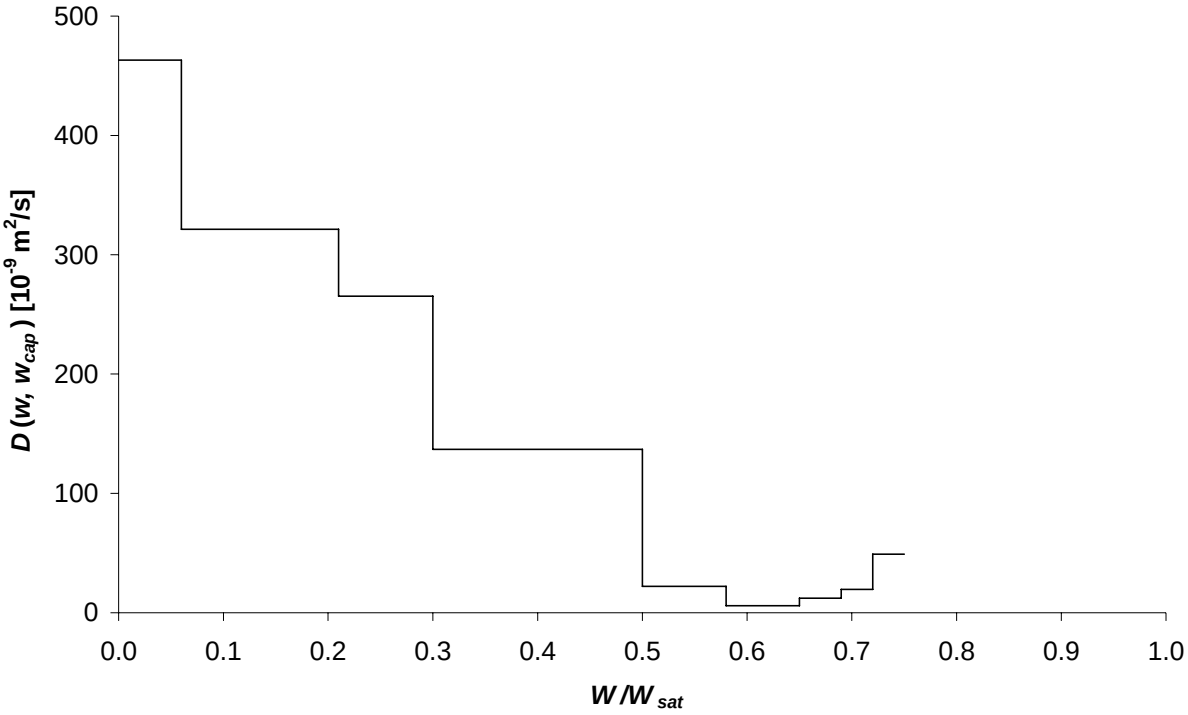

Figure 3.19 Moisture diffusivity, $D(w, w_{cap})$, as a function of the degree of vacuum saturation at the starting point, W/W_{sat}, for specimens of lime–cement mortar.

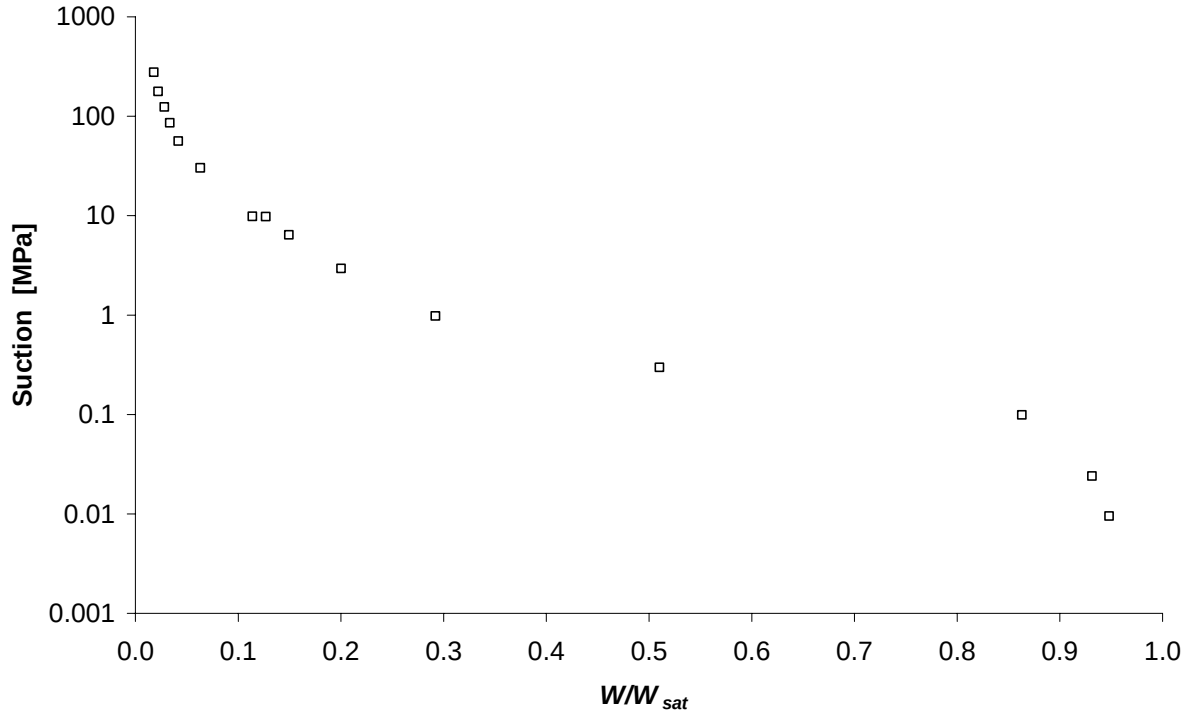

Figure 3.20 The complete desorption isotherm for lime–cement mortar measured using the pressure plate and sorption balance methods.

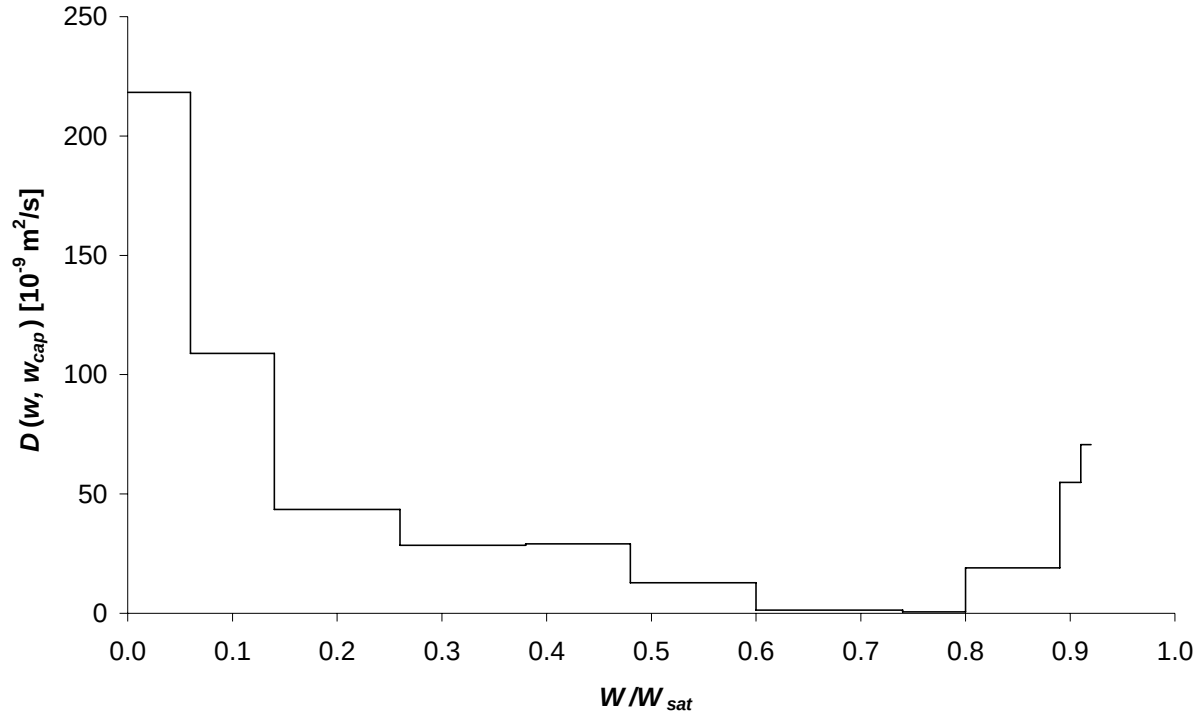

Figure 3.21 Moisture diffusivity, D(w, w_{cap}), as a function of the vacuum saturation at the starting point, W/W_{sat}, for specimens of cement mortar.

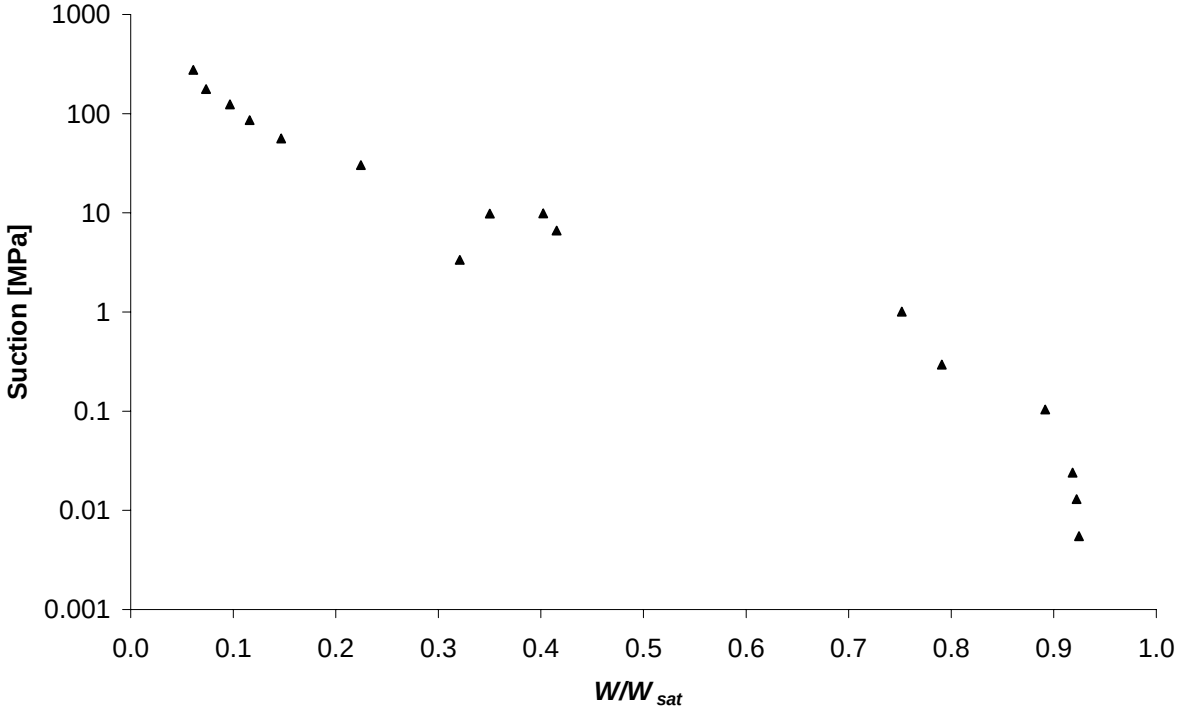

Figure 3.22 The complete desorption isotherm for cement mortar measured using the pressure plate and sorption balance methods.

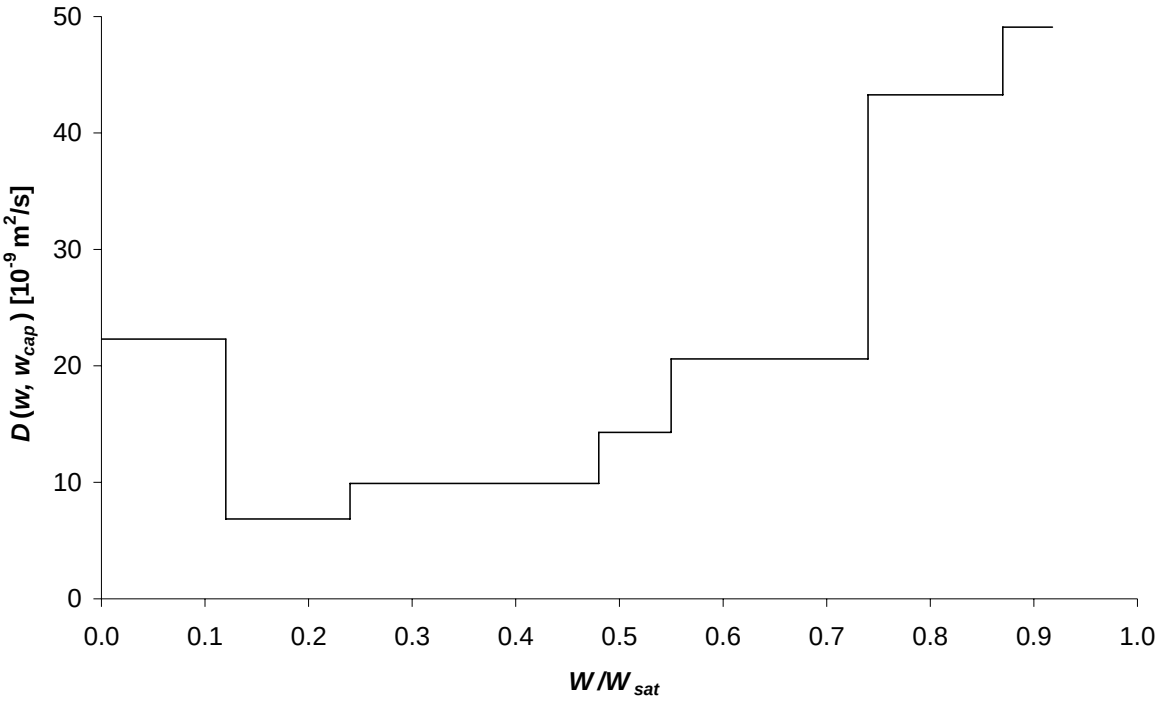

Figure 3.23 Moisture diffusivity, D(w, w_{cap}), as a function of the vacuum saturation at the starting point, W/W_{sat}, for specimens of lime–silica brick, batch 2.

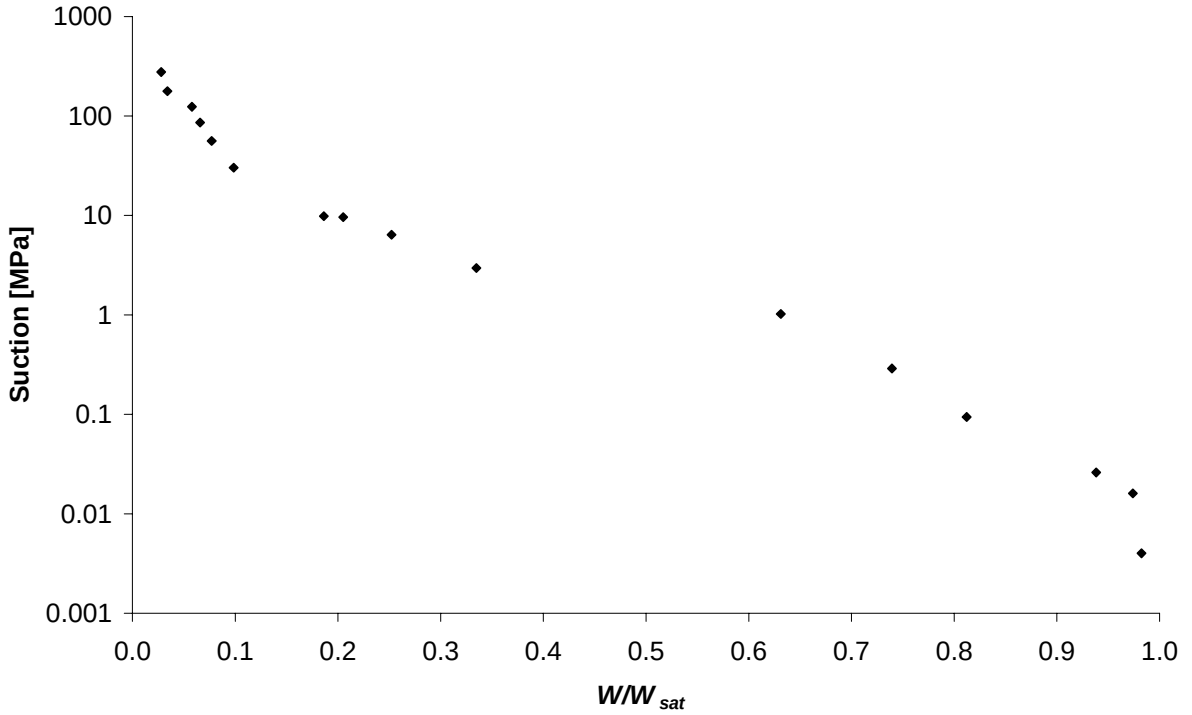

Figure 3.24 The complete desorption isotherm for lime–silica brick, batch 2, measured using the pressure plate and sorption balance methods.

The corresponding suction curves determined in Chapter 2 are shown in relation to the moisture diffusivities as Figures 3.20, 3.22, and 3.24 for the respective materials. A relationship could clearly be observed regarding moisture content, between where the maximum of the diffusivity appeared and where the suction curve was steeply sloped. The same type of relationship between suction curve and moisture diffusivity has also been observed in aerated concrete by, for example, van der Kooi (1971).

The variations in the moisture diffusivity can in principle be explained by the shape of the suction curve for the respective materials; the relationship between suction curve and moisture diffusivity can be explained by Equations 3.11–3.14.

$$g = -D_w \frac{\partial w}{\partial x} \tag{3.11}$$

$$g = -D_s \frac{\partial s}{\partial x} \tag{3.12}$$

$$D_w \cdot \frac{\partial w}{\partial x} = D_s \cdot \frac{\partial s}{\partial x} \tag{3.13}$$

$$D_w = D_s \cdot \frac{\partial s}{\partial w} \tag{3.14}$$

Equation 3.11 describes the moisture flow, g [kg/(m^2·s)], as a function of the driving potential expressed as the change in moisture content, w [kg/m^3], over distance x [m]. The moisture diffusivity is then expressed as D_w [m^2/s]. The moisture flow can likewise be described by Equation 3.12, in which the driving potential is expressed as the change in suction, s [Pa], over distance x [m], and the moisture diffusivity is expressed as D_s [(kg·m)/(N·s)]. By combining Equations 3.11 and 3.12, the moisture diffusivity, D_w [m^2/s], can be expressed by the moisture diffusivity, D_s [(kg·m)/(N·s)], and by the slope of the suction curve, $\partial s/\partial w$. Equation 3.14 clearly indicates that a moisture content at which the suction curve is most steeply sloped will also display maximal moisture diffusivity.

3.5 CONCLUSIONS

To evaluate moisture diffusivity, water absorption tests were performed on specimens with different initial moisture contents. The results of the capillary water uptake tests varied considerably, depending on the moisture contents of the particular specimens of a given material. These variations were observed among specimens from the same batch and exposed to identical external moisture loads. Since moisture diffusivities are normally evaluated from the sorption coefficient, that is, the slope of the line describing the amount of absorbed moisture as a function of the square root of time, moisture diffusivity will also vary considerably. In this work, the sorption coefficient was referred to in terms of an alternative sorption coefficient, describing the

degree of vacuum saturation as a function of the square root of time during capillary water uptake. By using the degree of vacuum saturation instead of the amount of absorbed water per square meter to define the moisture level, variation in moisture diffusivity according to specimen-specific variation could be decreased.

In this research, specimens conditioned to particular initial moisture contents were found to reach the capillary break point earlier and at a higher degree of saturation than a corresponding dry specimen did. The effect of the initial moisture content was most likely caused by material properties and did not correspond to the conditioning technique. The same type of effect has been described in other studies, in which a different conditioning technique was used.

Moisture diffusivities were determined according to the water content and were presented as a function of the degree of vacuum saturation. For all three tested materials, an unexpected appearance of the moisture diffusivity was found where both the high and the low moisture range showed a maximum. The moisture diffusivity according to moisture content can theoretically be described by the product of the slope of the suction curve and of the moisture diffusivity in terms of suction. A steeply sloping suction curve will therefore result in a high moisture diffusivity in terms of moisture content. The suction curve and moisture diffusivity in terms of the moisture content were compared for the tested materials. Generally, the suction curves sloped steeply for both the low and high moisture ranges. It was clear that a steeply sloping suction curve corresponded to a maximum moisture diffusivity in terms of moisture content for all tested materials.

4 METHODS FOR DETERMINING TRANSIENT MOISTURE PROFILES

4.1 INTRODUCTION

There are several methods for determining moisture profiles. The most accurate is probably the "slice–dry–weigh method", which measures the moisture content directly. In this method, the specimen is rapidly sliced into discs that are weighed, dried, and weighed again. The water in the disc evaporates during the drying, and the water content in mass by mass can be determined directly from the weight loss. This method is, however, quite time-consuming and can in some cases present practical difficulties. Besides, it might also be difficult to split the specimen into discs thin enough to enable evaluation of a very steep moisture front.

The non-destructive use of thermal imaging is a well-known method used in determining heat loss in the walls of buildings. In this method, thermal properties are used to indicate the moisture content of porous building materials. Thermal imaging makes it possible to measure the fluid distribution in porous materials during absorption. It is the same principle as was used by Sosoro (1998). The basic principle of the method is to measure the evaporation heat from the split surface of a specimen exposed to a known moisture load. The evaporation heat, i.e. the measured temperature drop, is proportional to the moisture content of the specimen. The split is made in the intake direction, implying that the measured temperature distribution will provide a measure of the moisture distribution. The temperature decrease is relatively constant over time.

X-ray attenuation offers another non-destructive method suitable for measuring moisture content. The method is widely used for clinical studies, for example, and is based on the attenuation of an x-ray beam as it passes through a specimen. When the x-ray beam is transmitted through a specimen, variations in the bulk density and the thickness of the specimen will result in different degrees of attenuation. Therefore, measurements performed on different specimens of the same material, but containing different amounts of moisture, will result in different degrees of attenuation. A clear correlation between moisture content and attenuation has been demonstrated by Bentz and Hansen (2000) for cement-based mortar. For wood, computer tomography using x-rays has been widely used (cf. Lindgren, 1992 and Wiberg, 2001). Moisture transport properties have been studied for inorganic building materials by computer tomography using x-rays (see Bentz et al. 2000 and Bjerkeli, 1990). Gamma-ray attenuation has frequently been used in a way similar to x-ray attenuation (see e.g. Nielsen, 1973 and Quenard and Sallee, 1989).

Of the non-destructive methods described in this chapter, nuclear magnetic resonance (NMR) is the most direct method for measuring moisture content. The method is used in both clinical studies and materials research. Measurements are based on the possibility of measuring the energy of the hydrogen nucleus during the transition between different orientations in a magnetic field. The number of free hydrogen nuclei in a material is proportional to the energy from the transition (see Torpgaard, 2003). One disadvantage of NMR is an extremely high equipment cost. A comparison between moisture content measurements for wood by computer tomography using x-rays and NMR has been performed by Rosenkilde (2002).

Several researchers have tried to improve the technique of measuring the relative humidity profiles of materials. When using relative humidity as a tool to determine moisture content, the sorption isotherm has to be known. A sorption isotherm is normally determined at a certain point in time and then directly used. This method for determining the moisture content requires that the material structure should remain constant during the measurements. For natural stone and brick that is the case, but cement-based materials have the ability to react with the moisture and carbon dioxide in the air. Contamination of the material by salt ions in the pore water will also change the original sorption isotherm.

For some materials, translating the relative humidity into the moisture content entails continuous measurements of the sorption isotherm. Making this nearly impossible is the fact that the material structure will change differently over its entire volume. This means that several sorption isotherms have to be measured to represent all parts of a specimen correctly.

Beside this fundamental weakness, accurate measurements of relative humidity above the hygroscopic range are very hard to obtain. It takes an absolutely stable temperature to avoid condensation on the measuring probe. Since the slope of the sorption isotherm is very steep in the high relative humidity range for most inorganic building materials, the precision of moisture content measurements will be very low in this range. A better way to obtain moisture profiles is to measure the moisture content directly.

In this chapter, four different methods for measuring of moisture profiles are presented in detail, and thereafter evaluated to various extents in studies. Two of the methods are further examined, the thermal imaging method in the Annex and the slice and dry method in Chapter 5.

4.2 SLICE AND DRY

4.2.1 General

One of the simplest and most direct ways to measure the moisture profiles of porous materials during moisture transport is simply to split the specimen into different parts. After the splitting, each slice can be weighed, dried, and then weighed again; the moisture content can then be determined from the difference in weight. The main advantages of the slice and dry method are its simplicity and the relative affordability of the equipment needed. Calibration procedures are not needed since the moisture content is measured directly. To achieve high spatial resolution the slices must be as thin as possible.

The aim of the measurements is to measure transient moisture profiles, i.e. the moisture content profile of the specimen during wetting, drying, or moisture redistribution. One suitable way is to slice the specimen into several pieces oriented perpendicularly to the moisture transport direction, so that the moisture content will be constant in the direction parallel to the cross-section. To avoid moisture transport between the remaining slices, all slices need to be cut more or less at the same time.

The mass of a dry specimen is defined by letting the material dry at 105ºC until there is no change in weight. In experiments involving the handling of cement-based materials, some

exceptions have been made, as temperatures as high as 105ºC have in some cases altered the material structure. It has also been observed that a cement-based material can display different capillary properties after drying at a relatively high temperature versus after drying at room temperature. It is thus of great importance that cement-based specimens be handled as carefully as possible during conditioning before capillary tests, and an exception to the normal conditioning and drying temperature has been made for cement-based specimens. Such specimens were instead dried at 50ºC for both conditioning before capillary testing and for drying specimen slices for the subsequent determination of the moisture content.

When all the slices cannot be cut simultaneously, there is of course the possibility of estimating the moisture redistribution occurring during the cutting time. In practice, it is unlikely that the amount of time required to cut each slice will be exactly the same. This will result in moisture redistribution in that part of the specimen that has not yet been cut. When performing tests using materials with relatively low moisture transport coefficients, the redistribution rate will be very low and its effect quite limited.

4.2.2 Method

A more robust way of performing the slicing is to make all the cuts in the whole specimen at the same time. Cutting a specimen of brick or plaster requires very rigid cutting equipment. Besides the demand for cutting equipment stability, the specimen should not contain significant cracks or artefacts. If a specimen contains cracks running in various directions, it will simply be crushed into small pieces during cutting instead of being sliced into even slices. To determine the mean moisture content in each slice after cutting, it is very important that the slices should be relatively intact. If the slices are partly crushed and divided into smaller pieces during cutting, there are two problems: it will be difficult to know with satisfactory certainty to what slice a specific piece belongs, and it will be difficult to handle the specimen during drying and weighing. Even if it is possible to “collate” most of the small pieces, and ensure that they are grouped with the correct slices, the increased evaporation caused by the larger relative surface area of the smaller pieces would still be a problem.

However, the method does allow one-dimensional moisture transport to be correctly evaluated. Using the slicing method for a two-dimensional application requires a slicing technique that enables cutting in two directions. Since a study of one-dimensional flow is sufficient for the purposes of the present project, this research was only concerned with developing an apparatus for one-dimensional slicing.

At the beginning of the study, specimens shaped as prisms were considered for cutting. However, after several unsuccessful initial cutting trials, the cutting technique was instead tried on cylindrical specimens. The cutting equipment was designed so that the cutting knife blades could be varied in type and quantity; each knife blade was put in a slit in the cutting rig, and the total number of slits was thirteen with a distance of 15 mm between them.

However, the smallest possible distance between the cut edges, depending on splitting properties, was found to be 30 mm (see Figure 4.1). The test was performed on cylindrical specimens of Gotland sandstone. Specimens of lime–silica brick, brick, and mortar were also studied, but no

successful slicing could be done for these materials. Both cylindrical and prism-shaped specimens were tested.

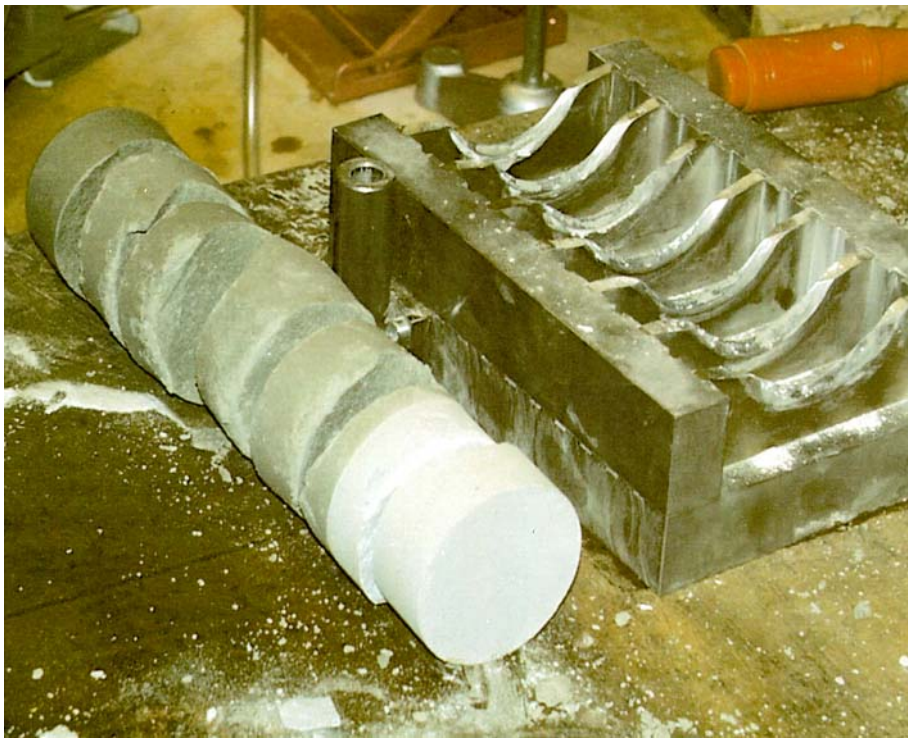

Figure 4.1 Cylindrical specimen of Gotland sandstone after cutting; total length 210 mm, diameter 62 mm. The slices were approximately 30 mm thick.

During the water intake phase, one end of the cylindrical specimen was put into contact with a water surface, i.e. the specimen was placed vertically in a plastic basin with a completely permeable interlayer between the specimen and the water to ensure a continuous water supply to the specimen. The level of water in the basin was adjusted so that only the end of the specimen made contact with the water. If the basin contains too much water during the water intake phase, there is always the risk that the water will not be in contact only with the end of the specimen, but also with the mantle surface; in that case the area of the wetted surface will be difficult to estimate.

Another more sophisticated way to perform the wetting phase is to mount a nozzle on one end of the cylinder. This nozzle can, for example, be made of plastic and sealed around the edge of the cylinder's end with a soft rubber gasket (see Figure 4.2); a screw clamp is then used to attach the base to the specimen. This technique was developed to avoid the need to have sealing compounds such as silicone in contact with the specimen (the hydrophobic effect of sealing compounds such as silicone and beeswax was noted during the research). Then the nozzle is connected to a tube that sucks water from a cup. To estimate the capillary water intake during the wetting phase, the cup containing the water is placed on a balance (the setup is shown in Figure 4.2b). A second tube was connected to the upper part of the nozzle, to make it possible to start

the wetting process by evacuating the air from the nozzle; when the air has been evacuated from the nozzle, a valve was closed.

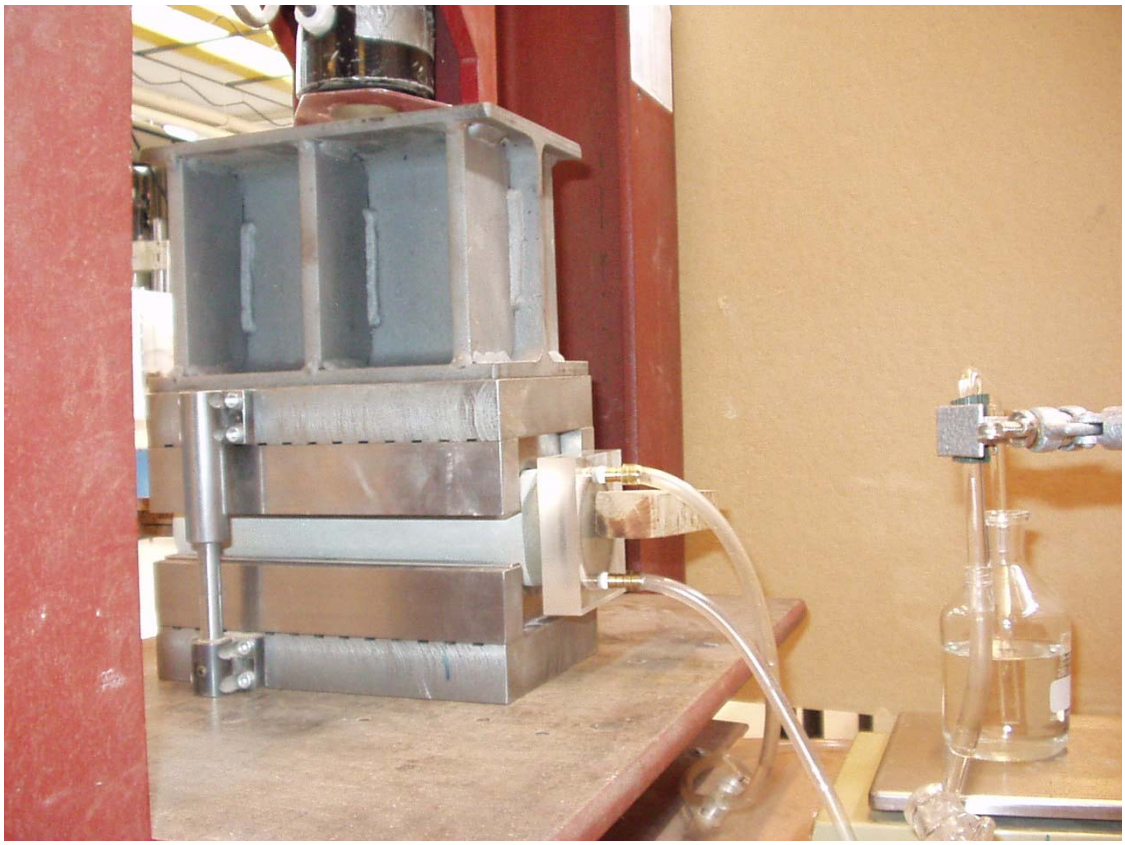

Figure 4.2a Cutting equipment with the stabilization beam attached on top. The complete equipment setup is placed in a rig equipped with a hydraulic jack. Tests were performed on Gotland sandstone prepared as a cylindrical specimen.

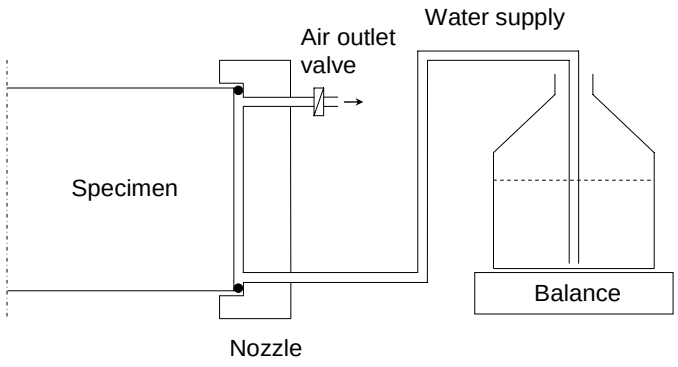

Figure 4.2b Schematic of the measuring setup for a cylindrical specimen during water absorption.

When a basin instead of a nozzle is used to supply the specimen with water during the wetting phase, there will definitely be a redistribution of moisture in the interval between the end of wetting and slicing. Such redistribution was avoided by using the plastic nozzle, since the specimen was placed in the cutting rig during the wetting phase; thus the wetting phase was followed immediately by the cutting without any redistribution.

4.2.3 Results

Different materials were used for the evaluation tests, materials such as lime–silica brick and cement mortar according to Section 2.2. Tests were also performed on brick and Gotland sandstone. Of the tested materials, only the Gotland sandstone could successfully be used with the slicing procedure (see Figure 4.1). The other two materials simply crumbled during the cutting process, as described in Section 4.2.2.

The Gotland sandstone used in the test has an approximate bulk density of 2060 kg/m^3 and a total porosity of 23%. The capillary porosity has been experimentally shown to be approximately 16%, resulting in a moisture content of 160 kg/m^3 in terms of capillary saturation.

Figure 4.3 shows the results of a test of capillary water intake for Gotland sandstone. The specimens tested were cylinder shaped, having a total length of 240 mm and a diameter of 62 mm. Before the test started, the specimens were allowed to dry at 105ºC until no change in weight was noted. The mantle surfaces of the specimens were covered with plastic film wrap to prevent evaporation during the test. The water intake phase, redistribution, and splitting were all performed at room temperature. The distance between the edges was 30 mm, and the total number of slices was eight. During the water intake phase, one end of the cylinder was put into contact with deionized water using the nozzle, as depicted in Figure 4.2.

The duration of the water intake phase was 1 h for all five specimens. Good correspondence between the mean moisture contents of the different specimens was found after the water intake phase. After the water intake phase or the redistribution, the specimens were immediately cut into slices using the cutting equipment. Redistribution was performed with the nozzle still mounted on the specimen, so the specimens were completely sealed during the redistribution phase. The time for redistribution ranged between 1 h and 24 h, according to the explanation on Figure 4.3. The interval between the end of water intake or redistribution and the commencement of cutting was only a few minutes. After cutting, each slice was put into a separate plastic container, covered with a lid to prevent water evaporation before weighing. A balance with a precision of thousandths of a gram was used for the weighing. Each slice was removed from its plastic container and weighed. After the first weighing, all the slices were dried at 105ºC until no change in weight was noted. Since the bulk density of Gotland sandstone was determined during the research, the bulk volume of each slice could easily be estimated once the dry weight was known. The moisture content of each slice after capillary suction was estimated by comparing the weight after cutting with the dry weight of each slice. The thickness of the individual slices varied slightly, but nearly corresponded to the 30 mm predetermined by the cutting equipment (see Figure 4.3).

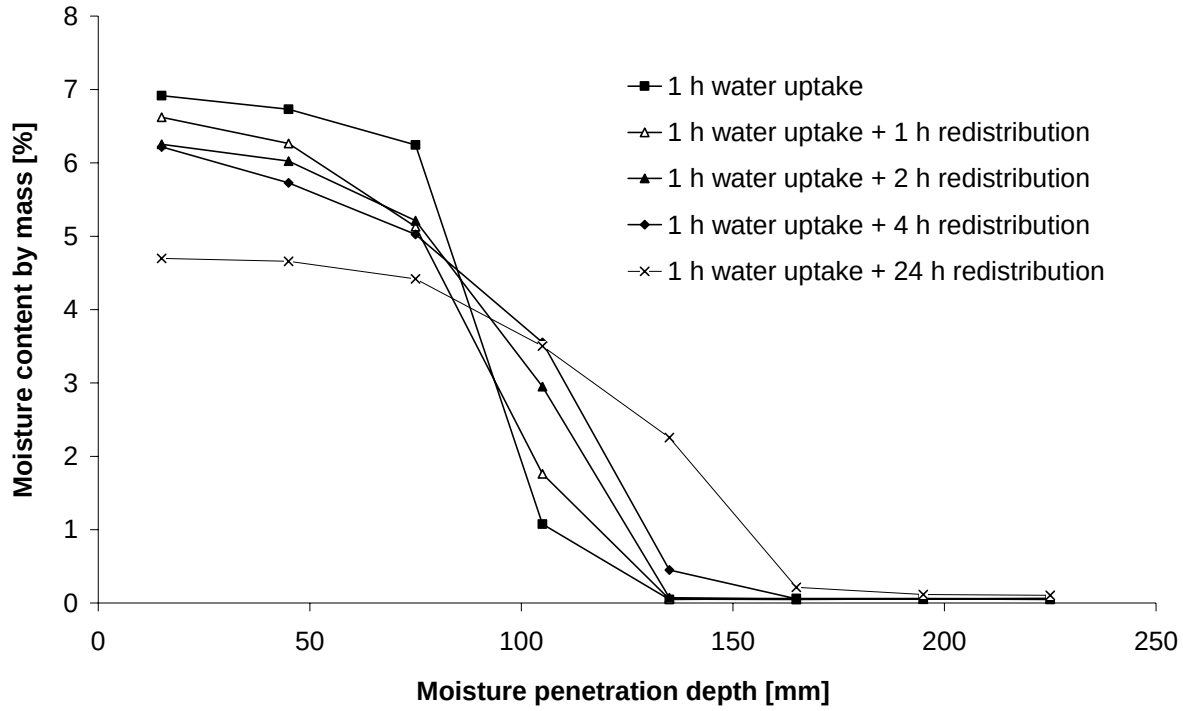

Figure 4.3 Moisture content as a function of penetration depth for individual cylindrical specimens of Gotland sandstone after 1 h of capillary water intake and various redistribution times.

4.2.4 Discussion

The primary strength of the slice and dry method is its simplicity. Since the moisture content measurements are based on simple weighing, they are hard to question. However, the specimens must be handled very carefully during the various steps. For example, evaporation from the wetted specimen must be prevented and the slices must be handled carefully to avoid damaging them.

A major disadvantage of the method was the difficulty of splitting specimens of inorganic material into thin and even slices. Problems performing the cutting arose when the thickness of the slices was less than 30 mm. The cutting technique was tried for several materials but was only successful for cylindrical specimens of Gotland sandstone. A spatial resolution of better than 30 mm in the water intake direction could not be achieved.

4.3 THERMAL IMAGING

4.3.1 General

Thermal imaging has been widely used in searching for heat bridges in the walls of buildings. The method has also been used on concrete bridges to determine areas with a higher chloride content and thus a higher moisture level. A higher moisture level on the concrete surface will result in a temperature decrease that can be registered using the thermal imaging principle.

4.3.2 Method

This measurement method is based on the fact that evaporation from the surface of a porous material will decrease the temperature of the surface. When a material has a moisture content corresponding to a higher relative humidity (RH) than that of its surroundings, evaporation will occur, resulting in a temperature decrease on the surface. If the moisture content is found to be the same in all measurements, the temperature decrease will also be the same, provided the surrounding conditions remain unchanged in terms of temperature and relative humidity. In most cases, differences in moisture create differences in evaporation and heat transfer to the surface; this will cause differences in surface temperatures.

The temperature decrease was measured with a precision of 0.1ºC using an active infrared camera placed one meter from the specimen. The tests were performed in a climate chamber. Specimens were thus exposed to a relatively constant climate, with only slight variations in temperature, relative humidity, and air velocity experienced during all the thermal measurements. The air pressure during the measurements was equal to atmospheric pressure. In the climate chamber the variations in each parameter were as follows: temperature 20.0 ± 0.1°C, relative humidity 33 ± 1%, and air velocity 0.7 ± 0.05 m/s.

The specimens of Gotland sandstone used for the test had an approximate bulk density of 2060 kg/m^3 and a total porosity of 23%. The capillary porosity was shown experimentally to be approximately 16%, resulting in a moisture content of 160 kg/m^3 in terms of capillary saturation.

The specimens were blocks of 200 × 150 × 30 mm. The surface that was exposed to water was 150 × 30 mm, i.e. absorption took place in the longitudinal direction of the specimen. The maximum penetration depth was consequently 200 mm. During capillary absorption the specimen was placed in a tub, and covered to prevent evaporation from the water surface. The water thus was the same temperature as the climate chamber was. The specimen was positioned so that the absorption direction was vertical. A plastic film was applied to the surface of the specimen during the capillary penetration phase to prevent evaporation and hence temperature decrease.

Before the specimens were used for the test, they were dried at 105°C for two days to ensure complete dryness. To keep the specimens dry, they were packed in double plastic bags and stored in a closed plastic box containing silica gel. The silica gel reduced the relative humidity in the box to a few per cent, and thus prevented the specimens from absorbing water from the air. The specimens were stored for a week in the climate chamber before the absorption tests were performed, so their temperature undoubtedly was the same as that of the climate chamber.

The procedure for measuring the surface temperature was the same on all measuring occasions. The specimens were split over a sharp edge along the capillary intake direction and exposed to the climate in the climate chamber. A fan, mounted half a meter from the specimen, created a turbulent air flow with a velocity of approximately 0.7 m/s over the split surface. The thermal measurement of the split surface was performed exactly 1 min after splitting the specimen. When the specimen is split, evaporation starts and the surface temperature begins to decrease. The amount of temperature decrease will differ along the length of split surface, depending on the moisture content, and there will be heat flow inside the specimen because of this. The part of the

specimen with the highest moisture content, and consequently the largest temperature decrease caused by evaporation, will be provided with heat from the rest of the specimen. Because the interval between splitting the specimen and commencement of thermal measurement was no more than 1 min, it could be assumed that the energy flow inside the specimen was negligible. The thermal measurements could not be successfully done directly after the splitting, as the evaporation requires approximately 0.5 to 1 min to produce a measurable temperature change. If the evaporation continues for more than 1 min, the temperature decrease will increase still further.

To calibrate the measured drops in temperature to the related moisture contents, specimens were conditioned to different initial moisture contents. The specimens were first dried at 105°C until no change in weight was observed; after that, every specimen was conditioned to a certain moisture content, from completely dry to capillary saturation in steps of approximately 20 kg/m^3. Containers filled with water were placed in the specimen storage boxes to keep the relative humidity as close to 100% as possible, preventing the specimens from losing any moisture through the plastic bags in which they were wrapped. Before splitting took place, the temperature of the specimens was the same as that of the climate chamber.

To achieve as homogenous moisture distribution as possible in the specimens, they were packed in double-sealed plastic bags and stored in sealed plastic boxes. The boxes were stored in the climate chamber for a month to give the moisture content of the specimens enough time to distribute itself as uniformly as possible by the time of the absorption test. The moisture distribution could never be completely uniform, since the conditioning consisted of a certain degree of absorption followed by a distribution phase. During the redistribution process, the outer parts of the specimen were subject to the desorption isotherm while the inner parts were subject to the absorption isotherm. For materials in which there is a difference between the absorption and the desorption isotherms, a certain difference in moisture content between the outer and inner parts of the specimen will always be present at the equilibrium state.

After the redistribution phase, specimens were exposed to water for 1 or 2 h. A total of six specimens were used in the test, i.e. three specimens for each test duration. After capillary water intake, the surface temperature decrease was measured using thermal imaging.

4.3.3 Results

Before the tests, a calibration procedure was performed by measuring the surface temperatures of specimens with known moisture contents. Figure 4.4 shows the surface temperatures of several specimens with known moisture contents. Some specimens had to be rejected because the moisture distribution in them was not uniform, which was clearly evident from differences in surface temperatures between the outer and inner parts of the specimens. The temperature of a completely dry specimen should have been 20.0ºC instead of the present 20.8ºC. This difference was caused by the fact that the emission factor of the specimen did not correspond to the settings of the camera. This had no influence on the results, since both calibration and profile measurements were performed on the same material and with the same settings of the camera. To increase the evaporation, the relative humidity in the climate chamber could be decreased, contributing to a more sensitive scale.

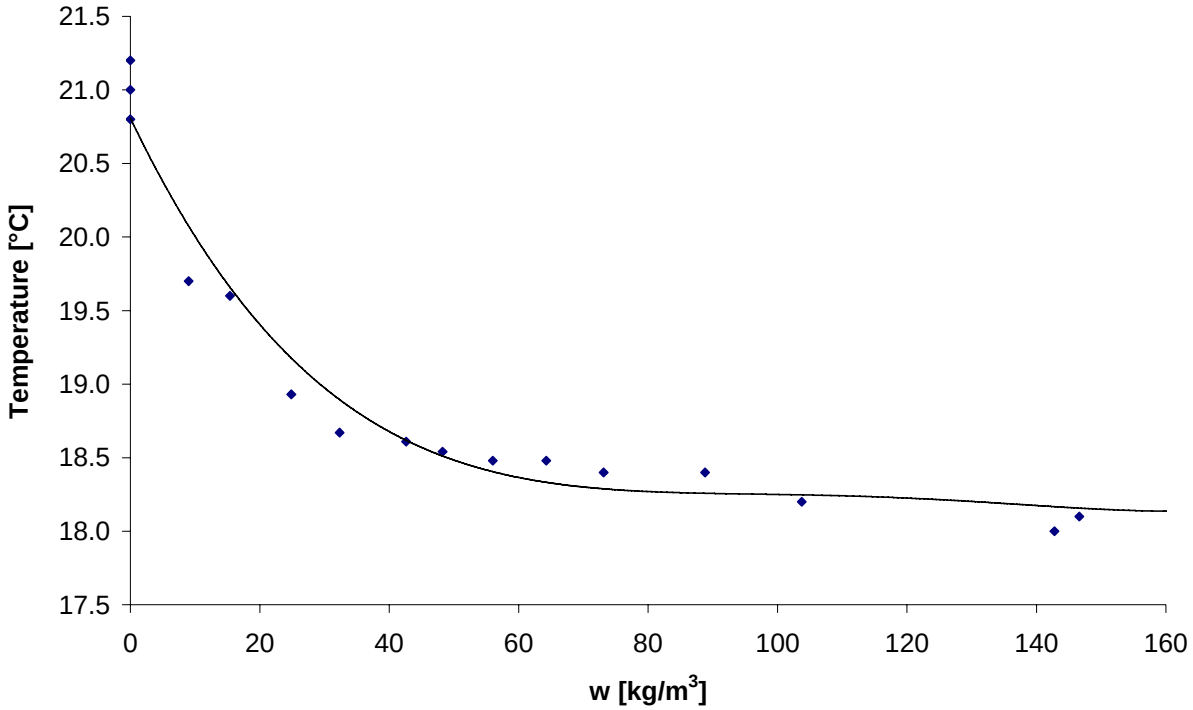

Figure 4.4 Surface temperature after splitting various specimens of Gotland sandstone conditioned to specific moisture contents.

Figures 4.5 and 4.6 show the surface temperature as a function of penetration depth after 1 and 2 h capillary absorption, respectively. The temperatures are transformed to moisture contents in Figures 4.7 and 4.8 using the temperature–moisture relationship depicted in Figure 4.4. Observe that the temperature distributions, and thus the moisture contents, of the different specimens are relatively equal behind the water penetration front, causing some of the points to be hidden.

The measured temperatures to the left in Figures 4.5 and 4.6 represent surface temperatures close to the wetted end. These temperatures are clearly lower than the lowest temperature in the calibration curve according to Figure 4.4. Therefore, the temperatures in this area could not be converted into moisture contents, resulting in the corresponding points being missing from Figures 4.7 and 4.8.

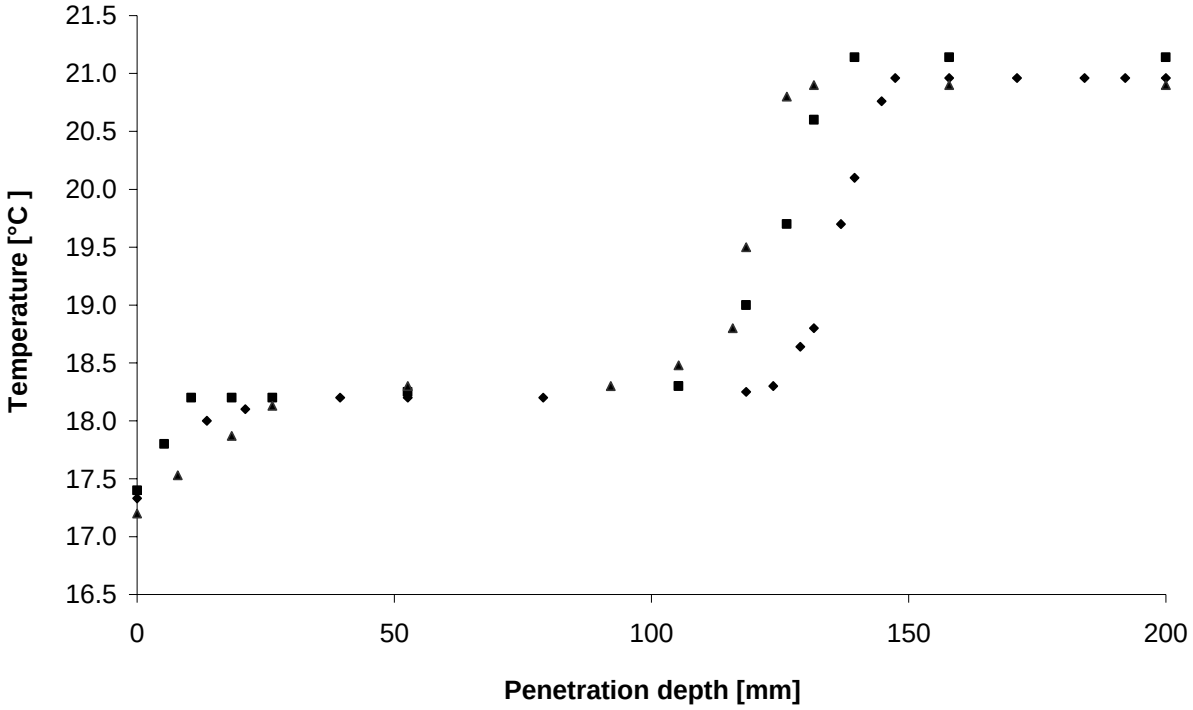

Figure 4.5 *Surface temperature as a function of penetration depth for three independent specimens of Gotland sandstone after 1 h of capillary absorption.*

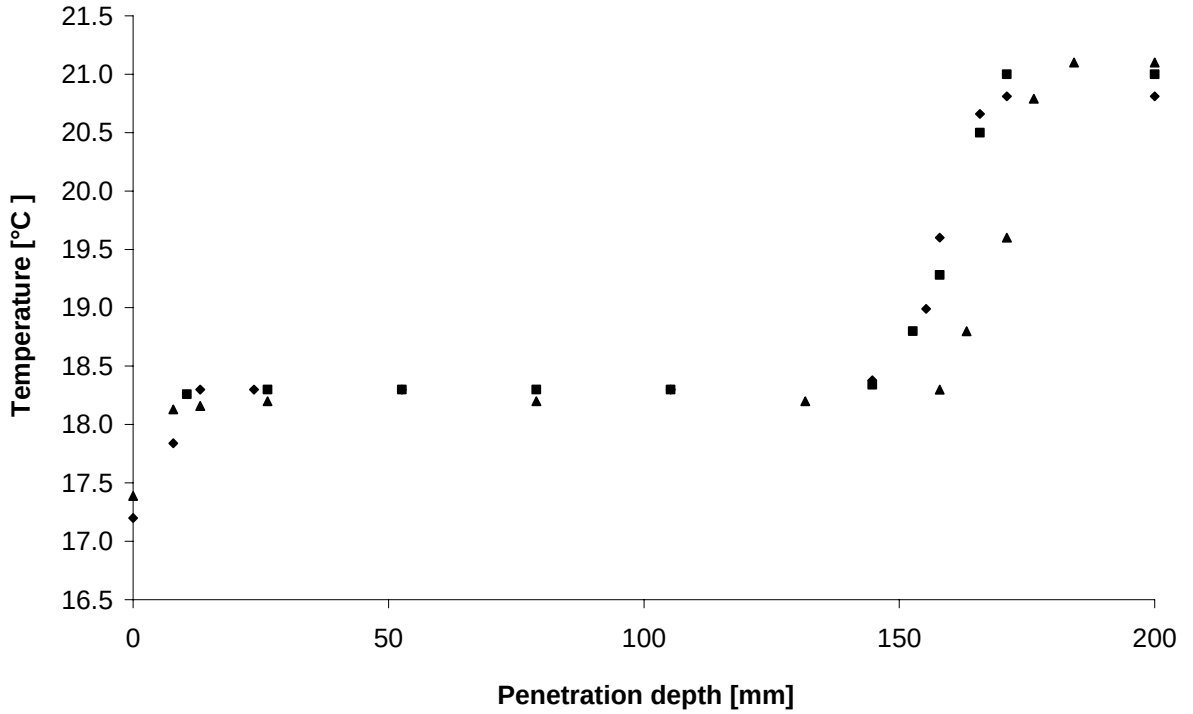

Figure 4.6 *Surface temperature as a function of penetration depth for three independent specimens of Gotland sandstone after 2 h of capillary absorption.*

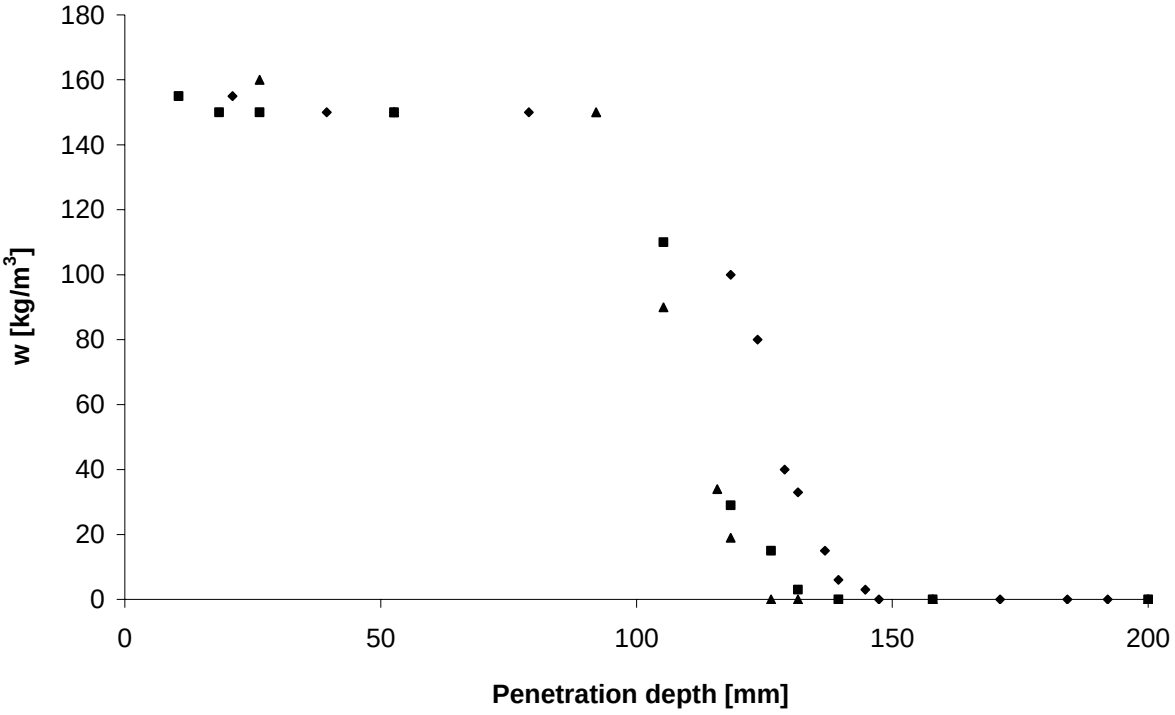

Figure 4.7 Moisture content as a function of penetration depth for three independent specimens of Gotland sandstone after 1 h of capillary absorption.

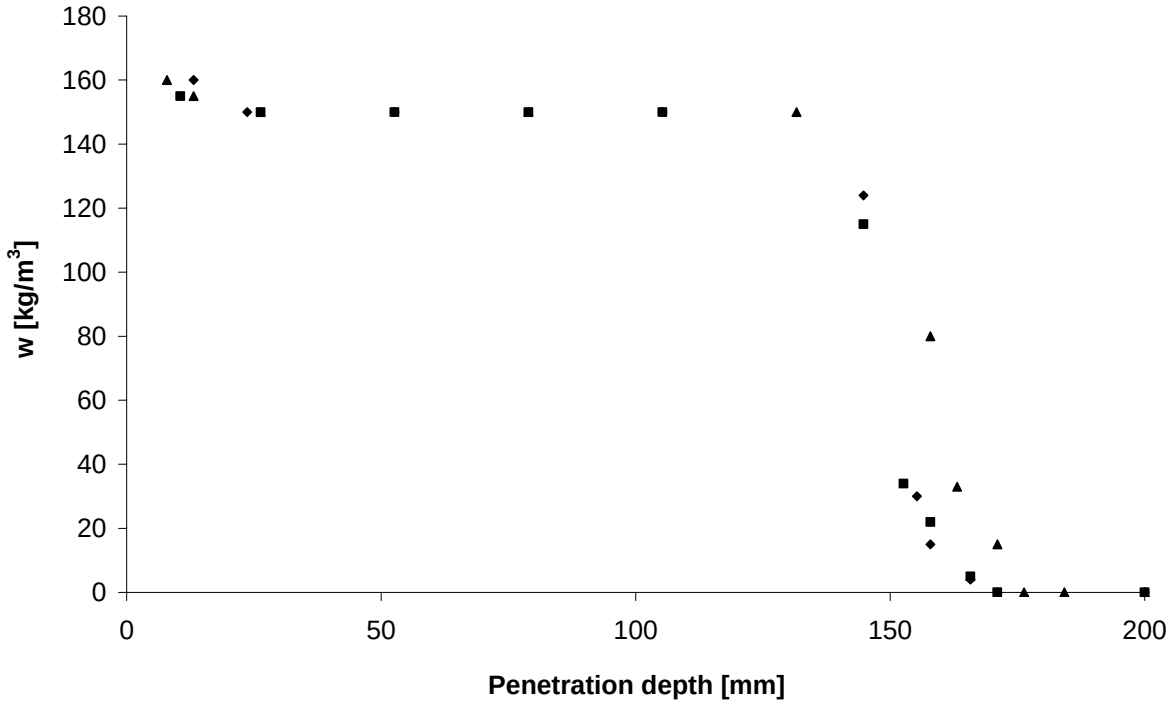

Figure 4.8 Moisture content as a function of penetration depth for three independent specimens of Gotland sandstone after 2 h of capillary absorption.

4.3.4 Discussion

The thermal imaging method, like the slice and dry method, is a relatively simple and inexpensive method. Using the thermal imaging technique to measure moisture profiles requires a calibration procedure, since the surface temperature decrease is what is being measured, instead of the moisture content directly. During calibration, the surface temperature decrease is determined as a function of moisture content. The calibration procedure is described in section 4.3.2.

Moisture contents in the area close to the wetted surface could not be determined from the calibration curve, since the low temperatures that appeared were not represented by the calibration curve. These low temperatures arose because evaporation was able to take place from both the previously wetted end and the mantle surfaces.

Better results can be obtained if the specimens are split along the water intake direction, instead of the measurements being directly made on the original surface. Hence, the cutting procedure prevents the same specimens from being used in repeated testing. A major disadvantage of the method is the relatively low resolution in the high moisture range, i.e. from a moisture content of 50 kg/m^3 and up to capillary saturation, as shown in Figure 4.4. The decrease in resolution is caused by the slope of the sorption isotherm, which is almost vertical in the moisture range from 50 kg/m^3 and up to saturation (see Janz, 2000). Because of the steep slope of the sorption isotherm, a change in the moisture content will not significantly affect the relative humidity and thus not significantly affect the surface temperature. The use of the thermal imaging method for determining transient moisture profiles is further discussed in Johansson (1999) and in the Annex.

4.4 X-RAY ABSORPTION

4.4.1 General

The x-ray absorption method is a non-destructive testing method which distinguishes this method from those mentioned in Sections 4.2 and 4.3. It is a major advantage to be able to reuse the same specimens in repeated testing. The x-ray absorption method is widely used for clinical studies and for material testing. For example, in material testing the method is used in the inspection of welding seams. The study of x-ray absorption described in Section 4.4.2 was performed at the Technical University of Denmark in Lyngby.

4.4.2 Method

The technique is based on the attenuation of x-rays, emitted by a transmitter, as they pass through a specimen of tested material. When using this technique to perform moisture profile measurements, a proxy parameter is measured instead of the moisture content directly. Therefore, the relationship between moisture content and degree of attenuation must be established before the moisture profiles can be determined. The method described in this section has been developed by the Danish company GNI®, and has been used by several researchers, including Bentz and Hansen (2000). Since the x-ray attenuation technique basically measures the density of a material, the method is most suited for measuring moisture content distribution in a

specimen. Figure 4.9 presents a schematic diagram of a setup for measuring moisture content using the x-ray technique. The amount of x-ray radiation transmitted through a composite material is shown in Equation 4.1 as Beer's law.

$$I = I_0 \cdot e^{-\sum \mu \rho t} \tag{4.1}$$

where

I_0 is the x-ray radiation from the source,

I is the x-ray radiation transmitted through the specimen,

μ is the mass attenuation coefficient of the tested material,

ρ is the density of the specimen, and

t is the thickness of the specimen.

Depending on the density of the specimen and its moisture content, various portions of the x-ray radiation will be absorbed in the specimen. A detector based on an NaI crystal measures the transmitted radiation, where a certain energy level corresponds to a certain density and thus a certain moisture content of the specimen (see Bentz and Hansen, 2000). Variations in the density, for example, caused by the presence of aggregate in a material, will produce variation in the amount of absorbed radiation. These variations can be considerable for materials such as mortar and concrete, in which there is a difference in density between the aggregate phase and the paste. Because of this, it is very important to control the path of the x-ray beam.

During the measurement process, the x-ray beam passes through a filter that divides it into two energy levels. After passing through the filter, the x-ray beam will have a constant diameter of 1.0 mm as it passes through the specimen (see Bentz and Hansen, 2000). Use of a collimated x-ray beam is necessary to control the volume exposed to radiation. The filters can easily be changed, and all filters contain a 0.1 mm copper layer and a 3.0 mm aluminium layer to protect human tissue from radiation exposure. The specimen type in combination with the voltage applied to the x-ray tube will determine the choice of filter.

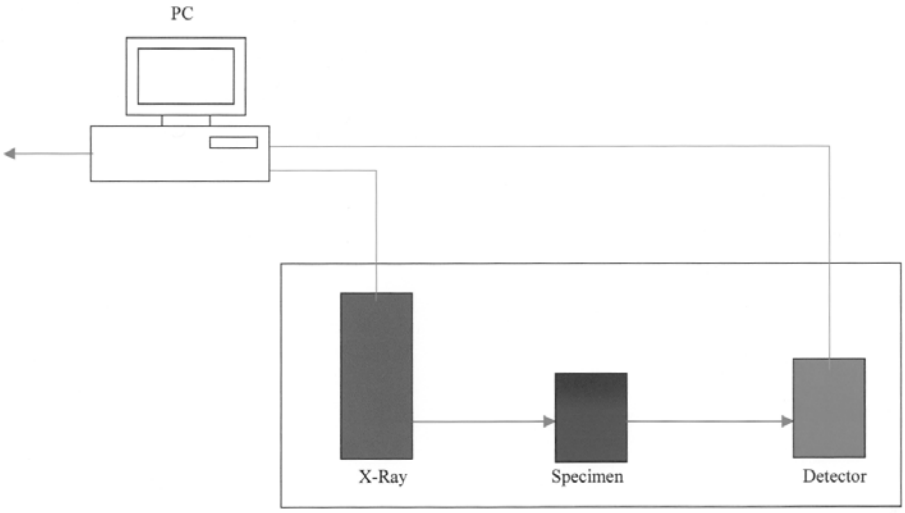

Figure 4.9 A schematic setup for measuring of moisture content using the x-ray attenuation technique. Drawing by GNI®.

During ongoing measurement the specimen can be scanned in two directions to determine different x and y values. This scanning can be performed since both the x-ray source and the receiver block are mounted on a frame (see Figure 4.10). The frame can be moved in the x direction, since it is attached to an approximately 800 mm long rail and driven by an electric motor. To perform measurements along the y axis, the x-ray source and the receiver block can be moved approximately 410 mm in relation to the frame. The distance between the x-ray source and the detector can be varied in the range of 350 mm. When moving the detector as close as possible to the x-ray source, the intensity of radiation can be up to sixteen times higher than when using a normal distance between the x-ray source and the receiver.

Obtaining repeated measurements of a specific specimen is crucial when determining moisture profiles during wetting or drying. One should bear in mind that the precision of movement is ±0.1 mm in each of the three directions (Bentz and Hansen, 2000). In an unfavourable case, for example, when repeated measurements are being performed on a specific specimen, the centre of the measuring point may deviate by up to 0.2 mm. This maximum deviation of 0.2 mm should be considered in relation to the 1.0 mm diameter of the measuring cylinder exposed to x-ray radiation. When performing repeated measurements, for example, when determining moisture profiles during wetting or drying, the deviation will mean that it is impossible to measure the moisture content in exactly the same cylinder on each measurement occasion; there will always be uncertainty as to the exact location of the measured volume.

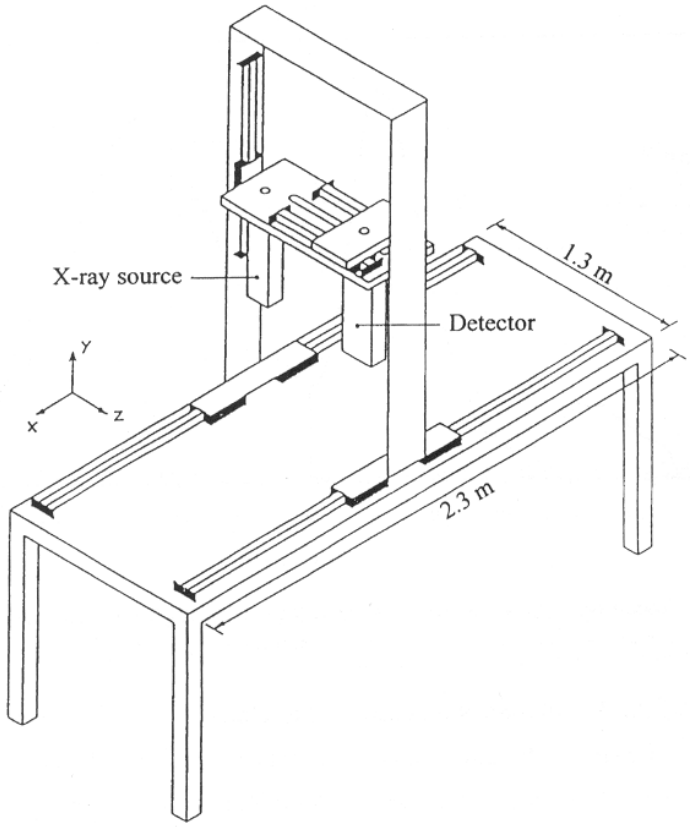

Figure 4.10 Setup for scanning using the x-ray attenuation technique, GNI®.

The testing equipment shown in Figure 4.10 was placed in a test chamber of 2500 × 1600 × 1000 mm. A test chamber was used, partly to reduce radiation exposure and partly to provide a climate shell for controlling the measurement conditions. The shielding of the chamber consists of 3 mm thick steel that reduces the outside radiation to less than 5 μS per h, measured 5 cm from the surface of the chamber. The observation window chosen also serves as a radiation shield, and consists of a 7 mm thick lead-containing glass. A climate control unit was attached to the chamber, providing it with air that was conditioned to the required relative humidity and temperature. The test chamber and the climate control unit were connected by ventilation ducting that together formed a sealed system. After the conditioned air leaves the climate control unit, it enters the test chamber through a long permeable hose to produce a diffused and low rate of air flow. The temperature can be varied between 10ºC and 90ºC, with an accuracy ±1ºC up to room temperature and ±0.5ºC in the range above. The relative humidity can be varied between 30% and 95%, with an accuracy of ±3%.

There are two ways to derive the moisture content of a porous material using x-ray technique. In the literature (e.g. Jensen, Damkilde, and Krabbenhøft, 2001), a theoretical method is often described and applied in which a derivation of Beer's law is used.

Another more robust method is to determine the correlation between moisture content and the amount of x-ray radiation, I , transmitted through specimens containing different amounts of water. For example, a number of specimens of the studied material can be conditioned to

different moisture contents, ranging from completely dry up to vacuum saturation. Before measurements are performed on the specimens, it is crucial that the moisture distribution in each should be uniform. The conditioning of materials to ensure uniform moisture distribution is described in Chapter 3.

The theoretical method requires that the mass attenuation coefficient, μ, from Equation 4.1 be known. The constant is material specific and is mentioned relatively frequently in the literature. However, in most studies the mass attenuation coefficient is measured individually for the different substances comprising the composite material of which the moisture content is to be measured.

For example, when measuring moisture content of cement paste, both the density and mass attenuation coefficient of the paste and water have to be known. A predetermined depth of water is exposed to the x-ray beam, and the x-ray radiation transmitted through the specimen, I, according to Equation 4.1 is measured. Since the density and thickness of the water are known, the mass attenuation coefficient, μ, can be derived. Using the same procedure, μ can also be derived for cement paste. When all the parameters relating to Beer's law are known for both components of the composite (i.e. water and cement paste), x-ray measurements of the composite can be made. During evaluation, Beer's law is used in instances in which the mass attenuation coefficient and thickness of the two components are known. Since the bulk density of the cement paste is also known, the only unknown variable is the concentration of water; the concentration of water describes the water content per volume in the composite specimen, and thus differs from 1000 kg/m^3.

A preliminary study was performed as part of the present research. Its aim was to analyze the possibility of measuring the moisture content of mineral-based materials with reasonable precision. Another issue that came up during the literature study was how the measurement method would react when measurements are performed on inhomogeneous materials. This is a highly relevant matter, since many building materials are inhomogeneous, for example, concrete, mortar, and lime–silica brick.

Lime–silica brick was used in the preliminary study, partly because it has been studied using other measurement methods in this work, and partly to investigate how the x-ray attenuation technique responds to an inhomogeneous material. The difference in density between the aggregate of limestone and the lime phase in the brick is smaller than the difference in density between the aggregate and the paste phase in concrete. The approximately bulk density of the lime–silica brick used in this study was 1895 kg/m^3 with a porosity of 28%.

4.4.3 Results

For the preliminary study, a number of 50 × 50 × 100 mm material prisms were prepared. After drying, the specimens were conditioned to particular moisture contents ranging from completely dry up to vacuum saturation, according to a method developed during the research and described in Chapter 5. The results of tests of three prisms with various moisture contents are shown in Figure 4.11. The first data series shows the level of x-ray radiation transmitted through a completely dry specimen. The specimen was scanned from end to end along its longest side;

there were 18 measurement points, spaced 5 mm apart. During the test, three specimens with varying moisture contents (see the figure label) were placed side by side on the frame.

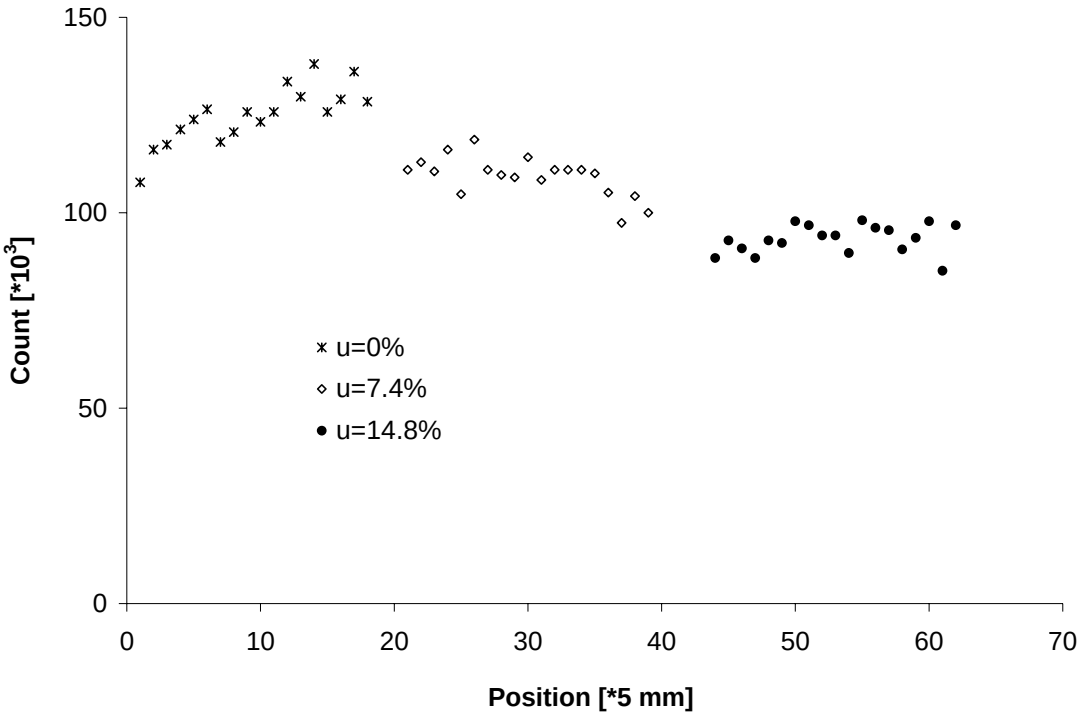

Figure 4.11 Results of the x-ray measurements for three different specimens of lime–silica brick with various moisture contents. In the figure, u represents the moisture content mass by mass.

4.4.4 Discussion

Figure 4.11 shows considerable scatter for a specimen of dry lime–silica brick in different positions. The scatter is most likely caused by variations in the bulk density of the material. Compared to the completely water-saturated specimen having a moisture content by mass of 14.8%, the scatter is less because the porous areas with lower densities are now saturated. Results for the dry specimen and the specimen with a moisture content by mass of 7.4% are hard to distinguish in several positions. Therefore, one can conclude that the x-ray technique is more suitable for homogenous materials of lower bulk density.

4.5 NUCLEAR MAGNETIC RESONANCE

4.5.1 General

The nuclear magnetic resonance phenomenon, here referred to as NMR, was discovered in 1946 by E. M. Purcell and F. Bloch, a discovery that earned them the Nobel Prize in physics. The measurement technique is often referred to as magnetic resonance tomography (MRT), magnetic

resonance imaging (MRI), or simply magnetic resonance (MR); these terms are most likely used to emphasize that the method is not associated with nuclear radioactivity.

One advantage of the NMR measurement method is that it is selective for different nuclear particles. For example, the hydrogen proton can be studied, such that the NMR signal will be proportional to the water content of the material. The NMR technique makes it possible to determine the moisture content directly, instead of by measuring a proxy parameter.

4.5.2 Method

The technique is based on the direct measurement of the number of free hydrogen nuclei in a specimen. When nuclei subject to a static magnetic field change positions in response to variations in a second, variable magnetic field, an electric current is induced in a receiving coil. The NMR measuring equipment consists of a primary magnet that produces a magnetic field, and three separate coils. The three separate coils are oriented orthogonally in relation to each other, and generate magnetic gradients in the three orthogonal directions, *x*, *y*, and *z*. Besides the main magnet and the three orthogonal coils, the equipment has a separate coil referred to as the RF coil, because it transmits and receives electromagnetic signals of radio frequency. In several types of equipment, the RF coil can be replaced with other coils of different sizes. Generally, the RF coil gives a better signal when it is placed as close as possible to the specimen.

NMR equipment used in medical applications normally has a main magnetic field of 1.5 to 2.0 T, that is, 30,000 times stronger than that of the earth. The main field, B_0 , causes the hydrogen nuclei in the field to spin in the field direction at a certain frequency, called the Larmor frequency, ω, according to Equation 4.2.

$$\omega = \gamma \cdot B_0 \tag{4.2}$$

where

ω is the Larmor frequency of spin for the hydrogen nucleus [MHz],

γ is the gyro magnetic ratio for hydrogen [MHz/Tesla], and

B_0 is the main magnetic field [Tesla].

The three gradient coils create a magnetic field, the field intensity of which is a function of the spatial position. The variations in the field intensity result in different values of the Larmor frequency for different positions in the field, according to Equation 4.2. The gradients in the magnetic field make it possible to determine the spatial position of a result in the field, *x*, *y*, and *z*.

To measure the number of hydrogen nuclei, the RF coil temporarily transmits a magnetic field. The spin is then oriented in the direction of the field of the RF coil. When the RF coil is deactivated, the spin returns to its original position, thus transmitting an electromagnetic pulse.

The intensity of the pulse is a function of the number of hydrogen nuclei in each spatial position. Both the electromagnetic pulse and the Larmor frequency are registered by the RF coil for each spatial point. An electric current is then be induced in the RF coil and recorded by a computer.

The results of the NMR measurement of a specimen are normally presented as a grey-scale image, in which the shade of grey is related to the NMR signal. A certain shade in the grey-scale image corresponds to a certain number of hydrogen nuclei, and the number of hydrogen nuclei also indicates the moisture content.

Testing was performed in co-operation with the Department of Radio Physics at Lund University Hospital to determine whether the NMR technique is suitable for making moisture profile measurements of inorganic materials. The NMR equipment used was delivered by Siemens® and designed for clinical studies. Before the tests took place, cement mortar, lime–cement mortar, and lime–silica brick, batch 1 (described in Section 2.2), were conditioned to different moisture levels (lime–silica brick, batch 1, will subsequently be referred to simply as "lime–silica brick"). It was known while preparing for the measurements that a certain iron content could disrupt the measurement process. Therefore, white cement instead of ordinary Portland cement was used so as to reduce the iron content of the tested mortars. Also, sawing the specimen with a conventional blade would have added small particles of iron to the specimen, enough to make measurement impossible. Therefore, a special iron-free blade had to be used in sawing the specimen.

Fifteen specimens, measuring 50 × 50 × 100 mm, of each of the three materials were conditioned; the specimens ranged from completely dry up to vacuum saturation. After conditioning, the specimens were stored to allow the moisture to distribute itself homogenously throughout the volume of the specimen. Both the conditioning and redistribution procedures are described in detail in Chapter 3. After the redistribution phase, individual measurements were performed on each specimen; the output was a grey scale, representing the concentration of hydrogen nuclei in a selected volume of the specimen.

Moisture profiles were also measured for water uptake durations of 3 and 6 h for lime–silica brick using NMR. The specimens were 50 × 50 × 100 mm, the wetted face being one of the short sides. Before wetting took place, the specimens were dried in a heating cabinet at 40ºC until no change in weight could be registered. To prevent evaporation during the wetting phase, the remaining sides were isolated with a thin plastic film.

4.5.3 Results

The most convenient method for determining the calibration coefficient, i.e. the relationship between the output signal and the moisture content, is to systematically measure the output signal for specimens with differing moisture contents. Such measurements have been performed for the three tested materials. Of the tested materials, only the lime–silica brick provided an output signal (grey scale) that could be evaluated. The output signal from the two other tested materials displayed too much distortion to be evaluated.

Figure 4.12 shows results of an NMR test of fifteen different prisms of lime–silica brick. The prisms were 50 × 50 × 100 mm and were conditioned to different moisture levels before the

measurements were made. The output of the NMR measurement process was a grey scale representing the concentration of hydrogen nuclei in a selected volume of the specimen. For the calibration evaluation, a mid-section (i.e. internal) volume of the specimen was chosen measuring 50 × 100 × 1 mm. If a volume close to the surface had been chosen for evaluation, boundary effects could have influenced the results. The grey-scale output was then digitized by a graphic processing program.

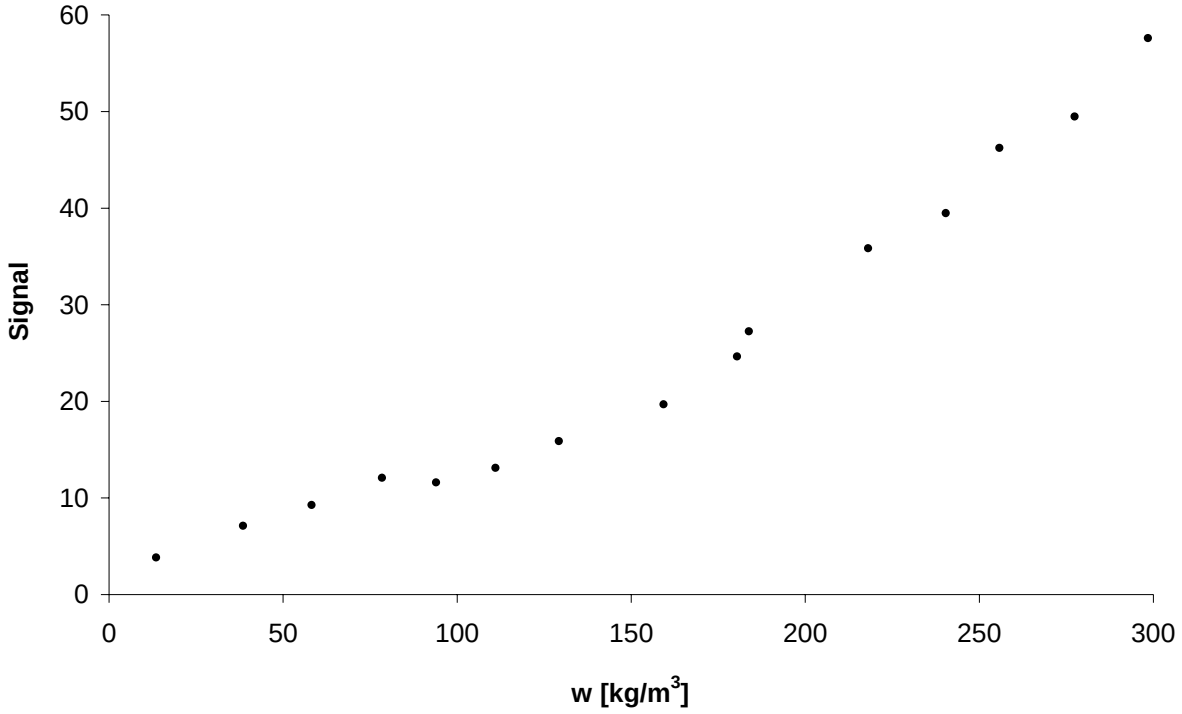

Figure 4.12 A calibration curve for fifteen different specimens of lime–silica brick, measured using NMR. The specimens were shaped as prisms and conditioned to certain moisture contents.

For both the moisture profile measurements presented in Figures 4.13 and 4.14, the wetted end was to the left and the mid section was chosen for the evaluation, as was the case in the calibration measurements. To transform the output signal into the corresponding moisture contents (see Figure 4.14), the relationship between the output signal and the moisture contents according to Figure 4.12 was used. A spatial resolution of 5 × 50 × 1 mm was chosen for the moisture profile evaluations. The length, height, and depth of the volume of a mid section parallel to the water intake direction were 5, 50, and 1 mm, respectively. In other words, the NMR signal for each point in Figure 4.13 was based on the concentration of hydrogen nuclei in a volume of 5 × 50 × 1 mm.

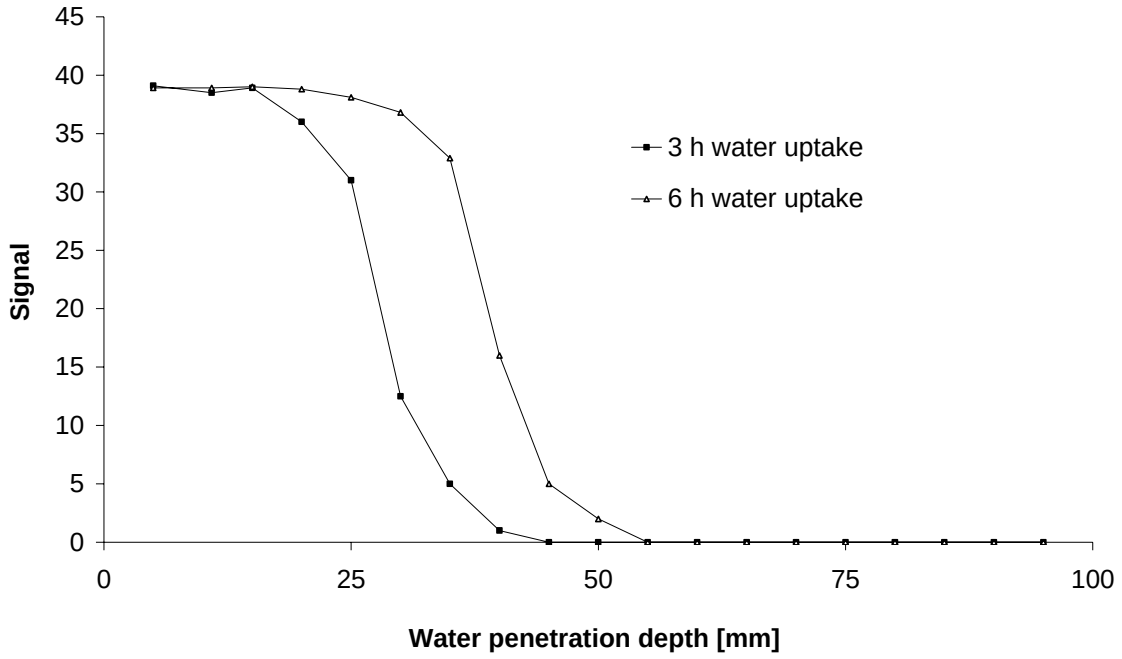

Figure 4.13 NMR signal as a function of penetration depth for individual specimens of lime–silica brick.

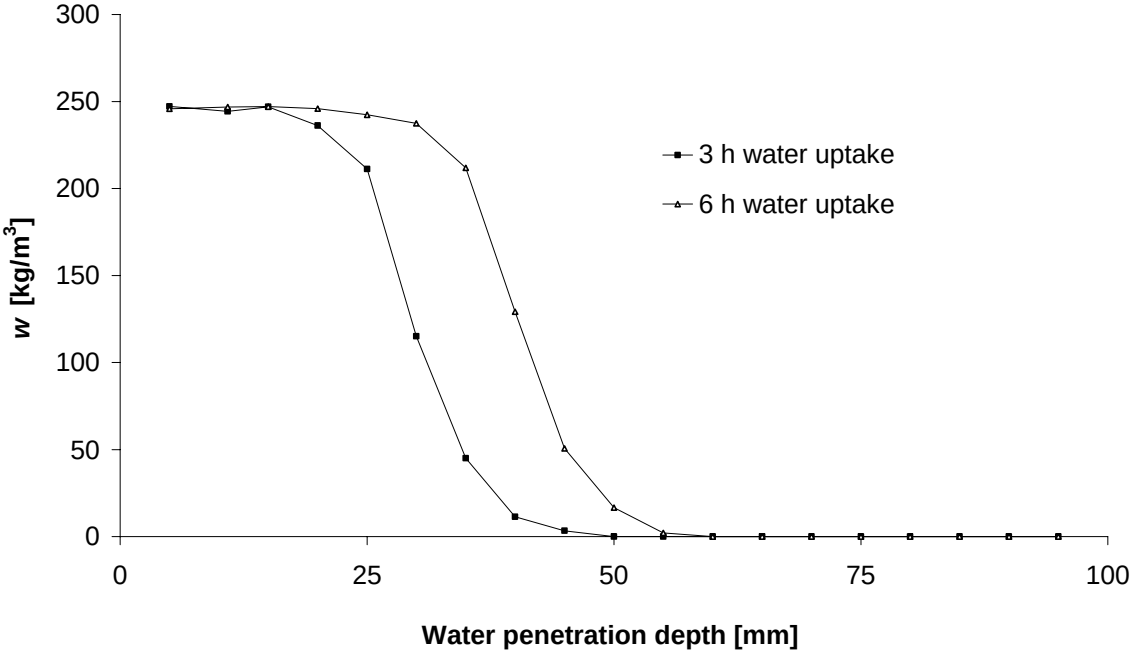

Figure 4.14 Moisture content as a function of penetration depth for individual specimens of lime–silica brick.

4.5.4 Discussion

When performing NMR measurements on materials that contain magnetic substances, the spatial resolution is affected. Fe and Mn are both strongly magnetic substances, and Portland cement, for example, contains approximately 3% Fe_2O_3. Even when Portland cement was excluded from the tested mortars and white cement (containing approximately 0–0.3% Fe_2O_3) was used instead, the output signal from the NMR was disturbed.

The additional iron content added via wear of the saw blade during specimen preparation was sufficient to disturb the measurements. When an iron-free saw blade was used for specimen preparation, useful results were obtained for the lime–silica brick. Output disturbances were still evident for the two mortars, despite the use of the iron-free saw blade, so we must conclude that the disturbance stems from the iron content of the white cement. To perform measurements on specimens that contain magnetic substances, special NMR equipment adapted to such conditions is required. Equipment that can be used on substances containing up to 6% Fe ions is described by Pel (1995).

The relationship between the output signal (grey scale) of the NMR testing and the water content (see Figure 4.12) was used as the calibration curve. Since the NMR technique measures the number of hydrogen nuclei in a given volume of specimen, the calibration curve was expected to follow a straight line passing through the origin of the co-ordinates. The measured calibration curve for the lime–silica brick followed the expected straight line through the origin of coordinates relatively well. Moisture profiles, according to Figure 4.14, were evaluated using the calibration curve. Both the penetration depth of the frontline of the moisture profiles and the moisture content behind the frontline corresponded fairly well to the measurements presented in Chapter 5.

The NMR equipment used provided a spatial resolution of 1 × 1 × 1 mm where the depth of the studied section was 1 mm. When digitizing the grey scale, so as to quantify the concentration of hydrogen nuclei, a height and width of 50 and 5 mm of the specimen was chosen to reduce the disruption of the NMR output. If the spatial resolution in the water intake direction had been set to 1 mm, the disturbance would have increased considerably.

4.6 CONCLUSIONS

The four studied measurement methods were evaluated for the measurement of moisture profiles during ongoing water absorption. All the methods had both strengths and weaknesses. For example, the NMR method had a very high resolution, both spatially and in terms of moisture content. However, with the NMR measuring equipment used for these tests, no useful results could be obtained for mortar, since even the minimal iron content of the white cement was sufficient to disturb the measurement process. Moisture profile measurements of lime–silica brick were successfully performed, however. Previous research has shown that NMR measurements, made using specially adapted equipment, can be performed on specimens with Fe ion contents up to 6%. Since the NMR technique allows a high spatial resolution, it is most suitable for moisture profile measurements of combined materials comprising a relatively thin

layer of mortar on an underlying material. The main reasons for not using the NMR technique for further research, despite its great precision, was equipment inaccessibility in combination with sensitivity to the iron content of the specimen.

As with NMR measurements, x-ray measurements also provide high spatial resolution. Since the x-ray technique measures variations in density, the method is unsuitable for inhomogeneous materials. Variations in density between the aggregate and the cement paste in mortar may be comparable to the variations in density between dry and wet portions of a specimen. Because of this sensitivity to variations in density within dry specimens, the x-ray technique had to be excluded from further moisture profile studies.

The thermal imaging method is relatively simple. To perform the measurements, all that is needed is a climate chamber with stable temperature and relative humidity levels as well as a thermal imaging camera. It is advantageous if the relative humidity in the climate chamber can be kept as low as possible, since the measurements are based on the temperature decrease caused by evaporation. However, the method is characterized by low resolution at high moisture contents.

During the thermal imaging tests we observed that the temperature decrease was unexpectedly great in the area close to the wetted end, resulting in the calibration curves not being applicable in this region. This anomalously low temperature was caused by evaporation from both the short end and the split surface of the specimen. Even if the short end was covered with plastic film immediately after the wetting phase, so as to prevent evaporation, the unexpected temperature decrease could only be reduced but not eliminated. Since this method was intended for making moisture profile measurements of composite materials, such as thin layers of mortar on an underlying material, in which the moisture content of the mortar is of a particular interest, the thermal imaging camera was excluded from use in further studies.

Of the tested measuring methods, the slice and dry method was the simplest, being based on weighing a specimen after a wetting phase. To determine moisture profiles, the specimens were sliced perpendicularly to the water intake direction directly after the wetting phase. It was difficult to make uniform slices of very brittle specimens, resulting in various thicknesses of the slices. If a highly accurate balance is used to weigh the slices and relatively uniform slices can be made, the slice and dry method is outstanding, considering the moisture content resolution it can provide.

For the studies of moisture profiles presented in Chapter 5, the slice and dry method was chosen for its high resolution of moisture content over the complete moisture range. However, the spatial resolution offered by the method did not completely meet the requirements, so small modifications had to be made for the studies presented in Chapter 5.

5 MEASURED TRANSIENT MOISTURE PROFILES

5.1 INTRODUCTION

A main purpose of performing the moisture profile measurements was to enable examination of the effect of an outer layer of plaster attached to masonry. Tests were performed on both single and combined materials. The combined materials were supposed to simulate masonry with an outer layer of mortar. A common opinion expressed in the literature is that the process of masonry break-down, caused by rain in combination with freezing, is largely determined by the properties of the outer layer of mortar.

Moisture profiles during wetting were thus measured for combined specimens comprising a background material corresponding to masonry and an outer layer of mortar with various properties. During the tests, both the moisture properties and the thickness of the outer layer of mortar were varied while the properties of the underlying masonry remained constant. Three materials were tested; the chosen underlying material represented the brick in masonry and the outer layer comprised one of two different mortars with different moisture properties. The compositions of the two mortars were specified so there would be a clear difference in their moisture properties, resulting in different sorption isotherms, suction curves, and moisture diffusivities.

Another important reason for performing the moisture profile measurements was to allow comparison between moisture profile simulations (see Chapter 6) and moisture profile measurements.

5.2 METHOD

5.2.1 General

Specimens of both single and combined materials were used for transient moisture profile measurements. The materials used for the transient moisture profile tests described in this chapter were lime–silica brick, lime–cement mortar, and cement mortar. Basic material data regarding properties of the tested materials, properties such as porosity and density, were presented in Chapter 2 along with the sorption isotherms of the materials. The corresponding moisture diffusivities were presented in Chapter 3.

Different methods for measuring transient moisture profiles during water uptake were analyzed in Chapter 4. Two of the studied measuring methods, the NMR and the slice and dry methods, could potentially be of interest for performing moisture profile measurements of the three studied materials. However, the iron content of the two mortars meant that NMR could not be used for the two types of mortars (see Chapter 4). In cases in which the moisture profile of only the lime–silica brick, but not of the outer layer of the mortar, is of interest, NMR can be used. However, since the moisture profiles of both mortars and lime–silica brick were of interest, another method had to be used for making the measurements (see Sections 5.2.2 and 5.2.3).

The slice and dry method was also evaluated in Chapter 4, where it was shown that only the specimen of Gotland sandstone could be successfully sliced. All three materials used for the moisture profile measurements presented in this chapter were unsuccessfully tested using the slice and dry method, since they could not be uniformly sliced. These materials cracked and broke during slicing, most likely because they were more brittle than the Gotland sandstone was. Therefore, without modification the slice and dry method could not be used in determining the moisture profiles of the materials studied in this chapter.

Tests showed that it was possible to slice the specimens of lime–silica brick by slicing off only one slice at a time. To perform the sawing so as to produce uniform slices without much cracking, notches had to be made on two of the long sides of the specimen (see Figures 5.1, 5.2, 5.5, and 5.6). Since redistribution of the absorbed water could occur in the interval between the end of the wetting phase and the completion of specimen splitting, the time used for splitting was minimized. The time required to saw off one slice was estimated to be approximately 5 s. Considering that the maximum number of slices was 12 for the specimens of combined materials, the total amount of time required to complete the slicing was approximately 1 min. When the time for slicing is considered in relation to the shortest duration of the wetting phase for the combined materials, i.e. two days, it is obvious that any redistribution occurring during slicing would have only a marginal effect.

Before the water uptake tests took place, all specimens were sawn to the required size, according to Figures 5.1, 5.2, 5.5, and 5.6. After sawing, the specimens were placed in a heating cabinet at 40°C. The heating cabinet was placed in a very well-ventilated laboratory, where the absolute vapour content of the indoor air corresponded to that of the outdoor air, i.e. the absolute vapour content in the heating cabinet was equivalent to the vapour content of the outdoor air at an equilibrium state. The absolute vapour content of the outdoor air was estimated using climate data, allowing for the time of year when the drying phase took place. Since the temperature in the heating cabinet was known and varied only slightly, the vapour content at saturation could be determined with great certainty. By relating the absolute vapour content of the air to the saturation point, the relative humidity of the air in the heating cabinet could be determined.

All specimens were sealed with several layers of plastic film on their long sides before the wetting phase took place. It was only the wetted side, seen as the short side to the left in Figures 5.1, 5.2, 5.5, and 5.6, that was not sealed. The short side opposite the wetted side was covered with a plastic bag held in place by a rubber band. Plastic film was not applied continuously on the short side as well, to make it easier for displaced air to leave the specimen during the wetting phase.

During wetting, the uncovered end of the specimen was put into contact with a water surface by placing the specimen vertically in a plastic basin. To secure the water supply, a completely permeable interlayer was placed between it and the specimen. The surface of the water was kept level by using the communicating vessel principle, so variations in water level were avoided during the water intake phase. When performing water absorption tests without using the communicating vessel principle, the level of the surface will sink as the specimen absorbs water. Since the surface of the water had to be adjusted very carefully, so that only the short end of the specimen was allowed to be in contact with the water surface, any drop in water level could

result in the specimen losing contact with the surface. On the other hand, too high a water level can result in the wetted area inadvertently increasing as water is sucked upwards along the long sides of the specimen. Even a minor rise in water level on the long sides of the specimen will result in a considerable increase in the wetted area. By using the communicating vessel principle, the water supply was stabilized during the complete testing process and the wetted area could be held constant.

During preliminary water absorption tests, it was observed that a layer of water could be transported between the specimen and the plastic film, if the film was allowed to be in contact with the surface of water. Since the formation of a layer of water between the plastic film and the specimen would affect the absorption rate considerably, precautions had to be taken. In the main water absorption experiments, the plastic film along the sides of the specimen was shortened by approximately 5 mm, so that the sides of the specimen were uncovered from the wetted side and 5 mm up the sides. In this way, the risk of water being transported between the specimen and the plastic film was eliminated. However, evaporation could occur via the 5-mm gap between the wetted side and the start of the plastic film. To prevent this, the entire basin setup used for the water uptake tests was put in a sealed plastic chamber. Since the plastic chamber was sealed, the relative humidity was just below 100% and evaporation from the uncovered part of the specimen was significantly reduced. The tests were performed in a climate-controlled laboratory, at a temperature of 20 ± 1°C.

Because of the use of only a single specimen for each wetting duration, the variation in the results could not be estimated. The specimens were sliced, as defined by the notches seen in Figures 5.1, 5.2, 5.5, and 5.6. Immediately after slicing, each slice was put on a balance so the wet weight could be registered before any evaporation could take place. After the splitting and weighing had been performed, the slices were dried in a heating cabinet at 40°C. To ensure that no material from the slices was lost during handling, each slice was put in an individual aluminium form immediately after slicing. Since the weight of these forms was known, the slices could be weighed and dried without being taken out of the forms.

After the slices had been dried and weighed, the moisture ratio, u [% by weight], of each slice could be determined. Then all slices were vacuum saturated again according to the process described in Section 2.4.2. During vacuum saturation, the complete open porosity became water filled under an external overpressure. After vacuum saturation, all the specimens were weighed again and the moisture ratio at vacuum saturation, u_{sat} [% by weight], was determined. Then the degree of vacuum saturation, u/u_{sat} , was determined for the individual slices after the wetting phase. The degree of vacuum saturation, u/u_{sat}, rather than the moisture ratio u [% by weight], was used as a measure of the moisture content of the specimen, since it was shown in Chapter 3 that the variation in degree of saturation at the capillary saturation point was smaller than the variation of the moisture content.

5.2.2 Single materials

Moisture profile measurements were performed on the single materials, lime–silica brick, lime–cement mortar, and cement mortar, after the continuous wetting phase. The duration of the wetting phase ranged from 6 h to seven days for the lime–silica brick, and from 0.5 h to 7 days

for the mortars (see Figures 5.7, 5.8, and 5.9). Five specimens of lime–silica brick and 9 specimens of each of the two mortars were tested.

The total length of the specimens of lime–silica brick was 240 mm and the total length of the specimens of lime–cement mortar and cement mortar was 100 mm. The lime–silica brick was obtained on the market, and the longest pieces that could be procured were 240 mm, corresponding to the general length of conventional bricks. The mortars tested were cast as part of this research project (see Section 2.2). During the casting, the fresh mortar was placed into 50 × 50 × 500 mm forms. After the curing phase (see Section 2.2), the mortars generally showed cracks perpendicular to the length of the forms. The cracks were regularly distributed over the length of the specimens, and thus the maximum possible length of a continuous specimen was approximately 100 mm.

After the specimens were dried and then sealed with plastic film to prevent evaporation (see Section 5.2.1), the capillary water uptake phase started. Briefer wetting phases were used for the mortars, since the length of the specimen used was just 100 mm. The specimens were cut immediately after the wetting phase. According to the cutting routine described in the previous section, the time required to cut each slice was estimated to be 5 s, resulting in total cutting times for the lime–silica brick and the two mortars (lime–cement and cement mortar) of 35 and 20 s, respectively. After being cut, each slice was dried and the moisture content was determined as a mean value for each slice.

Water absorption tests were performed on the single materials, lime–silica brick, lime–cement mortar, and cement mortar. The dimensions of the lime–silica brick are as shown in Figure 5.1, where lengths A, B, C, and D were 5, 40, 26.5, and 4 mm, respectively. The total length of the specimen was 240 mm with a width of 50 mm. The division of the specimen into slices by cutting is shown by the dotted lines. Water absorption was performed in five time steps, ranging in length from 6 h to 7 days, one specimen being used for each time step.

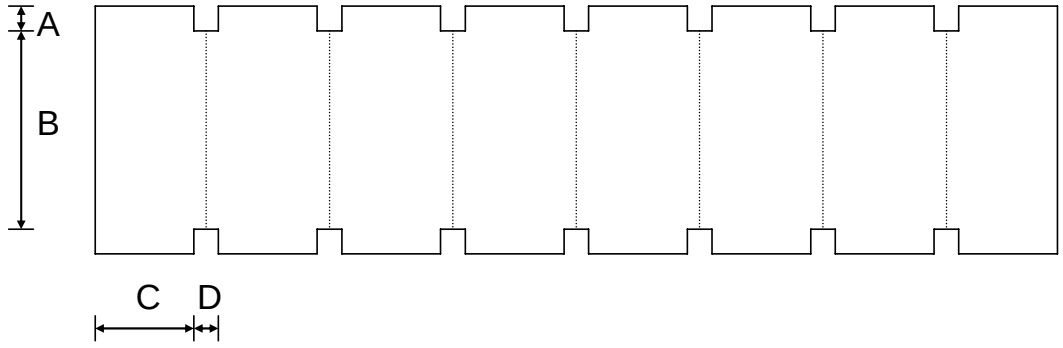

Figure 5.1 Principal dimensions of the lime–silica brick used for moisture profile simulations.

The single materials lime–cement mortar and cement mortar were also tested. The length of the specimens used for the moisture profile measurements was 100 mm (instead of 240 mm in the case of the lime–silica brick). The proportions of the specimens can be seen in Figure 5.2, where lengths A, B, C, and D were 4, 42, 16.8, and 4 mm, respectively. The division of the specimen

into slices by cutting is shown by the dotted lines. Both materials were exposed to continuous wetting for nine different time steps, ranging in length from 0.5 h up to 7 days. Shorter durations were needed here, since the specimens depicted in Figure 5.2 were considerably smaller. One specimen was used for each time step.

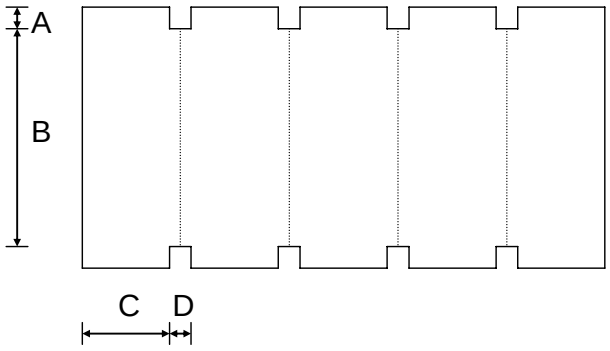

Figure 5.2 Principal dimensions of the lime–cement mortar and cement mortar specimens used for moisture profile simulations.

5.2.3 Combined materials

Water absorption tests were performed on combined materials as well. The combined materials were generally composed of an outer layer of mortar attached to an underlying specimen of lime–silica brick. The thickness of the mortar layer was either 7 or 14 mm, and both the lime–cement mortar and the cement mortar were tested in both thicknesses. The length of the underlying lime–silica brick was 240 mm (see Figures 5.5 and 5.6). The lime–silica brick was here divided into 12 slices rather than the 8 slices described in the previous section. While preparing for the tests of combined materials, it was discovered that the slices could be thinner than those of the single materials. To make the thinner slices, sharper knifes were used on the cutting equipment. Thinner slices resulted in better spatial resolution, since the moisture content was presented as the mean value of the moisture content of each slice.

The outer layer of mortar could not be sliced because of its thinness, so only a mean moisture level could be presented instead of a moisture gradient. Before the outer layer of mortar and underlying lime–silica brick were assembled, both materials were dried in a heating cabinet at 40°C. The mortars were separately cast in sealed forms (see Section 2.2). The mortars were not cast directly on the underlying lime–silica brick to avoid variation in the mortar properties. When mortar is cast on an underlying material which itself has absorbing properties, the water–cement ratio will, for example, decrease in the part of the mortar close to the underlying material, while the rest of the mortar retains the original quality.

Since the mortars were cast separately, the two well-defined materials were then assembled according to Figures 5.5 and 5.6 before the water uptake tests were performed. Before the materials were assembled, the surfaces facing the interface were plane ground to facilitate perfect hydraulic contact between the mortars and the underlying lime–silica brick. Initial tests showed that the capillary waterfront was hindered by the interface between the two materials, despite the

very smooth and flat appearance of the surfaces. That the waterfront was hindered was easily observed, by comparing the waterfront depths of specimens with and without an internal interface. The discontinuous hydraulic contact was most likely caused by small irregularities on the respective surfaces, hindering a continuous water phase between the two materials.

Since the hydraulic contact failed between the two materials, despite considerable effort put into making the surfaces as flat and smooth as possible, various intermediate layers were tested. An intermediate layer was used to even out the irregularities of the surfaces. Several possible intermediate layer materials were tested; to be suitable, the material should be able to maintain continuous contact between the two materials in both the capillary and hygroscopic moisture ranges.

A systematic method was developed for testing moisture transferring properties in both the capillary and hygroscopic ranges. The ability to provide continuous contact across an interface was tested by comparing the capillary absorption rates of two specimens of lime–silica brick. The specimens were 50 × 50 × 100 mm; the sides were covered with a thin plastic film, but both of the short ends were uncovered. One specimen was provided with an interface, i.e. it was sawn into two equal pieces of 50 × 50 × 50 mm, while the other specimen was kept intact. Then capillary water absorption tests were performed concurrently on both the undivided specimen and the two-piece specimen with the interface. Concurrent water absorption tests on the two specimens clearly revealed that the interface considerably hindered the capillary contact. Since the poor capillary contact across the interface was most likely caused by the roughness of the surfaces, different intermediate layer materials were tested. The materials tested included paper from filter bags, different types of polishing and dish cloths, and a piece of cotton cloth. Of the tested materials, the cotton cloth proved to be the only one that worked as an intermediate layer, providing a satisfactory contact between the two materials in the capillary range (see Figure 5.3).

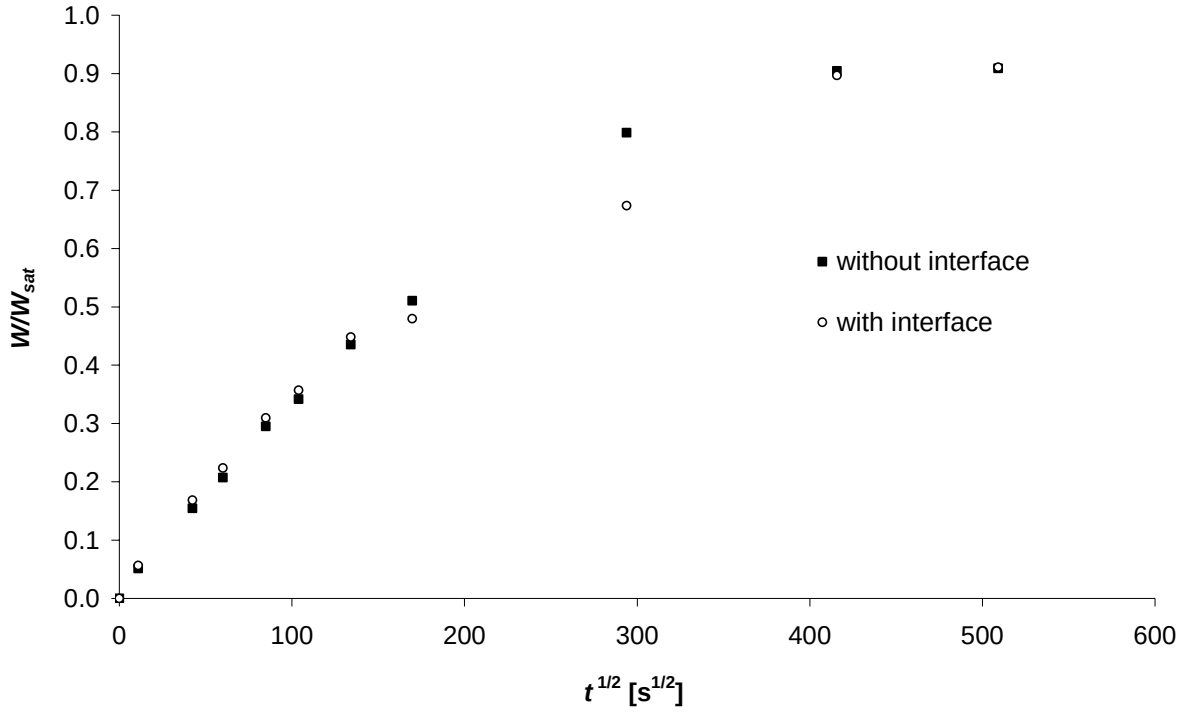

Figure 5.3 Capillary water uptake tests for two individual specimens of lime–silica brick. The specimen with an interface had an intermediate layer of cotton cloth.

Since the cotton cloth was shown to provide a perfect contact across the interface in the capillary moisture range, the resistance caused by the interface was tested in the hygroscopic range as well. For the tests, the well-known cup method was applied, described in detail by Hedenblad (1993). The specimens of lime–silica brick were 50 × 50 × 40 mm; the sides of the specimens were covered with a thin plastic film, but both short ends were uncovered. One specimen was provided with an interface, i.e. it was sawn into two equal pieces of 50 × 50 × 20 mm, while the other specimen was kept intact. Then both the undivided and the divided specimens were each put into a cup. In the cup, a free surface of water kept the relative humidity close to 100%. As one uncovered end was put into contact with the climate in the cup, while the other uncovered end was exposed to the room air in the laboratory, a moisture flow arose from the cup, via the specimen, to the room air. Since the two cups holding the two specimens were placed in the same room, the outer relative humidity experienced by both was equal; thus, the identical moisture loss from both cups proved that the moisture diffusivity was equal for both the divided and undivided specimens. Results of tests conducted with and without an intermediate layer of cotton cloth revealed no significant difference in the amount of evaporated water, despite the fact that the test duration was approximately 70 days.

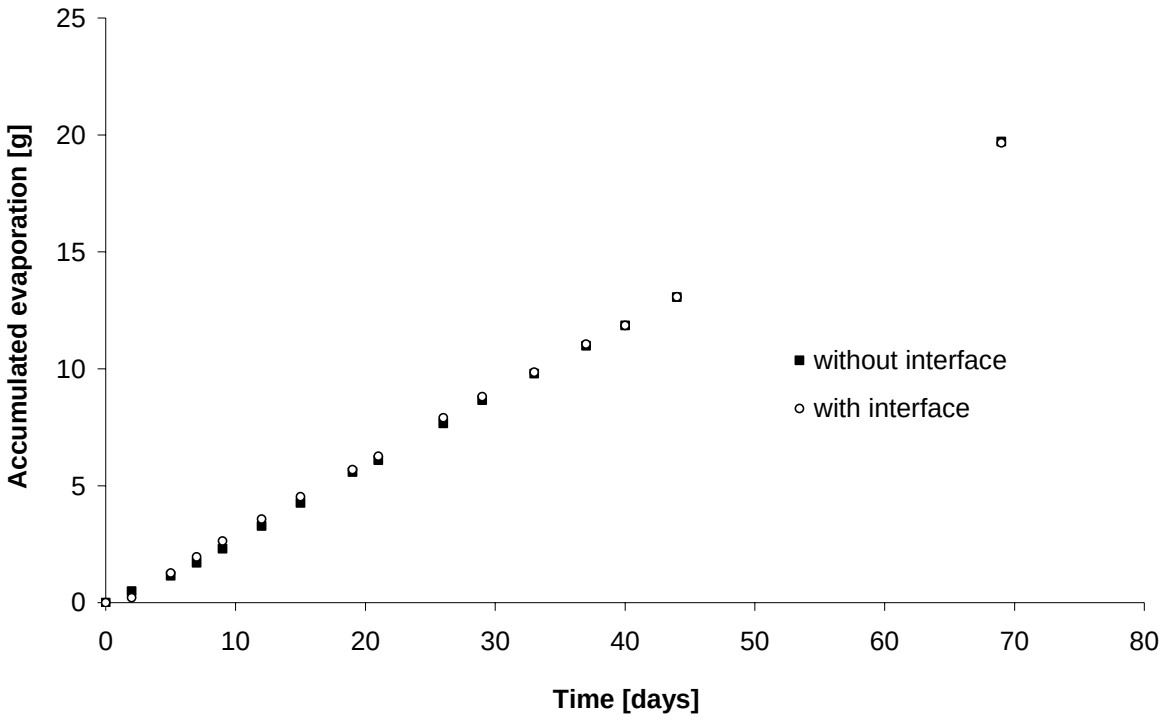

Figure 5.4 Cup method tests of two individual specimens of lime–silica brick. The specimen with an interface had an intermediate layer of cotton cloth.

Moisture profile measurements were performed on combined materials in which the underlying material was lime–silica brick for all material combinations. The outer layer was either lime–cement mortar or cement mortar, seen as the shaded areas in Figures 5.5 and 5.6. Figure 5.5 depicts a specimen of combined materials, in which the shaded area represents a 0.007 m layer of mortar and the rest of the specimen is lime–silica brick. The wetted area was the short end on the left of the combined specimen. The measurements A, B, C, D, and E in Figure 5.5 were 4.5, 41, 7, 17, and 4 mm, respectively, the shaded area representing mortar and the rest of the specimen being lime–silica brick. The total length of the specimen was 246.5 mm with a width of 50 mm.

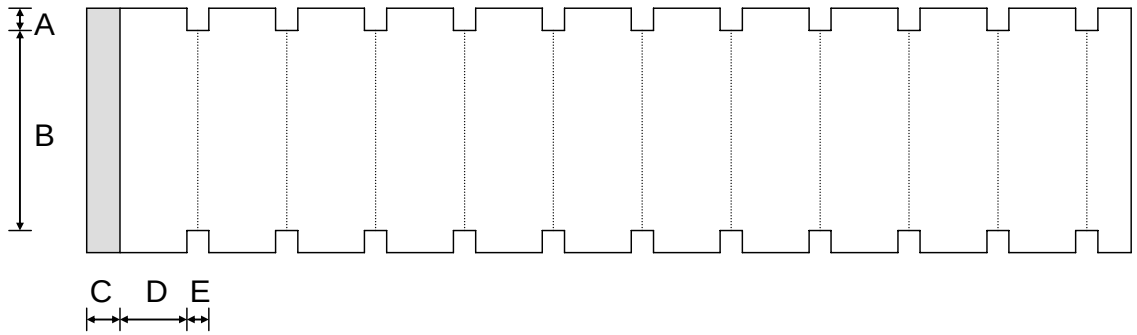

Figure 5.5 Principal dimensions of a specimen composed of 7 mm of mortar and lime–silica brick.

Figure 5.6 depicts the same type of combined specimen as Figure 5.5 does, except that the mortar layer is 0.014 m thick. Dimensions A, B, C, D, and E were 0.0045, 0.041, 0.014, 0.017, and 0.004 m, respectively, the shaded area representing mortar and the unshaded area lime–silica brick. The total length of the specimen was 0.2535 m and the depth was 0.05 m. In both Figures 5.5 and 5.6 the division into slices after cutting is indicated by the dotted lines.

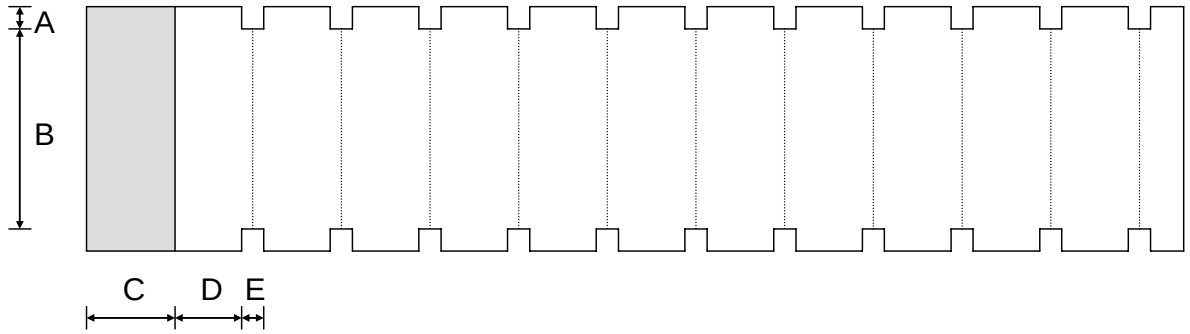

Figure 5.6 Principal dimensions of a specimen composed of 14 mm of mortar and lime–silica brick.

5.3 RESULTS

5.3.1 Single materials

Results of the moisture profile measurements for lime–silica brick can be seen in Figure 5.7. Each dot represents the mean value of the degree of vacuum saturation, w/w_{sat}, for the specific slices. The moisture profiles display a typical frontline appearance.

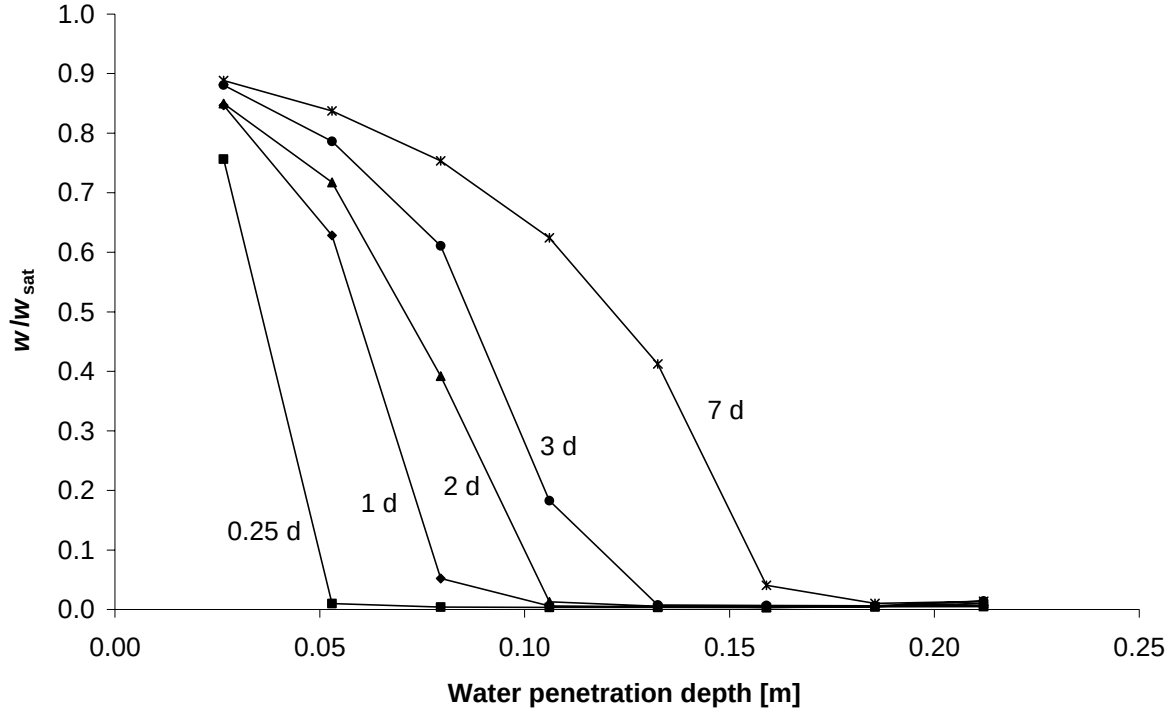

Figure 5.7 Moisture profiles for individual specimens of lime–silica brick exposed to continuous wetting by contact with water.

Results of the moisture profile measurements for lime–cement mortar and cement mortar can be seen in Figures 5.8 and 5.9, respectively. Each dot represents the mean value of the degree of vacuum saturation, w/w_{sat}, for the specific slices. The clear frontline of the moisture profile seen for the lime–silica brick could not be seen for either the lime–cement mortar or the cement mortar. Comparing the penetration depth for the three materials after one day of wetting, the lime–silica brick and the cement mortar displayed a penetration depth of 60 mm and 45 mm, respectively, while the lime–cement mortar displayed a penetration depth clearly exceeding 100 mm.

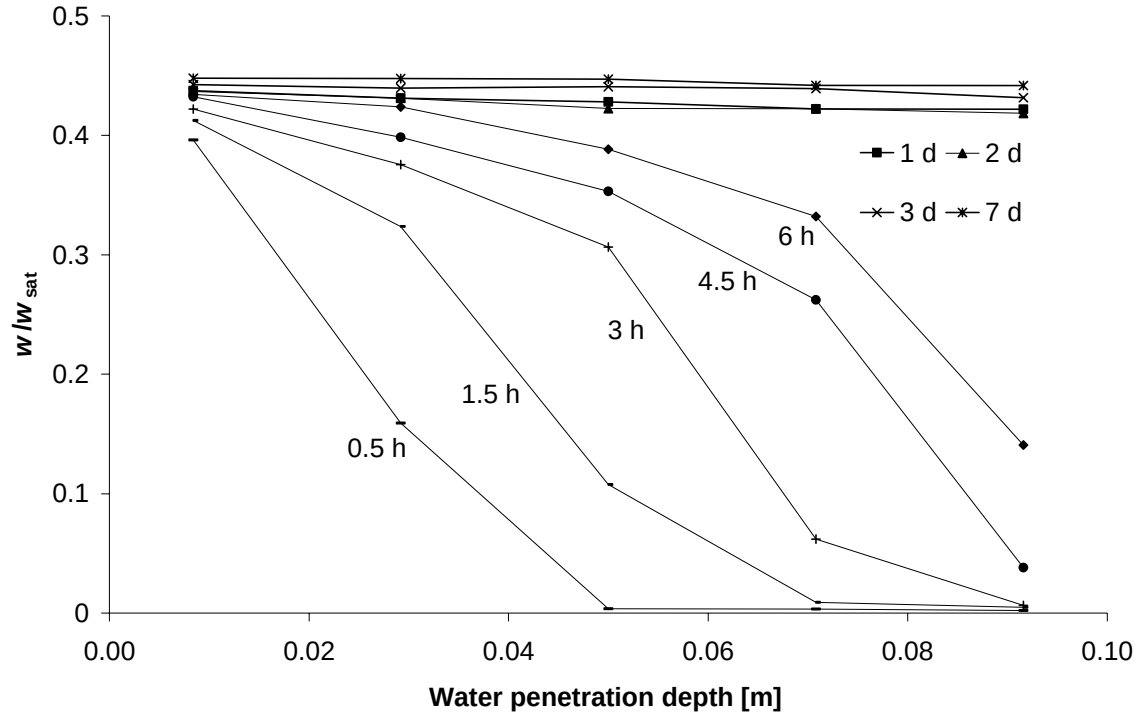

Figure 5.8 Moisture profiles for individual specimens of lime–cement mortar exposed to continuous wetting.

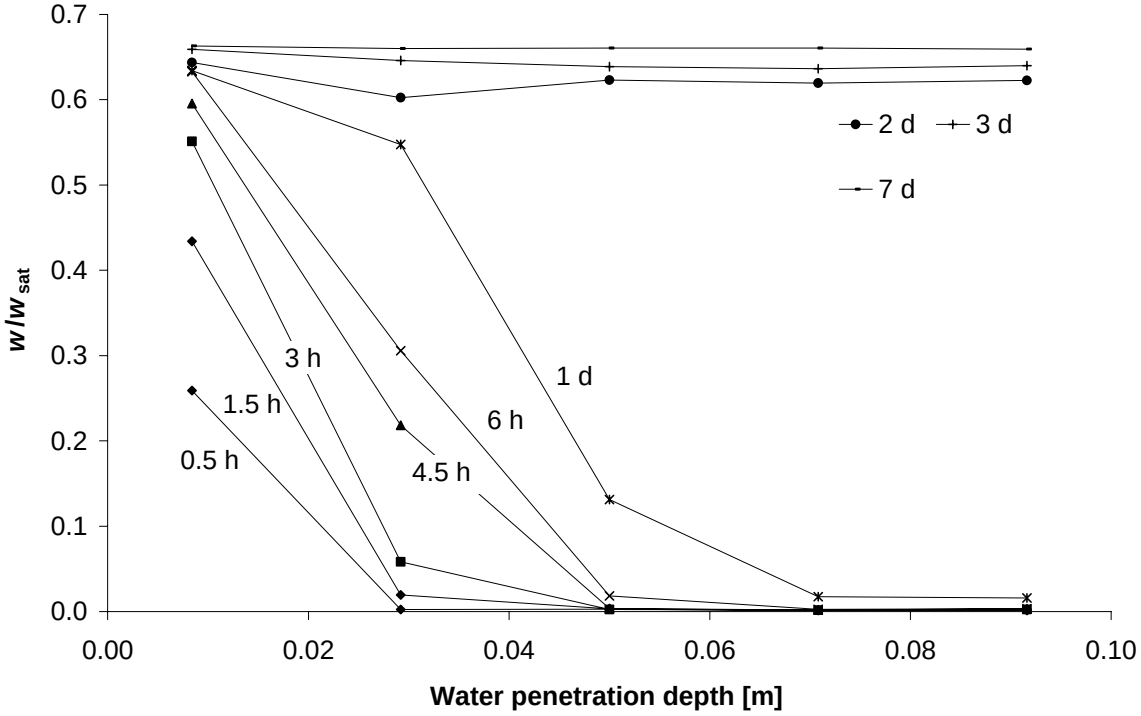

Figure 5.9 Moisture profiles for individual specimens of cement mortar exposed to continuous wetting.

5.3.2 Combined materials

Figures 5.10 to 5.13 present moisture profiles determined from water absorption tests of combined material specimens. The moisture level is represented by the degree of vacuum saturation, w/w_{sat}, which varied less than the moisture content, w [kg/m^3], did according to the tests presented in Chapter 3. The outer layer was either lime–cement mortar or cement mortar, and the underlying material was lime–silica brick. The unfilled dots represent the degree of vacuum saturation of the mortar, while the filled dots represent that of the underlying lime–silica brick. Since the slices of mortar could not be split, the results for the mortar are shown as a mean value. The slices of the lime–silica brick used here were thinner than those used in the tests of single materials presented in Section 5.3.1, giving a better spatial resolution.

It was clearly observed from both the 2- and 7-day water absorption tests that the specimen with an outer layer of cement mortar displayed a smaller penetration depth than did the specimen with an outer layer of lime–cement mortar. Also, the moisture levels in the underlying lime–silica brick were considerably lower for the specimens with cement mortar. An interesting observation was that the moisture level close to the interface in the lime–silica brick was almost constant for the respective material combinations for both the 2- and 7-day wetting tests.

In Figures 5.10 to 5.13 the results are separated according to the type of mortar. Results of the 2- and 7-day wettings in which lime–cement mortar was used as an outer layer are presented in Figures 5.10 to 5.11. It is clear that the thickness of the mortar is of minor importance to the penetration depth of the moisture front after a certain wetting duration. Even if the moisture content was only measured as a mean value for the layer of mortar, a slightly declining moisture gradient could be indicated, since the moisture level was a little lower for the 14-mm than for the 7-mm layer. The underlying lime–silica brick reached moisture levels close to capillary saturation in the area approaching the interface with the mortar.

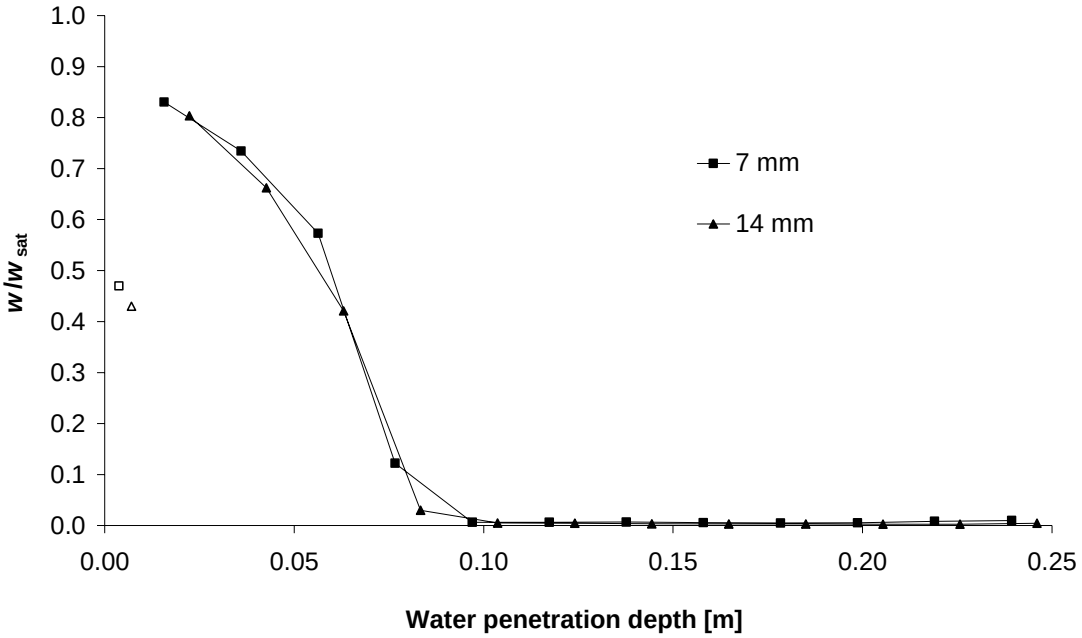

Figure 5.10 Moisture profiles for combined specimens with an outer layer of lime–cement mortar exposed to continuous wetting for two days.

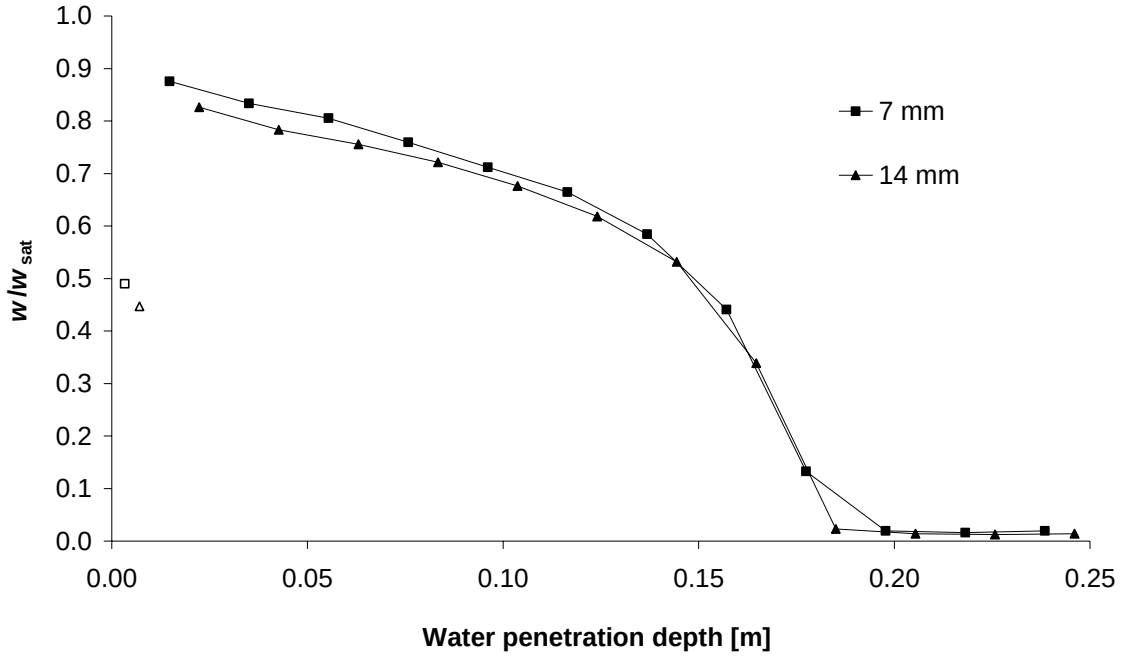

Figure 5.11 Moisture profiles for combined specimens with an outer layer of lime–cement mortar exposed to continuous wetting for seven days.

The results presented in Figures 5.12 to 5.13 are from the 2- and 7-day wettings in which cement mortar was used as an outer layer. Unlike when the lime–cement mortar was used as an outer layer, the moisture penetration depth was in this case somewhat dependent on the thickness of the cement mortar. The thickness of the 14-mm cement mortar layer clearly delayed the moisture profile compared to when the 7-mm layer was used. The mean moisture content of the cement mortar corresponded well to the capillary saturation point (see Chapter 3). No clear moisture gradient could be observed here for the layer of cement mortar. The moisture level of the underlying lime–silica brick was considerably lower here than when lime–cement mortar formed an outer layer. Also, the moisture profile penetration depth was less for specimens with a layer of cement mortar.

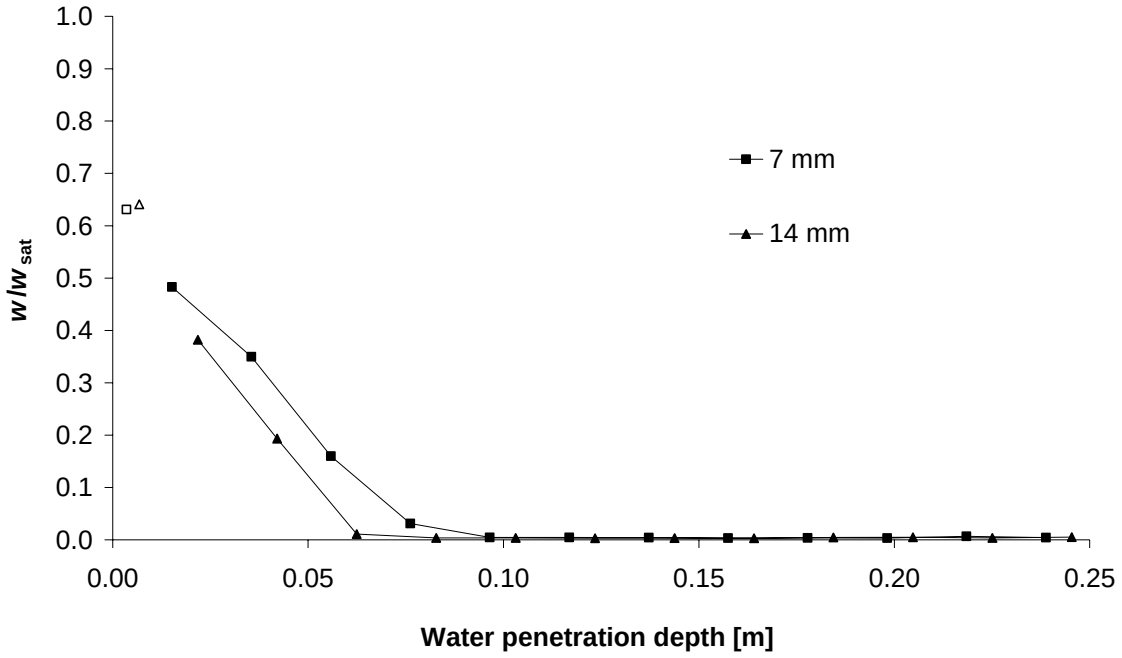

Figure 5.12 Moisture profiles for combined specimens with an outer layer of cement mortar exposed to continuous wetting for two days.

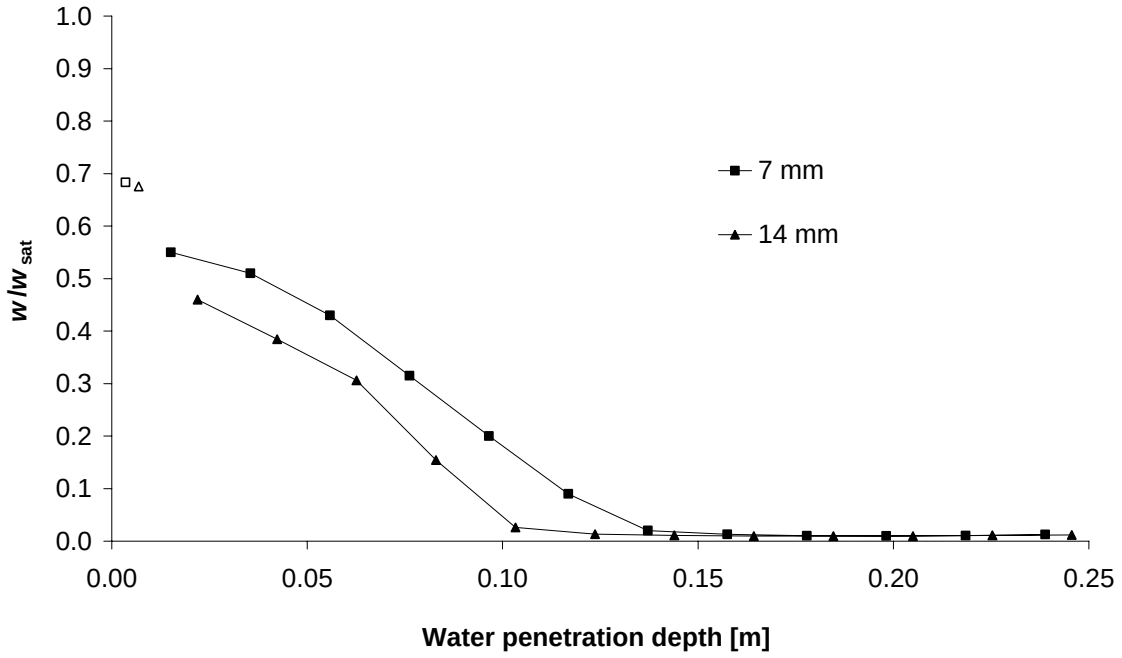

Figure 5.13 Moisture profiles for combined specimens with an outer layer of cement mortar exposed to continuous wetting for seven days.

5.4 ANALYSIS AND DISCUSSION

It was discovered during the water absorption tests presented in Chapter 3 that the scatter in the results obtained from different specimens of the same materials could be decreased if the degree of vacuum saturation was used instead of the moisture content to indicate the moisture level. Therefore, results pertaining to moisture levels are expressed as the degree of vacuum saturation, w/w_{sat}, instead of as the moisture content, w [kg/m^3], in this chapter as well.

The shape of the moisture profiles for the lime–silica brick were clearly distinguishable from those for both the lime–cement mortar and the cement mortar. The moisture profiles for the lime–silica brick were shaped like a frontline with a relatively steep slope, but the moisture profiles for the two mortars were flatter in appearance, without a marked frontline.

By studying the moisture diffusivities determined in Chapter 3 as a function of the moisture contents of the studied materials, the shapes of the different moisture profiles can be explained. The moisture diffusivity for the lime–silica brick, seen in Figure 3.23, indicated a relatively high moisture diffusivity in both the low and high moisture ranges, but a considerably lower moisture diffusivity in the mid moisture range. The lower moisture diffusivity in the mid moisture range resulted in a steeper moisture profile in the corresponding moisture range. The steeper moisture profile and thus the higher moisture gradient in this range were necessary to maintain the moisture transport, despite the low moisture diffusivity in this moisture range. The moisture profiles for the two mortars were slightly flatter than those for the lime–silica brick; this can be explained by the different moisture diffusivities, according to Figures 3.19 and 3.21, of the respective materials. Since the moisture diffusivities of the mortars did not display a minimum in the mid moisture range, but instead strictly decreased with increased moisture content, the frontlines of the moisture profiles were flatter.

After the water absorption phase, the specimens were cut according to the predetermined notches. Difficulties cutting all of the slices simultaneously for the tested materials meant that each slice had to be cut separately. The approximate time required to cut each slice was 5 s, resulting in a total cutting time for the single materials of 40 s for the lime–silica brick and 25 s for the mortar specimens. The cutting time for the combined materials was a little longer, since the underlying lime–silica brick specimens were cut into thinner slices. However, if the total cutting and moisture redistribution times are compared to the total duration of the wetting phase, one may regard the effect of any redistribution that may occur as negligible.

The results for the combined materials were determined in the same way as for the single materials. One difference was that the outer layers of mortar had to be left undivided, since they were too thin and brittle to cut. The use of undivided slices of mortar meant that the moisture levels of the outer mortar layers could only be determined as mean values, and that no gradient could be determined. However, a gradient could still be estimated by comparing the moisture levels in 7- and 14-mm mortar layers subject to the same wetting durations. These layers were expected to have the same moisture content in the region near the exposed surface; however, the mean values for the entire layers were different, indicating that there was a difference in moisture gradient.

The moisture content of the underlying lime–silica brick was generally lower when cement mortar rather than lime–cement mortar was used as an outer layer (see Figures 5.10 to 5.13). The obvious difference in the moisture content of the underlying material can be explained by the difference in the moisture diffusivities and sorption isotherms between the respective mortars and the underlying lime–silica brick.

For the combination of the lime–cement mortar and lime–silica brick it was clear that the underlying material would reach the capillary saturation point as soon as the water penetration front had passed through the outer layer of mortar; this was revealed by studying the moisture diffusivities presented in Figures 3.19 and 3.23 as well as the sorption isotherms in Figures 2.19 and 2.20. Comparing the moisture diffusivities for the entire moisture range up to the capillary saturation point revealed that the moisture diffusivity of the mortar was much higher than that of the underlying material. This difference meant that the underlying material could be provided with water with little hindrance from the outer mortar layer. Despite the higher moisture diffusivity of the mortar, a slight gradient in the moisture content was observed, with a declining moisture content moving away from the wetted surface and towards the interface between the two materials.

The sorption isotherm of lime–cement mortar depicted in Figure 2.20 slopes steeply in the high moisture range, indicating that the moisture content in this range can decrease considerably with even slight changes in the relative humidity and the pore water pressure. Thus a decreasing moisture gradient from the wetted surface to the interface in the lime–cement mortar would not necessarily mean that the underlying material was subject to a relative humidity level much below the saturation point. It was most likely that the underlying material was able to reach the capillary saturation point despite the fact that the lime–cement mortar displayed a decreasing moisture profile. By studying the moisture profiles in Figures 5.10 and 5.11, it can be seen that the thickness of the lime–cement mortar did not significantly influence either the shape or the moisture penetration depth of the moisture profile. The lack of influence of the mortar thickness was most likely caused by the fact that the moisture diffusivity of the mortar exceeded that of the underlying lime–silica brick in the actual moisture range.

The moisture profiles in Figures 5.10 and 5.12 indicate that when the cement mortar formed the outer layer, the frontline of the moisture profile was delayed compared to when the lime–cement mortar was used. Also, the moisture levels of the underlying lime–silica brick were influenced by the cement mortar, and reached little more than half-way to the capillary saturation point in the area close to the internal interface. The delay of the moisture profile frontline and the generally lower moisture contents of the underlying lime–silica brick were most likely caused by the difference between the moisture diffusivities of the mortar and of the underlying material, in combination with the difference in the sorption isotherms. The moisture diffusivities and sorption isotherms for the two combined materials are shown in Figures 3.21 and 3.23 and in Figures 2.19 and 2.21, respectively.

By comparing the moisture diffusivities of the mortar and of the underlying materials, it was observed that the mortar had a lower moisture diffusivity in the actual moisture content close to the capillary saturation point, while the underlying lime–silica brick had a higher moisture diffusivity over the complete moisture range. This difference in moisture diffusivities was most

likely the main reason for the delayed moisture profile frontline, since the outer layer of cement mortar was unable to provide the underlying material with the same moisture flow as the lime–cement mortar was. That the delay of the moisture profile frontline was caused by the lower moisture diffusivity of the cement mortar was also confirmed by the results presented in Figures 5.12 and 5.13, in which the increase in the thickness of the cement mortar from 7 mm to 14 mm was found to delay the frontline utterly. The higher moisture diffusivity in the underlying material than in the outer layer of cement mortar most likely caused a moisture gradient in the mortar, and the moisture content decreased with increasing distance from the wetted surface. By studying the sorption isotherms for the two combined materials in Figures 2.19 and 2.21, it was observed that the sorption isotherm of the outer layer of cement mortar was much flatter than that of the lime–silica brick in the high moisture range. Therefore, a decrease in the moisture content of the cement mortar from the capillary saturation point resulted from a decrease in the relative humidity. Since the sorption isotherm of the underlying lime–silica brick sloped steeply in the corresponding moisture range, a decrease in the relative humidity resulted in a considerable decrease in the moisture content. The decrease in the moisture content of the underlying material when the cement mortar was used as an outer layer is obvious in Figures 5.12 and 5.13.

Observe that the sorption isotherms presented in Figures 2.19 to 2.21 (as discussed above) reflect desorption. Since the tests presented in this chapter were performed at absorption, the relevance of the desorption isotherms can be called into question for a comparison of direct values but still be of interest for a qualitative discussion. The estimated absorption isotherms are presented in Figures 6.2 to 6.4.

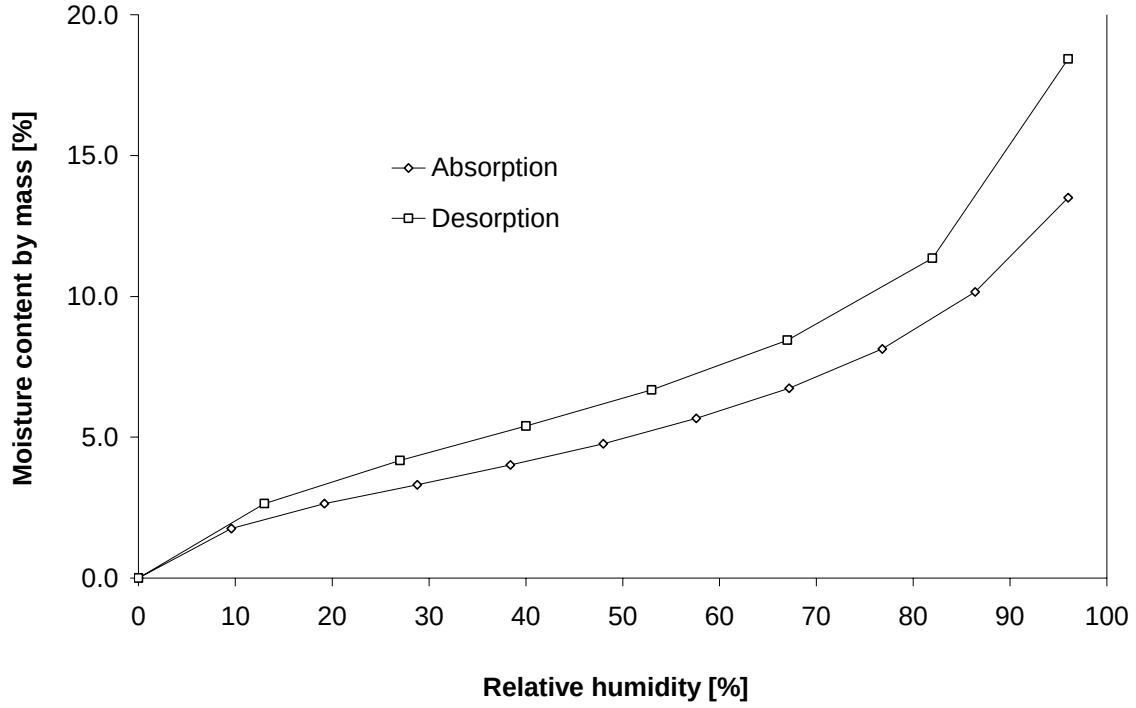

Figure 5.14 Sorption isotherms for the intermediate layer of cotton cloth.

The hydraulic contact between two combined materials was discussed in Section 5.2.3. Different methods for obtaining a good contact for moisture transport in both the hygroscopic and the capillary moisture ranges were tested. When a piece of cotton cloth was used as an intermediate layer between the two combined materials, moisture transport in both the hygroscopic and capillary moisture ranges was unhindered across the interface between the two materials (see Figures 5.3 and 5.4). In Figure 5.14 the absorption and desorption isotherms of the intermediate layer of cotton are shown for the hygroscopic range. However, the absorption isotherm above the hygroscopic range is crucial for the capillary water uptake.

6 SIMULATED TRANSIENT MOISTURE PROFILES

6.1 INTRODUCTION

Simulations of moisture profiles in the hygroscopic range are often performed, for example, when the risk of condensation in a building structure is being investigated. Accepted values for the moisture diffusivities and sorption isotherms required as input for moisture profile simulations in the hygroscopic range are fairly available in the literature (see Hedenblad, 1993 and 1996).

On the other hand, moisture profile simulations and corresponding moisture profile measurements are seldom mentioned in the literature. One of the major problems experienced when performing moisture profile simulations in the high moisture range is that the moisture transport data needed, such as moisture diffusivity and suction curves, are difficult to determine. For the hygroscopic range, several well-established methods are available for determining the sorption isotherms and moisture diffusivities.

In this work, sorption isotherms were determined above the hygroscopic range using the pressure plate method (see Chapter 2). The pressure plate method is a relatively well-tried method, but its original field of application was soil mechanics. For determining the moisture diffusivities of the studied materials, a method developed by Arfvidsson and Janz (1994) and Claesson (1994) has been used. The method is further described in Chapter 3.

One of the main objectives of this research was to verify the reliability of a method for determining moisture diffusivities in the high moisture range. Therefore, the moisture profile simulations in Section 6.3 were performed using the moisture diffusivities determined in Chapter 3 for the studied materials. Sorption isotherms corresponding to the moisture diffusivities were presented in Chapter 2. The software used for the moisture profile simulations was the well-established JAM-2 program, described in Arfvidsson (1989); it is capable of simulations for both single and combined materials.

To verify the moisture profile simulations and thus the method for determining moisture diffusivities, corresponding measurements of transient moisture profiles were performed as presented in Chapter 5. The materials used for the moisture profile measurements were also used in determining the input data for the computer simulations. Since both the material properties and boundary conditions were identical for both the moisture profile measurements discussed in Chapter 5 and the moisture profile simulations in this chapter, the results should be directly comparable (see Section 6.5.2).

6.2 GENERAL

Capillary water absorption has been simulated for specimens of single materials as well as for specimens composed of two different materials. One reasons for performing absorption simulations beyond a certain external moisture load for combined specimens as well, was to be able to determine the influence of an outer layer of mortar on the moisture conditions in the

masonry. Interest was particularly focused on the interface between the masonry and the outer mortar. The outer layer of mortar was varied in thickness and moisture transport properties.

In performing verification measurements, the interface between materials can be difficult to evaluate since considerable spatial resolution is required. Different methods for measuring moisture contents during transient moisture uptake were evaluated in Chapter 4. Measured results corresponding to the simulations discussed in the present chapter were presented in Chapter 5.

Two kinds of mortar with very different absorption properties were used for both the simulations and for the corresponding water absorption tests presented in Chapter 5. Since the two kinds of mortar displayed different moisture transport properties, variation in the overall transport properties of the combined masonry and attached mortar could be analyzed as a function of the transport properties of the mortar. The effect of the thickness of the mortar was also studied during the simulations, and the water absorption was determined for lime–silica brick combined with the two types of mortar on the outer side, in thicknesses of 7 and 14 mm. Therefore, the absorption rate of the material combinations could be studied as a function of the properties and thickness of the mortar. At the beginning of the study, a hypothesis was that even a relatively thin layer of mortar attached to the outer surface of the masonry would be able to change the absorption properties of the combined materials to a considerable degree.

6.3 METHOD

6.3.1 General

Altogether, three materials were used for the simulations: lime–silica brick, representing the properties of masonry, and both lime–cement mortar and cement mortar representing the mortar. Basic material properties such as density, compact density, and porosity were determined in Section 2.2, where the preparation and the curing of the three materials were also described.

For the computer simulations, each type of specimen was divided into cells. In the computer program, the maximum number of computational cells in each of the two directions was fifty. The interface connecting the lime–silica brick and the mortar was assumed to provide a perfect hydraulic contact over the complete moisture range. The materials used were assumed to have identical material properties throughout their complete volumes.

In an actual case where mortar is cast in contact with a relatively dry porous material, for example, masonry, that part of the mortar that is close to the dry material will have considerably different material properties from those of that part of the mortar at a certain distance from the dry material. Variations in the material properties of mortar cast in contact with masonry are very common in actual structures. In the computer simulation it was possible to consider this effect, and the material properties of the mortar can be varied in the cells close to the boundary. If this is done, an extended range of input data regarding material properties will of course be necessary. However, in the experimental work the mortars were cast separately from the underlying material, so variations in material properties within the volume of the specimen could be disregarded.

6.3.2 Theory

The equation of conservation of mass for three dimensions can be written as Equation 6.1, where w [kg/m^3] represents the moisture content of a porous material, t [s] represents the time and g_x, g_y, and g_z [kg/m^2·s] represent the moisture flow in directions x, y, and z, respectively.

$$\frac{\partial w((x,y,z)t)}{\partial t} = -\frac{\partial g_x}{\partial x}, -\frac{\partial g_y}{\partial y}, -\frac{\partial g_z}{\partial z} \tag{6.1}$$

A more common way to describe the moisture flow, g, is to use Fick's law according to Equation 6.2, in which the driving potential is described by the vapour pressure, p [Pa], and the moisture diffusivity, D_p [kg/(m·s·Pa)]:

$$g = -D_p(p)\frac{\partial p_v}{\partial x} \tag{6.2}$$

The moisture flow, g, can also be described by Equations 6.3 to 6.6, in which the moisture flow was described in one dimension in the x direction. The driving potentials can be chosen as either the relative humidity, ϕ, the vapour content, v [g/m^3], the moisture content, w [kg/m^3], or the suction, s [Pa]. When the moisture diffusivity then was used, according to Fick's law, for determining the moisture flow, g [kg/m^2·s], the type of driving potential had to be considered, so the variables would match. The following equations can of course also be described for the three dimensions x, y, and z, as with the equation of conservation of mass (Equation 6.1).

$$g = -D_\phi(\phi)\frac{\partial \phi}{\partial x} \tag{6.3}$$

$$g = -D_v(v)\frac{\partial v}{\partial x} \tag{6.4}$$

$$g = -D_w(w)\frac{\partial w}{\partial x} \tag{6.5}$$

$$g = -D_s(s)\frac{\partial s}{\partial x} \tag{6.6}$$

Equations 6.3 to 6.6 could generally be described by Equation 6.7, in which the different possible driving potentials, ϕ, v, w, or the suction, s, were replaced by φ as a general driving potential.

$$g = -D_{\varphi}(\varphi)\frac{\partial \varphi}{\partial x} \tag{6.7}$$

The moisture flow calculations performed by the computer program, JAM-2, are based on the fundamental flow potential, ψ [kg/m·s]. According to Arfvidsson (1998), the use of a transport coefficient is an unnecessary complication. When moisture flow measurements are performed on materials transporting water as a function of the driving potential over the material, the fundamental flow potential, ψ [kg/m·s], is actually measured instead of the moisture flow coefficients.

In simulations performed by the JAM-2 program, the moisture diffusivity was transformed into the fundamental flow potential, ψ [kg/m·s]. The transformation from the moisture flow coefficient, D_{φ} (φ), was performed by the program. The fundamental flow potential was described by Equation 6.8 as the area below the function D_{φ} (φ) in the moisture range from φ_{ref} to φ, according to Arfvidsson (1998).

$$\psi = \psi_{ref} + \int_{\varphi\ ref}^{\varphi} D_{\varphi}(\varphi)d\varphi \tag{6.8}$$

Since the fundamental flow potential represents the accumulated area below curve D_{φ} (φ) for moisture potentials from φ_{ref} to φ, the fundamental flow potential at φ_{ref} is always zero according to Equation 6.9. The equation can thus be written as Equation 6.10 instead.

$$\psi_{ref} = \psi(\varphi_{ref}) = 0 \tag{6.9}$$

$$\psi = \int_{\varphi\ ref}^{\varphi} D_{\phi}(\varphi)d\varphi \tag{6.10}$$

The derivative of $\psi(\varphi)$ from Equation 6.10 is shown in Equation 6.11, in which the moisture transport coefficient is expressed as a function of the fundamental flow potential. The flow g [kg/m^2·s], from Equation 6.7 can now be expressed as a function of the gradient of the fundamental flow potential in Equation 6.12, according to Arfvidsson (1998).

$$\frac{\partial \psi}{\partial \varphi} = D_{\varphi}(\varphi) \tag{6.11}$$

$$g = -\frac{\partial \psi}{\partial \varphi} \cdot \frac{\partial \varphi}{\partial x} = -\frac{\partial \psi}{\partial x} \tag{6.12}$$

The general driving potential described as φ in Equations 6.7 to 6.12, can optionally be changed to either of the previously described potentials in Equations 6.3 to 6.6. If the moisture content, w, for example, is used instead of the general driving potential, φ, the transport coefficient, D, and the moisture flow, g, should also be expressed as a function of the fundamental potential, as a function of the moisture content, w [kg/m^3]. Equations 6.13 to 6.14 describe the moisture flow and the fundamental flow potential, with the moisture content, w [kg/m^3], as a driving potential.

$$g = -D_w(w)\frac{\partial w}{\partial x} \tag{6.13}$$

$$\psi = \int_{w\ ref}^{w} D_w(w)dw \tag{6.14}$$

$$\frac{\partial \psi}{\partial w} = D_w(w) \tag{6.15}$$

$$g = -\frac{\partial \psi}{\partial w} \cdot \frac{\partial w}{\partial x} = -\frac{\partial \psi}{\partial x} \tag{6.16}$$

The main advantage of Equations 6.12 and 6.16 for moisture transport calculations using a forward difference method is that the moisture transport coefficient, D_ψ, will always assume the value of 1.

The moisture flow calculations performed internally by the JAM-2 program use the fundamental flow potential, ψ [kg/m·s], and the moisture content, w [kg/m^3], as variables. By combining Equations 6.1 and 6.16, a principal relationship between the fundamental flow potential, ψ [kg/m·s], and the moisture content, w [kg/m^3], is described (see Equation 6.20).

The relationship in Equation 6.20 is determined by that in Equation 6.1, which in turn is described by Equation 6.17 (only applicable to the x axis). The moisture flow, g, is more clearly expressed if Equation 6.17 is rewritten as Equation 6.18.

$$\frac{\partial w}{\partial t} = -\frac{\partial g}{\partial x} \tag{6.17}$$

$$g = -\frac{\partial w \cdot \partial x}{\partial t} \tag{6.18}$$

Then Equations 6.16 and 6.18 can be combined, according to Equation 6.19, in which the moisture content, w, is described as a function of the fundamental potential, ψ.

$$w = \partial \psi \cdot \partial t \tag{6.19}$$

Equation 6.19 can be described by a more general expression, Equation 6.20. The principal relationship expressed in Equation 6.20, between the fundamental flow potential, ψ, and the moisture content, w, was then used for calculating the moisture contents by the JAM-2 program, according to Arfvidsson (1989).

$$w = w(\psi) \tag{6.20}$$

In the boundary between two combined materials, A and B, in direct contact with each other, the relative humidity will display a continuous value across the boundary. As in Equation 6.20, the relative humidity, ϕ, can be described as a function of the fundamental flow potential according to Equation 6.21. Since the relative humidity is continuous across the boundary section, Equation 6.21 can be combined for the two materials A and B across the boundary. The combined equation is shown as 6.22. According to Equation 6.22, the fundamental flow potential will display discontinuous behaviour across the boundary.

$$\phi = \phi(\psi) \tag{6.21}$$

$$\phi_A(\psi_A) = \phi_B(\psi_B) \tag{6.22}$$

The computer program is able to consider the outer boundaries in three alternative ways, of which the relative humidity at the surface of the material and the relative humidity in the surrounding air are two. When the relative humidity in the surrounding air is given as an outer boundary condition, the moisture resistance across the surface also has to be given. The third alternative in defining the boundary condition is to give the moisture flow at the boundary. Both

the relative humidity and the moisture flow could be defined as stepwise variables over time or as sinus functions with both the period and amplitude as variables.

6.3.3 Input data

General

To perform simulations for single materials, in terms of material input data, only moisture diffusivity, D, was needed for the considered material. Since the moisture diffusivity is normally dependent on the moisture level of the material, the diffusivity needs to be described as a function of the actual moisture level. When the diffusivity, D_w, for example, was used as a function of the water content, w, the moisture levels expressed as w could be calculated without the use of a sorption isotherm. The boundary conditions must then be given as water content as well.

In a comparable case, in which the boundary conditions were given in terms of relative humidity, and the moisture level after a certain external moisture load was required as the water content, w, the sorption isotherm of the studied material must be used as input for the simulations. Also, when simulations are performed for combined materials (see Section 6.4.3), the sorption isotherms as well as the moisture diffusivities of the separate materials would be needed. For the combined materials, sorption isotherms would always be needed, since the moisture levels in the separate materials across the boundary vary according to the sorption isotherm of the separate materials.

Transient water absorption simulations were performed using a computer model of two-dimensional moisture transport, JAM-2, according to Arfvidsson (1989). The water absorption simulations had to consider two dimensions, since the specimens used in making the corresponding measurements (see Chapter 5) had notches in their sides. All of the specimens were shaped as rectangular parallelepipeds, with two of the long sides, in opposite directions, provided with notches. The notches were made to simplify the cutting of the specimen into separate slices during the moisture profile measurements described in Chapter 5.

The geometry of the different types of specimen used for the simulations as well as for the measurements presented in Chapter 5 can be seen in Figures 6.8 and 6.10 for the single materials. The geometry depicted in Figures 6.13 and 6.14 refers to the specimens composed partly of lime–silica brick and partly of attached lime–cement mortar or cement mortar. The shaded areas in the figures represent the mortar and the remaining parts represent the lime–silica brick. Figures 6.13 and 6.14 depict the combined specimens in which the mortar was either 7 or 14 mm thick. All specimens had a width and height of 50 mm and the sections of mortar were free from notches. The total lengths of the specimen, including the mortar, ranged from 100 mm to 253.5 mm depending on the type of material. Note that the figures depicting the geometry simply provide schematic outlines and are not correct in scale.

The input options for the computer program in terms of material data comprised five different alternatives, only one of which used a combination of moisture diffusivities and sorption isotherms. Since both the sorption isotherms and moisture diffusivities were measured for the studied materials, this alternative was chosen. The moisture diffusivity was unfortunately defined

differentially by the measurements in Chapter 3 and by the computer program. In the computer program, the moisture diffusivity, D_ϕ, was defined as a function of the relative humidity, ϕ, while the measured diffusivity, D_w, was defined as a function of the moisture content, w [kg/m^3]. Therefore, the measured diffusivity, D_w, was transformed by Equation 6.24 into D_ϕ before the moisture profile simulations were performed.

Sorption isotherms

As input for the calculations, the moisture diffusivities and sorption isotherms were experimentally established in Chapters 3 and 2, respectively. Since the moisture diffusivity originally was determined by absorption tests, the moisture profile measurements described in Chapter 5 were also performed for absorption. A more relevant comparison could then be made between the simulations and the moisture profile measurements using the absorption phase in both cases. Since only the desorption isotherms of the studied materials could be experimentally determined in the high moisture range area, an assumption was made (see Figure 6.1).

The sorption isotherms were determined using two different methods, the sorption balance method for the low moisture range, and the pressure plate method for the high moisture range. The pressure plate method was originally designed for determining only desorption isotherms; to determine absorption isotherms over the complete moisture range, the pressure plate equipment would have to be modified. Part of an absorption isotherm was determined, but the equilibrium state could not be established (see Chapter 2). Since the modifications to the pressure plate apparatus were not successful, it was only the complete desorption isotherms that could be determined for the studied materials.

As shown in Figure 6.1, the experimentally determined desorption isotherm was used as an approximation of the absorption isotherm between the origin and point A, marked in the figure. Point A represents the highest measured value of the desorption isotherms, that is, just below the capillary saturation point, marked C in the figure. The moisture content at the capillary saturation point is well known for the studied materials from the capillary uptake tests reported in Chapter 3. An assumed absorption isotherm was then described by the experimentally determined desorption isotherm from the origin to point A, and then further on along the straight line to point C, representing the capillary saturation point in the water uptake phase with an originally dry material. The upper part of the measured desorption isotherm from point A to the vacuum saturation point, marked B, was not used at all.

Another way to estimate an absorption isotherm from a measured desorption isotherm would be to rotate the complete desorption isotherm clockwise, with the origin fixed, until the curve touches the capillary saturation point, marked C. The part of the desorption isotherm representing moisture contents above the capillary saturation point could simply be left out. A main disadvantage of using this method to estimate the absorption isotherm is that the curve would be drawn without any underlying values, besides the origin of the co-ordinates and the capillary saturation point at C.

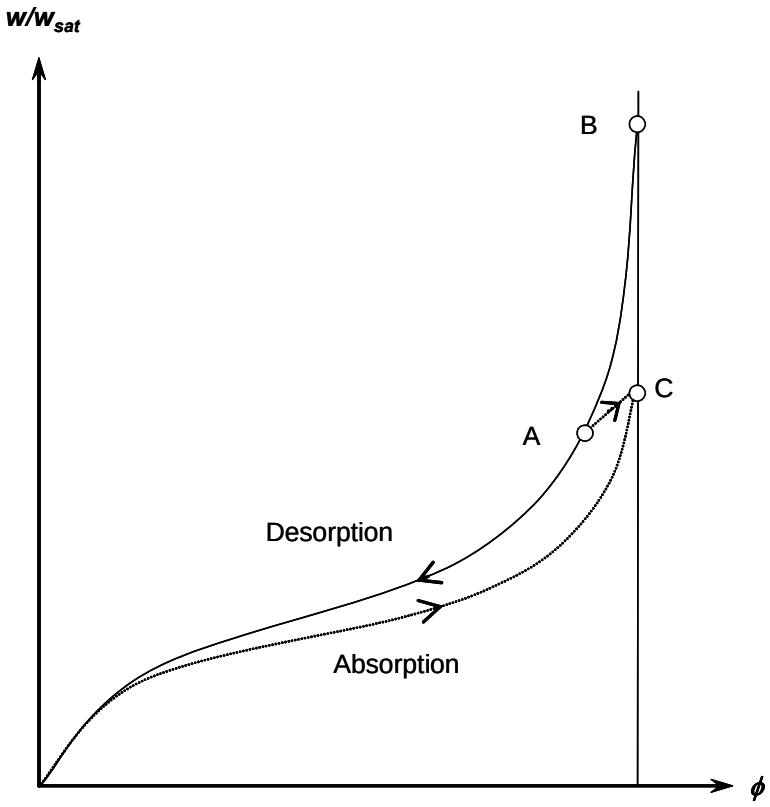

Figure 6.1 The principal appearance of the absorption and the desorption isotherms.

Absorption isotherms for the studied materials are presented in Figures 6.2 to 6.4. The isotherms were estimated according to the principle shown in Figure 6.1, using the experimentally determined desorption isotherms as well as the capillary saturation point. The program used for the moisture profile simulations was designed to use the moisture content, w [kg/m^3], to define the moisture level, instead of using the degree of vacuum saturation, w/w_{sat}, that has been used to define the moisture level elsewhere in this work. Before the sorption isotherms were used as input for the simulations, the degrees of vacuum saturation, w/w_{sat}, in Figures 6.2 to 6.4 had to be transformed into the moisture content, w. To perform the transformation, the different values of w/w_{sat} were multiplied by the mean moisture content at vacuum saturation, w_{sat}, for the separate materials (see Section 2.2).

The absorption isotherms were then input into the computer program as a series of numbers corresponding to the relative humidities and the corresponding moisture contents. The gaps between the points were made wider in the hygroscopic than in the capillary range, since the original desorption isotherms almost followed a straight line here (see Chapter 2). During the simulations, the computer program used an absorption isotherm estimated by joining the given points with straight lines.

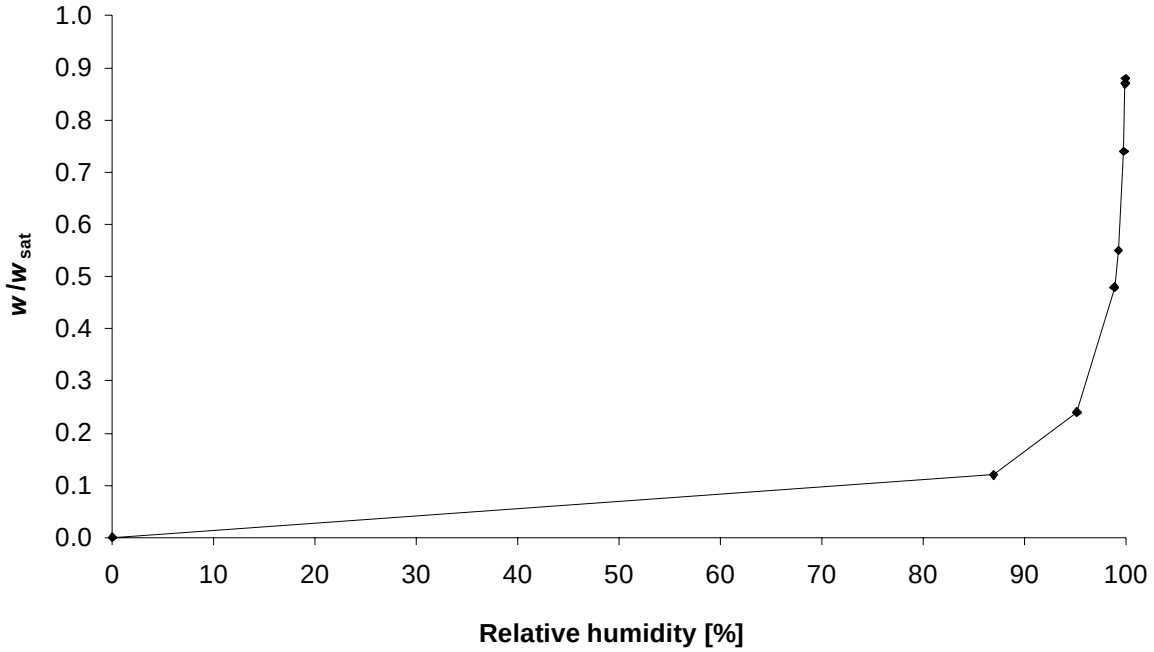

Figure 6.2 Absorption isotherm for lime–silica brick as input for simulations.

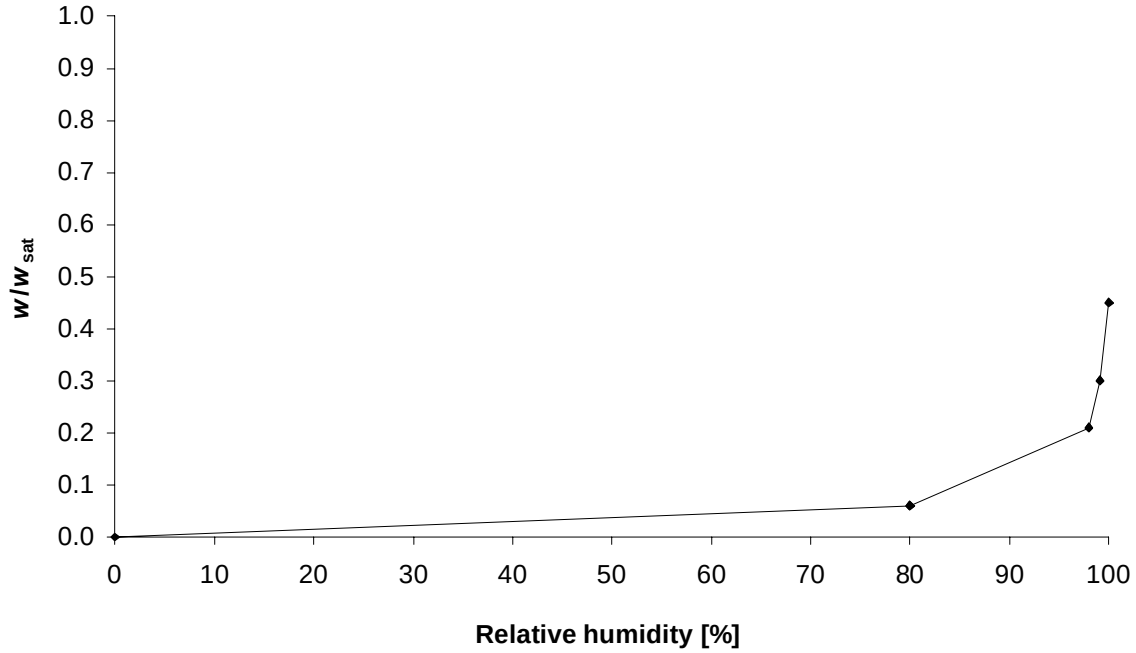

Figure 6.3 Absorption isotherm for lime–cement mortar as input for simulations.

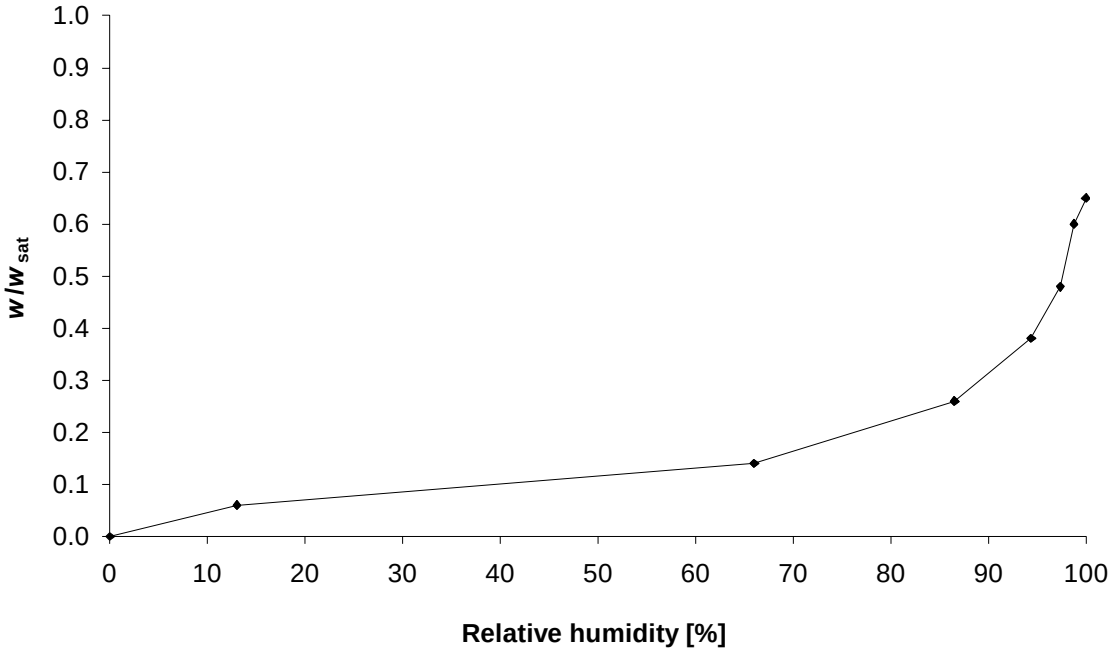

Figure 6.4 Absorption isotherm for cement mortar as input for simulations.

Moisture transport data

The moisture transport coefficient, D_w, was determined for the studied materials during the capillary water absorption phase (see Chapter 3). Since the transport coefficient was evaluated from absorption tests, both the redistribution and the drying phases were omitted during the simulations. To perform simulations of the redistribution and evaporation phases, an extended range of moisture diffusivities ands suction curves would be needed.

Transport coefficients evaluated from the water absorption tests presented in Chapter 3 are defined as D_w, where the transport coefficients are expressed as functions of the actual water contents in relation to the water contents at vacuum saturation, w/w_{sat}. Moisture diffusivities as presented in Chapter 3 for the actual materials are here shown in Tables 6.1 to 6.3. The most suitable input option, considering the transport coefficients used by the computer program, was D_ϕ, in which ϕ is the relative humidity. The transport coefficient, D_ϕ, must be given as a function of the relative humidity as input into the computer program.

The measured transport coefficient, D_w, from Chapter 3 was transformed into D_ϕ using Equations 6.23 and 6.24. Also, the degree of vacuum saturation, w/w_{sat}, was transformed into relative humidity using the sorption isotherms presented for the separate materials in Chapter 2.

$$-g = D_\phi \cdot \frac{\partial \phi}{\partial x} = D_w \cdot \frac{\partial w}{\partial x} \tag{6.23}$$

$$D_\phi = D_w \cdot \frac{\partial w}{\partial \phi} \tag{6.24}$$

Tables 6.1 to 6.3 present input data for the computer simulations for the three studied materials. The moisture content, w, and the corresponding relative humidity levels, ϕ, represent the absorption isotherms transformed from a desorption isotherm, according to the principle shown in Figure 6.1.

For the transformation of the moisture diffusivity, the slope of the corresponding sorption isotherm, $\partial w/\partial \phi$, is needed. Since the slopes of the actual absorption isotherms are most likely nearly equivalent to the slopes of the experimentally determined desorption isotherms, the $\partial w/\partial \phi$ relationship obtained from the measured desorption isotherms was used. The $\partial w/\partial \phi$ relationship represents the slope of a straight line in the different moisture intervals (see Tables 6.1 to 6.3).

If the absorption isotherms estimated according to the principle described in Figure 6.1 were instead used for determining the $\partial w/\partial \phi$ relationship, the slope would probably be underestimated for the high moisture range between points A and C. Underestimating the slope would result in lower moisture diffusivities for this moisture range. The high moisture ranges of the sorption isotherms are especially sensitive to changes in slope, and even a little change in this region where the sorption isotherms already showed a steep slope, would significantly affect the $\partial w/\partial \phi$ relationship. On the other hand, changing the slope of the sorption isotherms in the low moisture range region, where the slope was initially relatively flat, would not significantly affect the $\partial w/\partial \phi$ relationship. Since the slopes of the sorption isotherms directly affect the magnitude of the moisture diffusivity, D_ϕ, the choice of sorption isotherm slopes was crucial.

Table 6.1 Input data for lime–silica brick.

w/w_{sat}	w [kg/m^3]	ϕ [%]	$\partial w/\partial \phi$ [kg/m^3]	$D_w\ 10^{-9}$ [m^2/s]	$D_\phi\ 10^{-9}$ [kg/(m·s)]
0	0	0			
			0.384	22.3	8.56
0.12	33.24	87			
			6.15	6.86	42.189
0.24	66.48	95.2			
			20.77	9.9	205.62
0.48	132.96	98.9			
			48.47	14.3	693.12
0.55	152.35	99.3			
			95.69	20.6	1971.21
0.74	204.98	99.85			
			300.08	43.3	12993.46
0.87	240.99	99.97			
			886.4	49.1	43522.24
0.88	243.76	100			

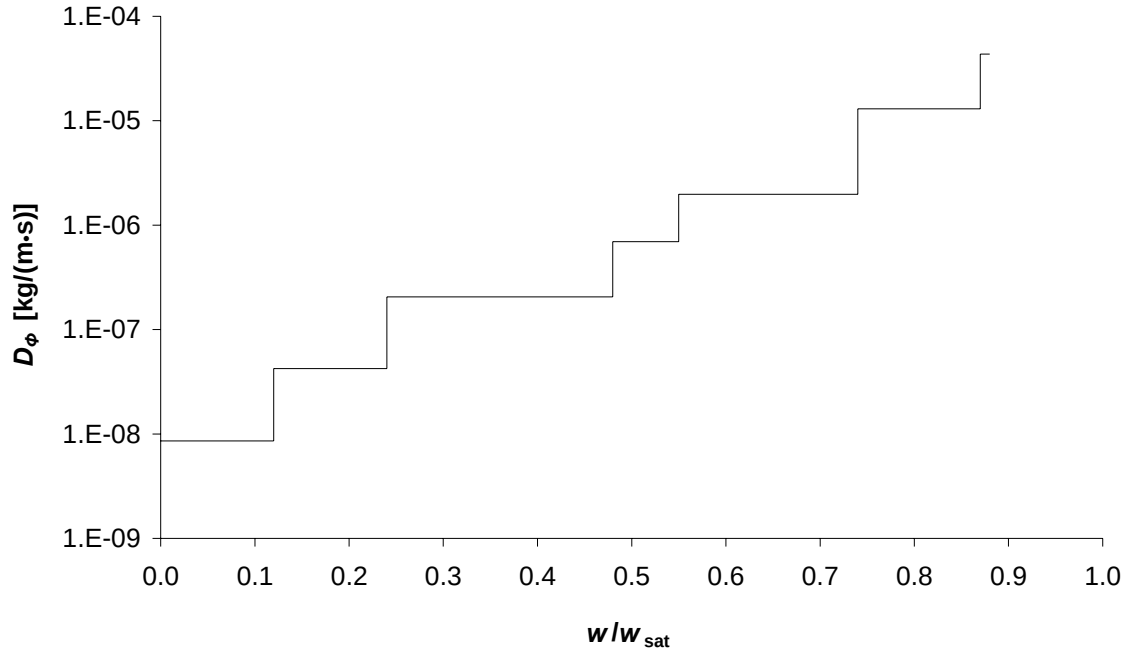

Figure 6.5 Moisture diffusivity, D_ϕ, as a function of moisture content, w/w_{sat}, for specimens of lime–silica brick.

Table 6.2 Input data for lime–cement mortar.

w/w_{sat}	w [kg/m^3]	ϕ [%]	$\partial w/\partial\phi$ [kg/m^3]	D_w 10^{-9} [m^2/s]	$D_\phi \cdot 10^{-9}$ [kg/(m·s)]
0	0	0			
			0.273	463	126.4
0.06	21.84	80			
			3.033	321	973.6
0.21	76.44	98			
			29.778	265	7891.2
0.3	109.2	99.1			
			158.26	137	21681.6
0.45	163.8	100			

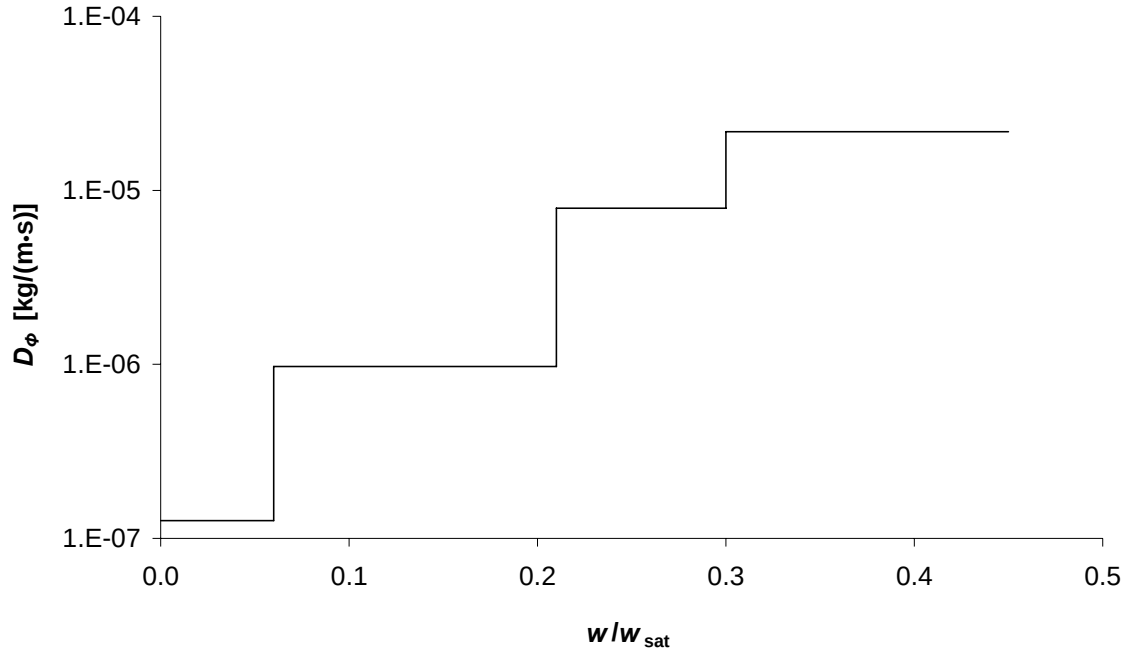

Figure 6.6 Moisture diffusivity, D_ϕ, as a function of moisture content, w/w_{sat}, for specimens of lime–cement mortar.

Table 6.3 Input data for cement mortar.

w/w_{sat}	w [kg/m^3]	ϕ [%]	$\partial w/\partial\phi$ [kg/m^3]	$D_w \cdot 10^{-9}$ [m^2/s]	$D_\phi \cdot 10^{-9}$ [kg/(m·s)]
0	0	0			
			1.192	218	259.8
0.06	15.48	13			
			0.390	109	42.51
0.14	36.12	66			
			1.509	43.5	65.65
0.26	67.08	86.5			
			3.919	28.6	112.08
0.38	98.04	94.4			
			8.746	29.1	254.51
0.48	123.84	97.35			
			22.113	12.8	283.05
0.6	154.8	98.75			
			45.15	1.36	61.40
0.65	167.7	100			

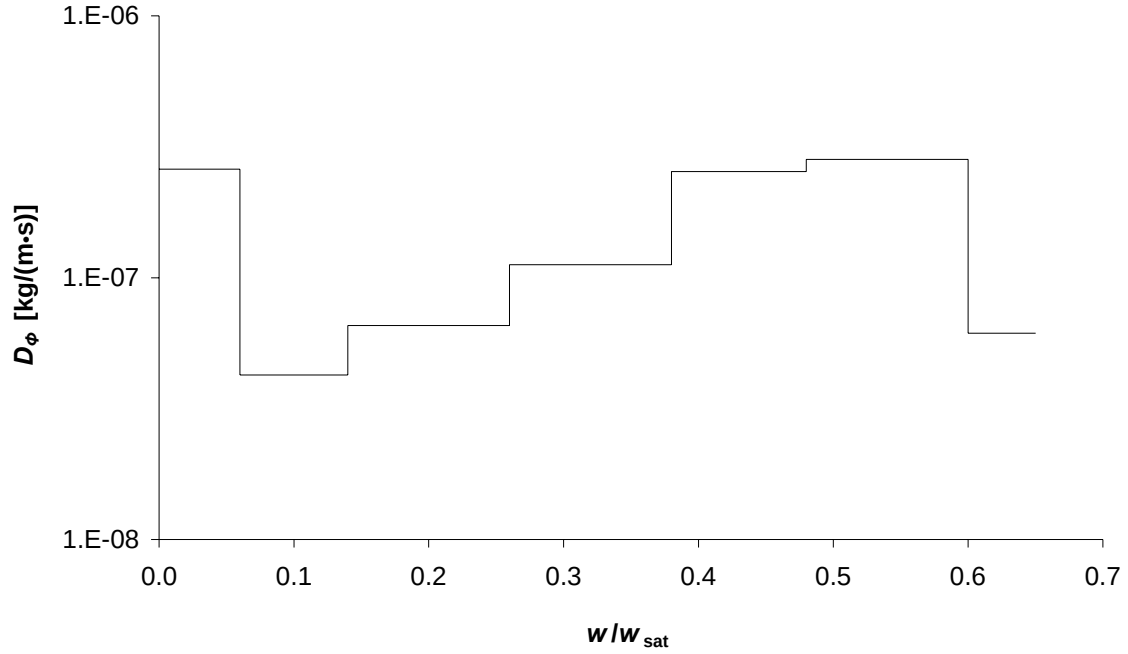

Figure 6.7 Moisture diffusivity, D_ϕ, as a function of moisture content, w/w_{sat}, for specimens of cement mortar.

Initial and boundary conditions

The input data was given as both initial moisture and boundary conditions. For simulations for single as well as combined materials, a relative humidity of 0% was used as an initial condition.

For simulations for the single materials, the boundary condition at the wetted boundary was set to 100% relative humidity. The remaining sides were regarded as completely insulated in terms of moisture exchange with the surroundings. For simulations for the combined materials, the wetted end was defined as the end of the mortar specimen parallel to the boundary between the two materials, and the boundary condition was here defined as 100% relative humidity at the surface. The boundary conditions representing the remaining sides of both the mortar and the lime–silica brick were defined as completely insulated in terms of moisture exchange with the surroundings.

6.4 RESULTS

6.4.1 General

Output from the computer simulations was provided as moisture content, w [kg/m^3], where w represents the mean value of the moisture content for each cell. The subdivision of the specimen geometry into cells is illustrated in the figures representing the different specimen geometries. Since the computer program uses moisture content as an input, the output was also given as moisture content. Just as the original input was transformed into moisture contents, the output

was transformed back into degrees of vacuum saturation using the same moisture content at vacuum saturation, w_{sat} , as had been used in transforming the input. The w_{sat} values used for the transformations were derived from the general material data for each of the three tested materials (see Section 2.2).

6.4.2 Single materials

Moisture profile simulations performed for specimens of single materials are presented in this section, and for combined materials in Section 6.4.3. The single materials are lime–silica brick, lime–cement mortar, and cement mortar. The geometry of the specimens used for simulations for lime–silica brick is shown in Figure 6.8, where the dimensions A, B, C, and D are 5, 40, 26.5, and 4 mm, respectively. The total length of the specimen was 240 mm and the width was 50 mm. The cell divisions chosen for the simulations are shown by the dotted lines.

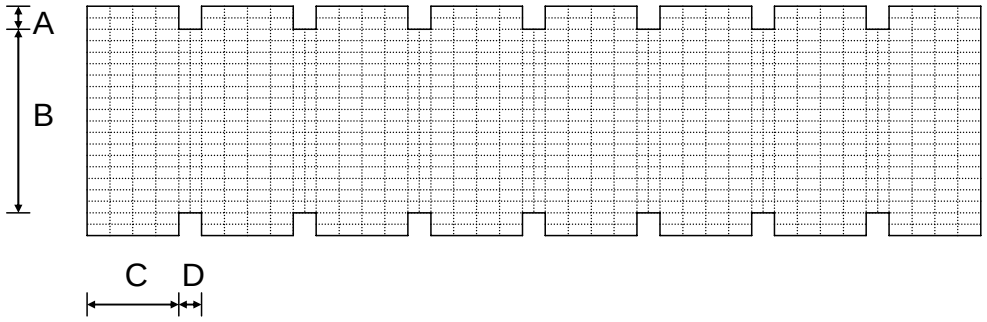

Figure 6.8 Specimen geometry used for moisture profile simulations for lime–silica brick.

The results of moisture profile simulations for lime–silica brick as a single material are shown in Figure 6.9. The simulations were performed for different water absorption durations ranging from 6 h to 7 days. It can clearly be seen that the moisture profile, representing the 7-day simulation, was becoming more flat than the other profiles were. The flatter appearance of the profiles representing higher time ranges in the simulation is of course caused by the moisture front reaching the top of the specimen. Since moisture transport across all boundaries apart from the wetted end was hindered, the moisture content will increase rapidly when the moisture flow has reached the top of the specimen.

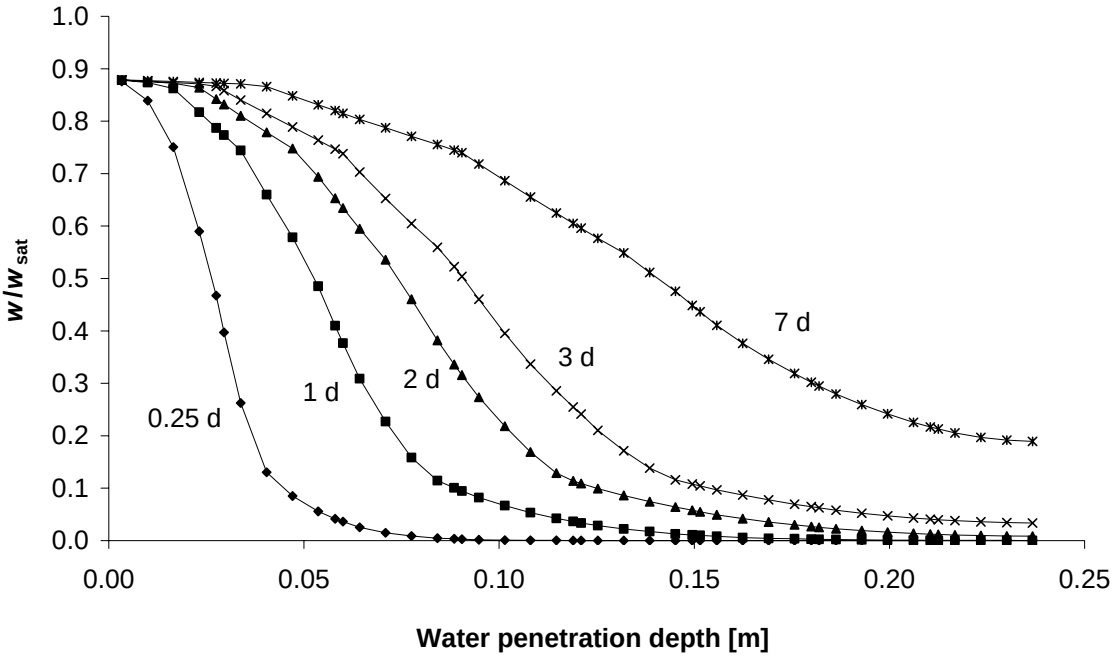

Figure 6.9 Specimens of lime–silica brick exposed to a free surface of water for different durations.

The geometry depicted in Figure 6.10 was used for moisture profile simulations for lime–cement mortar and cement mortar considered as single materials. The dimensions A, B, C, and D were 4, 42, 16.8, and 4 mm, respectively. The total length of the specimen was 100 m and the depth was 50 mm. The cell divisions chosen for the simulations are shown by the dotted lines. The inputs for the simulations are described in detail in Section 6.3.3.

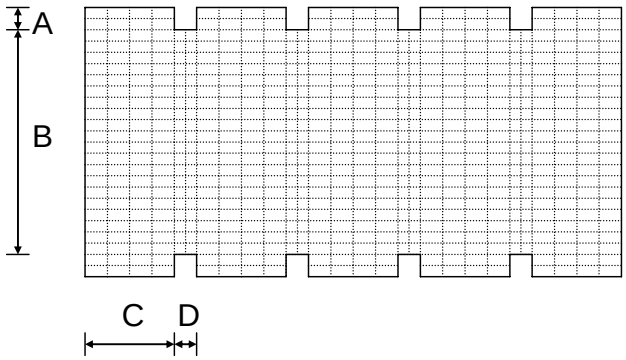

Figure 6.10 Principal specimen geometry used for moisture profile simulations for lime–cement mortar and cement mortar.

Results of moisture profile simulations for lime–cement mortar and cement mortar are presented in Figures 6.11 and 6.12, respectively. The simulations were performed for different wetting durations, ranging from 0.5 h to 7 days.

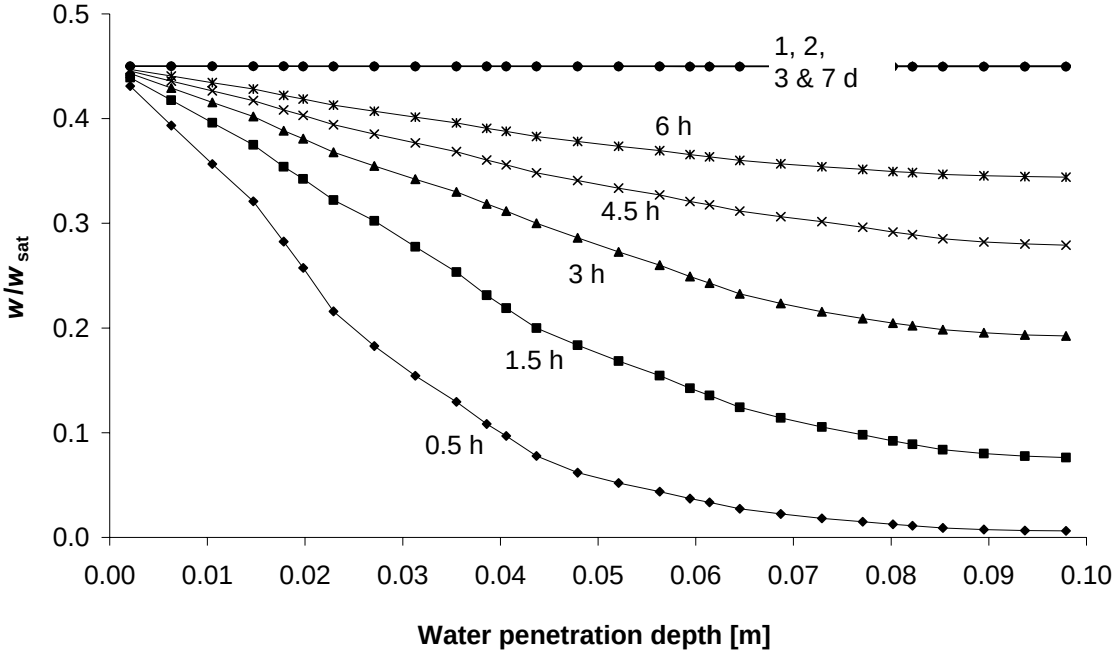

Figure 6.11 Specimens of lime–cement mortar exposed to a free surface of water for different durations.

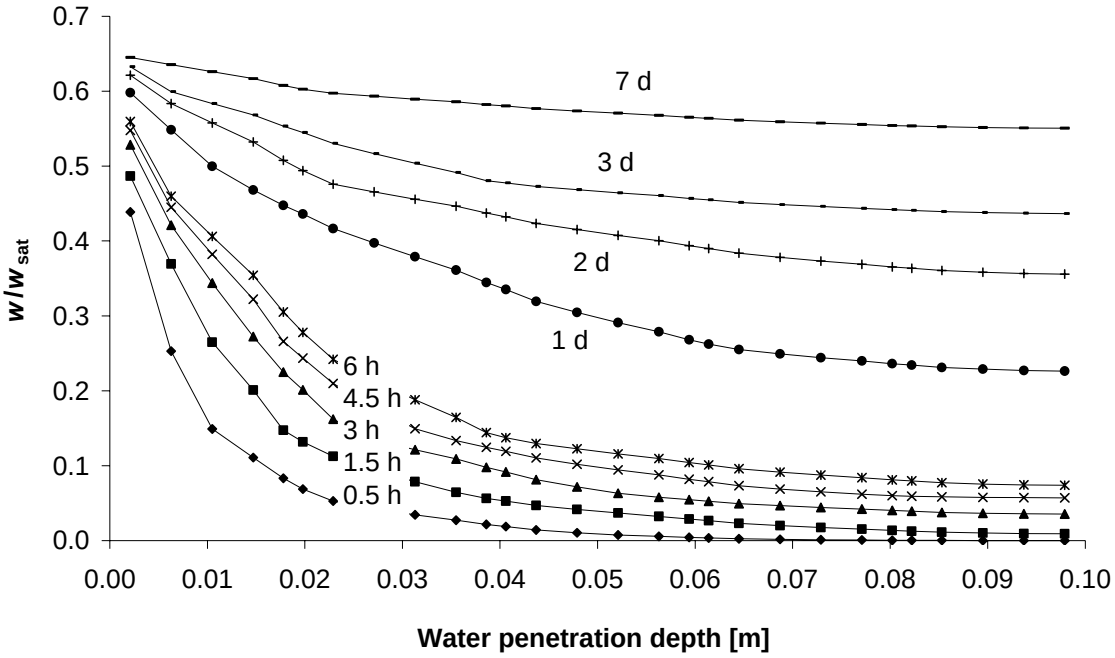

Figure 6.12 Specimens of cement mortar exposed to a free surface of water for different durations.

6.4.3 Combined materials

Moisture profile simulations were also performed for specimens of combined materials, in which an underlying specimen of lime–silica brick had a thin layer of mortar attached. The mortar was either lime–cement mortar or cement mortar, and is represented by the shaded area to the left in Figures 6.13 and 6.14. The total length of the specimen shown in Figure 6.13 was 0.2465 m and the depth was 0.05 m. The dimensions A, B, C, D, and E in Figure 6.16 were 4.5, 41, 7, 17, and 4 mm, respectively. The cell divisions chosen for the simulations are shown by the dotted lines.

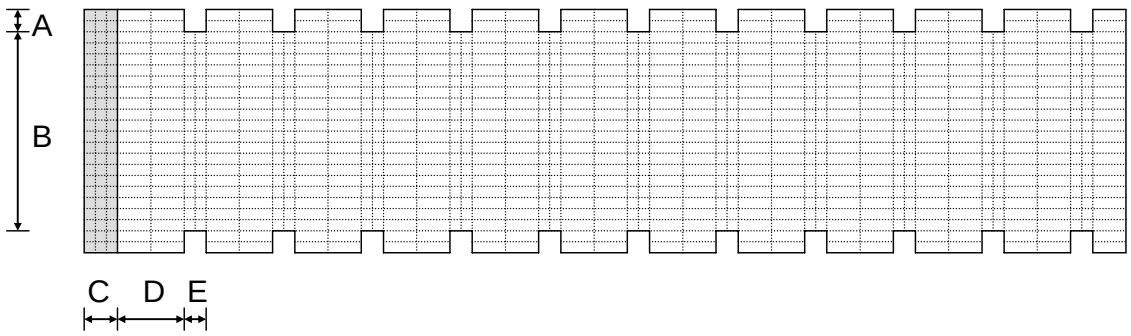

Figure 6.13 Schematic drawing showing the geometry of a specimen composed of a 7-mm mortar layer and lime–silica brick.

Figure 6.14 shows the geometry of combined materials, in which the thickness of the mortar layer is 14 mm. The dimensions A, B, C, D, and E are 4.5, 41, 14, 17, and 4 mm, respectively. The total length of the specimen was 253.5 mm and the depth was 50 mm. The cell divisions chosen for the simulations are shown by the dotted lines.

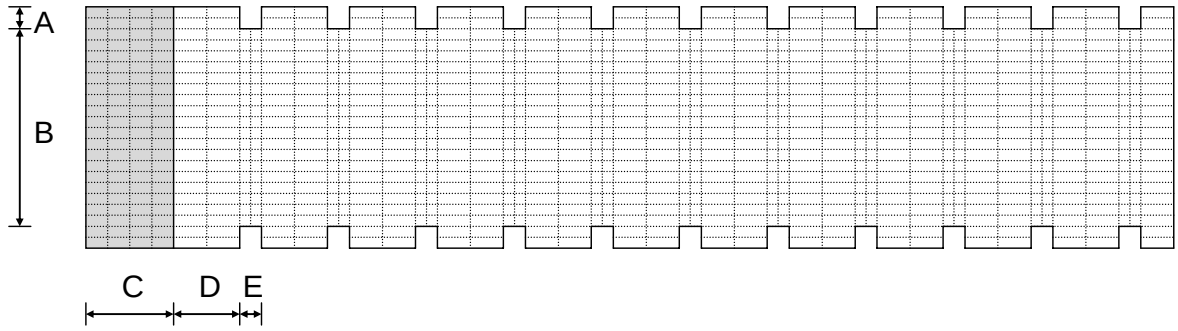

Figure 6.14 Schematic drawing showing the geometry of a specimen composed of a 14-mm mortar layer and lime–silica brick.

Results of moisture profile simulations for mortar attached to lime–silica brick (as combined materials) are shown in Figures 6.15 and 6.16. Each dot in the figures represents the mean value of the degree of vacuum saturation for the corresponding vertical row of cells. The unfilled circles and squares represent the moisture levels of the mortar. To make the results more obvious, the dots are connected by lines. The simulations were performed for water absorption phase lasting 2 and 7 days. As can be seen in the figures, the types of mortar used as an outer layer were lime–cement mortar and cement mortar in thicknesses of 7 and 14 mm. It can clearly be seen in Figures 6.15 to 6.20 that the thickness of the mortar was of minor importance for the penetration depth of the moisture profile front. On the other hand, the type of mortar used did affect the depth of the water penetration front, and using a layer of cement mortar instead of lime–cement mortar was found to delay the water front considerably.

A clear gradient in terms of the degree of vacuum saturation could be seen for the cement mortar, resulting in a lower moisture content in the underlying material. This behaviour was not observed in simulations using layers of lime–cement mortar corresponding in thickness to that of the cement mortar layers.

For the 7-day simulations, the moisture profiles generally displayed a flatter moisture profile. The relatively flat appearance of the moisture profiles could be observed when a layer of either lime–cement mortar or cement mortar was attached. In both cases the moisture flow reached the upper, sealed boundary.

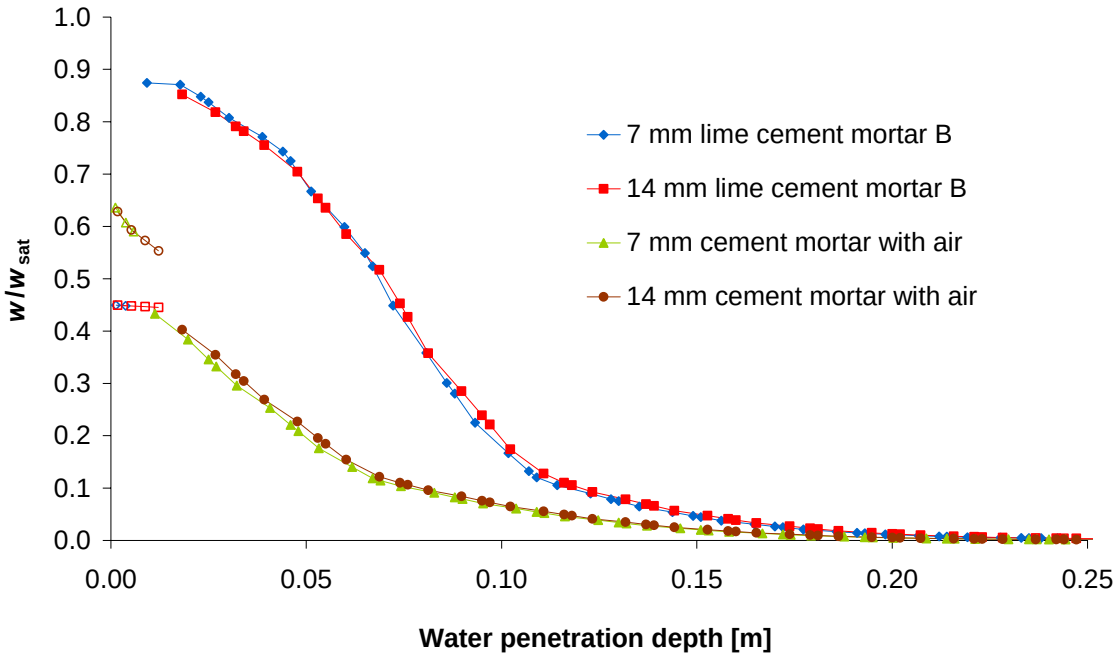

Figure 6.15 Specimens of lime–silica brick with a layer of mortar attached. The surface of the mortar was exposed to a free surface of water for two days.

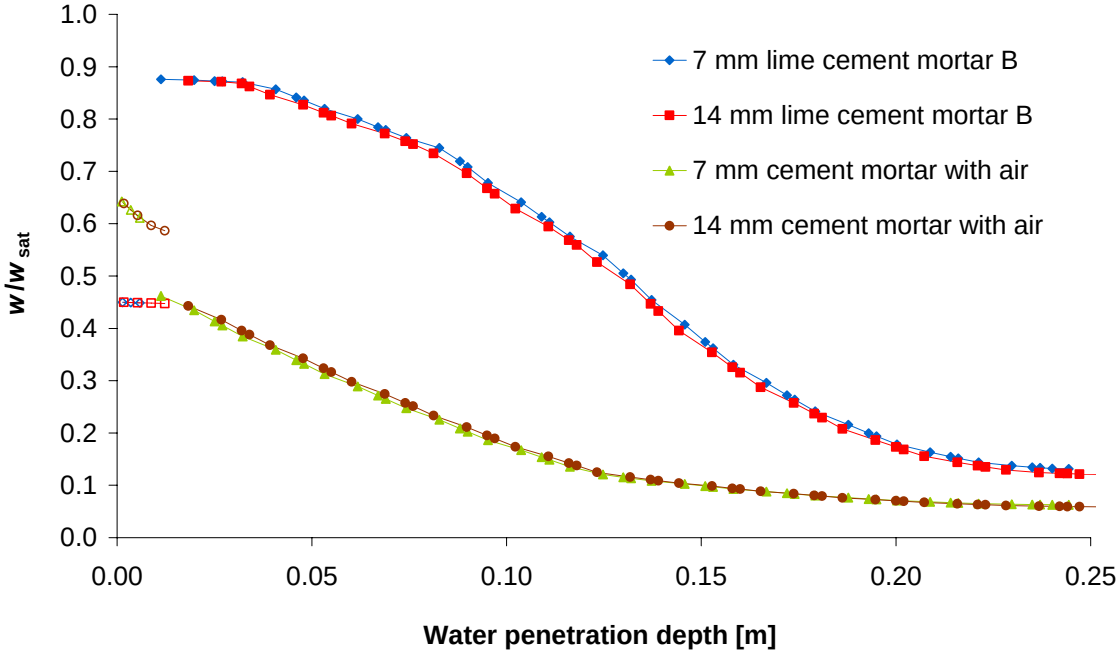

Figure 6.16 Specimens of lime–silica brick with a layer of mortar attached. The surface of the mortar was exposed to a free surface of water for seven days.

In Figures 6.17 to 6.20 moisture profiles are shown separately for combined specimens with attached lime–cement mortar or cement mortar layers. The simulations include both 2- and 7-day wetting phases, and the results are shown in different figures. It can clearly be seen that the thickness of both lime–cement mortar and cement mortar layers were of minor importance to the position of the moisture profiles; instead, the duration of the wetting phase and the type of mortar used were crucial for the position of the moisture profiles.

The two types of mortar affected the moisture level of the underlying material very differently. When the lime–cement mortar was used, the moisture levels in the underlying lime–silica brick corresponded to the capillary saturation level in the area close to the boundary between the two materials (see Figures 6.17 to 6.18 and Table 6.1). As can be seen in the figures, the moisture level in the lime–cement mortar was evenly distributed throughout both the 7-mm and the 14-mm layers, in which the moisture level also corresponded to capillary saturation (see Table 6.2).

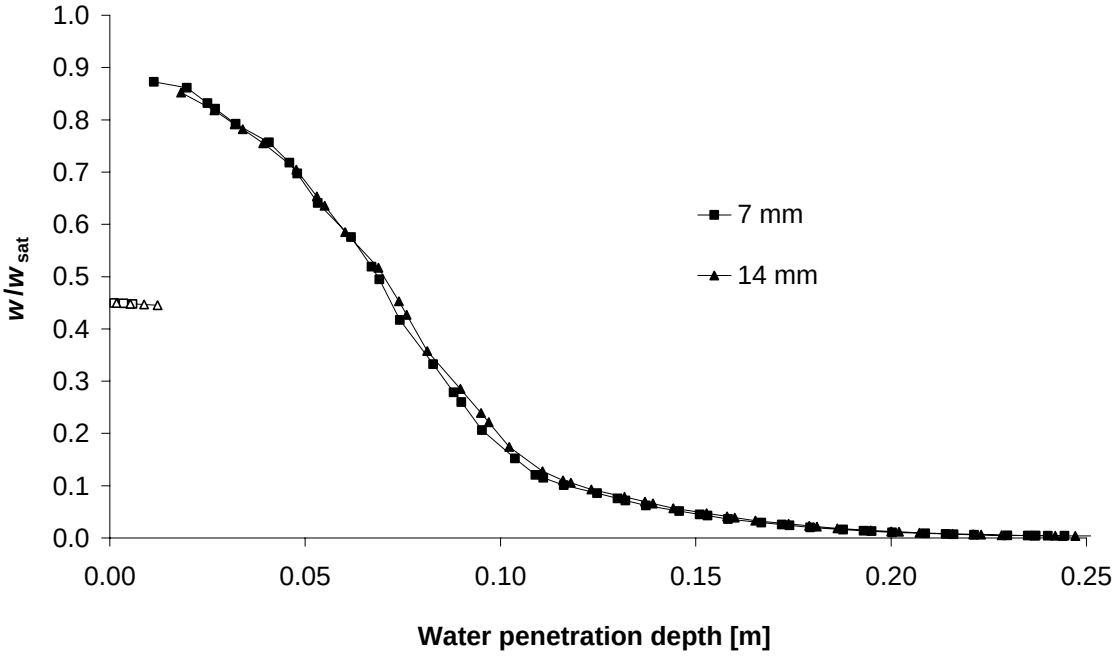

Figure 6.17 Specimens of lime–silica brick with a layer of lime–cement mortar attached. The surface of the mortar was exposed to a free surface of water for two days.

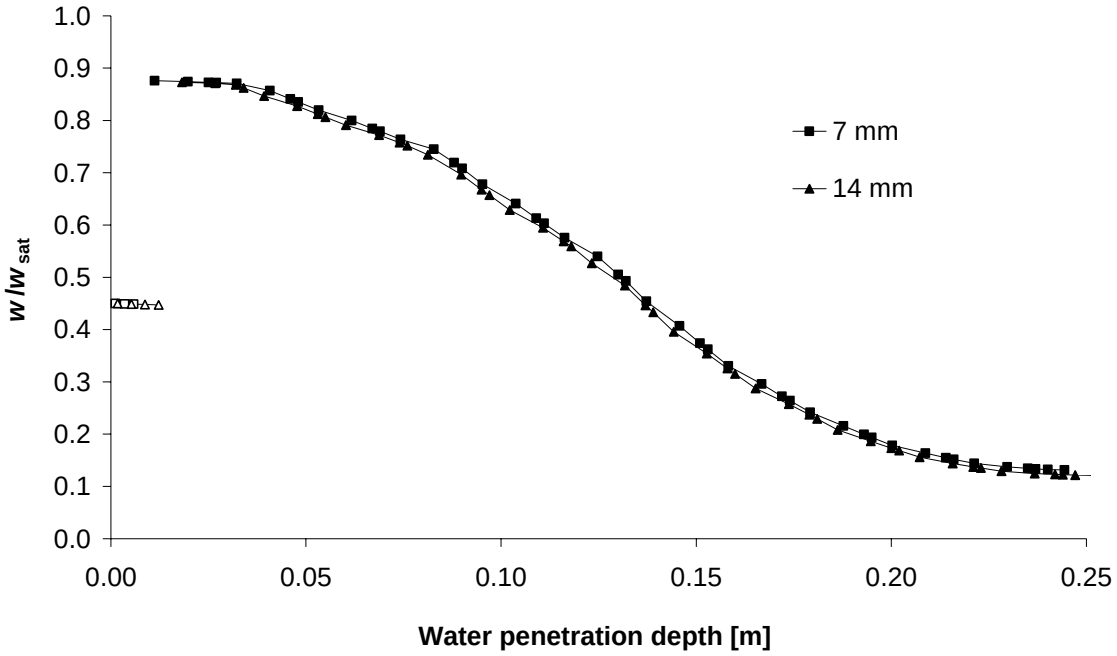

Figure 6.18 Specimens of lime–silica brick with a layer of lime–cement mortar attached. The surface of the mortar was exposed to a free surface of water for seven days.

For simulations in which cement mortar was attached to lime–silica brick, the moisture levels in the underlying lime–silica brick reached on half of the moisture level corresponding to capillary saturation (see Figures 6.19 to 6.20 and Table 6.1). The moisture levels in the cement mortar, unlike in the lime–cement mortar, displayed a clearly decreasing moisture gradient from the wetted surface to the boundary between the two materials. As with the lime–cement mortar, the moisture level of the wetted surface of the cement mortar corresponded to capillary saturation.

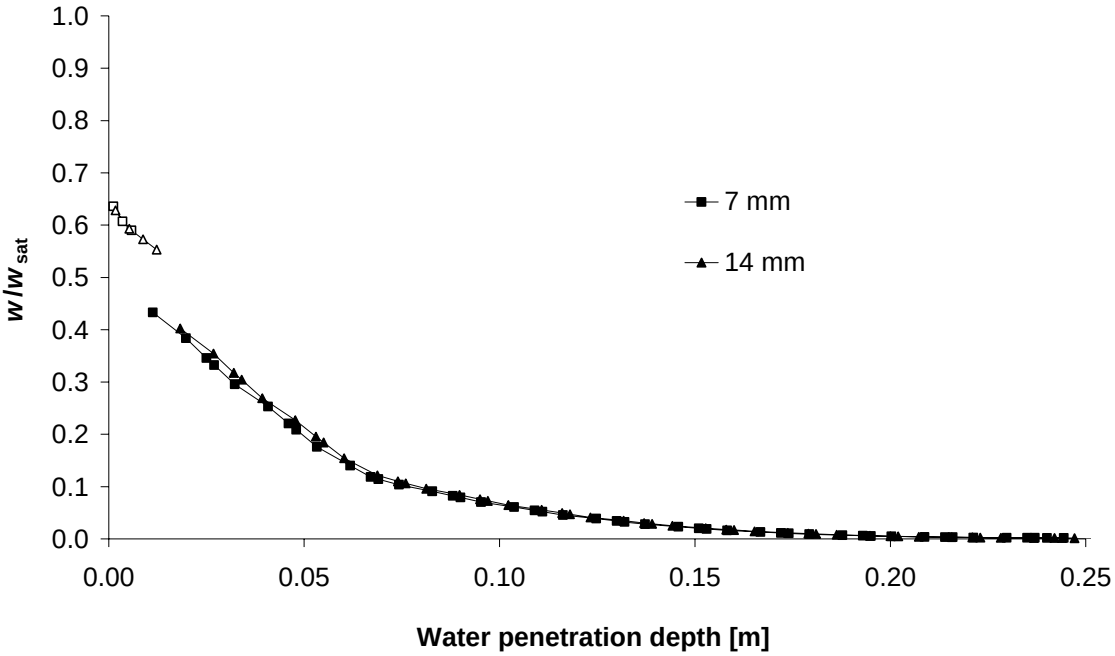

Figure 6.19 Specimens of lime–silica brick with a layer of cement mortar attached. The surface of the mortar was exposed to a free surface of water for two days.

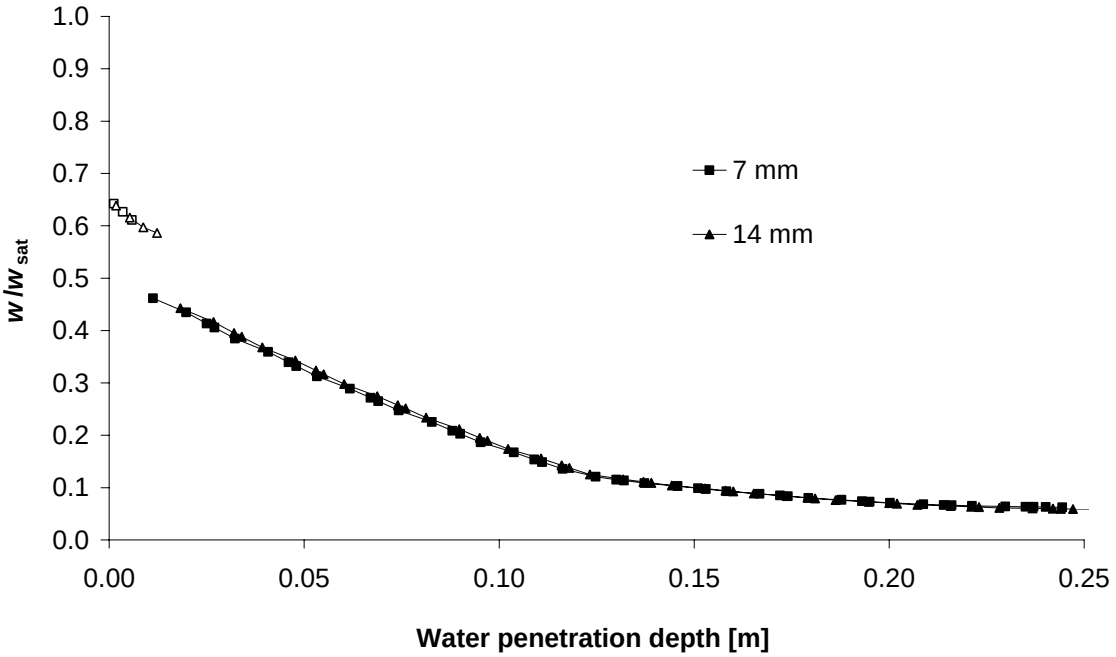

Figure 6.20 Specimens of lime–silica brick with a layer of cement mortar attached. The surface of the mortar was exposed to a free surface of water for seven days.

6.4.4 Effect of notches

The results of the simulations presented in Sections 6.4.2 and 6.4.3 were based on a specimen geometry including notches. The effect of notches in potentially delaying the moisture front was studied by comparing the measured with the simulated results. The geometry used for specimens with notches can be seen in Figure 6.8, while a corresponding geometry without notches is presented in Figure 6.21. Besides the presence of notches, the dimensions of the two geometries were identical. In Figure 6.21 dimensions A and B were 0.05 and 0.24 m, respectively. The cell divisions chosen for the simulation are shown by the dotted lines.

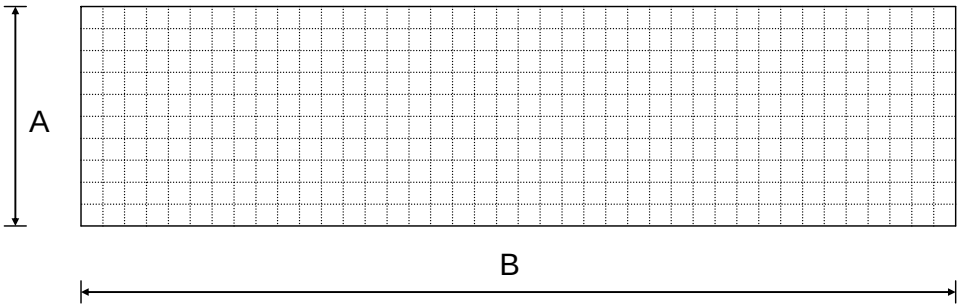

Figure 6.21 Schematic drawing of a specimen without notches, used for the simulation of water absorption.

Results of simulations for specimens with and without notches can be seen in Figure 6.22. The results presented are both for 2- and 7-day wetting phases. For the 2-day simulations, the moisture profiles of specimens with and without notches agreed completely, and no significant differences could be observed between the two curves. For the 7-day simulations, however, a small difference is seen for the specimen without notches. This difference was expected, since the specimen with notches had a smaller continuous cross-sectional area than the specimen without notches did, though the cross-sectional area between the notches was the same as in the un-notched specimen. The larger cross-sectional area between the notches providing a storage effect, resulting in a slight delay of the moisture profile front, as can be seen in Figure 6.22.

However, the delay was not noticeable for the simulation with the 2-day wetting phase. This lack of delay most likely happened because by the end of the simulation, the moisture profile front had just passed one notch, while the storage effect only became active in the first space between two notches. On the other hand, the moisture profile front for the 7-day simulation passed several notches, resulting in the activation of a larger storage space.

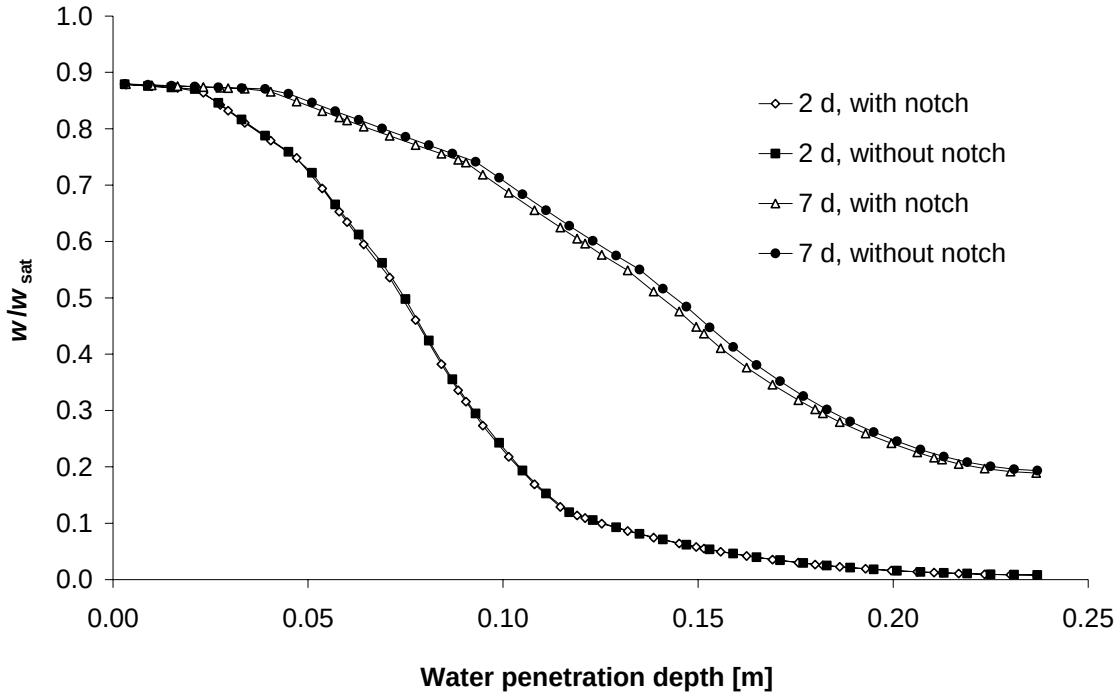

Figure 6.22 Specimens of lime–silica brick in which the surfaces of the specimens were exposed to a free surface of water for seven days.

6.5 ANALYSIS OF RESULTS

6.5.1 Analysis of simulations

Effect of sorption isotherm

Since the slope of the measured desorption isotherms most likely were a little steeper than the real absorption isotherms, the moisture diffusivies D_ϕ, were most likely a little overestimated. An overestimation of the moisture diffusivities D_ϕ, were resulting in a slightly shorter time range to reach a certain moisture profile.

The estimated absorption isotherms used as input for the simulations generally overestimated the degree of vacuum saturation, w/w_{sat} , for a certain relative humidity (see Figure 6.1). As can be seen in the figure, in estimating the absorption isotherm the true values at origin and at the capillary saturation point, C, were assumed. For the moisture profile simulations for single materials presented in Section 6.4.2, only the capillary saturation point was used from the absorption isotherm. Since the boundary condition at the wetted surface was set to equal 100% relative humidity, the estimated absorption isotherms did not influence the results of the moisture profile simulations.

For the simulations for combined materials presented in Section 6.4.3, the boundary condition of 100% relative humidity at the wetted surface was also applied. The moisture absorption isotherms were not only used at the wetted boundary, but also at the boundary between the two

materials. At the boundary between the two materials, the moisture transport was based on the difference in relative humidities, determined using the actual w/w_{sat} and the absorption isotherms. Since the absorption isotherms slightly overestimated w/w_{sat}, the relative humidities at the boundary were underestimated. The relative humidities of both the combined materials were underestimated, so the defects in the assumed absorption isotherms were estimated to have minor effects on the moisture profiles. In a case where the underestimations of the relative humidities of both of the materials were equal, the effect of the assumed absorption isotherms would not appear.

Effect of moisture diffusivity

Generally, connections between the appearance of the moisture diffusivity as a function of the moisture content and the slope of the moisture profile can be found. The moisture profile during the water absorption phase can normally be characterized as a moving boundary, with a frontline moving from the wetted surface into the specimen. A comparison of the moisture levels in two nearby points behind the frontline of the moisture profile, indicates that the moisture flow must be almost equivalent, since the capillary saturation point was reached behind the frontline. In a case in which the moisture profile shows different gradients, or slopes, in two nearby points, a corresponding difference in the moisture diffusivity can be observed. For example, if the moisture diffusivity was lower for one of the points a higher moisture gradient would result.

When the shapes of the moisture profiles are compared for the three studied materials, fundamental differences are discovered. The moisture profile for the lime–silica brick displays a clear frontline, the gradient of which is relatively steep (see Figures 6.23 and 6.24). The moisture profile has a flat distribution, both in front of and behind the steep frontline. Examining the underlying moisture diffusivities as a function of the moisture content, allows the appearance of the moisture profile to be explained. In Figure 6.26 it can be seen that the moisture diffusivity for the lime–silica brick increases with increasing moisture content, with the exception of the lowest moisture step. There, the observed shape of the moisture profile for the lime–silica brick is as expected, since the moisture diffusivity is relatively high both in the lower and the upper moisture ranges; the lowest moisture diffusivity is found in the mid moisture range. Therefore, it is expected that the moisture profile should be more flat in both the upper and lower moisture ranges, while a steeper profile is expected in the mid moisture range.

The moisture profiles for both the lime–cement mortar and the cement mortar did not display the typical frontline appearance found in the lime–silica brick (see Figures 6.23 and 6.24). A particularly flat moisture profile is observed for the lime–cement mortar. The relatively flat moisture profile is expected, considering the moisture diffusivity evident in Figure 6.28. The moisture diffusivity for lime–cement mortar varies only slightly as a function of the moisture content, where the moisture diffusivity decreases with increasing moisture level. This results in a relatively low moisture flow, even close to the wetted surface where the moisture gradient was high at the beginning of the wetting phase. Then further into the specimen, at a certain distance from the wetted surface, a lower moisture gradient could result in a moisture flow almost as high as at the surface, since the moisture diffusivity shows higher values in this lower moisture range.

Besides the effect of the increasing moisture diffusivity with decreasing moisture content, the moisture profile for lime–cement mortar displays an even flatter appearance in Figure 6.24. The cause of this flatter appearance is most likely that the frontline of the moisture profile is reaching the bottom of the specimen; since all sides except the wetted side of the specimen were sealed to prevent moisture transport, the moisture level is simply increasing.

The moisture profile for cement mortar also displays a flat appearance, flatter than that of the lime–silica brick (see Figures 6.23 and 6.24). However, the moisture profile for the cement mortar is steeply sloping close to the wetted surface. Examining moisture diffusivity as a function of moisture content, reveals that it regularly decreases with increasing moisture content. As can be seen in Figure 6.30, the moisture diffusivity is particularly low in the highest moisture step. The relatively steep slope only for the high moisture content close to the wetted surface can thus be explained by the characteristic low moisture diffusivity in this area.

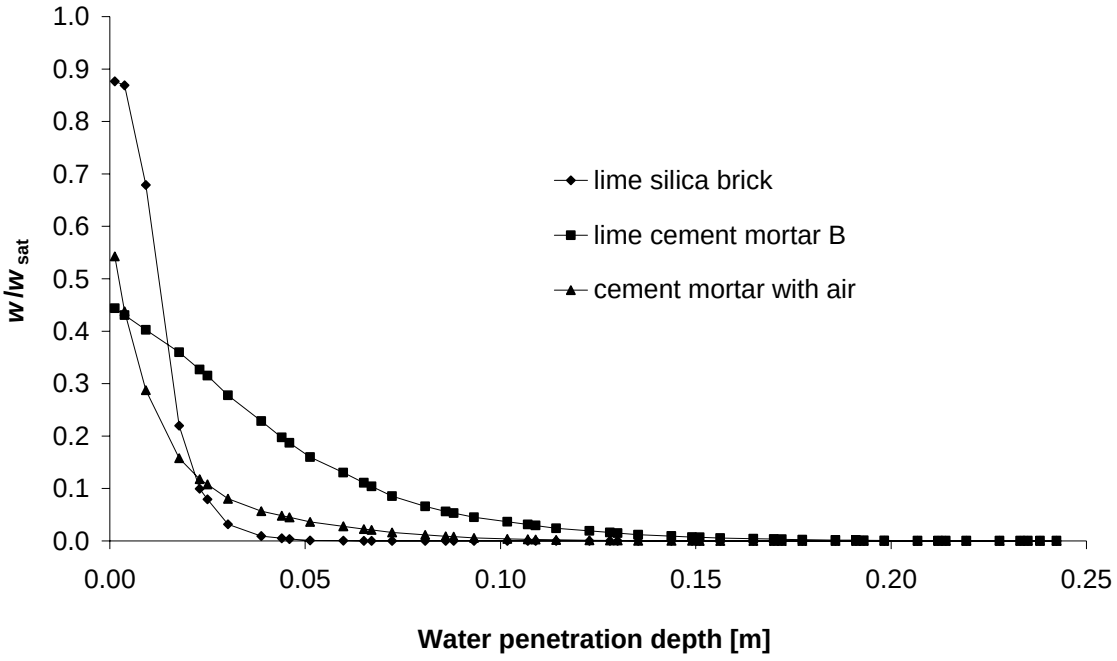

Figure 6.23 Single materials exposed to a free surface of water for 1.5 h.

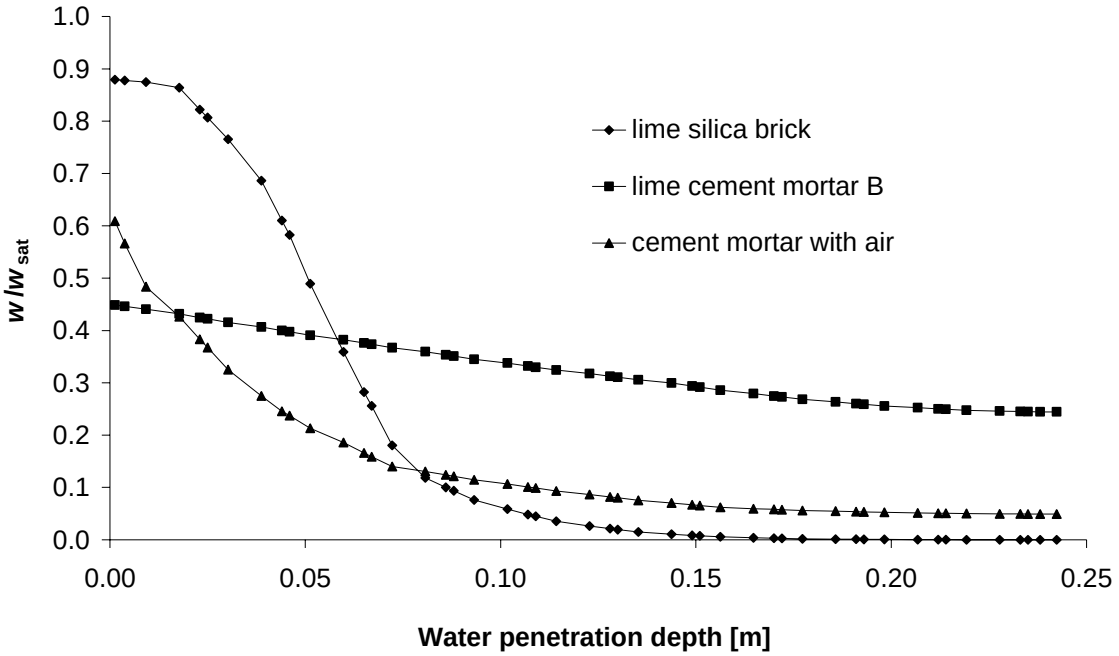

Figure 6.24 Single materials exposed to a free surface of water for one day.

Associated with the previous discussion of changes in the slope of the moisture profile caused by variations in the moisture diffusivity, moisture profiles and moisture diffusivities were compared. By using the same *x*-axis variable for both the moisture profiles and the moisture diffusivities, any possible effect of moisture diffusivities on the moisture profiles can more easily be pointed out. The results of water absorption simulations for the studied materials were originally presented in Section 6.4.2 as Figures 6.9, 6.11, and 6.12. Now, however, the moisture profiles are instead transformed so that the water penetration depth is expressed as a function of the degree of vacuum saturation, w/w_{sat} (see Figures 6.25, 6.27, and 6.29).

In connection with the moisture profiles, the corresponding moisture diffusivities are presented in Figures 6.26, 6.28, and 6.30. The moisture diffusivities are expressed as a function of the degree of vacuum saturation, w/w_{sat}. Comparison of the moisture profiles with the moisture diffusivities at a certain value of w/w_{sat} reveals that a change in the slope of the moisture profile regularly corresponds to a leap in the moisture diffusivity. The relationship between a leap in the moisture diffusivity and the change in slope of the moisture profile was observed for all three studied materials.

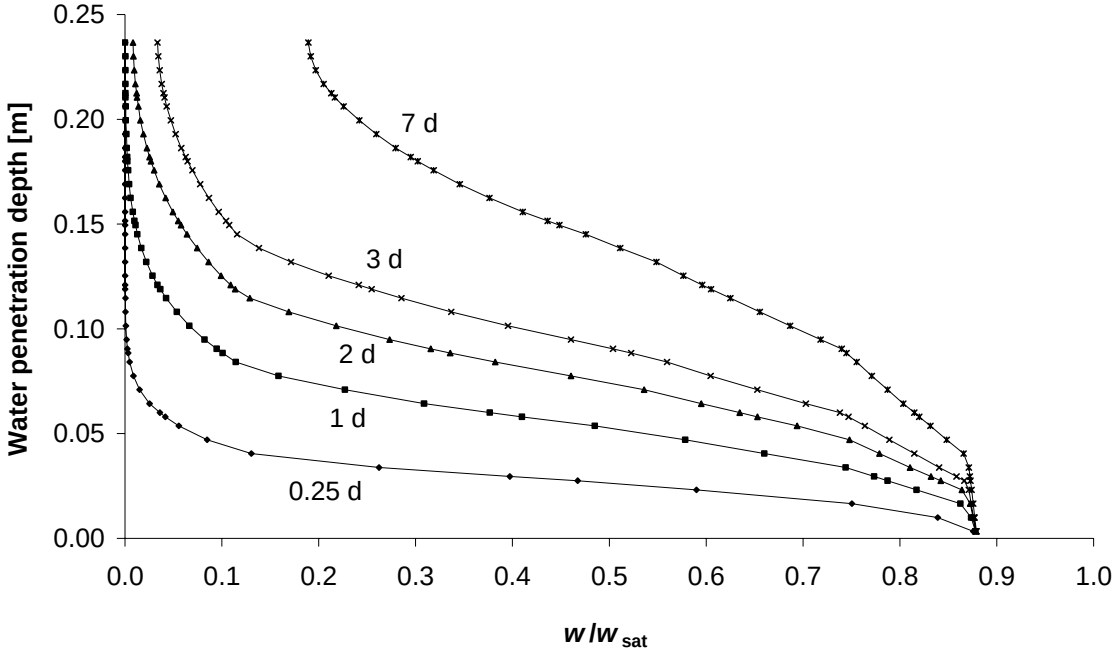

Figure 6.25 Specimens of lime–silica brick exposed to a free surface of water for different durations.

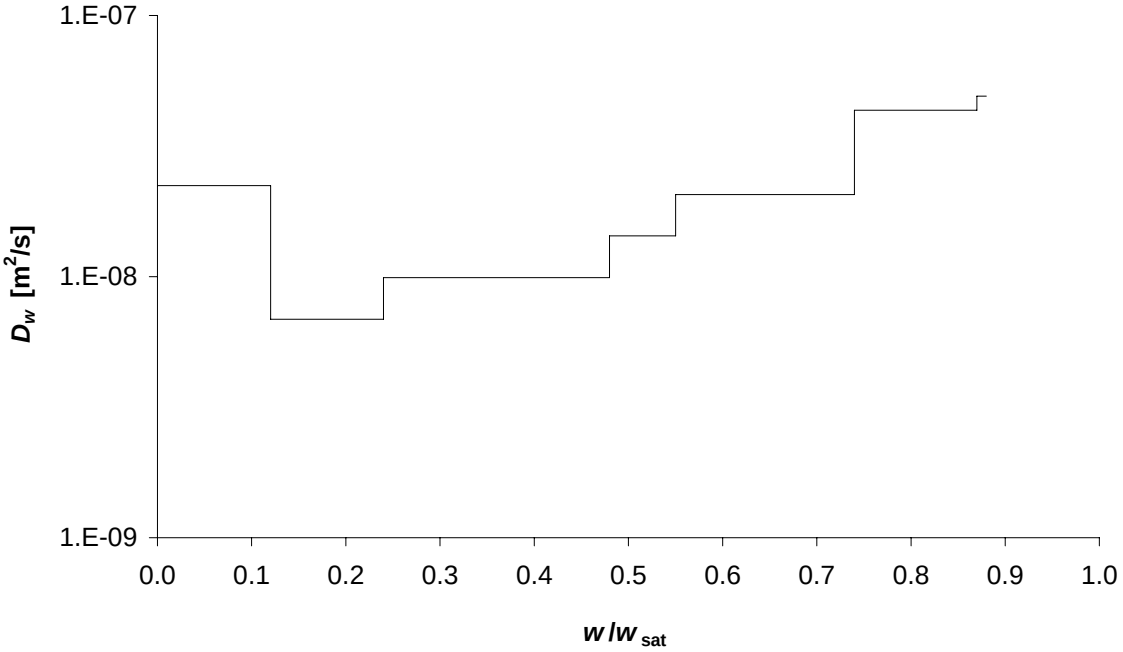

Figure 6.26 Moisture diffusivity, D_w, as a function of the degree of vacuum saturation, w/w_{sat}, for lime–silica brick.

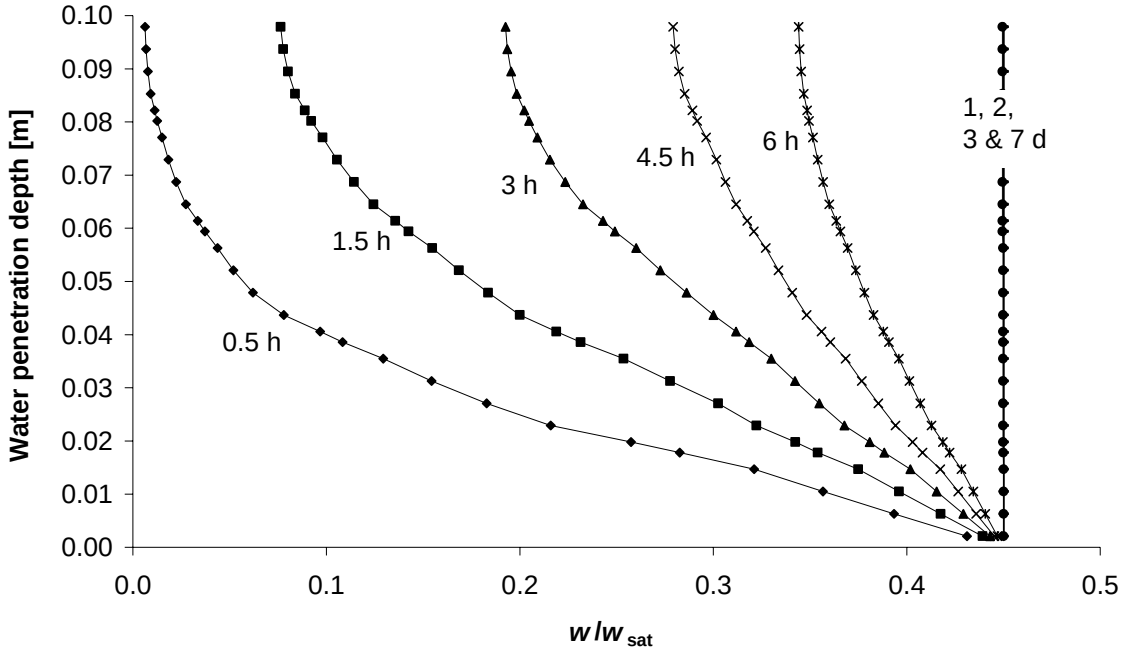

Figure 6.27 Specimens of lime–cement mortar exposed to a free surface of water for different durations.

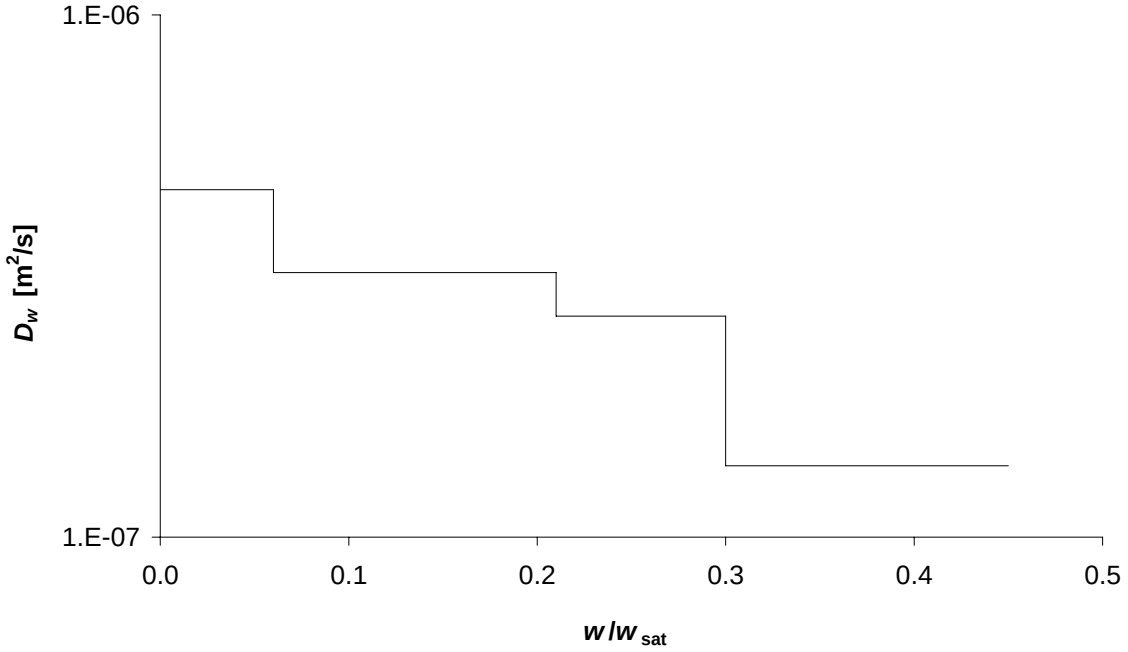

Figure 6.28 Moisture diffusivity, D_w, as a function of the degree of vacuum saturation, w/w_{sat}, for lime–cement mortar.

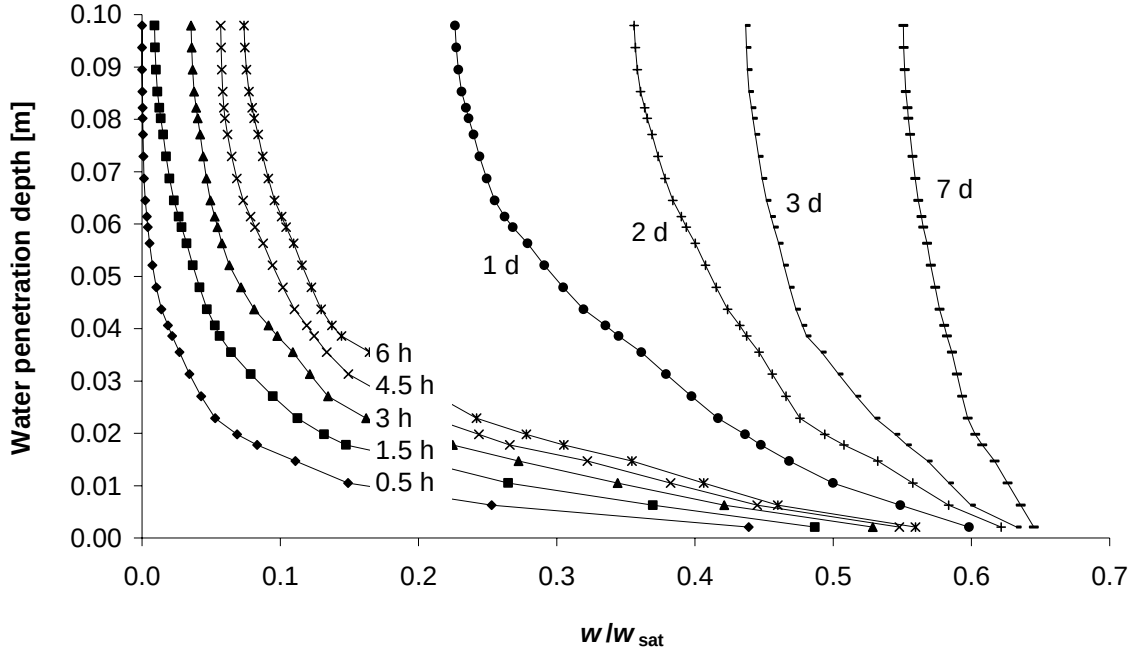

Figure 6.29 Specimens of cement mortar exposed to a free surface of water for different durations.

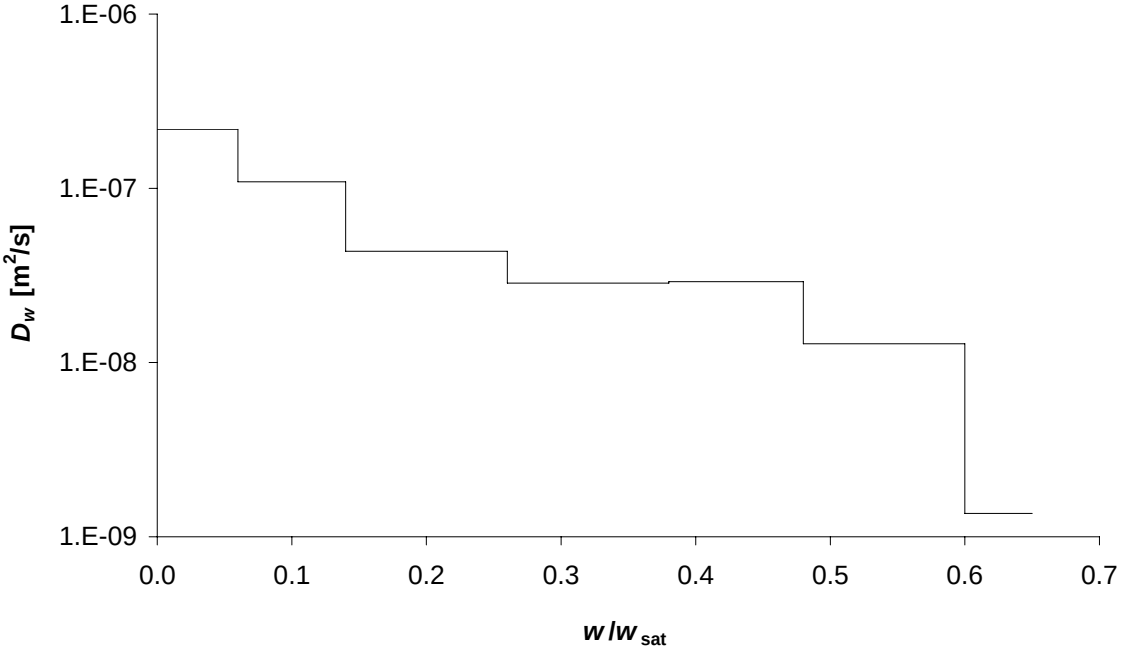

Figure 6.30 Moisture diffusivity, D_w, as a function of the degree of vacuum saturation, w/w_{sat}, for cement mortar.

Effect of combined materials

The shape of the moisture profiles for the underlying lime–silica brick were completely different depending on whether lime–cement mortar or cement mortar was used for the outer layer. Since the wetting was applied to the mortar, the material properties of the mortar were crucial for the water absorption rate of the combined specimen.

According to Figures 6.15–6.20 in Section 6.4.3, where the moisture profiles for the combined materials were presented, the moisture properties of the different mortars are crucial for the shape of the moisture profile in the substrate. When cement mortar was used for the outside layer of mortar, a clear gradient, given the degree of vacuum saturation, w/w_{sat} , was observed for the layer of mortar. By studying the moisture diffusivities, D_{ϕ}, used as input for the simulations of both the cement mortar and the underlying lime–silica brick, it was seen that the moisture diffusivity of the mortar was approximately 1% of the moisture diffusivity of the underlying material in the actual moisture range. The difference in the moisture diffusivity between the two materials caused a clear moisture gradient in the mortar.

Since the mortar had a relatively flat absorption isotherm compared to that of the underlying material in the high moisture range, the relative humidity decreased considerably in the mortar with the decreasing gradient of w/w_{sat}. An effect of the decrease in relative humidity of the mortar was that the underlying lime–silica brick, having a relatively steep absorption isotherm in the high moisture area, did not reach the capillary saturation point. Therefore, the relatively lower moisture diffusivity of the cement mortar, in combination with the flatter absorption isotherm of the underlying material, hindered the underlying material from reaching moisture contents approaching the capillary saturation point.

For lime–cement mortar used as the mortar layer, almost no gradient in w/w_{sat} was observed in the outer layer. The underlying lime–silica brick reached the capillary saturation point in the area close to the boundary between the two materials, and the capillary saturation point was reached through the layer of mortar in both the 2- and 7-day simulations. No moisture gradient could be observed in the mortar, since the moisture diffusivity of the mortar was approximately five times that of the underlying material in the high moisture range. In addition to the difference in moisture diffusivities, the absorption isotherm of the lime–cement mortar displayed a relatively steep slope in the high moisture range; the result was that a minor moisture gradient in the mortar would not significantly affect the relative humidity. Therefore, the underlying material was not particularly sensitive to changes in the moisture content of the lime–cement mortar.

As can be seen in all the figures, the thickness of the mortar was of minor importance, and was overshadowed by the differences in moisture diffusivities and absorption isotherms between the two mortars and the underlying lime–silica brick.

6.5.2 Comparison with measured moisture profiles

General

Results of the moisture profile measurements presented in Chapter 5 were compared with the results of corresponding moisture profile simulations presented in Sections 6.4.2 and 6.4.3.

Examining this comparison indicated how the appeared discrepancies could be used as a tool for analyzing the reliability of the simulations, and thereby the underlying input data.

Comparison between the simulations and the measurements could be accomplished quite realistically, since the actual materials used had definitely characterized properties. Also, the boundary conditions and initial moisture contents were adapted by the simulations so as to correspond to the boundary conditions for the moisture profile measurements. A comparison between measured and simulated moisture profiles for both single and combined materials can be seen in Figures 6.31 to 6.37.

Single materials

Moisture profiles for single materials of lime–silica brick, lime–cement mortar, and cement mortar are presented in Figures 6.31 to 6.33, respectively. The results of both moisture profile simulations and measurements are presented parallel to each other in the figures, to make comparison easier. The dotted lines represent the results of the simulations and the unbroken lines represent the results of the corresponding measurements. For practical reasons, the spatial resolution of the moisture profile measurements was limited (see Section 5.2.1).

The results presented in Figure 6.31 for lime–silica brick indicate generally satisfactory agreement between the measured and simulated values. It should be observed that the results of the measurements generally represent individual measurements instead of mean values obtained from numerous specimens; these results in a wider spread than if the results were based on mean values. However, the simulated moisture profiles displayed a flatter frontline appearance, particularly in the case of the 7-day simulation.

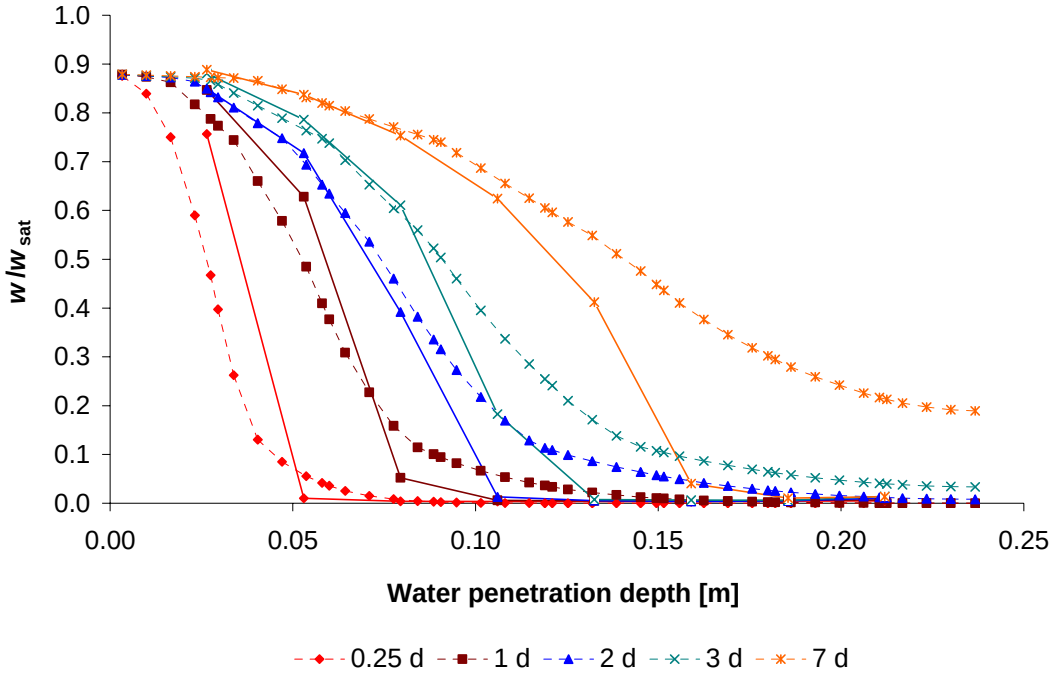

Figure 6.31 Specimens of lime–silica brick exposed to a free surface of water for different durations.

Results of moisture profile measurements and simulations for lime–cement mortar and cement mortar are presented in Figures 6.32 and 6.33, respectively. As with the lime–silica brick results presented in Figure 6.31, the conditions for both the measurements and simulations for the two mortars intentionally corresponded, so as to facilitate valid comparison. A difference between the mortars and the lime–silica brick was that the length of the specimens was just 0.1 m for the two mortars compared to 0.24 m for the lime–silica brick. The specimens of mortar were shorter because of cracking during the curing phase. Since shorter specimens were used for the mortars, shorter wetting durations were also applied to prevent the moisture profiles from reaching the bottom of the specimen. Despite the shorter wetting durations, the majority of the moisture profiles determined by simulations did reach the bottom of the specimen for both lime–cement mortar and cement mortar.

The range of wetting durations, from 0.5 h to 7 days, was applied for both the lime–cement mortar and the cement mortar in nine different time steps. As with the lime–silica brick, the moisture profile measurements were performed on individual specimens of the two mortars as well. It is clearly seen from Figures 6.32 and 6.33 that the measured moisture profiles display a steeper frontline than the simulations do. The difference in the frontline slope was simply not observed in profiles that had reached the bottom of the specimen and in moisture profiles that could still be considered semi-infinite, i.e. where the moisture profile had not reached the top of the specimen. Despite the difference between the slopes of the measured and simulated moisture profile frontlines, the measured and simulated moisture profiles corresponded relatively well for the lime–cement mortar up to a penetration depth of 0.06 m. For higher penetration depths of the moisture profiles, the moisture contents were overestimated by the simulations.

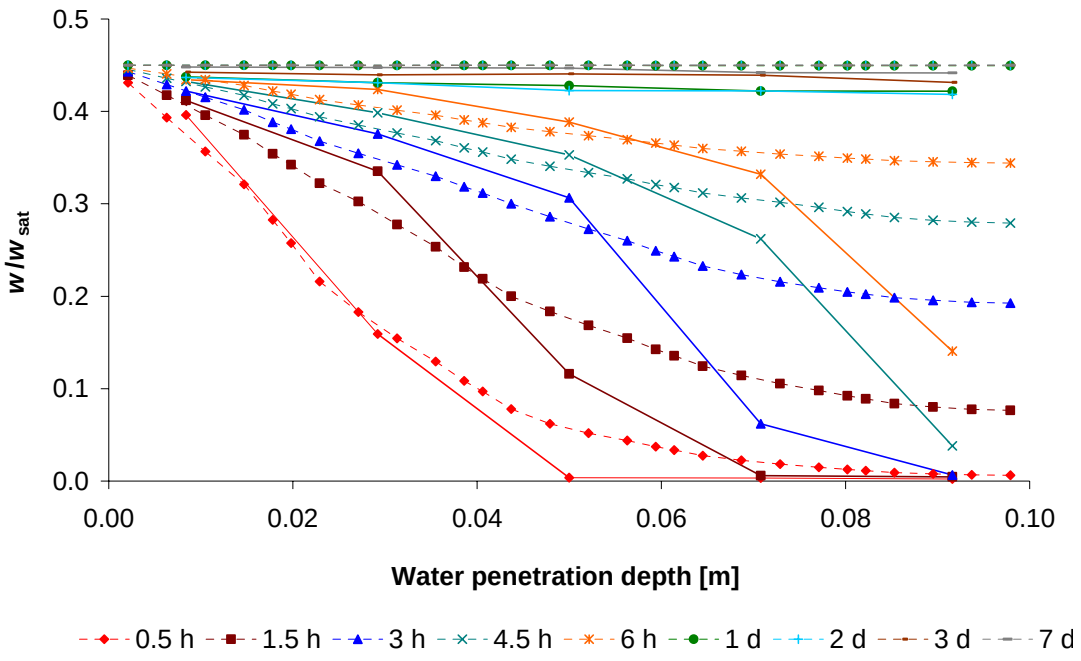

Figure 6.32 Specimens of lime–cement mortar exposed to a free surface of water for different durations.

In Figure 6.33, corresponding measured and simulated moisture profiles are shown for the cement mortar. The agreement between the penetration depths of the measured and simulated moisture profile frontlines was good for wetting durations of up to 1 day.

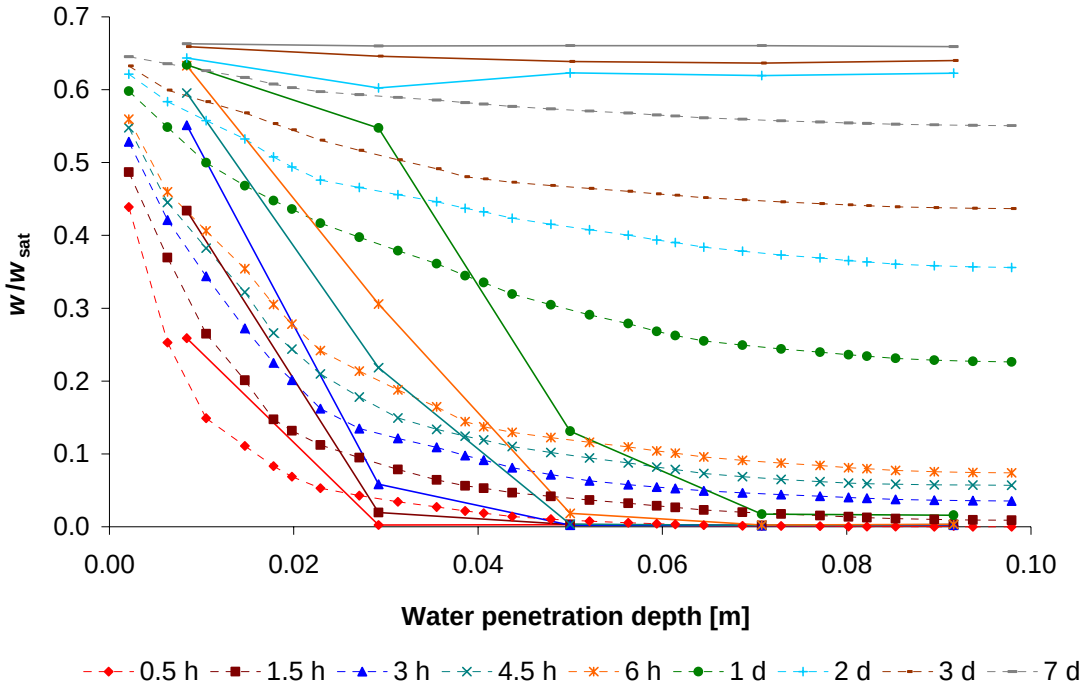

Figure 6.33 Specimens of cement mortar exposed to a free surface of water for different durations.

For both the lime–cement mortar and the cement mortar the measured slope of the moisture profile frontline was generally steeper than the simulated value. For wetting durations of over 1 day, a considerable difference in the moisture level was observed between the measurements and the simulations.

Combined materials

A comparison of simulated and measured moisture profiles was performed for combined materials as well. The combined materials were produced with an outer layer of either lime–cement mortar or cement mortar attached to an underlying layer of lime–silica brick; the outer layer was either 7 mm or 14 mm thick. The wetting time was also varied for the tests, and continuous wetting phases of two and seven days were applied.

In Figures 6.34 to 6.37, results of both moisture profile simulations and measurements are presented for lime–silica brick with an outer layer of either lime–cement mortar or cement mortar. In the figures, the results of the simulations are represented by blue dots and the results of the measurements are represented by red dots. The unfilled dots represent the moisture level of the outer layer of mortar and the filled dots represent the moisture levels of the underlying lime–silica brick. From the measurements of the moisture profiles, just one value of the moisture level

of the outer layer of mortar could be obtained, seen as the red single unfilled dots to the left in the figures.

In Figures 6.34 and 6.35, where the lime–cement mortar was used as an outer layer of mortar for the combined specimen, good correlation was found between the absolute moisture levels in the simulations and the measurements. For the 2-day wetting phase, the frontline of the simulated moisture profiles showed a greater moisture penetration depth than did the measurements for either the 7-mm of 14-mm mortar. As with the moisture profile results for the single materials, the moisture profile results for the combined materials generally displayed a greater slope for the simulated than for the measured moisture profile frontline.

By studying the moisture levels of the outer layer of lime–cement mortar it was observed that the actual moisture levels corresponded to the moisture level of the capillary saturation point as determined in the tests presented in Chapter 2. For the measurements, a moisture gradient indicating decreasing moisture with increasing distance from the wetted surface was seen for the outer layer of mortar. The observation of a moisture gradient was based on the difference between the moisture levels of the 7-mm versus the 14-mm layer of lime–cement mortar, where the 14-mm layer displayed a lower moisture level then the 7-mm layer did for wetting durations of both 2 and 7 days. The moisture level of the lime–silica brick in the area close to the interface corresponded to the capillary saturation point for both the 2- and 7-day measurements.

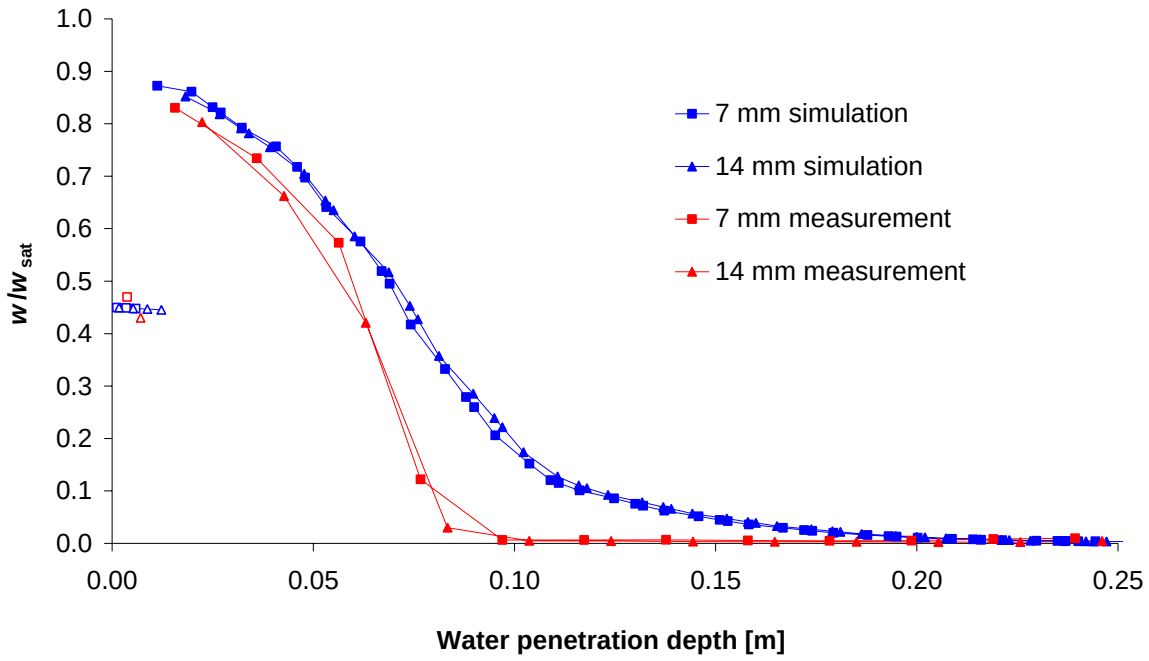

Figure 6.34 Specimens of lime–silica brick with a layer of lime–cement mortar attached. The surface of the mortar was exposed to a free surface of water for two days.

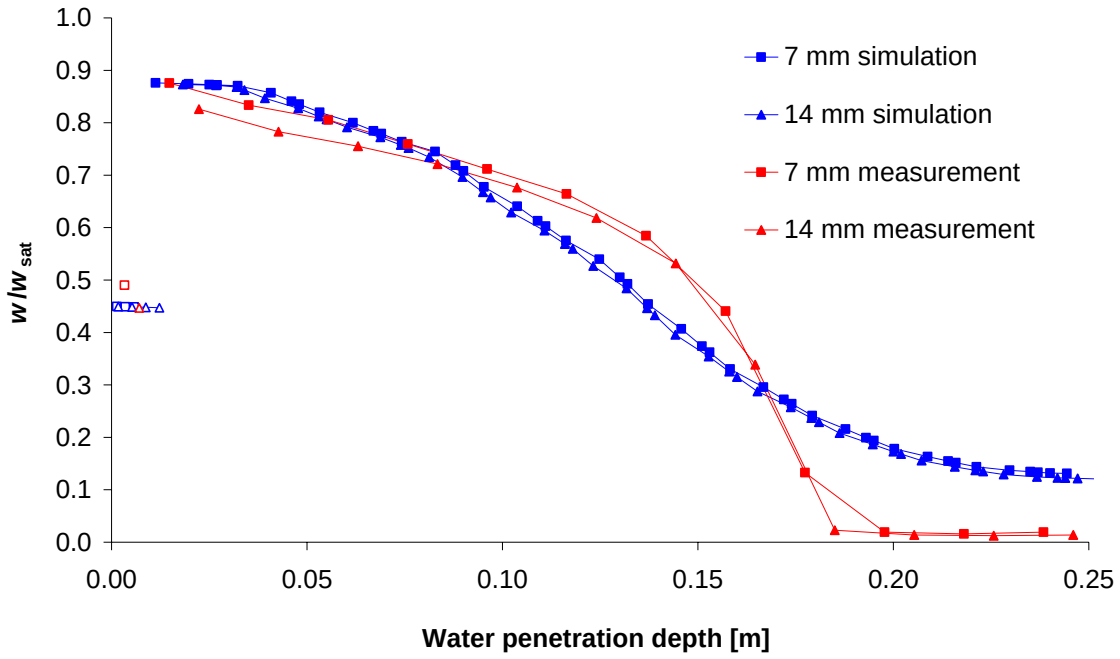

Figure 6.35 Specimens of lime–silica brick with a layer of lime–cement mortar attached. The surface of the mortar was exposed to a free surface of water for seven days.

In Figures 6.36 and 6.37 the results of both moisture profile measurements and simulations are presented for 2- and 7-day wetting phases. An outer layer of cement mortar, either 7 mm or 14 mm thick, was attached to an underlying lime–silica brick. Generally, the results of the moisture profile simulations indicate a flatter profile than the measurements do, where the moisture profile frontline was more clearly marked. By studying the moisture levels in the cement mortar, a clear moisture gradient was observed for the simulations. The moisture levels in the cement mortar correspond to the moisture levels at the capillary saturation point. Since the measured moisture levels in the mortars are only represented by mean values, a possible gradient could not be determined. The measured and simulated moisture levels in the lime–silica brick at the interface correspond very well for the 14-mm cement mortar and relatively well for the 7-mm cement mortar layer.

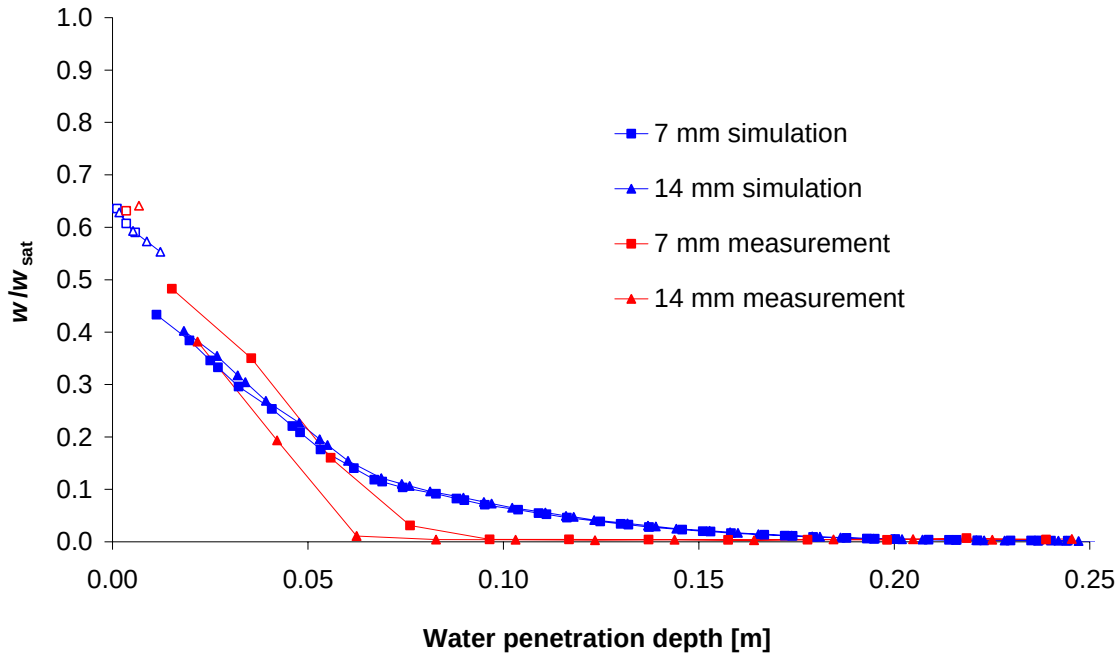

Figure 6.36 Specimens of lime–silica brick with a layer of cement mortar attached. The surface of the mortar was exposed to a free surface of water for two days.

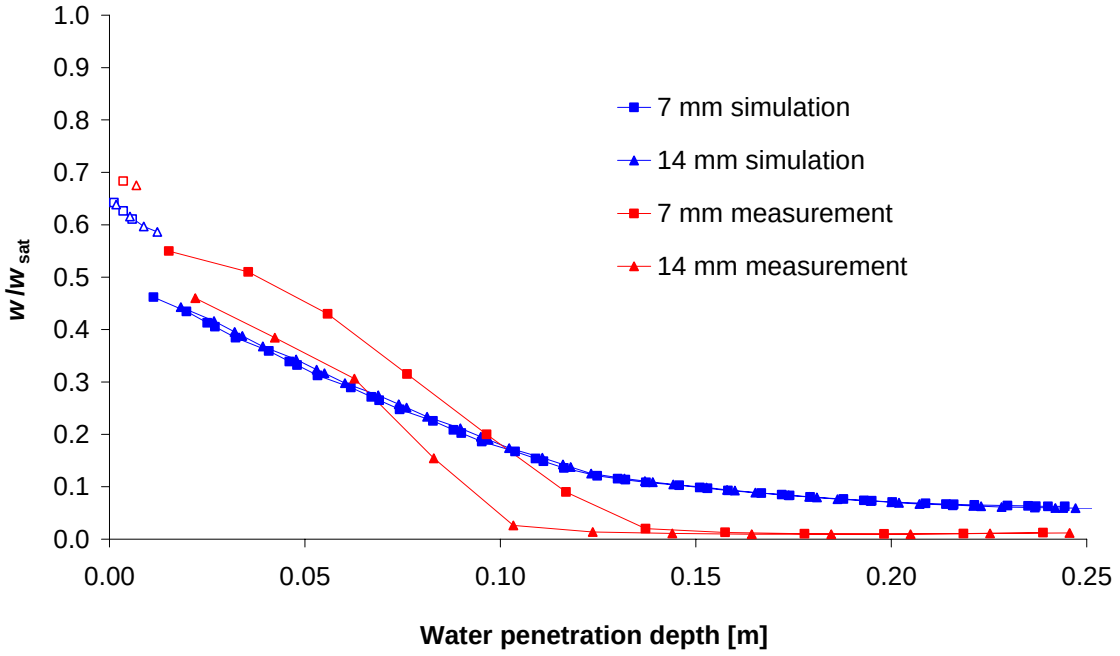

Figure 6.37 Specimens of lime–silica brick with a layer of cement mortar attached. The surface of the mortar was exposed to a free surface of water for seven days.

6.5.3 Alternative simulations

General

Since the measured and simulated moisture profiles did not agree well enough, some alternatives to the original simulations performed in Section 6.4.2 are presented in this section. The alternative simulations are performed for the cement mortar, since the agreement between the simulations and measured values presented in Section 6.5.2 was unsatisfactory.

Method

As input for the alternative simulations for the cement mortar, data according to Section 6.3 are generally used. Only the moisture diffusivity and the sorption isotherm data, initially determined in Chapters 3 and 2, respectively, are modified. The results of the original simulations especially diverge from the shape of the measured moisture profiles, in such a way that the simulated moisture profiles do not display a clear frontline. For the original moisture profile simulations, moisture diffusivity values up to a moisture content corresponding to a degree of vacuum saturation, w/w_{sat}, of 0.65 were used (see A in Figure 6.38). This moisture content corresponds to the capillary saturation point for initially dry specimens. However, since the moisture diffusivities were determined during capillary water uptake for specimens initially conditioned to different moisture contents, the capillary saturation point was reached at moisture contents corresponding to a degree of vacuum saturation, w/w_{sat}, of 0.92 (see B in Figure 6.38).

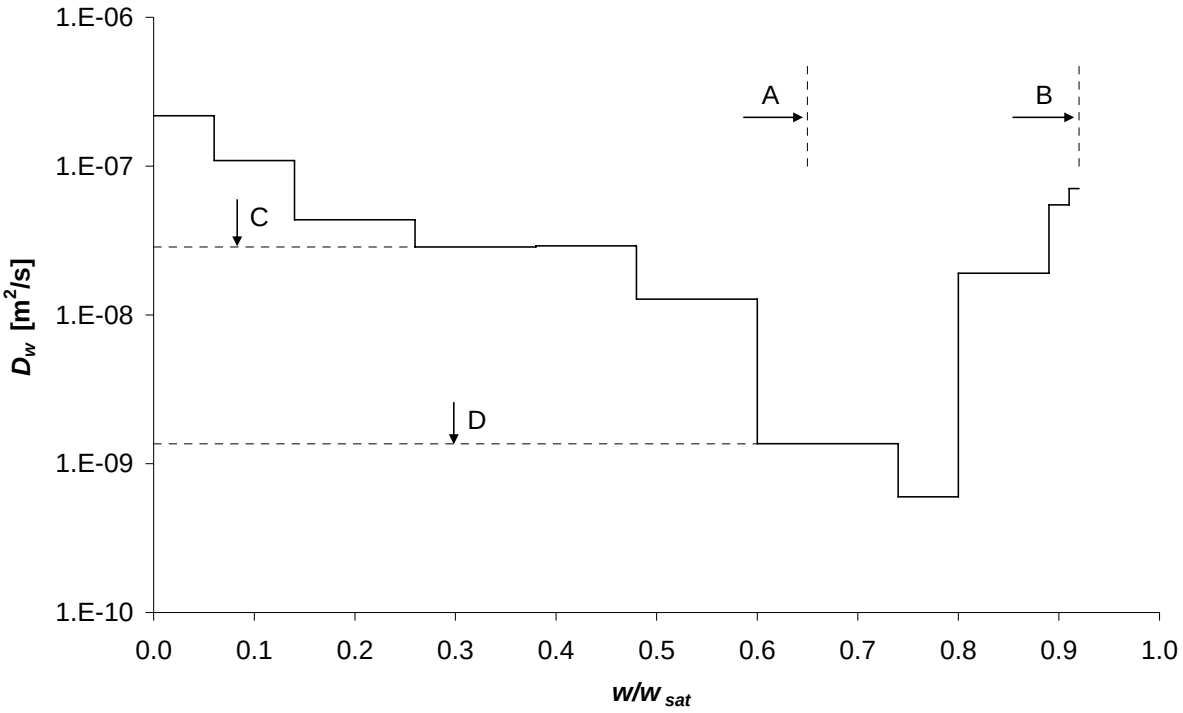

Figure 6.38 Moisture diffusivity, D_w, over the complete moisture range as a function of the degree of vacuum saturation, w/w_{sat}, for cement mortar, according to Chapter 3.

To achieve a clear frontline of the moisture profile, the moisture diffusivity is expected to display a minimum in the mid moisture range and a maximum in both the high and low moisture ranges (cf. Equation 6.5). Therefore, the moisture diffusivity in the moisture range up to B in Figure 6.38 was used at the same time as the desorption isotherm according to Chapter 2 was used as an absorption isotherm. The desorption isotherm was transformed into an absorption isotherm corresponding to a maximum degree of vacuum saturation, w/w_{sat}, of 0.92 using the procedure described in Section 6.3.3.

A computer program was used to evaluate the moisture diffusivities presented in Chapter 3, in which the evaluation was performed stepwise from the high to the low moisture range. The evaluation procedure is designed so that systematic deviation in the high moisture range would increase at each moisture level, thus showing the largest deviation in the low moisture range. To analyze the effect of a possible fault in the moisture diffusivity in the low moisture range, two different simulations were performed in which the moisture diffusivities were estimated to correspond to the dotted lines marked C and D, respectively (see Figure 6.38). For these simulations, the moisture diffusivity was used up to a moisture content corresponding to B in Figure 6.38 as well.

To clarify the influence of the sorption isotherm on the input of the simulations, an alternative simulation was performed for the cement mortar. It was suspected that the fault would arise when the moisture diffusivity originally expressed as the moisture content, D_w, was transformed into the moisture diffusivity expressed as the relative humidity, D_ϕ, using the slope of the absorption isotherm (see Equation 6.24). Therefore, an alternative simulation was performed in which the fundamental potential, ψ, was used as input instead of the moisture diffusivity, D_w.

Results

All the alternative simulations were performed using a wetting duration of 1 day and are compared to a measured moisture profile marked M in Figure 6.39, as well as to the original simulated moisture profile marked A. The measured and the original simulated moisture profiles were originally presented in Chapter 5 and in Section 6.4.2, respectively.

Since the alternative simulated moisture profiles, marked B, C, and D in Figure 6.39, use a higher degree of vacuum saturation for the capillary saturation point, the results are standardized according to the moisture levels.

For simulation B, a clearer moisture profile front is seen, compared to the results of the original moisture profile simulations. Since the moisture levels are still overestimated in front of the moisture profile, the moisture diffusivities are further modified. For the simulation alternatives marked C and D, the moisture diffusivities are assumed to take lower values in the low moisture range compared to the moisture diffusivity values determined in Chapter 3. The results of the moisture profile simulations with moisture diffusivities according to the dotted lines marked C or D in the low moisture range in Figure 6.38, show that the simulated moisture profiles are approaching the shape of the measured moisture profile, marked M.

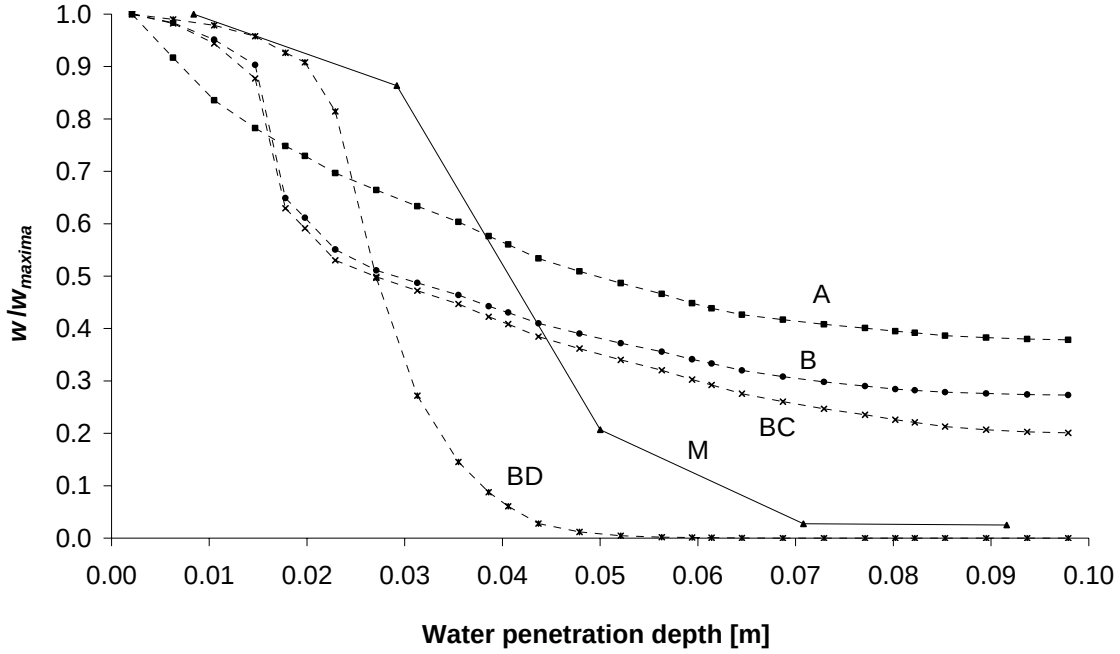

Figure 6.39 Measured and simulated moisture profiles for specimens of cement mortar exposed to a free surface of water, for a wetting duration of one day.

The alternative simulation in which the fundamental potential, ψ, was used instead of the moisture diffusivity, D_w, produced results that were unchanged from those of the original simulation, marked A.

6.6 SUMMARY AND CONCLUSIONS

Moisture profile simulations are fundamentally based on a moisture flow equation in which relative humidity is used as a driving potential. As input for the simulations, the moisture diffusivity over the complete moisture range was determined in Chapter 3. Sorption isotherms were also used as input for the studied materials and were determined in Chapter 2. However, the sorption isotherms from Chapter 2 could only be determined for desorption over the complete moisture range, so an estimation had to be performed in Section 6.3.3 to transform the desorption isotherms into absorption isotherms. The transformation had to be performed, because the moisture diffusivities were determined by absorption, and because transformation of the diffusivities was estimated to produce a more uncertain result than would estimation of the absorption isotherm from the desorption isotherm. The absorption isotherms were known for the hygroscopic range, and the capillary saturation point was well known from the tests presented in Chapter 3, so a satisfactory estimation of the absorption isotherm over the complete moisture range could be performed.

The relatively new and untested method for estimating moisture diffusivities from the results of single capillary water absorption tests for specimens conditioned to different moisture levels remains to be validated. By studying the evaluation procedure it was discovered that a possible

deviation in the high moisture range resulted in an accumulated deviation in the lower moisture range. A possible way to check the accuracy of the moisture diffusivity results for the low moisture range would be to perform corresponding diffusivity measurements using the well-reputed cup method.

The moisture profile simulations were performed on three different materials that were supposed to reflect commonly used masonry façade materials in terms of moisture transport behaviour. The materials were exposed to continuous wetting for different durations and tested as both single and combined materials. The output moisture levels were expressed as the degree of vacuum saturation instead of moisture content, since it was discovered in Chapter 3 that a considerable part of the variation in the moisture level due to inhomogeneities could be excluded by instead using the degree of vacuum saturation.

For the moisture profile simulations, all conditions, such as the initial moisture content, specimen geometry, and wetting durations, were found to correspond to the moisture profile measurements presented in Chapter 5. Since both the measurements and simulations were performed on the same materials and using corresponding conditions, the results could be compared directly. Comparison between the moisture profile measurements from Chapter 5 and the moisture profile simulations was performed in Section 6.5.2. The comparison was performed for both single and combined materials, and a surprisingly good agreement was found for both. Generally, however, the simulations showed a flatter slope of the moisture profile frontline than the measurements did; furthermore, the frontline was more distinctly marked in the measured than in the simulated results.

In Section 6.5.3, alternative simulations were performed on cement mortar to study the influence of the moisture diffusivities on the shape of the moisture profile. The alternative simulations clearly demonstrated that the flatter shape of the frontline of the simulated moisture profiles, compared to that of the measured moisture profiles, is partly caused by an overestimation of the moisture diffusivities in the low moisture range. The flatter shape is also caused by an underestimation of the moisture diffusivity in the high moisture range.

The overestimation of the moisture diffusivities in the low moisture range most likely happens when determining the moisture diffusivity from the results of water uptake tests (see Chapter 3). Since the moisture diffusivities are determined stepwise, working from high moisture contents to low moisture contents, and since the diffusivity for each moisture step is partly based on the moisture diffusivities of the higher moisture steps, a certain systematic deviation will increase with decreased moisture content.

The underestimation of the moisture diffusivities in the high moisture range is most likely caused by the conditioning procedure for the determination of the moisture diffusivities (see Chapter 3). Since the specimens used for the water uptake tests presented in Chapter 3 were vacuum saturated and dried to different moisture levels during the conditioning procedure, the moisture levels at the capillary saturation point became altered. The results showed that a specimen with a higher initial moisture content did reach the capillary saturation point, but at a higher moisture content. Therefore, the moisture diffusivities at higher moisture contents are more accessible than the moisture contents are that could be reached by the capillary water uptake of an initially

dry specimen. Because of this, the moisture diffusivities determined for the high moisture range were not used during the original simulations presented in Section 6.4. Consequently, the moisture diffusivities in the upper moisture range were not used, resulting in the moisture diffusivities for both the lime–cement mortar and the cement mortar not displaying a minimum in the mid moisture range. Since a minimum in the mid moisture range did not appear, a sharp front in the simulated moisture profiles also did not appear.

For the combined materials, both in the measurements and the simulations, considerably lower moisture contents were observed in the underlying lime–silica brick when the cement mortar instead of the lime–cement mortar formed the outer layer of mortar. The lower moisture content in the underlying material is most likely caused by the difference in moisture diffusivity between the outer cement mortar layer and the underlying lime–silica brick. The diffusivity in the actual moisture range is considerably lower for the outer layer, resulting in a moisture content gradient. Since the sorption isotherm of the cement mortar is relatively flat, the gradient of the moisture content resulted in a relative humidity gradient across the outer layer of cement mortar. The pore water pressure in the interface between the two materials clearly differs from the pore water pressure corresponding to the saturation point, thus preventing the underlying lime–silica brick from reaching the capillary saturation point even after long wetting durations.

7 CONCLUSIONS AND FUTURE STUDIES

7.1 CONCLUSIONS

To determine sorption isotherms over the complete moisture range, two different methods must be used. With the cup method, both absorption and desorption isotherms could successfully be determined in the hygroscopic moisture range. With the capillary moisture range, the pressure plate method had to be used; however, the pressure plate equipment used only allowed desorption isotherms to be determined. To determine absorption isotherms in the capillary moisture range as well, while still using the same method, the pressure plate equipment would have to be extensively modified. Desorption isotherms determined using the two methods have an overlap of approximately 93% RH and thus correspond very well.

Moisture diffusivities were determined by evaluating a series of water absorption tests using Boltzmann transformation. Different specimens were conditioned to different moisture levels representing the complete moisture range from completely dry up to vacuum saturation. Using this method, the moisture diffusivities could be determined over the complete moisture range. Results of moisture profile simulations based on moisture diffusivities indicate that the moisture diffusivities are overestimated in the low moisture range.

Different methods for measuring transient moisture profiles were evaluated. All the tested methods had both advantages and disadvantages. One of the methods, the x-ray technique, could be excluded almost immediately from application in testing. The most interesting methods were the NMR and the slice and dry methods. Since equipment accessibility limits application of the NMR technique, as does the impossibility of performing measurements on specimens containing a certain content of iron, the method was excluded from further study. The method that demonstrated great versatility was the slice and dry method, and this method was chosen for performing larger-scale measurements.

The larger-scale moisture profile measurements were performed on specimens of both single and combined materials. Three different materials were used for the tests. All the materials were tested as single materials, and then different combinations of the three materials were tested. During the tests the wetting durations were varied widely, so that moisture profiles could be determined at the various time steps.

Moisture profile simulations with boundary conditions and sorption isotherms expressed as relative humidity produced satisfactory results, since relative humidity levels between 99% and 100% can be determined with sufficient accuracy. Moisture profile simulations were successfully performed for both single and combined materials.

Comparison between simulated and measured moisture profiles for both single and combined materials was performed. The measured and the simulated moisture profiles for the combined materials showed a most satisfactory agreement. However, comparison of the results for two of the single materials revealed deviations between the measured and the simulated moisture profiles. These deviations were found to stem from inaccuracies in the moisture diffusivities, and both the conditioning principle and an accumulated error in evaluating the moisture diffusivities were decisive.

7.2 FUTURE STUDIES

In this study, absorption isotherms above the hygroscopic moisture range were estimated using absorption isotherms for the hygroscopic moisture range in combination with knowledge of the moisture contents at the capillary saturation point. To perform moisture profile simulations with satisfactory accuracy, both complete absorption and desorption isotherms must be determined. To determine the absorption isotherms above the hygroscopic moisture range, the pressure plate equipment used for the tests must be further modified. Scanning curves for the complete moisture range will also be required for the simulation of redistribution and drying over the complete moisture range.

To perform moisture profile simulations over the complete moisture range for both absorption and desorption, moisture diffusivities must also be determined for the desorption phase. The moisture diffusivities determined in this research for the absorption phase will most likely not be valid for the desorption phase, since the evaporation process over the surface took considerably longer than the wetting phase did when the surface of the material was exposed to a free surface of water. Additional desorption tests for specimens with various initial moisture contents will most likely provide a sufficient basis for determining the moisture diffusivities using the step response method. The moisture diffusivities determined using the Boltzmann principle seemed to be overestimated in the low moisture range. Therefore, additional measurements of moisture diffusivity should be performed in the low moisture range. The additional measurements should preferably be made using the cup method.

Moisture profile simulations over the complete moisture range, considering absorption, desorption, and redistribution, should be compared to free-standing measurements of transient moisture profiles. This will allow analysis of the reliability of the available methods for calculating the redistribution and desorption phases as well.

Non-destructive moisture profile measurements should be performed using the NMR method, a method that allows a single specimen to be used repeatedly in testing. Variations in material properties can thus be excluded when evaluating the results produced by this method. The NMR method also provides high spatial resolution in studies of moisture gradients across interfaces.

REFERENCES

Ahlgren, L., Bergström, S. G., Fagerlund, G. and Nilsson, L-O. (1976), 'Moisture in concrete' (in Swedish), CBI educational training, Stockholm.

Anderberg, A. and Wadsö, L. (2004), 'Moisture in self-levelling flooring compounds. Part II. Sorption isotherms', Nordic Concrete Research, Publication No. 32, 2/2004.

Arfvidsson, J. (1989), 'Computer model for two-dimensional moisture transport. Manual for JAM-2.0' (in Swedish), Division of Building Physics, Lund Institute of Technology.

Arfvidsson, J. (1998), 'Moisture transport in porous media: Modelling based on Kirchhoff potentials', Report TVBH-1010, Division of Building Physics, Lund Institute of Technology.

Arfvidsson, J. and Janz, M. (1994), 'Determination of moisture transport coefficients at very high moisture levels by series of capillary absorption tests' (in Swedish), Part of Report TVBH-7180, Division of Building Physics, Lund Institute of Technology.

Bentz, D.P. and Hansen, K.K. (2000), 'Preliminary observations of water movement in cement pastes during curing using X-ray absorption', Cement and Concrete Research, Volume 30, No. 7, July 2000, pp. 1157-1168.

Bentz, D.P., Quenard, D. A., Kunzel, H.M., Baruchel, J., Peyrin, F., Martys, N.S. and Garboczi, E.J. (2000), 'Microstructure and transport properties of porous building materials. II: Three-dimensional X-ray tomographic studies', Materials and Structures, Vol. 33, April 2000, pp 147-153.

Bjerkeli, L. (1990), 'The use of X-ray thomography for measuring water absorption in concrete' (In Norwegian), Report STF65 A90008, Forskningsinstituttet for Cement og Betong, Norway.

Bomberg, M. (1974), 'Moisture flow through porous building materials', Report 52, Division of Building, Technology, Lund Institute of Technology.

Brocken, H. J. P. (1998), 'Moisture transport in brick masonry: The gray area between bricks', Eindhoven University of Technology, Netherlands.

Burström, P. G. (2001), 'Building materials' (in Swedish), textbook, Studentlitteratur, Lund, Sweden.

Christensen, K. and Strømdahl, K. (1996), 'Vejledning till pressure plate extractor' (in Danish), Serie 1, No. 1, Department of Structural Engineering and Materials, Technical University of Denmark.

Claesson, J. (1994), 'Determination of moisture transport coefficients at very high moisture levels by series of capillary absorption tests' (in Swedish), Division of Building Physics, Lund institute of Technology.

Fagerlund, G. (1973), 'Determination of pore size distribution by suction porosimetry', Materials and Structures, Vol. 6, No. 33, pp. 191-201.

Fagerlund, G. (1977), 'The critical degree of saturation method of assessing the freeze/thaw resistance of concrete', Materials and Structures, Vol. 10, No. 58.

Hall, C. and Hoff, W. D. (2002), 'Water transport in brick, stone and concrete', Taylor and Francis, London.

Hedenblad, G. (1993), 'Moisture permeability of mature concrete, cement mortar and paste', Division of Building Materials, Report TVBM-1014, Lund institute of Technology.

Hedenblad, G. (1996), 'Materialdata för fukttransportberäkningar' (In Swedish), Byggforskningsrådet, T19: 1996, Stockholm.

Hinderson, G. (1958), 'Kalk- och kalkcementbruk, Invändig puts på betong' (in Swedish), Statens nämnd för byggforskning, Rapport 46, pp. 6, Stockholm.

Hjorslev, H. M. (1998), 'Retention curves measured using pressure plate and pressure membrane apparatus', SBI-report 295, SBI, Denmark.

Hus AMA 98, (1998), National material and working instructions for Buildings (in Swedish), AB Svensk Byggtjänst, pp. 108, Stockholm.

Janz, M. (1997), 'Methods of measuring the moisture diffusivity at high moisture levels', Report TVBM 3076, Division of Building Materials, Lund Institute of Technology.

Janz, M. (2000), 'Moisture transport and fixation in porous materials at high moisture levels', Doctoral thesis, Report TVBM 1018, Division of Building Materials, Lund Institute of Technology.

Jensen, S.K., Damkilde, L. and Krabbehøft, K. (2001), 'Non-destructive assessment and FEM-simulations of moisture profiles in Sitka spruce (Picea Sitchensis) during drying', 3rd European COST E15 Workshop on wood drying, 11-13 June 2001, Helsinki, Finland

Johannesson, B. and Janz, M. (2002), 'Test of four different experimental methods to determine sorption isotherms', Materials and Structures, Vol. 14, No. 6, pp. 471-477.

Johansson P. (1999), 'A thermal imaging method for measuring moisture distribution in porous building materials', Proceedings of the 5th Symposium on Building Physics in the Nordic Countries, Göteborg, August 24-26, pp.297-304.

Kieβel, K. and Krus, M. (1991), 'NMR-measurements of capillary penetration behavior of water and hydrophobing agent in porous stone and derivation of new capillary transport values', Report FtB-12e, Fraunhofer-Institut für Bauphysik, Holzkirchen.

van der Kooi, J. (1971) 'Moisture transport in cellular concrete roofs', Doctoral thesis, Uitgevery Waltman, Delft, Netherlands.

Krus, M. and Kieβl K. (1991), 'Vergleichende untersuchungen zur bestimmung der porenradienverteilung von natursandsteinen mittels saugspannungsmessungen und quecksilber druckporosimetrie' (in German), FtB-11/1991, Fraunhofer-Institut für Bauphysik, Holzkirchen.

Krus, M. and Kieβl, K. (1998), 'Determination of the moisture storage characteristics of porous capillary active materials', Materials and Structures, Vol. 31, pp. 522-529.

Levoguer, C. L. and Williams, D. R. (1997), 'The determination of permeability and diffusion rates in polymer films and packaging materials', Pharm. Technol. Europe, April 25-30.

Lindgren, O. (1992), 'Medical CT-Scanners for non-destructive wood density and moisture content measurements', LuTH 1992:111 D ISSN 0348-8373, Luleå University of Technology.

Lykow, A.W. (1958), 'Transporterscheinungen in kapillarporösen körpern', Akademie-Verlag, Berlin, Germany.

Nielsen, A.F. (1973), 'Measurements of drying-out of cellular concrete', Thermal Insulation Laboratory, Meddelelse Nr. 26, Technical University of Denmark.

Nielsen, A.F. (1974), 'Moisture distributions in cellular concrete during heat and moisture flow', (in Danish), Thermal Insulation Laboratory, Meddelelse Nr. 29, Technical University of Denmark.

Nokken, M. R. and Hooton, R. D. (2002), 'Dependence of absorption on degree of saturation of concrete' Cement, Concrete and Aggregates, CCAGDP, Vol. 24, No. 1, June 2002, pp. 20-24.

Nordtest standard (1997), 'Retention curve and pore size distribution', NT BUILD 481.

Pel, L. (1995), 'Moisture transport in porous building materials', Eindhoven University of Technology, Netherlands.

Plagge, R., Grunewald, J., Haeupl, P. and Bomberg, M. (2004), 'Analysis of water uptake experiments of building materials: Methods, functions and parameters', Proceedings of the 'CIB W40 Conference papers Thursday 2 September 2004', September 1-2, Glasgow.

Quenard, D. and Sallee, H. (1989), 'A gamma-ray spectrometer for measurement of the water diffusivity of cementitious materials', Mat. Res. Soc. Symp. Proc. Vol. 137, Materials Research Society.

Richards, L. A. (1948), 'Porous plate apparatus for measuring moisture retention and transmission by soil', Soil Science, Vol. 66, pp. 105-109.

Rosenkilde, A. (2002), 'Moisture content profiles and surface phenomena during drying of wood', Division of Building Materials, KTH- Royal Institute of Technology.

Sandin, K. (1980), 'The effect of the rendering on the moisture balance of the façade-sub report I-VIII', (in Swedish), Report TVBM-1005, Division of Building Materials, Lund Institute of Technology.

Schwarz, B. (1972), 'Capillary water absorption in building materials' (in German), Gesundheits-Ingenieur, Heft 7, Nr. 93, pp. 206-211.

Sosoro, M. (1998), 'Transport of organic fluids through concrete', Materials and Structures, Vol. 31, April 1998, pp. 162-169.

Svensk standard (1988), SS 13 72 42, BST Byggstandardiseringen, (in Swedish), edition 1, pp. 1.

Torpgaard, D. (2003), 'Nuclear magnetic resonance studies of water self-diffusion in porous systems', Doctoral thesis, Center for Chemistry and Chemical Engineering, Physical Chemistry, Lund University.

Vos, B. H. and Tammes, E. (1968), 'Flow of water in the liquid phase', Report No. BI-68-38, TNO. Bouw, Rijkswijk, The Netherlands.

Wiberg, P. (2001), 'X-ray CT-scanning of wood during drying', Thesis No. 2001:10, Luleå University of Technology.

ANNEX

Janz, M. and Johansson, P, ‘Evaluation of thermal imaging as a method of measuring moisture profiles over an interface between cement-lime mortar and brick’ (submitted for publication).

Evaluation of thermal imaging as a method of measuring moisture profiles over an interface between cement-lime mortar and brick.

Mårten Janz and Peter Johansson
Division of Building Materials, Lund University, P.O. Box 118, SE-221 00 Lund, Sweden

ABSTRACT

Moisture profiles reveal much about the moisture behavior of a material or combination of materials. Measured transient moisture profiles can also be used to verify and evaluate moisture diffusivities. One possible method of measuring these profiles is thermal imaging. This paper evaluates this technique applied to bricks with and without cement-lime mortar attached. The measured temperature profiles are transformed to moisture profiles through calibration curves obtained by measuring the temperature decrease on preconditioned specimens. The use of calibration curves avoids problems arising from possible difference in emittance between wet and dry surfaces.

1 INTRODUCTION

There are several methods of determining moisture profiles. The most accurate is probably the "slice-dry-weigh method," which measures moisture content directly. In this method, the specimen is rapidly sliced into discs that are weighed, dried, and weighed again. The water in the disc evaporates during the drying and the water content in mass by mass can be determined directly from the weight loss. This method is, however, quite time-consuming and can in some cases present practical difficulties. Besides, it might also be difficult to split the specimen into discs thin enough to evaluate a very steep moisture front.

Other methods of determining moisture content rely on measuring other physical attributes, such as electrical conductivity, electrical capacitance, gamma-ray attenuation, nuclear magnetic resonance, and the temperature loss when liquids evaporate. These and other methods are briefly outlined in Janz (1997). The method used in this paper is thermal imaging; i.e. measurement of the decrease in temperature when water evaporates.

Moisture diffusivity can be determined from moisture absorption profiles or redistribution profiles. Two of the most common methods of doing this are the Boltzmann transformation method and the profile method. These methods are described in de Freitas et al. (1995). Measurements of moisture distribution obtained through such techniques as thermal imaging can also be used to verify measured moisture diffusivities. Such verification is important in order to estab-

lish correlations between empirically measured distributions and existing models of transport properties so as to develop better models.

The combination of mortar and brick can be sensitive to frost attack. Although both the brick and the mortar may themselves be frost resistant, the combination can cause failure. In some cases a thick layer of mortar protects the brick, while a thin layer increases the risk of frost attack. The critical degree of saturation of the brick will, of course, not change in this combination. However, the quality of the mortar may change, because the brick sucks water from the fresh mortar. This effect is dependent on the thickness of the mortar, with a thin layer being proportionately more affected than a thick layer.

The main reason for the increase or decrease in frost resistance is the moisture levels reached in the brick. The mortar will always have some influence on these moisture levels. It may, for example, lower the moisture content in the brick by reducing moisture absorption during driving rain. However, it will also simultaneously lower the capacity of the brick to dry out, which may increase the moisture content in the brick.

The moisture levels reached in a multi-layer construction will depend on both the moisture diffusivity and the moisture storage capacity of all the construction materials. The moisture diffusivity determines the rate of moisture transport within a specific material, while the moisture storage capacity determines the moisture equilibrium at interfaces between materials and at the boundary to the surrounding environment. Current models for calculating moisture transport and transport properties in homogenous materials do not show satisfactory agreement with measured moisture distributions for many materials. The agreement is even worse for multi-layer constructions. There is clearly a need for methods of measuring actual moisture distribution. One such method is thermal imaging.

2 PRINCIPLE OF THERMAL IMAGING

Thermal imaging is a simple method of determining moisture distribution, or the distribution of any volatile fluid. This method makes use of a split surface of the specimen, and hence it is destructive, with one specimen used every time the moisture profile is measured.

Immediately before measuring, the specimen is split into two halves, parallel to the moisture flow direction. As the moisture in the specimen starts to evaporate from the split surface, the temperature of the surface drops. An infrared camera registers the temperature distribution over the split surface, and this distribution is used to construct a moisture profile.

It should be noted that thermal imaging measures the radiation from a surface, rather than the surface temperature. The camera computes the surface temperature from the measured radiation, and in order to do so the emittance of the surface must be known. The magnitude of the total radiation from a certain surface with a temperature equal to the temperature of the surrounding air is described by

$$q_{rad} = \varepsilon E_b + (1-\varepsilon) q_{in} \tag{1}$$

where

q_{rad} is the total radiation [W/m^2];
ε is the emittance [–];
E_b is the total emitted radiation from a black body [W/m^2];
q_{in} is the incident radiation in the object measured on [W/m^2].

The first term in Equation 1 describes the total emitted radiation from the surface while the second term describes the reflected radiation.

The total emitted radiation from a black body is given by Stefan-Boltzmann's equation:

$$E_b = \sigma T^4 \tag{2}$$

where σ is the Stefan-Boltzmann constant with a magnitude of $5.68 \cdot 10^{-8}$ W/(m^{2}K^4) and T is the absolute temperature [K] of the surrounding air.

Liquid water will evaporate when a split surface of a specimen with raised moisture content is exposed to the surrounding air. This process requires a certain amount of heat, and hence the evaporation decreases the surface temperature. The magnitude of the heat of vaporization is dependent, among other things, on the moisture content, the rate of moisture transport to the surface, the rate of vapor transport from the surface, the specific heat of vaporization, and the temperature.

The decrease in the surface temperature of a wet surface results in the total radiation of the wet split surface being lower than the total radiation of a dry surface. The total radiation of a surface with a moisture content u (moisture content mass by mass) can be described by

$$q_{rad,u} = \varepsilon_u \sigma T_S^4 + (1-\varepsilon_u) q_{in} \tag{3}$$

where $q_{rad,u}$ is the total radiation from a surface with the moisture content u, ε_u is the emittance of a surface with a moisture content u, and T_S is the decreased surface temperature.

The decrease in radiation emitted from the surface is proportional to the evaporation, and consequently also to the moisture content. Thus the moisture content in the material can be described in terms of the difference between the radiation from a dry surface and a wet surface:

$$\Delta q_{rad} = \sigma \left(\varepsilon_0 T_0^4 - \varepsilon_u T_S^4 \right) + q_{in} \left(\varepsilon_u - \varepsilon_0 \right) \tag{4}$$

where ε_0 is the emittance of a dry surface and T_0 is the temperature of a dry surface.

The output from an infrared camera is the temperature. Thus, in order to measure the correct surface temperature, the emittance of the surface must be known and programmed into the camera. Since only one emittance at a time can be pro-

grammed into the camera, the surface temperature measured will be incorrect when ε_0 differs from ε_u.

This problem can, however, be avoided by using a method of calibration proposed by Janz (1997). In this method the temperatures of the split surface on which the profile is measured are calibrated against the temperatures of split surfaces of well-conditioned specimens. The calibration is performed on specimens of the specific material with different, known moisture contents. The measuring procedure and conditioning procedure must take place in a climate room with constant relative humidity and temperature, and the image must be taken at the same time after splitting the specimen. Both the calibration and the measurement of profiles must, of course, be performed with the same camera settings. Since the emittance at a specific moisture level is the same independent of whether the temperature is measured on a calibration specimen or on a specimen with a moisture distribution, the magnitude of the emittance is insignificant. A specific temperature decrease always implies a definite moisture level, even if the measured temperature is incorrect. While the conditioning procedure is time-consuming, the accuracy of the measured water content is high. This is the method used to evaluate the profiles presented in this paper.

Another method of evaluating moisture profiles without any calibration is given in Sosoro and Reinhardt (1995). They claim that the moisture profile in a specimen with a constant cross-section over depth can be calculated by:

$$\psi(x) = \frac{\left(T - T_S(x)\right)^2}{\frac{S}{V_{fl}} \cdot \int_0^{\ell} \left(T - T_S(x)\right)^2 dx} \tag{5}$$

where

- ψ is the water content volume per volume [m^3/m^3];
- T is the temperature of the surrounding air [K];
- T_S is the surface temperature [K];
- x is the co-ordinate in the direction of water transport [m];
- S is the surface area exposed to fluid [m^2];
- V_{fl} is the total absorbed test fluid [m^3];
- ℓ is the specimen length [m].

Measured profiles of different liquids and laboratory arrangements are described in Sosoro et al. (1995), Sosoro (1995), Sosoro (1998) and Johansson (1999).

2.1 Limitations

Since evaporation involves cooling of the evaporating surface, thermal imaging can never be used to detect moisture contents directly after a period of desorption. Some absorption time must always precede the imaging so that the specimen is at the same temperature as the climate room. Hence it follows that the moisture distribution cannot be studied immediately after a period of drying.

3 MATERIALS AND METHOD

3.1 Specimens

The test was performed on bricks with or without mortar attached. The attached mortar consisted of cement-lime mortar CL 50/50/650. The porosity, density, and sorption coefficient of both the brick and the mortar had been measured. The porosity and density were determined according to Archimedes' principle (weighing vacuum saturated specimens in air and water). The sorption coefficient was determined on specimens dried in, and in equilibrium with, normal room climate. The porosity, density, and sorption coefficient of the brick were 26%, 1978 kg/m^3 and 0.35 kg/(m^2 s^{½}), respectively. For the cement-lime mortar the same properties were 30%, 1853 kg/m^3 and 0.091 kg/(m^2 s^{½}), respectively.

The specimens were manufactured by sawing a brick in two, yielding pieces of approximately 250 x 120 x 30 mm^3. An edging was attached around the 120 x 30 mm^2 surface in which the cement-lime mortar was to be cast. The edgings were 2 and 10 mm in height, reflecting the desired thickness of the mortar. Some variation occurred, however, especially in the thin mortar layer.

Before the mortars were attached, the bricks were stored in water for a week. The purpose of this water saturation was to prevent the bricks from sucking water from the cement-lime mortar during the casting and curing, and so to obtain the same characteristics in the 2 mm mortar and the 10 mm mortar. This saturation procedure also avoided differences at varying depths of the 10 mm mortar. After casting the specimens were stored at room climate for at least 4 months so that all the mortar was carbonized when tested.

In total, 57 specimens were manufactured: 17 with a 2 mm thick mortar, 34 with a 10 mm thick mortar and 6 without any mortar. Of the 34 specimens with a 10 mm thick mortar, 19 were used in the calibration procedure. All the other specimens were used for measurements of the moisture distribution.

3.2 Camera

The camera used was AGEMA, Thermovision 900. The camera has, according to its manual, a sensitivity of 0.1°C at 30°C.

3.3 Calibration procedure

Measurement of the surface temperature of specimens with known and well-conditioned moisture contents produced calibration curves. These curves were used to determine moisture distributions from measured temperature profiles.

At the start of the calibration procedure, the mortar and brick were separated with a diamond saw, making it possible to condition the mortar and the brick separately. The conditioning process started with drying the specimens in an oven at a temperature of 60°C until no changes in weight were observed, whereafter they were vacuum-saturated with water. The vacuum saturated specimens were then dried to the desired moisture content.

To achieve homogenous moisture distribution, the specimens were wrapped in plastic film and stored for at least 2 months in a climate chamber. A water-filled container was placed in the chamber with the specimens in order to keep the relative humidity in the chamber as close to 100% as possible, so preventing moisture loss through the plastic during the storage period. During this period the moisture in each specimen was redistributed so that the specimens would have a uniform distribution when the surface temperature was measured. Two weeks before the temperature measurement, the climate chamber was placed in the climate room were the surface temperature was to be measured. Thus the specimen was at the same temperature as the climate room when measured.

The temperatures of the calibration specimens were measured using thermal imaging in a climate room with a temperature of 20.6 ± 0.1°C and 19 ± 1% relative humidity. The procedure for measuring the surface temperature was identical on all measuring occasions. The specimens were split with a sharp cutting edge and exposed to the climate in the climate room. A fan, mounted half a meter from the specimen, generated turbulent air flow with a velocity of approximately 0.7 m/s over the split surface. Thermal imaging of the split surface took place exactly one minute after the specimen was split. The specimen was during the imaging placed 1 m from the camera. After the thermal imaging, the exact moisture content mass by mass of the specimen was determined by weighing it, drying it at 105°C, and finally weighing the specimen again.

The calibration curves obtained for the brick and cement-lime mortar are shown in Figure 1 and Figure 2. Possible differences between individual specimens were avoided by using the relative moisture content and relative temperature rather than the actual moisture content and temperature. Hence the moisture content was represented as the relative moisture content u/u_{cap}, where u is the actual moisture content mass by mass and u_{cap} is the moisture content at capillary saturation for the specific specimen. The temperature is represented by $(T_0–T_S)/(T_0–T_{S,cap})$ where T_0 is the temperature of the dry surface of the specimen, T_S is the actual surface temperature, and $T_{S,cap}$ is the temperature of the capillary saturated surface of the specimen. On average T_0 and $T_{S,cap}$ were 20.60°C and 17.76°C for the brick and 21.70°C and 16.03°C for the cement-lime mortar. The standard

deviation of T_0 and $T_{S,cap}$ were 0.15°C and 0.36°C for the brick and 0.13°C and 0.39°C for the cement-lime mortar.

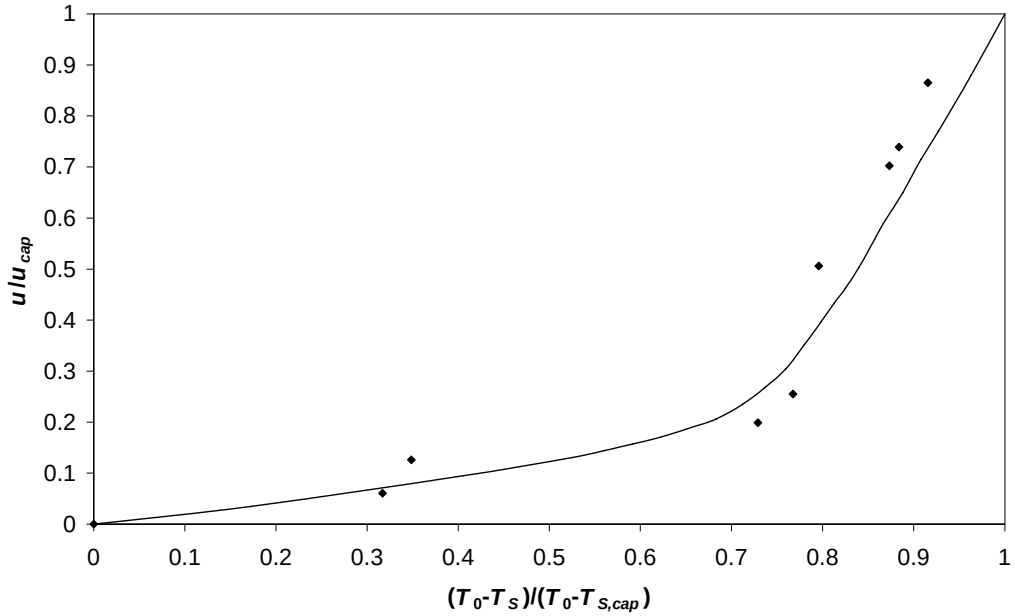

Figure 1 *Calibration curve of the brick. The relative decrease in surface temperature is plotted against the relative moisture content.*

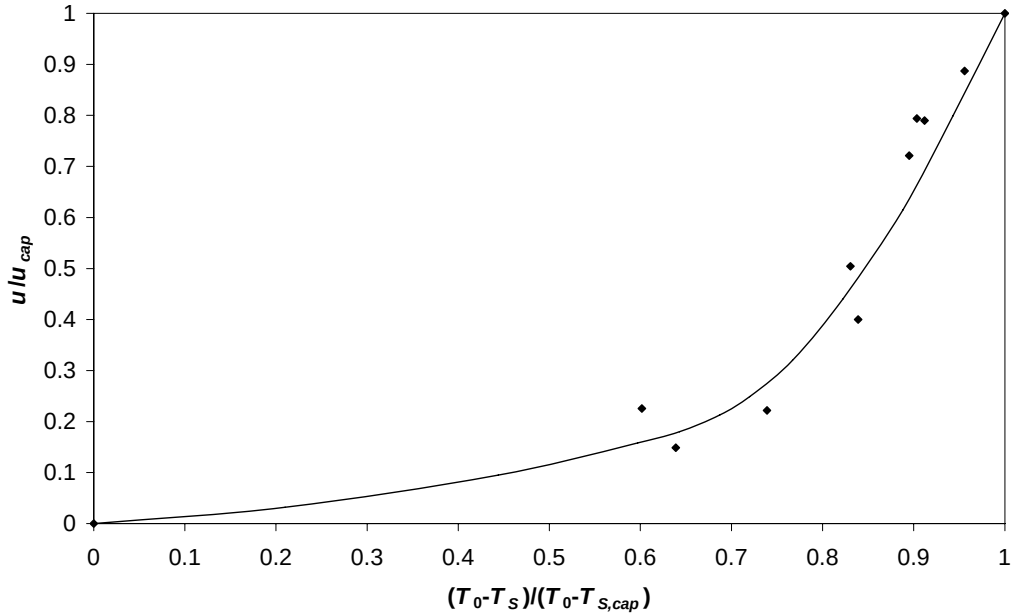

Figure 2 *Calibration curve of the cement-lime mortar. The relative decrease in surface temperature is plotted against the relative moisture content.*

3.4 Measurement of temperature profiles

The temperature profiles, and thus indirectly also the moisture profiles, were measured on dry specimens (dried at 60°C) subjected to different moisture loads. The dry specimens were wrapped in plastic film and stored for 2 weeks in the climate room where the surface profiles were to be measured so that the specimens were at the same temperature as the climate room. Conditions in the climate room were identical to those maintained when measuring the calibration curves, i.e. the temperature was 20.6 ± 0.1°C and the relative humidity was 19 ± 1%.

Before the temperature profiles were measured, the mortar-coated sides of the specimens were exposed to liquid water or the climate in the climate room for varying times. Moisture transport was prevented on all other sides of the specimens. Thus the moisture transport in the specimen during absorption and drying took place in only one direction. The water used for the absorption was acclimatized to the temperature of the climate room so that it was at the same temperature as the specimens.

Once a specimen had been subjected to the desired moisture load, it was split with a sharp cutting edge parallel to the direction of absorption and desorption. Thermal imaging of the split surface was conducted as described in section 3.2.

4 RESULTS AND DISCUSSION

The measured temperature profiles were compared to the calibration curves that had been obtained (see Figure 1 and Figure 2). The emitted radiation at a certain moisture level in the moisture distribution measurement was the same as the emitted radiation on the calibration specimen with the same moisture content. Any differences in emittance between a wet and dry surface were therefore insignificant in the tests performed here. Both the calibration curves obtained were very similar. If this is a coincidence or if there is any physical explanation for the similarity is not analyzed in this paper. If the similarity is a coincidence could however be checked by measuring calibration curves for more materials.

Figure 3 shows a typical measured temperature profile. The brick in question was exposed to water for 12 hours followed by 12 hours of desorption at 75% relative humidity, and finally by an additional 12 hours of absorption before the temperature profile was measured with thermal imaging. Figure 4 shows a moisture profile derived from the measured temperature profile. The derivation was performed using the calibration curves shown in Figure 1 (brick) and Figure 2 (cement-lime mortar).

As can be seen in Figure 3, the slope of the temperature profile is not perfectly sharp at the interface between mortar and brick. Consequently near the interface the moisture content is below capillary saturation in the cement-lime mortar and above capillary saturation in the brick (see Figure 4).

This phenomenon is a product of the limitations in the spatial resolution of the camera used. Figure 5 shows a temperature profile over an interface between

cellular plastic and a steel plate. On this occasion, the cellular plastic had a temperature of 20.9°C and the steel a temperature of 16.6°C. There is thus a sharp temperature profile between the steel and cellular plastic, but the camera cannot register this sharp step. Therefore, the thermal imaging shows an inclined temperature profile. Thus, if using a camera and camera settings similar to the one used in this investigation, this method cannot register sharp temperature profiles, making it impossible to measure moisture levels close to the interface. From Figure 5 it appears that the spatial resolution of the camera and camera setting used in this investigation is approximately 11 mm. Moisture profiles with very large gradients will thus to some extent be incorrect.

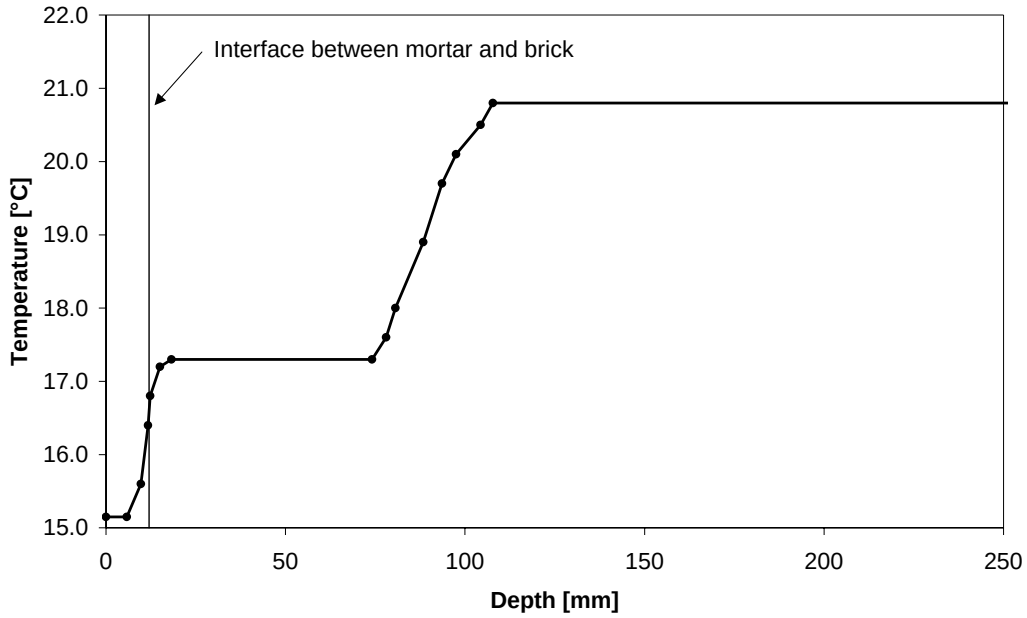

Figure 3 *Measured temperature profile on a brick with 12 mm mortar. The brick was exposed to water for 12 hours, followed by 12 hour desorption at 75% relative humidity, and finally an additional 12 hours absorption.*

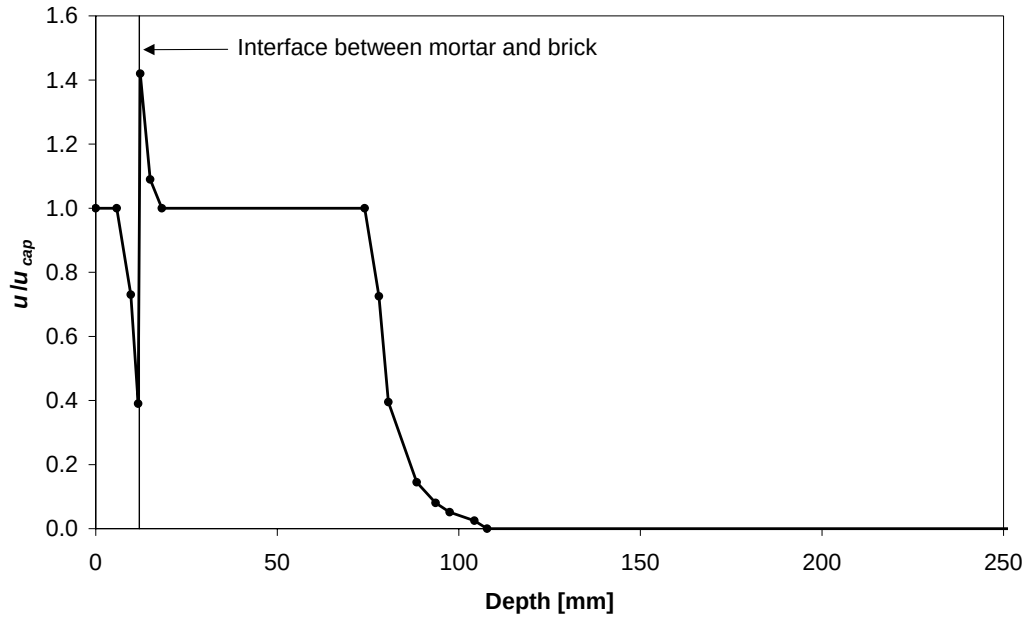

Figure 4 *Moisture distribution derived from Figure 3 with the calibration curves of brick (Figure 1) and cement-lime mortar (Figure 2).*

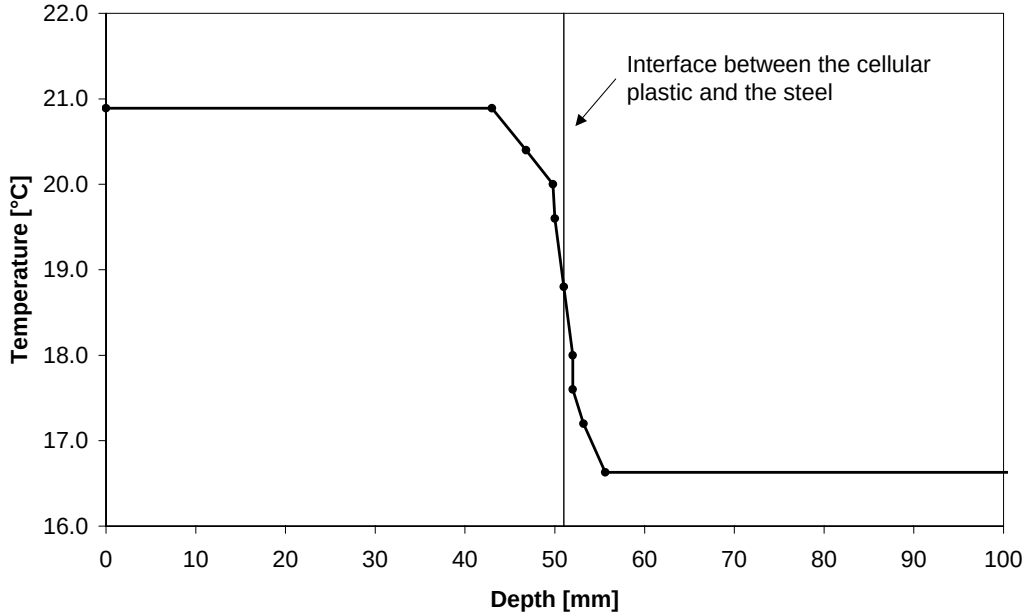

Figure 5 *Temperature profile measured over the interface between a steel plate and cellular plastic.*

However, even though the details in sharp moisture fronts may be incorrect due to problems with spatial resolution, the total penetration depth is correct. Figure 6 shows the relations between the penetration depth (defined as the depth were the moisture content has decreased 50%) of the wet capillary saturated face and the exposure time for specimens without mortar, for specimens with an average of 3.9 mm mortar, and for specimens with an average of 11.5 mm mortar. The penetration depth is clearly directly proportional to the square root of time, even for the specimens with mortar attached. It is also clear that the penetration rate is considerably lower for the specimens with a thick layer of mortar. Surprisingly, the difference between specimens without mortar and specimens with a thin layer of mortar is very small. This may explain why a thin layer of mortar sometimes increases the risk of frost attack while a thick layer protects the bricks. Even if a thin layer of mortar only has a very slight effect on the water absorption, it may prevent desorption and trap water in the brick. Unfortunately this possibility could not be investigated because thermal imaging cannot be used to measure moisture profiles directly after periods of desorption.

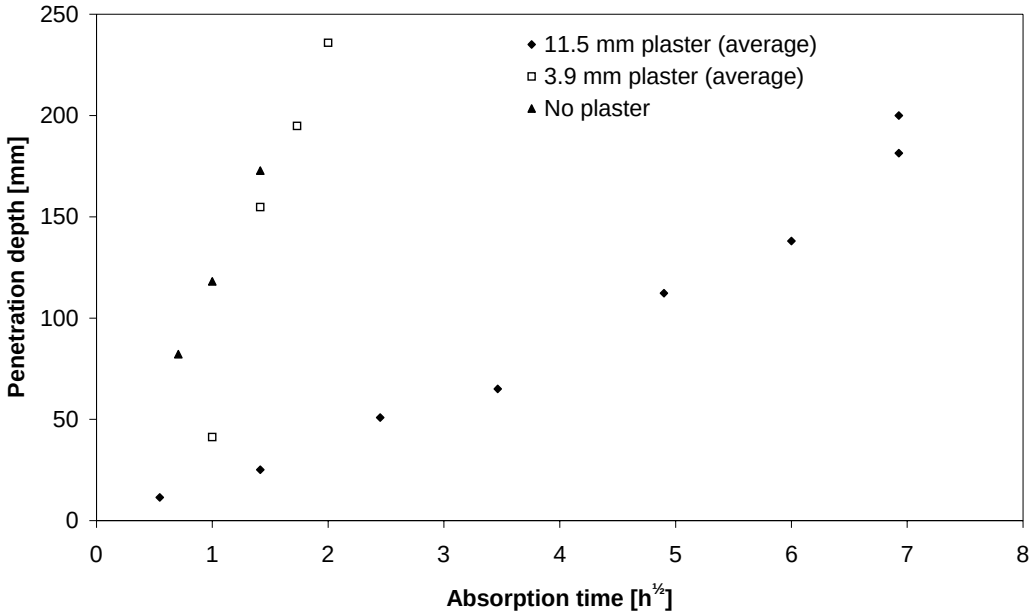

Figure 6 *Penetration depth of the wet face after different exposure times on specimens without mortar, with an average of 3.9 mm mortar, and with an average of 11.5 mm mortar.*

The temperature profiles of specimens that were first exposed to water, followed by varying periods of redistribution, are shown in Figure 7 to Figure 9. During the redistribution period, the specimens were wrapped in plastic film so that no water could leave them. Figure 7 shows profiles measured on specimens without mortar, Figure 8 profiles measured on specimens with a thin layer of mortar, and Figure 9 profiles measured on specimens with a thick layer of mortar.

Unfortunately it was impossible to recalculate the temperature profiles to moisture profiles since the values of $T_{S,cap}$ and T_0 were unspecified for the specimens tested. At the measuring occasion the relatively great variation of $T_{S,cap}$ and T_0 was unknown and therefore not measured separately. During an absorption test these values appear directly from the temperature profile whereupon the moisture profiles can be calculated. In future studies the values of $T_{S,cap}$ and T_0 will be measured in separate tests for each specimen.

From the profiles it appears that during redistribution the water penetrates the specimen only to a certain level, where penetration more or less stops. The stop in moisture flow is probably due to the decreased moisture gradient resulting in a marked decrease in moisture diffusivity.

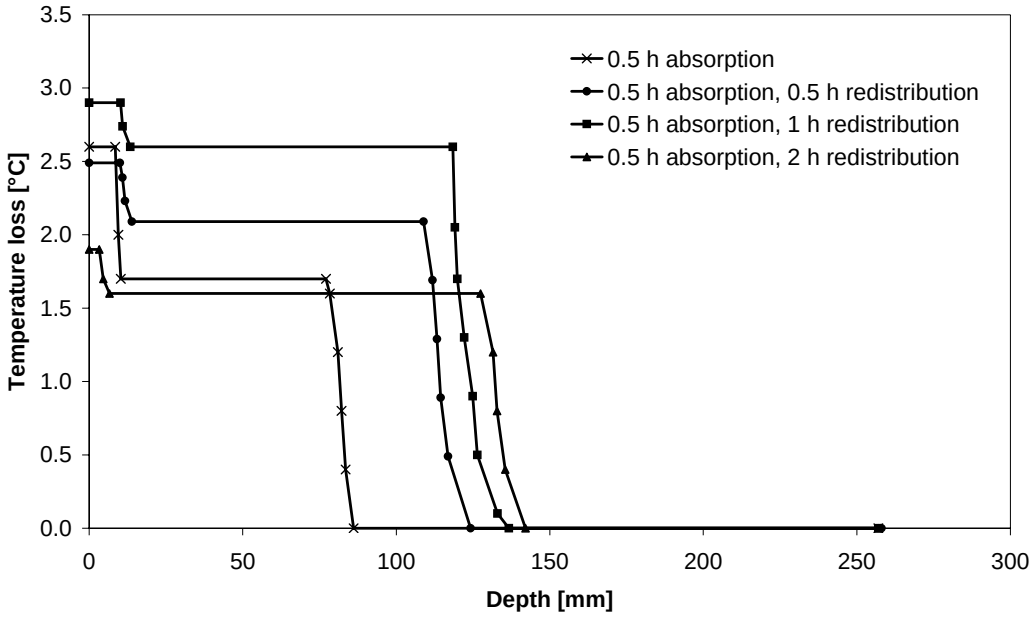

Figure 7 Temperature profiles measured on bricks without mortar.

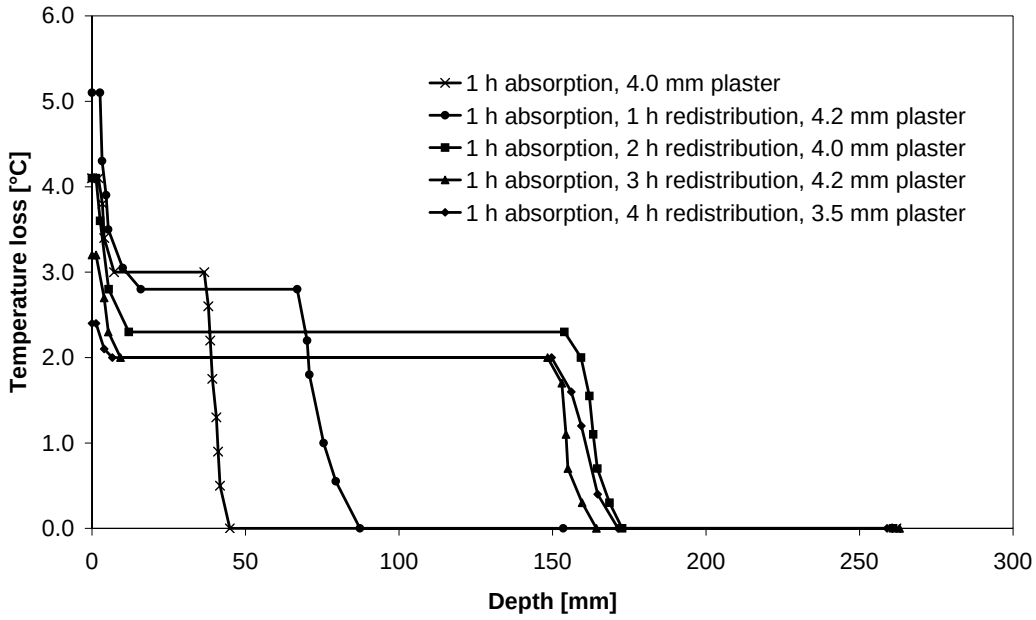

Figure 8 *Temperature profiles measured on bricks with a thin layer of mortar attached.*

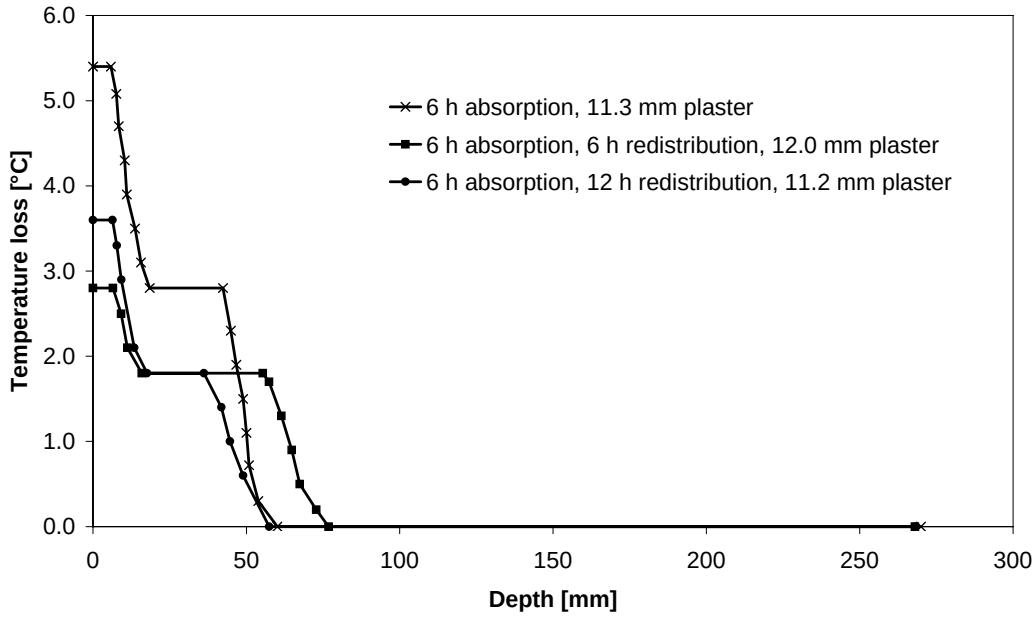

Figure 9 *Temperature profiles measured on bricks with a thick layer of mortar attached.*

5 CONCLUSIONS

Thermal imaging provides a quick and easy way of measuring penetration depth and the shape of the moisture profile. Compared to other methods of measuring transient moisture profiles, this method is relatively inexpensive and requires no major technical outlays other than for the camera. Moreover, thermal imaging eliminates the need for any special geometry in the specimens. The only requirement is that it must be possible to split the specimen parallel to the moisture flux.

Time-consuming calibration is needed if exact moisture levels are to be derived from the temperature profiles. In such cases a climate room is needed in addition to the camera.

The major weakness of thermal imaging is that it cannot be used directly after periods of desorption since evaporation cools the evaporating surface and disturbs the imaging. A period without desorption must always precede imaging to ensure that the specimen is at the same temperature as the surrounding air.

The partial resolution of the camera used in this study was rather low, making it impossible to evaluate the moisture content near the interface between mortar and brick.

6 ACKNOWLEDGMENT

The financial support of the Development Fund of the Swedish Construction Industry and the Swedish Council for Building Research is gratefully acknowledged. The authors also wish to express their gratitude to Mr. Ingemar Larsson for his assistance in the experimental work.

7 REFERENCES

De Freitas, V. P., Krus, M., Künzel, H. and Quenard, D. (1995), 'Determination of the water diffusivity of porous materials by gamma-ray attenuation and NMR', *Proceeding of the International symposium on Moisture Problems in Building Walls, Porto, 11–13 Sept*, pp. 445–460.

Janz, M. (1997), '*Methods of Measuring the Moisture Diffusivity at High Moisture Levels*'. Report TVBM-3076. Division of Building Materials, Lund Institute of Technology, Lund.

Johansson, P (1999), 'A thermal imaging method for measuring moisture distribution in porous building materials', *Proceedings of the 5th Symposium on Building Physics in the Nordic Countries, Göteborg, August 24–26*, Vol. 1, pp. 297–304.

Sosoro, M. (1995), 'A model to predict the absorption of organic fluids in concrete' (in German), *Deutscher Ausschuß für Stahlbeton*, Heft 446, Beuth Verlag GmbH, Berlin.

Sosoro, M. and Reinhardt, H. W. (1995), ‘Thermal imaging of hazardous organic fluids in concrete’, *Materials and Structures*, Vol. 28, pp. 526–533.

Sosoro, M. (1998), ‘Transport of fluids through concrete’, *Materials and Structures*, Vol. 31, pp. 162–169.